

ELVE

THE ACTIVATION AND DEACTIVATION OF

PLATINUM / RHODIUM CATALYSTS FOR

AMMONIA OXIDATION

by

James Anthony Busby, C. Chem, M. R. I. C.

November 1975

A thesis submitted for the
degree of Doctor of Philosophy of the
University of London

Dept. of Chemical Engineering and
Chemical Technology

Imperial College

London, S. W. 7.

ABSTRACT

The object of this study has been to investigate the activation and deactivation of platinum/rhodium wire mesh catalysts used to oxidise ammonia.

Two experimental parameters give an indication of the reactivity of the gauzes: the temperature at which rapid reaction starts and the gauze activity, as judged by product yields. The importance of different effects on activation has been studied, using these parameters as a measure of success.

Surface contamination has been shown to increase light-off temperature substantially. Contaminants can be removed by a solvent washing method.

Electron spectroscopy has been used to monitor the changes occurring in alloy composition. Attempts have been made to quantify this technique. The platinum/rhodium ratio has been examined with respect to the variations arising during the activation and reaction processes.

The effect of surface geometry on catalyst activity has been studied. The effect of heating the gauzes in oxidising, inert and reducing gases has been correlated with pitting and/or grain boundary groove formation. Optical microscopy has been used to follow the rearrangements induced by the individual gases and by the ammonia oxidation reaction.

The nature of any electronic effects arising from changes occurring in the catalyst has been studied using electron spectroscopy.

Adsorption on the catalyst, and 'in situ' reactions, were studied by ultraviolet photoelectron spectroscopy.

The results have been used to assign a relative importance for each factor in determining the initial activity of the gauze.

Doping of platinum/rhodium catalysts with metal oxides has been undertaken with a view to reducing the weight loss of the platinum/rhodium gauze. These dopants are found to deactivate the catalyst to different

extents. The conversion and light-off temperatures arising from doped catalysts have been correlated with induced geometric, electronic, and alloying mechanisms.

Finally, a numerical method for estimating the platinum loss occurring in ammonia oxidation has been improved and extended to cover high pressure plant data.

A comprehensive review of the aspects of heterogeneous catalysis in its relation to ammonia oxidation is also included together with an extensive review of the literature.

ACKNOWLEDGEMENTS

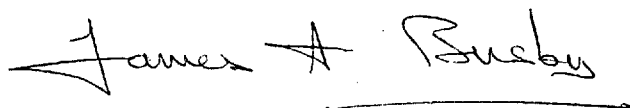
I should like to express my thanks to Dr. D. L. Trimm for his help and supervision during this project.

My thanks must also go to the technical staff and my colleagues for their help and companionship during the last three years.

Valuable assistance from Johnson, Matthey and Co., Ltd. is gratefully acknowledged.

Finally, I should like to express my thanks to the Staff of Slough College of Technology for their help and encouragement earlier in my career.

November 1975

A handwritten signature in cursive script that reads "James A. Busby". The signature is written in dark ink and is positioned above a horizontal line.

Dept. of Chemical Engineering and Chemical Technology

Imperial College

London, S. W. 7.

To Mum, Dad

and Alison.

CONTENTS

CHAPTER 1	INTRODUCTION	9
CHAPTER 2	EXPERIMENTAL	92
CHAPTER 3	RESULTS	114
CHAPTER 4	WEIGHT LOSS CALCULATIONS	189
CHAPTER 5	DISCUSSION	205
CONCLUSIONS		250
APPENDIX		253
REFERENCES		290

CHAPTER 1

INTRODUCTION

		Page.
1. 1.	<u>Industrial aspects of ammonia oxidation</u>	
1. 1. a.	Historical background	9
1. 1. b.	Catalyst system	11
1. 1. c.	Nitric acid plant and manufacture	14
1. 1. d.	Design of the ammonia burner	16
1. 1. e. (i)	Pt/Rh gauzes	21
	(ii) Activation of Pt/Rh gauze catalysts	21
	(iii) Deactivation of Pt/Rh gauze catalysts	22
	(iv) Pickling of Pt/Rh gauze catalysts	24
1. 1. f.	Platinum loss and recovery	25
1. 2.	<u>Heterogeneous catalysis - Introduction</u>	
1. 2. a.	Mass transfer in heterogeneous catalysis	33
1. 2. b.	Heat transfer in heterogeneous catalysis	35
1. 2. c.	Adsorption in heterogeneous catalysis	36
1. 2. d.	Kinetics of heterogeneous catalytic reactions	39
1. 2. e.	The geometric factor in heterogeneous catalysis	51
1. 2. f.	The electronic factor in heterogeneous catalysis	57
1. 3.	<u>Modern analytical methods used in this work</u>	
1. 3. a.	X-ray photoelectron spectroscopy	61
1. 3. b.	Ultraviolet photoelectron spectroscopy	72
1. 3. c.	Electronprobe Microanalysis	73
1. 3. d.	Energy dispersion analysis of X-rays (EDAX)	77

1.4.	<u>The mechanism of catalytic ammonia oxidation</u>	80
1.5.	<u>The kinetics of catalytic ammonia oxidation</u>	88
1.6.	<u>Present work</u>	89

1. 1. Industrial Aspects of Ammonia Oxidation

1. 1. a. Historical background

During the latter half of the nineteenth century, scientists were beginning to draw the public's attention to the depletion of natural resources - in this case, sodium nitrate or 'Chile Saltpetre'. This substance was at that time, the major naturally occurring compound from which nitrogenous fertilizers were produced.

Military strategists were also worried that in the event of an outbreak of war, these Chile nitrates which were needed for the manufacture of nitric acid for explosives, might become inaccessible to either side. Thus, the fixation of nitrogen, or 'The Nitrogen Problem' as it later became known, received ample stimulus and very rapidly established itself as a major industry which has undergone very little basic change to the present day.

By 1900, Wilhelm Ostwald had occupied the chair of chemistry at Leipzig for thirteen years, and he immediately began an investigation into the nitrogen fixation problem using catalysis. Two possible approaches to the problem became apparent. Either free nitrogen and oxygen of the air could be combined, or ammonia, which was then produced as a by-product in the gas industry, could be oxidised to give nitric acid. It was the latter approach that Ostwald adopted, basing his approach on earlier work by Kuhlmann.

Kuhlmann had studied the work of Lavoisier on the composition of ammonia, and was familiar with the discoveries of Humphry and Edmund Davy in catalysis. The agricultural uses of nitrogen products were also of interest to him, and so he began work by passing a mixture of ammonia and air over a platinum sponge catalyst heated to 300°C in a glass tube. Using this method he obtained nitric acid and filed a patent application in 1838.

Using this work as a base, Ostwald began work to determine the theoretical basis of the ammonia oxidation reaction. Though the first experiments using platinised asbestos gave only low yields, it clearly showed that the conversion to nitric acid was possible, though difficulties lay in the absorption of the reaction products.

Further experiments were performed using a glass tube 2mm. in diameter and a coiled strip of platinum as the catalyst. With the tube heated to red heat, a conversion to nitric oxide of the order of 50% was obtained. Increasing the gas velocity gave an 85% conversion, and Ostwald deduced that the nitrogen oxides formed could decompose to free nitrogen and oxygen if the catalyst contact time was excessive. Further work followed on the effects of variations in the ammonia/air ratio, contact time and gas temperature, and following this, in 1904, Ostwald and Brauer constructed a pilot plant. Thus, the foundations were laid for the production of nitric acid from ammonia, though in one area, that of type of catalyst, work still remained.

The first large scale plant was constructed at Gerthe, near Bochum, to produce 300 kg. of nitric acid per day. The catalyst used consisted of a roll of corrugated platinum strip 2 cm. wide, heated initially by a hydrogen flame. This type of catalyst had disadvantages in that a relatively large amount was required per unit of acid produced, accurate temperature control was not possible, and catalyst life was short, of the order of 4 to 6 weeks.

Finally, Kaiser filed patents in 1909 for a process involving preheating of the ammonia/air mixture to between 300° and 400°C , using four platinum gauze catalysts, constructed from 0.06 mm. diameter wire woven to 1,050 mesh per cm^2 , the specification for catalysts still widely used today.

Other earlier methods included one by Caro, in which a thorium oxide/cerium oxide catalyst was used. This process failed as a result of the catalyst sintering, the resulting impermeability rendering the catalyst inactive. Further work in this field led to a process based on a single platinum gauze, heated electrically, though this was subsequently replaced by multiple gauzes and the electrical heating was discontinued.

Thus by the outbreak of the first world war, the basic method for the oxidation of ammonia to nitric acid had been developed, and whilst large increases in plant size and throughput have been achieved, using higher pressures and platinum/alloy gauzes, the basic manufacturing process has changed little since the first decade of the twentieth century.

1. 1. b. Catalyst System

The catalyst systems at present in use in the oxidation of ammonia to nitric oxide are variations on a type of metal catalyst first used over 60 years ago. In his paper on the commercial oxidation of ammonia to nitric acid, Parsons (1) outlines a process using a platinum gauze catalyst. The nature and form of the catalyst have changed very little since these early plants went into operation (2).

Parsons (1) also noted that platinum wire cannot be drawn unless it contains a hardening element. It was for this reason that alloys of platinum with other precious metals were evolved. Palladium and iridium were first considered as being suitable alloying agents. Whilst a palladium gauze was more active than a platinum catalyst for the reaction, its useful life was very limited, giving only a maximum of ten hours. A platinum gauze containing 10 to 20 per cent palladium in platinum did not affect the catalyst efficiency but did not activate as easily as a gauze containing only a few per cent iridium. Thus a platinum/iridium alloy was the first alloy gauze used in the ammonia oxidation process.

With the advent of high pressure ammonia oxidation plants, catalyst loss became a serious economic problem. Thus, alloys, besides being used for strengthening were now studied for their potential in lowering catalyst loss by evaporation.

Handforth and Tilley (3) carried out an economic appraisal of various alloy catalyst systems. With an increase in plant running pressure from atmospheric to 100 p. s. i. , an increase in both speed and efficiency of conversion of ammonia to nitric oxide was achieved, together with smaller plant and a higher final acid strength. However, higher pressures require higher running temperatures, resulting in a more rapid deterioration of the catalyst. Initial experiments carried out by Handforth and Tilley used platinum/iridium alloys, but these proved to be unsatisfactory under ammonia oxidation conditions. Further work with platinum/rhodium alloys showed that a 5 to 10 per cent rhodium/platinum alloy was both the most

advantageous and the most economical. Thus, the Pt/10% Rh gauze catalyst was adopted as the catalyst for ammonia oxidation.

It was well known that all platinum metals oxidise and volatilise rapidly at high temperatures in oxidising atmospheres. Below 900°C , there should be little or no volatilization of platinum. Handforth and Tilley (3) have shown that in the ammonia oxidation process, platinum is volatilised from the surface at lower temperatures. Further testing showed that this loss, at a given temperature and with a given alloy, to be proportional to the weight of oxygen in the reacting gas mixture passed over the catalyst. This has led several workers to postulate that it is the platinum oxide that volatilises and, further, that it is the oxide and not the platinum metal itself, which is the catalyst for the ammonia oxidation process. This is discussed further in section 1.1.f. Sikora (4) has used platinum oxide, PtO_2 , as the catalyst instead of platinum, and has obtained the catalytic oxidation of ammonia to nitric oxide as low as 300°C with no prior activation treatment. This must be contrasted with the platinum catalyst which requires a thorough cleaning and heating to high temperature in a hydrogen burner before it can efficiently catalyse the reaction.

Despite the use of alloying techniques, the problem of catalyst loss is still not completely removed. Work was undertaken with alternative catalysts, such as iron and chromium oxides, though these proved to have an efficiency below that which could be considered economical. However, work recently carried out by Dobrovol'skaya et al. (5) and Epshtein (6) uses a two step oxidation process, by passing an ammonia/air mixture first through several platinum metal catalyst gauzes, followed by further catalytic conversion using iron oxide and chromium oxide. This resulted in higher ammonia conversion and lower platinum catalyst losses.

Other catalysts which have been employed in the oxidation of ammonia include bismuth/molybdenum catalysts reviewed by Alkhozov et al. (7) and crystalline cuprous oxide catalysts used by Holbrook and Wise (8). These systems are not suitable for ammonia oxidation to nitric oxide and they tend to produce nitrogen and nitrous oxide as

predominant products. Work by Delaney and Manogue (9) used 0.5% platinum on alumina support at temperatures up to 350°C. The yield was predominantly nitrous oxide, but catalyst sintering at higher temperatures reduced the nitrous oxide yield to give almost complete conversion to nitrogen. Thus it would seem that supported systems are inadequate to dissipate the heat produced in the exothermic reactions of ammonia and oxygen.

At present therefore, it appears that variations of the Pt/Rh catalyst system still offer the most economical method of producing nitric acid, provided platinum loss can be further reduced.

A novel catalyst system for ammonia oxidation has been developed by Gillespie and Kenson (10). As the ammonia/air mixture passes down through the catalyst screen at 900°C and 100 - 125 p. s. i. g., a rapid reaction results with contact times of 10^{-3} seconds or less. It is therefore essential that the catalyst bed has a low length/diameter ratio, to avoid cracking of nitric oxide to nitrogen which occurs at longer contact times. Thus, in a 300 ton day⁻¹ plant, the catalyst bed is about $\frac{1}{4}$ " x 50" diameter. This very low l/d ratio produces a low pressure drop and difficulties occur with uniform distribution of gases to the catalyst pad, producing areas of catalyst operating at very high temperature, resulting in excessive platinum loss during the reaction. The top layers of the catalyst rearrange to form nodules, whereas layers at the bottom of the pack show very little rearrangement. Clearly, the reaction must be occurring on the top two thirds of the pack, whilst the remaining gauzes are not catalytically active. However, removal of these lower gauzes, results in the formation of ammonium nitrite, indicating that ammonia has passed through the catalyst pad unconverted. Thus, it appears that these lower gauzes do in fact take part in the reaction, though not in the oxidation itself, and may be present to increase pressure drop across the catalyst pad. Gillespie and Kenson (10) have therefore replaced the lower gauzes of the catalyst pad by a 'Random Pack', of 4 mesh $\frac{1}{8}$ " diameter coarse nichrome screen. This avoided the failure occurring with 80 mesh nichrome wire yet produced a randomly

oriented resistance path for gas flow. The use of this 'Random Pack', coupled with the 'Degussa Getter' outlined by Holzmann (11) (12) and reviewed later (section 1.1.f.) has resulted in the reduction of platinum losses by 25 - 30% without any loss of conversion efficiency.

1.1.c. Nitric acid plant and manufacture

The theory and practice involved in the manufacture of nitric acid has been reviewed by Sorgenti and Sachsel (13). Early ammonia oxidation processes, as described by Parsons (1), operated at atmospheric pressure. Since then however, both high pressure and intermediate pressure plants have been commissioned (14)(15).

In the atmospheric pressure process, the catalytic ammonia oxidation reaction and absorption of the nitrous gases are carried out at atmospheric pressure. After evaporation, the ammonia is mixed with air at 9.5 to 11.0 volume per cent, and preheated to between 150° - 200°C, which ensures that temperatures of between 750° and 800°C are maintained in the catalyst. After combustion, the products leave the converter to pass through an air preheater, waste heat boiler and a series of coolers, before entering the absorber system. The resulting acid is further treated in a bleaching tower, from which it emerges as 45 to 52% acid.

These early oxidation plants were replaced in the United States by the DuPont high pressure process (16). This process has been reviewed by Chilton (17) and Miles (18). Basically, the process involves compressing air to 100 p. s. i. g. and preheating it to 250° - 300°C. Anhydrous ammonia is vaporised, super heated and mixed with the air stream. The mixture burns in the converter, using a Pt/10% Rh catalyst gauze at 900°C. The product gases are cooled by passing them through a heat exchanger and a filter to remove traces of platinum catalyst. Following cooling, the gas stream is oxidised in a cascade type cooler, and the uncondensed gases fed to the base of an absorption column. The acid produced is withdrawn from the absorber tower at a strength of 57 - 60%. Bell (19) has

reviewed the operating conditions pertaining to this type of converter.

More recently, European chemical manufacturers have used intermediate pressure systems, operating at approximately 40 p. s. i. , with converter temperatures of approximately 800°C or 70°C cooler than the high pressure system. The main differences between the medium and high pressure processes are in the super heating and a recovery boiler, both of which are contained in the reactor shell. Design details are shown in Miles (18), and plant operation has been reviewed by Sloan and Staats (20).

Further methods to produce 98% nitric acid have been developed by Bamag of Germany using a modification of the Fauser Process. Ammonia is catalytically oxidised to nitric oxide by air at atmospheric pressure. Further oxidation is carried out and two thirds of the water of reaction is removed as a weak acid condensate. The remaining gas is compressed to 8 atmospheres pressure and the nitrogen oxides are removed as liquid nitrogen tetroxide in a condensation tower cooled to -10°C . The resulting nitrogen tetroxide is then autoclaved at 70°C and 50 atmospheres pressure to produce 98% nitric acid.

Clearly, no method has been developed to manufacture nitric acid at any strength. The choice of type of plant is influenced by economic and technical factors outlined by Holmes (21), Roudier (22) and Inskep and Henry (23). Processes utilising pressures greater than atmospheric offer advantages of higher acid strength, smaller plant and hence lower investment cost, as well as higher absorption efficiency. Though catalytic efficiency increases with increasing temperature, the efficiency decreases with increasing pressure. Also, with high pressure plants operating at higher temperatures, catalyst losses are correspondingly greater, and power consumption is increased. It is necessary to increase the amount of catalyst in the converter, thereby increasing the capital cost of the plant. A comprehensive review of production trends and operating costs has been undertaken by Bahari (24), and though this survey has recently been invalidated by the large increases in energy and raw material

prices, catalyst costs contribute between 1 and 7% of total operating costs (25). With manufacturing costs increasing, it has become increasingly important to reduce waste heat losses and catalyst losses to a minimum. The origin of these catalyst losses and their recovery are reviewed in section 1.1.f.

In an attempt to quantify all these effects, Uronen and Kiukanniemi (26) have reviewed the modelling and optimisation of the ammonia oxidation process for nitric acid manufacture. Their model included factors for the inlet gas temperature, mole fraction of ammonia in the feed, the number of gauze screens, the diameter of the catalyst wire, a characteristic factor of the screen representing the wire area/ screen area ratio, the amount of gas per square metre of catalyst per second and the conversion of ammonia. Operational experience showed that the model gave good agreement with data obtained for catalyst loss, variation in contact time, and increasing oxygen/ammonia ratio.

1.1.d. Design of the ammonia burner

In their work on a catalyst system for ammonia oxidation, Gillespie and Kenson (10) developed the 'Random Pack', coupled this with 'getters' and succeeded in reducing platinum loss by between 25 and 30%. However, little work has been done in the modification of burners since the work outlined by Handforth and Tilley (3). Holmes (21) has defined the problems associated with ammonia burners. These are related to temperature rise across a catalyst depending primarily on the ammonia concentration in the gas feed. The optimum conversion temperature is fixed by the catalyst loading and the concentration of ammonia in the gas stream. These two parameters determine the amount of preheating needed for efficient conversion to occur. Thus, in high pressure systems, the ammonia concentration has to be low to avoid the lower explosion limit of 13% NH_3 /air at 5 atmospheres. This in turn necessitates higher preheating temperatures to maintain the high operating

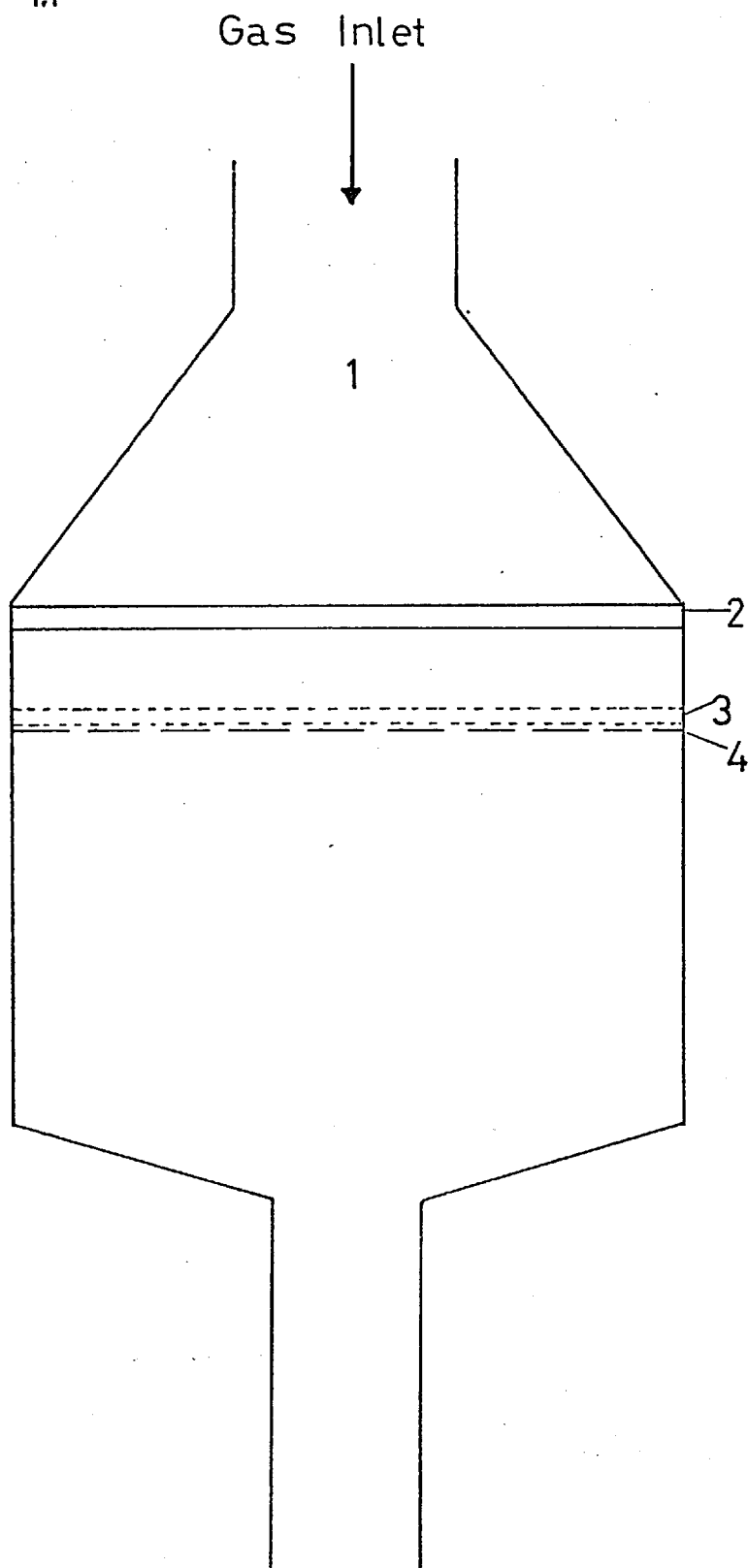
temperatures involved with high pressure work.

A platinum/rhodium gauze catalyst operating at 800° - 900°C has relatively little mechanical strength and must be supported to sustain the pressure difference due to flow of gas through the gauze. Gauze pads are therefore supported against downward flow by grids.

A complete review of the technological aspects of the catalytic combustion of ammonia with platinum gauze elements has been undertaken by Oele (27). A diagram of an ammonia burner is shown in Fig 1.1. As the gas enters the burner, the equalizer ensures that the gas velocity is uniform over the whole width of the tube. This alleviates the problem of local overheating outlined by Gillespie and Kenson (10). The gas then passes down through the catalyst, which is supported by a supporting grid constructed from heat resistant chromium - nickel alloy. Tables 1.1 and 1.2 show the more usual burner constructions and the structural data for commercial gauzes.

Burner design and turbulent gas flow are also important in the prevention of 'flickering' of catalytic gauzes. The phenomenon of temperature fluctuation has been studied by Ervin and Luss (28) and Edwards, Worley and Luss (29). Flickering is most predominant in ammonia oxidation on gauze catalysts and Ervin and Luss have concluded that coupling between chemical reaction and turbulence in the gas stream may cause large oscillations in the surface temperature. These temperature fluctuations are strongly affected by the frequency and intensity of the turbulence, the heat capacity of the wire and the specific chemical reaction. Gillespie and Kenson (10) have also shown that flickering in ammonia oxidation converters can be suppressed by inserting a porous, non-catalytic pad below the platinum gauze. It is clear that this flickering of the gauze catalyst is going to give rise to temperatures substantially greater than the average, with resulting increase in platinum loss. Ervin and Luss (28) postulate that flickering in an ammonia oxidation converter, running between 750° - 950°C , results in large platinum losses above those associated with hydrogen cyanide converters which operate at $1,150^{\circ}\text{C}$, but with very little flickering.

Fig 1.1



- 1 Diffuser
- 2 Equalizer
- 3 Pt/Rh gauzes
- 4 Supporting grid

Table 1. 1.

CATALYTIC ELEMENT	CHARACTERISTIC FORM	OXIDISING MEDIUM	DIRECTION OF FLOW	NAME OF DESIGN
Spirally wound Pt strip	Cup	Air at normal pressure	Upflow or Downflow	Ostwald
Cylindrical Pt gauze	Cylinder	Air at normal pressure		Parsons
3 - 4 flat Pt gauzes	Disk	Air at normal pressure Air at med. pressure Enriched Air/oxygen	Downflow Downflow Upflow	Bamag Montecatini Piesteritz
10 - 20 Pt gauzes	Tube	Air at normal pressure	Upflow	DuPont

Table 1.2.

Diameter of Wire (cm)	Meshes per linear inch	Total wire surface per square metre gauze surface (m^2/m^2)	Wire surface per kg Pt material (m^2/kg)
0.004	152	1.5	4.2
0.006	82	1.2	2.8
0.0046	80	1.5	2.2

1. 1. e. (i) Pt/Rh gauzes

The role of platinum alloy gauzes in the ammonia oxidation process has been reviewed by Connor (30)(31). Both platinum and Pt/10% Rh alloy are malleable and ductile, and thus are easily drawn into fine wires for weaving on modified conventional weaving looms. Platinum catalysts are sensitive to poisons, particularly iron and its oxides, and therefore the gauzes are pickled in concentrated hydrochloric acid to remove this iron before use.

Gauzes are used in many forms. The largest circular gauzes required by industry for atmospheric plants are approximately 12 feet in diameter, and though modern plants require circular gauzes, hexagonal and square catalyst screens are also required.

Catalyst loading is the most important factor in the operation of the ammonia burner. To ascertain the amount of ammonia which can be oxidised, it is essential to know the surface area of the gauze catalyst. Wire diameter and mesh are not therefore the most important factors, but if these are controlled in the production stage, then the weight of the gauze will be proportional to the surface area of the catalyst. This is obviously easier to monitor, and gauzes are preweighed before insertion in the burner. The gauze catalyst must be woven to a specified weight per unit area of 1.72 troy ozs. per square foot. Careful control of the degree of annealing occurring during weaving and tension on the looms produces gauzes which vary by less than 2% from the specified weight per unit area.

1. 1. e. (ii) Activation of Pt/Rh gauze catalysts

The efficiency of Pt/Rh gauze catalysts is seriously effected by surface contamination and dust. Therefore, before insertion into an ammonia burner, the gauzes are first pretreated as outlined in Hamforth and Tilley (3). Pickling in hydrochloric acid, followed by washing in distilled water, and a solvent wash is sufficient to remove any iron oxides, dirt and grease contamination arising from the manufacturing and weaving processes.

The activation of Pt/Rh gauze catalysts is usually carried out in the converter using a hydrogen flame or an electrically heated nickel - chromium wire (30). With the ammonia/air stream passing over the catalyst, ignition occurs and gradually spreads to cover the whole of the gauze (19), after which the igniter is removed. Initially, the conversion efficiency of a new gauze pack is low, of the order of 93 to 94%, but after 2 to 3 days running, 95 to 96% conversion efficiency can be obtained.

Various methods of activation have been used by authors in their work on activating platinum for various catalytic reactions. Eyraud (32) heated platinum ribbons in a mixture of methane/air prior to studying the combustion of methane/air mixture. Work carried out by Nutt and Kapur (33) involved preheating in oxygen at 1,300K for 2 hours, plus running in a mixture of ammonia/oxygen for $\frac{1}{2}$ hour. Pignet, Schmidt and Jarvis (34) have used Auger Electron Spectroscopy to study the effect of oxygen on the removal of carbon and sulphur from the surface of platinum foils. Samples heated in oxygen for more than one hour at temperatures in excess of 300°C produced a lower carbon content. A significant point arising from this work is that at no time was sufficient oxygen detected to allow for the existence of more than monolayer coverage of PtO₂. However, work carried out by Sikora (4) clearly shows that PtO₂ is the catalyst for ammonia oxidation as low as 300°C. The PtO₂ used by him did not require any preactivation, in contrast to the platinum catalyst which required heating to a high temperature in a hydrogen burner or burning ethanol on its surface. It is likely however, that the PtO₂ used by Sikora would probably be powdered and thus have a far greater surface area on which reaction can occur.

1. 1. e. (iii) Deactivation of Pt/Rh gauze catalysts.

In the manufacture of nitric acid, one of the most common causes of low catalyst conversion is that due to deposition of iron oxide on the gauze surface (31). Iron oxide is used as an ammonia

synthesis catalyst, and is therefore equally capable of catalysing the reverse reaction, the decomposition of ammonia to nitrogen and hydrogen. Iron oxide is also formed as a result of the presence of iron in the gauze at concentrations up to 200 p. p. m. and can arise from the use of mild steel components which are prone to rust formation.

Besides iron oxide, Connor (30) identifies lubricating oils, used in compressors for liquefaction, as the major cause of sulphur contamination. Synthetic ammonia is generally very pure, but ammonia produced from non-synthetic sources, such as coke oven liquors, contains high concentrations of sulphur, arsenic and other base metal impurities. These must be removed and levels above 2 p. p. m. total of arsenic and sulphur cannot be used.

Harbord (35) has studied used Pt/Rh gauzes by microscopy and X-ray diffraction. Gauzes possessing low conversion efficiency are usually contaminated, principally by α -Fe₂O₃ in fine particulate form which can be traced to poor air filtration. He also found traces of molybdenum disulphide from lubricating oil, yet this appears to have had little effect on efficiency. This seems to contrast with the results obtained by Arutyunyan et al (36) who studied the effect of oil contaminants in the ammonia/air stream. The use of 0.2 to 10 mg. of oil m⁻³ of gas mixture resulted in a rapid decrease in conversion efficiency which was not restored for up to 5 hours. An alloy composed of 15 - 25% palladium was not so susceptible to oil contamination.

Harbord (35) has used X-ray diffraction to study the excrescence formation occurring on Pt/Rh gauzes. Excrescence formation is accompanied by platinum loss, resulting in slight enrichment of rhodium over the gauze. However, in plants operating at medium pressure (4 atmospheres), the platinum excrescences on the active gauzes were masked by α -Rh₂O₃, leading to depletion from the gauze, and giving rise to compositions as low as 6% rhodium. This contrasts sharply with plants operating at one atmosphere pressure, in which rhodium concentration increases gradually with time. Plants operating at high pressure (8 atmospheres) also show evidence

of a blanket coverage of Rh_2O_3 .

Whilst pickling in concentrated hydrochloric acid is adequate for the removal of iron oxides, it is totally inadequate in dealing with Rh_2O_3 , which has to be reduced back to the metal, either by heating in an hydrogen flame, or by including the gauze in a pad for use in an atmospheric oxidation plant. Either method produces diffusion of rhodium back into the alloy. Harbord suggests that in atmospheric plants, the alloy tends to become rhodium rich by preferential loss of platinum as PtO_2 , which, according to Alcock and Hooper (37), volatilises more rapidly in a flowing gas stream than RhO_2 . In medium and high pressure plants, preferential oxidation occurs to a more stable Rh_2O_3 , giving depletion of rhodium in the alloy of the wire surface.

Philpott (38) has also studied the deactivation of catalyst gauzes occurring in medium pressure plants. He notes that treatment with boiling hydrochloric acid does not improve the efficiency of inactive gauzes, which always gave a chemical composition within the tolerance limits acceptable for gauze production. He quotes Holmes (21) who identified the nodules or 'brussel sprout' growths present on active gauzes. These growths show a clearly developed octagonal crystal structure, which is not present on the inactive gauze. Electron image examination of both active and inactive gauzes showed that the former were homogeneous, whereas the latter showed clearly defined concentrations of material which he suggests is probably rhodium present as Rh_2O_3 , associated with a surface concentration of $\alpha\text{-Fe}_2\text{O}_3$. The removal of $\alpha\text{-Fe}_2\text{O}_3$ by pickling is discussed in the next section.

1.1.e. (iv) Pickling of platinum/rhodium gauze catalysts

Blair and Gibb (39) have developed a method of determining the frequency of pickling using the cumulative sum (cusum) technique. Pickling must be carried out at intervals to prevent excessive build up of iron oxide on the catalyst surface.

The modified cusum technique takes into account the fact that regular acquisition of data may not be possible. Table 1.3 shows the figures produced from a nitric acid plant. Economics have dictated that efficiency must not drop below 93% conversion and so the datum is set at that figure.

The differences between duplicate determinations of conversion efficiencies and the datum line were calculated and their arithmetic mean \bar{x} evaluated. As daily determinations of efficiency were not available, the arithmetic mean of successive values of \bar{x} was calculated, and multiplied by the time interval between these successive determinations. The results were then added to each other to give a corrected cusum chart. Thus after 5 days, the mean for \bar{x} is 4.5. Averaging this figure with the previous \bar{x} value of 3.5 gives 4, which when multiplied by the time interval, 5 days, gives 20, addition of 3.5 to which gives a corrected cusum of 23.5. The results are then plotted in graph 1.1.

From the graph, between 0 and 20 days, the plant is running at an efficiency greater than 93%, and between 18 and 26 days, at an efficiency below 93%. To maintain an average efficiency of 93%, pickling must be carried out after approximately 28 days.

Alternatively, if pickling were carried out after 20 days, then efficiency could be maintained at a figure substantially above that of 93%.

1.1.f. Platinum loss and recovery

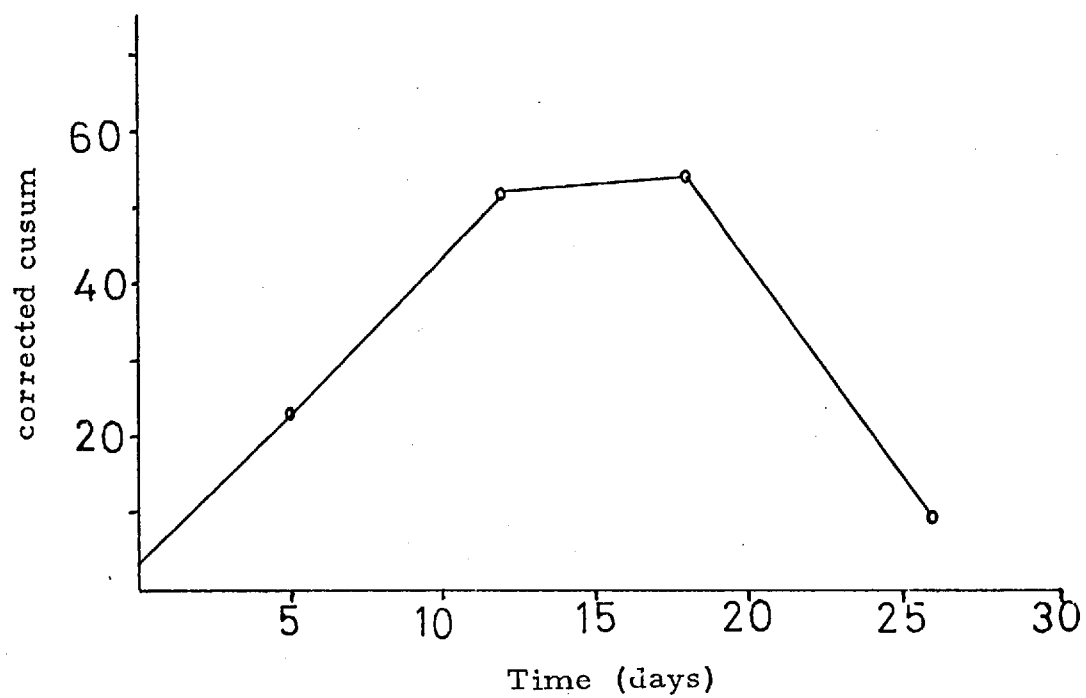
Platinum losses in catalytic ammonia oxidation are an important factor in considering the economics of operation (25), particularly following the development of high pressure plants which require higher inlet gas temperatures giving rise to greater platinum loss.

The exact nature of the mechanism of this platinum loss is still speculative. Miles (18) and Sikora (40) consider that mechanical loss of the oxide is the main cause of platinum loss, because the

Table 1.3.

day	conversion efficiency %		difference from datum		mean \bar{c}	corrected cusum
			\bar{c}			
0	97	97	4	3	3.5	3.5
5	97	98	4	5	4.5	23.5
12	96	97	3	4	3.5	51.5
18	90	91	-3	-2	-2.5	54.0
26	90	90	-3	-3	-3.0	10.0

Graph 1.1.



volatility of the metal at the temperatures reached in the catalytic oxidation process is too low, and the particles collected by the filters are too large. Sedasheva et al. (41) conclude that the loss of platinum in ammonia oxidation is dependent on the degree of exhaustion of the catalyst networks, because as the gauzes age, more platinum metal is lost by mechanical removal caused by the vibration occurring in plant operation. Ervin and Luss (28) deduce that flickering of the catalyst causes large temperature fluctuations, giving rise to excessive platinum loss, and Brack and Guenzel (42) ascribe platinum losses to the alternating expansion and contraction of the gauze wires produced by variations in temperature. They prevented these temperature variations by inserting a gas-permeable ceramic layer between adjoining gauzes.

More recently however, Connor (30) has reached the conclusion that whilst particle loss may be partially responsible for metal loss, particularly when surface growths are exposed to a high velocity gas stream at high temperature, this argument is insufficient to explain all the metal lost. Extensive work carried out by Handforth and Tilley (3) showed that Pt/10%Rh alloys gave low metal loss, whilst Connor (30) quotes Raub who showed that these alloys preferentially lose platinum. It is likely therefore that the transient formation of volatile oxides of platinum and rhodium play a role in metal loss under operating conditions.

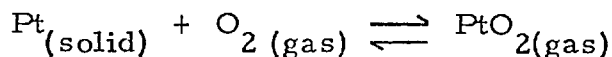
Extensive work has been carried out by many authors on the oxidation of platinum. Recently, Nowak (43)(44) has developed a formula put forward by Bartlett (45) to predict platinum losses arising from the ammonia oxidation reaction. The errors arising from Nowak's work, and their correction are discussed later (Chapter 4).

Studies of the high temperature oxidation of platinum and the platinum group alloys have been carried out by Raub (46), Lacroix (47) Krier and Jaffe (48), Alcock and Hooper (37) and Betteridge and Rhys (49). Basically, the high temperature oxidation of platinum metals is of two types, one involving the formation of a solid oxide on the metal

surface, whilst the other involves formation of a volatile oxide. Formation of solid oxide is favoured at temperatures below $1,000^{\circ}\text{C}$, whilst above this temperature the gaseous oxide reaction becomes important. A study of the enhanced oxidation of platinum in activated oxygen has been carried out by Fryburg (50)(51). This led to the conclusion that the oxide formed is PtO_2 , which may partly decompose to give the impression that PtO has been formed.

Platinum metal does not readily absorb appreciable quantities of oxygen, though at room temperature the solid metal forms a very thin strongly adherent layer of oxide, and at high temperatures this oxide appears to be resistant to further diffusion of oxygen into the platinum or of platinum away from the bulk metal.

At higher temperatures, the platinum-oxygen equilibrium involves the formation of a gaseous oxide which has been investigated by Alcock and Hooper (37)(52) and Schafer and Tebben (53). From their results Alcock and Hooper conclude that the equilibrium involved is,



The presence of platinum dioxide has been proved by Norman (54) using mass spectrometry. The vapour pressure of the gaseous oxide is given by

$$\log_{10} P = \frac{-8,585 \pm 74}{T} + (0.204 \pm 0.047)$$

for the temperature range $1,100^{\circ}\text{C}$ - $1,550^{\circ}\text{C}$. Alcock and Hooper also estimate that the rate of platinum volatilisation is 10^4 times greater in oxygen at $1,500^{\circ}\text{C}$ than in an inert gas at the same temperature.

Many factors are involved in platinum loss during its heating in oxygen. The actual weight loss occurring will depend on factors such as the rate of gas flow, degree of saturation of the atmosphere with volatile oxide and the thermal geometry of the system.

Phillips (55) has studied the oxidation of platinum metals in air and found that the oxidation rates of the metals in air between

800 - 1,400°C were in accordance with a linear weight law, and activation energies for the oxidation of platinum and rhodium were 15.4 and 29.6 k cal. mole⁻¹ respectively.

Chaston (56)(57)(58)(59)(60) has reviewed the work carried out on the reaction of oxygen with the platinum metals. He quotes Brewer that PtO₂ is a solid, having a heat of formation at 298K of -32 k cal. mole⁻¹. In air, a strongly adhered thin layer of oxide is formed on a bright platinum surface which is difficult to remove. After a small amount of oxide forms, equilibrium is reached and further reaction ceases. Raising the temperature at first causes the oxide skin to thicken. On further heating a temperature is reached at which PtO₂ cannot normally continue as a solid. This temperature, at which the dissociation pressure of PtO₂ becomes equal to one atmosphere, has not yet been accurately determined, though it is thought to lie between 280° and 450°C. Thus, between these temperatures, solid PtO₂ decomposes to platinum and oxygen. Below the dissociation temperature, the vapour pressure of platinum metal is higher than that of PtO₂, but above this dissociation temperature PtO₂ has the higher vapour pressure. Above the dissociation temperature, evaporation of PtO₂ will become more rapid owing to the increase in vapour pressure of PtO₂, and the thin oxide film is probably removed giving a clean platinum surface.

Fryburg and Petrus (61)(62) have developed a boundary layer diffusion mechanism to explain the loss of platinum oxide from heated platinum. Their mechanism depends on the fact that when platinum is heated in air or oxygen at 800°C or above, the volatile oxide PtO₂ forms which must be removed from the surface of the platinum. Thus the rate of oxidation depends on the ease with which the PtO₂ molecules may escape from the surface. Whilst the partial vapour pressure of PtO₂ is low, even at 1,250°C, 0.03 mg. of platinum will saturate a litre of oxygen. In the ammonia oxidation process where large volumes of hot moving air are involved, this low partial vapour pressure could still lead to significant catalyst losses.

The fact that this partial vapour pressure is low led Fryburg and Petrus (61) to study the reactions taking place on the surface of thin platinum ribbons heated by an electric current and surrounded by a low pressure oxygen atmosphere. It is significant that at a pressure of approximately 0.25 Torr, a direct proportionality is found between the oxygen pressure and the rate of oxide formation. In this low pressure region, the only factor controlling the loss of platinum is the rate of collision of the oxygen molecules with the platinum surface, and under these conditions, the molecules of PtO_2 can readily move away as they are formed. As the oxygen pressure is increased, the rate of oxidation falls below the proportional relationship, so that the rate at 1,000 Torr is only six times that at 1 Torr. It therefore appears that as the pressure is increased and more oxygen molecules collide with the surface, it becomes more difficult for the PtO_2 molecules formed to escape, and so they are back-reflected onto the foil, where they decompose to form platinum and oxygen. Thus Fryburg concludes that at low pressures, the mean free path of the volatilising oxide molecules in the surrounding gas is large compared with the width of the ribbon, and so the PtO_2 molecules escape. As the pressure increases, the mean free path decreases, and the oxide molecules undergo collision at distances closer to the ribbon. Thus, the chance of back-reflection, and hence apparent lowering of oxide vapour pressure is increased, giving platinum redeposited on the ribbon surface.

Heywood (63) has collected data from various types of ammonia oxidation plant and concludes that typical platinum loss rates vary between 0.05 to 0.11 g ton⁻¹ nitric acid produced for atmospheric plants, to 0.20 to 0.45 g ton⁻¹ nitric acid produced for high pressure plants. Clearly, this rate of loss not only contributes significantly to the production costs of nitric acid, but also provides a financial inducement to recover the lost platinum metal.

It is possible to trap any platinum volatilised in the reaction by passing the product gases through filters. Akerman et al. (64)(65) have used a platinum net containing 2% iridium, which had been

bombarded with neutrons to give ^{194}Ir . This platinum gauze was then inserted in the reactor, in a catalyst pad. After reaction, the radioactive iridium was found after the dry platinum filter, immediately following the high temperature reactor. Thus Akerman concludes that wet filters are essential before the gas is absorbed in water to give nitric acid.

Whilst doubt still exists about the actual mechanism of platinum loss, it is difficult to decide on the best means for its recovery. Several methods of lowering platinum loss and at the same time increasing the recovery of platinum have recently been devised. Acres et al. (66) have used gauze stacks of Immaculate 5(Ni21%, Cr 23%, Fe > 56% + traces Ag) Pt - Ni alloy with ruthenium to achieve this.

The most preferred methods however involve some form of catchment gauze. Holmes (21) outlines this process in which the hot gases pass through a bed of gold-plated ceramic rings, and the heat of the reaction alloys the platinum with the gold. The coating is then stripped, and refined to recover the platinum and gold for further use. The development of these Au-Pd catchment gauzes has been carried out by Holzmann (11)(67). Using the fact that platinum is lost in the vapour form, these catchment gauzes are particularly useful in medium and high pressure plants where filtration methods are insufficient to prevent platinum loss. The platinum lost is recovered by a getter grid consisting of 80:20 Pd-Au and a glass wool filter. Initial experiments showed that with six recovery grids and a glass wool filter, 99% of the lost platinum was recovered in the proportions 74% : 25% (7 atmosphere plant). Heywood (63) has studied the performance of these getters after several years running experience and concludes that over 60% of the gross platinum losses have been recovered. Variations on this method have also been developed, including one by Sikora et al (68), in which three gold plated Cr/Ni wire screens were inserted below the Pt/Rh gauzes. This method recovered approximately 80% of the dislodged platinum particles.

A further method for cutting catalyst losses and improving catalyst efficiency has been devised by Gillespie and Kenson (10). Using their Random Pack gas distributor outlined earlier, platinum loss by volatilisation has been reduced by approximately 30%.

Zasorin et al. (69) has used glass wool filters to recover 30% of the platinum loss. Further however, he has used four layers of 5-8mm. diameter tablets of zirconia, alumina and silica gel. These tablets can recover further amounts of platinum which can be recovered by dissolving the oxides in 50% sodium hydroxide at 16 atmospheres pressure and 250°C.

Further methods of capturing platinum lost in the catalytic reaction have been used by Atroschenko et al (70), Sikora (71)(72) and Zasorin et al (73). These workers have studied the effect of granular porous calcium oxide on the recovery of platinum. Recoveries range from 50% (71) to 80% (70). A study of these calcium oxide granules has also been carried out by Blasiak et al (74), Sikora (40) (71), Janiczek et al (75)(76) and Zasorin (73).

The work by Sikora compared the platinum containing deposits of CaO with those in which platinum dust / CaO mixtures and PtO_2 / CaO mixtures had been heated to 1,100°C. A new compound $\text{CaO} \cdot \text{PtO}_2$ was found, and from this he concludes that loss from gauzes during reaction is probably due to mechanical failure causing shedding of small particles of PtO_2 and not due to the evaporation of platinum metal from the gauze.

Janiczek et al (76) used X-ray and chemical methods of analysis. They compared samples of trapped platinum with prepared Pt/CaO compounds. Both were soluble in hydrochloric acid and precipitated with KCl to form K_2PtCl_6 . From this work they conclude that platinum losses are due to erosion of metallic platinum caused by disintegration of platinum wire and also due to volatilisation of platinum, possibly as PtO_2 .

Blasiak et al (74) used physical and chemical methods to identify a compound with an X-ray diffraction pattern identical to Ca_4PtO_6 . This, they conclude, is a new compound, $\text{PtO}_2 \cdot 4\text{CaO}$, formed by the reaction between calcium oxide and gaseous platinum dioxide.

1.2. Heterogeneous Catalysis : Introduction

Heterogeneous catalysis - used mainly in the sense of the conversion of gas to gas over solids is of enormous potential. Fully 95% of all industrial chemicals for example, involve a catalytic process at some stage in their manufacture. Of these, one of the oldest processes is the catalytic oxidation of ammonia over platinum. Many reviews have been written on all aspects of heterogeneous catalysis, for example by Thomas and Thomas (107) and Bond (108)(109).

A catalytic reaction can be divided into five basic stages. These include diffusion to the catalyst, adsorption at a catalyst site followed by reaction with another adsorbed molecule or a reaction with the gas phase. The product molecule must then desorb from the catalyst and finally diffuse away from the catalyst. It is on these initial and final stages of the catalytic reaction which involve diffusion that attention will now be focused.

1.2.a Mass transfer in heterogeneous catalysis

Besides involving chemical reaction, catalytic processes also involve diffusion of reactants to and from the catalyst surface. In a reaction as rapid as ammonia oxidation, and involving abnormally high flow rates, it is obvious that mass transfer effects will be involved in the overall catalytic process.

The five basic stages in a catalytic reaction have been outlined above. The first and last of these processes, diffusion to and away from the catalyst will involve mass transfer processes.

In the first process, reactants must pass through the gaseous phase surrounding the catalyst, to be adsorbed on the active sites. Similarly, products must also diffuse away through this gaseous layer, to the bulk mixture. This diffusion process is obviously important, because if it is rate controlling, then the catalyst may not be used at its maximum possible efficiency. Thus, it is important to recognise when mass transfer limitations are operating in a catalytic process. These conditions can easily be recognised by studying the following effects.

If the rate is increased by agitating the gas or liquid with respect to the catalyst, then mass transfer limitations are operative. Also, if the rate is not directly proportional to the weight of catalyst to the power of unity, but to a power less than unity, then mass transfer effects are also preventing complete reaction. Finally, gaseous diffusion processes do not obey the Arrhenius equation, their rates being proportional to $T^{\frac{1}{2}}$ (109).

Reviews by Dixon and Longfield (110) and Nowak (43) show that in the ammonia oxidation reaction, short contact times are involved, of the order of 10^{-3} sec or less and that this time requires very rapid mass transport to the catalyst for the reaction to be completely heterogeneous. If the mass transport rate is insufficient, then a heterogeneous initiation of a homogeneous chain reaction is possible.

Shah and Roberts (111), Satterfield and Cortez (112) and Gay and Maughan (113) have studied the mass transfer characteristics of woven-wire screen catalysts. Satterfield and Cortez conclude that the transport characteristics of screen catalysts were shown to be similar to those of infinite cylinders whilst Shah and Roberts concluded that wire diameter and opening or porosity of a typical screen were the most significant properties affecting mass transfer.

Finally Roberts and Gillespie (114) and Oele(27) have studied the technological aspects of catalytic ammonia oxidation. Roberts and Gillespie (114) conclude that operation at a higher mass velocity or with closer mesh screens would effectively reduce catalyst requirement, though the consequence of this would be lower catalyst strength and poor ageing qualities. Oele (27) has assumed that in excess oxygen, the transport of ammonia molecules to the platinum surface is the rate-determining step during the reaction. Using the approximation that ammonia transport may be described as a stationary diffusion process in a laminar flow, Oele has calculated mass transfer coefficients in the range 3.6×10^{-2} k mol. m^{-2} sec^{-1} atm^{-1} NH_3 and 2.3×10^{-2} k mol. m^{-2} sec^{-1} atm^{-1} NH_3 .

1. 2. b Heat transfer in heterogeneous catalysis

The oxidation of ammonia to nitric oxide is a highly exothermic reaction. The heat evolved must be removed if overall efficiency of the catalyst is to be maintained and damage to the catalyst averted. Whilst gas velocities are high, the heat evolved can rapidly transfer from the gauze to the ambient gas stream. An understanding of the nature of this transfer process is an essential factor in catalyst design, efficient plant economics and reclamation of the heat evolved.

Transfer of heat occurs from hot to cold surfaces. Whilst individual processes are basically very simple, their application to actual systems is somewhat complicated. The application of heat transfer theory to these systems has been covered by Ede (115) and McAdams (116).

Basic heat transfer can occur by three processes. The first of these, radiation, is caused by the thermal motion of elementary particles. This causes them to emit energy in the form of electromagnetic radiation. Higher temperatures produce more vigorous motion and hence a more intense radiation, which is analogous to that in radio waves, light waves etc. To compare this process with other modes of heat transfer, it is essential to study how the energy is lost by the emitting material and gained by the receiving object. Molecules lying on the surface of an emitting body must be in contact with a medium which is transparent to radiation. These molecules radiate energy in all directions, some of which will leave the emitting body, and travel until it encounters an absorbing material, to which will be transferred the energy of the emitted radiation.

Conduction however, involves a temperature gradient in which heat can be transferred from a hotter to a colder part of the same system, by the following mechanisms. The surface molecules of a radiating body may also transfer heat into the body by absorption of energy. Thus in the case of a molecule within a heated body, this process is the means by which it transfers its energy. It is continuously losing and gaining energy, and in a temperature equilibrium, these

two effects counterbalance each other, giving no temperature rise. In the presence of a temperature gradient however, a net transfer of heat will occur. Secondly, the molecules in a body interact with each other by means of intermolecular forces. Thus the thermal motion of one molecule is transmitted to its neighbours, and if one group of molecules is hotter than another, then a net transfer of heat will occur. Thus the basic difference between conduction and radiation is that conduction can only take place in the presence of matter.

The final process, convection, arises from the possibility that portions of a fluid may pass from one position to another. If a temperature difference exists between two regions in a fluid then heat transfer can occur by conduction. If however the fluid is stirred, some of the hotter fluid will be transferred to a position where the temperature is lower, giving rise to a net heat transfer.

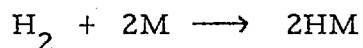
Once again, as in mass transfer, the application of these three processes to industrial and experimental systems gives rise to many complicated formulae and equations. However London, Mitchell and Sutherland (117) have studied the heat transfer and flow friction characteristics of crossed-rod matrices, whilst Oele (27) has covered the technological aspects of heat exchange at the gauze surface.

1. 2. c Adsorption in heterogeneous catalysis

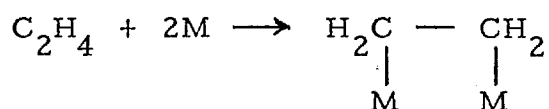
The adsorption, or interaction of molecules with surfaces is of vital importance in heterogeneous catalysis. The phenomenon of adsorption can be divided into two classes. The first, chemical adsorption, or chemisorption is a process which involves chemical bond formation at the surface. As an example, a fracture or defect in a solid will produce surface atoms with spare bonds available for chemical reaction (i. e. the coordination number of an atom at a defect will be lower than that in the bulk matrix).

Chemisorption may be either associative in which bonds linking the atoms in the adsorbing molecule remain intact, or dissociative, in which the adsorbing molecule breaks down into fragments.

The reaction of hydrogen with metals leads to dissociative chemisorption



However, molecules possessing π or lone pair electrons can undergo associative chemisorption, an example of which is provided by mono-olefin reactions with metals. This reaction is thought to proceed by chemisorption through rehybridisation of the carbon sp^2 bonds to sp^3 bonds leaving two free valencies for reaction with the metal (M)



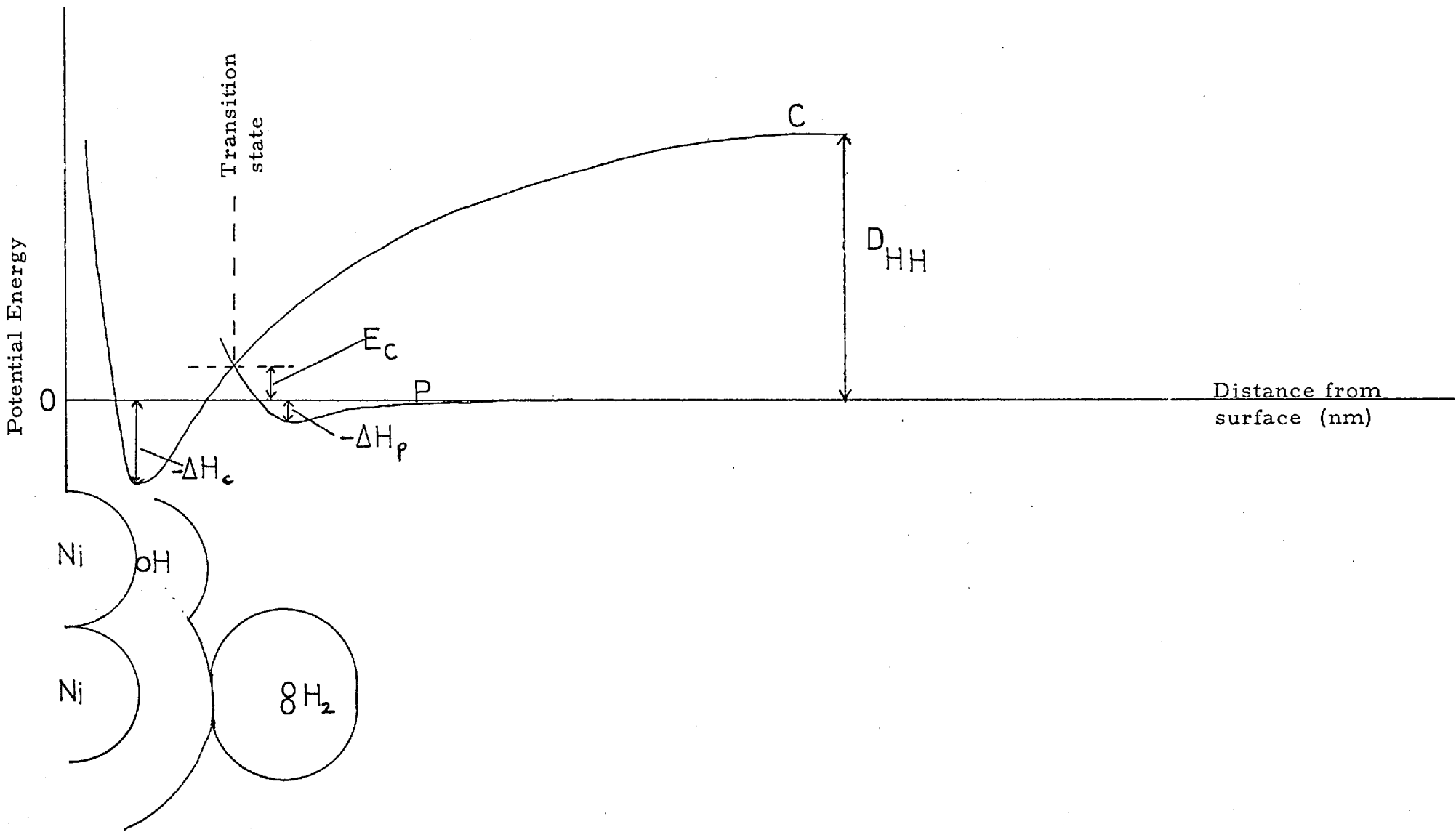
Chemisorption reactions generally give rise to heats of adsorption of between 40 and 800 kJ mol^{-1} , and give rise to monolayer formation only.

This contrasts with the second type of adsorption, physical or Van der Waal's adsorption, in which multilayer formation is possible and heats of reaction are much lower, usually between 8 - 20 kJ mol^{-1} . Physical adsorption arises through electrostatic attraction between the reactant molecules with permanent dipole moments and the surface of the catalyst, or dipoles induced in polarizable molecules. This method of adsorption involves no chemical bond formation but can be related to the physical properties of the adsorbing species, e. g. nitrogen adsorption will be weak at room temperature, but will become detectable as the temperature is lowered.

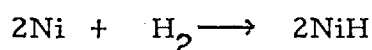
Adsorption, being a spontaneous process is usually exothermic. With spontaneous processes, ΔG is negative, and hence overall ($\Delta H - T\Delta S$) must also be negative. However, in an adsorption process, ΔS is negative, because the system is becoming more ordered. Therefore, for $T\Delta S$ to be greater than ΔH , ΔH must be negative.

Chemisorption requires energy before it can occur and how this activation energy arises is shown in figure 1.2. This represents the chemisorption of hydrogen on nickel. The diagram represents the variation in potential energy of a hydrogen molecule with its distance from the solid catalyst surface. A molecule at infinity has zero potential energy represented by the horizontal line. Physical adsorption, represented by curve P is shown to have a small heat of adsorption

Fig 1.2



$-\Delta H_p$, and no activation energy is necessary (i. e. the curve did not pass above the potential energy zero before physical adsorption occurred). The chemisorption process, represented by curve C must involve a dissociative energy D_{HH}



(434 kJ) the energy necessary to break a hydrogen bond. As the atoms approach the surface, chemisorption results in a large fall in potential energy $-\Delta H_c$.

However, the point where the two curves cross, above the zero P.E. line, represents the activation energy E_c for this reaction to occur. This is much less than the dissociation energy D_{HH} and thus it is here that the advantage of physical adsorption as a preliminary to chemisorption can be seen. Physical adsorption enables the hydrogen molecule to get within close proximity of the catalyst surface without any input of energy being necessary. Thus at the transition state, shown in figure 1.3, the nature of the adsorption changes from physical to chemisorption, without the dissociation energy D_{HH} being applied.

This potential energy method gives no idea of the quantitative aspects of catalysis which would enable the best catalyst from a series to be chosen.

Obviously, catalytic activity is going to be related to strength of chemisorption of the reactants. However if chemisorption is too strong for desorption to occur after reaction, then the surface molecule will behave as a catalyst poison, blocking further reaction at that site

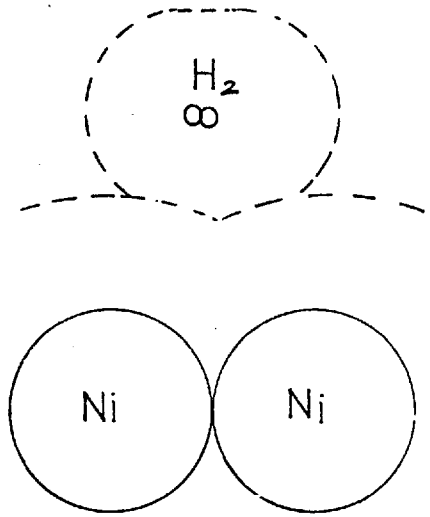
1.2.d Kinetics of heterogeneous catalytic reactions

Generally, the rate of a chemical reaction involving two reactants occurring at a catalyst surface can be expressed by

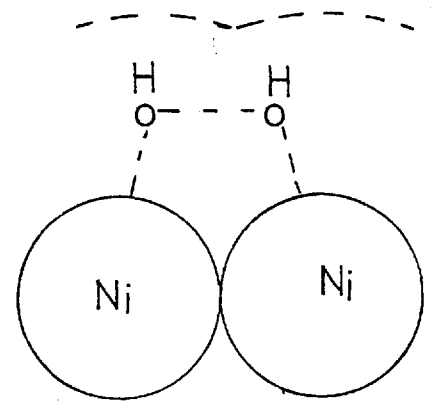
$$r = k\theta_A\theta_B$$

where θ_A represents the coverage of the surface of reactant A and θ_B the coverage of reactant B. The rate coefficient k will take into account the strengths of adsorption of both reactants, since these

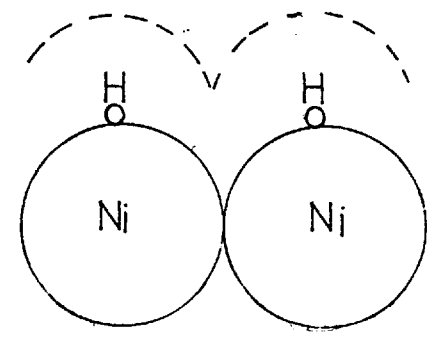
Fig 1.3



Hydrogen molecule
Physically adsorbed



Transition
state



Hydrogen atoms
chemisorbed

affect the energy of the transition state.

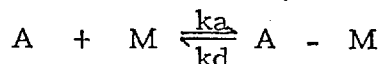
Having thus related reaction rate to coverage of the surface, it is now necessary to quantify the relationship between gas phase pressure and surface coverage.

When a catalyst surface is first outgassed, and then a reactant gas admitted, a proportion of the gas is adsorbed on the surface. The amount of gas adsorbed will vary with the pressure, if the temperature remains constant. This relationship gives rise to an adsorption isotherm, an example of which is shown in figure 1.4. If x is the amount adsorbed at a given pressure and x_m is the maximum amount the surface can adsorb then,

$$\frac{x}{x_m} = \theta$$

where θ is the fractional surface coverage.

A relationship between θ and the pressure P has been developed by Langmuir, who assumed that a given area of surface will consist of n sites, each of which can adsorb one molecule of the gas, and that all adsorption sites are of equivalent energy. The equilibrium reaction occurring can be represented by



where A is an adsorbing molecule and M is a single surface site. The complex formed is represented by $A - M$. Therefore,

$$\begin{aligned} \text{rate of adsorption} &= k_a [A] [M] \\ \text{and rate of desorption} &= k_d [A - M] \end{aligned}$$

$[A]$ can be replaced by P , the gas pressure, and $[M]$ the number of vacant sites by $n(1-\theta)$. Also $[A - M]$ can be given by $n\theta$. At equilibrium, the rate of adsorption will equal the rate of desorption, giving

$$k_a P n (1 - \theta) = k_d n \theta,$$

which rearranges to give

$$\theta = \frac{k_a P}{k_d + k_a P} = \frac{bP}{1 + bP}$$

where $b = k_a / k_d$ the adsorption coefficient or the equilibrium constant

Fig 1.4

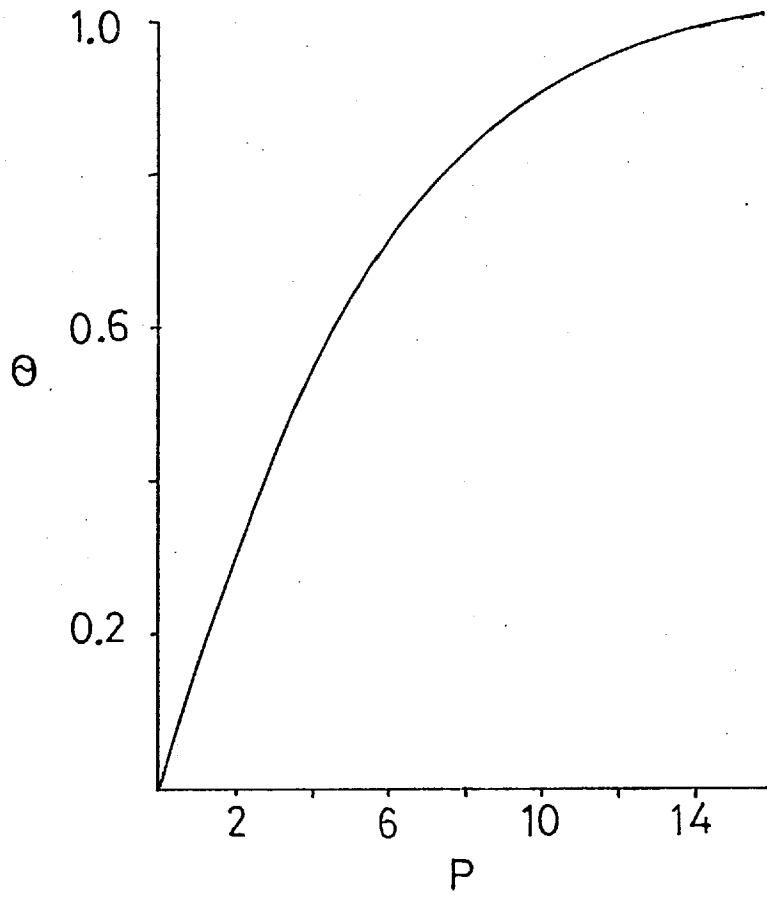
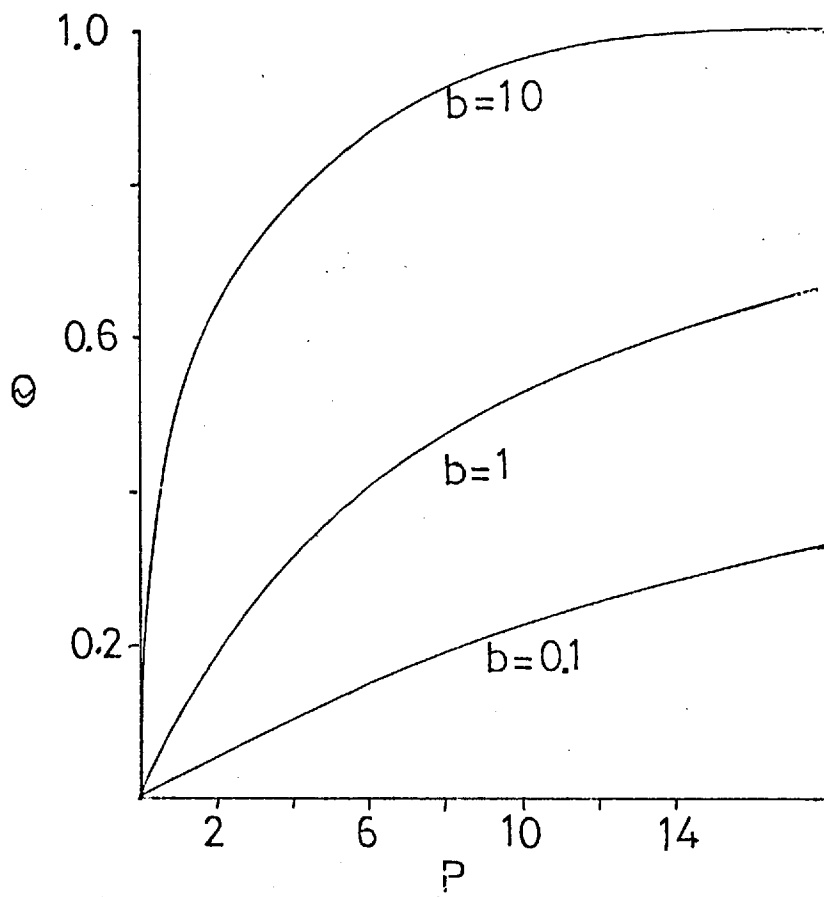


Fig 1.5



for the reaction process. Thus, with high values of b adsorption of A will be strong and this will be reflected in the shape of the isotherm, examples of which are shown in figure 1.5.

When two gases A and B are involved in a reaction then they will compete for surface sites on the catalyst. The total fraction of surface covered will become $1 - \Theta_A - \Theta_B$

$$\text{and } \Theta_A = \frac{b_A P_A}{1 + b_A P_A + b_B P_B}$$

$$\Theta_B = \frac{b_B P_B}{1 + b_A P_A + b_B P_B}$$

Isotherms have an important role to play in the determination of catalyst surface area. The activity of a catalyst is usually expressed as the rate per unit surface area (m^2) and provided no mass-transfer limitation processes are involved, then the rate will be directly proportional to the surface area of the catalyst.

Determinations of surface area are best carried out using the Brunauer, Emmett and Teller (B. E. T.) equation, at temperatures above the boiling point of the adsorbing gas

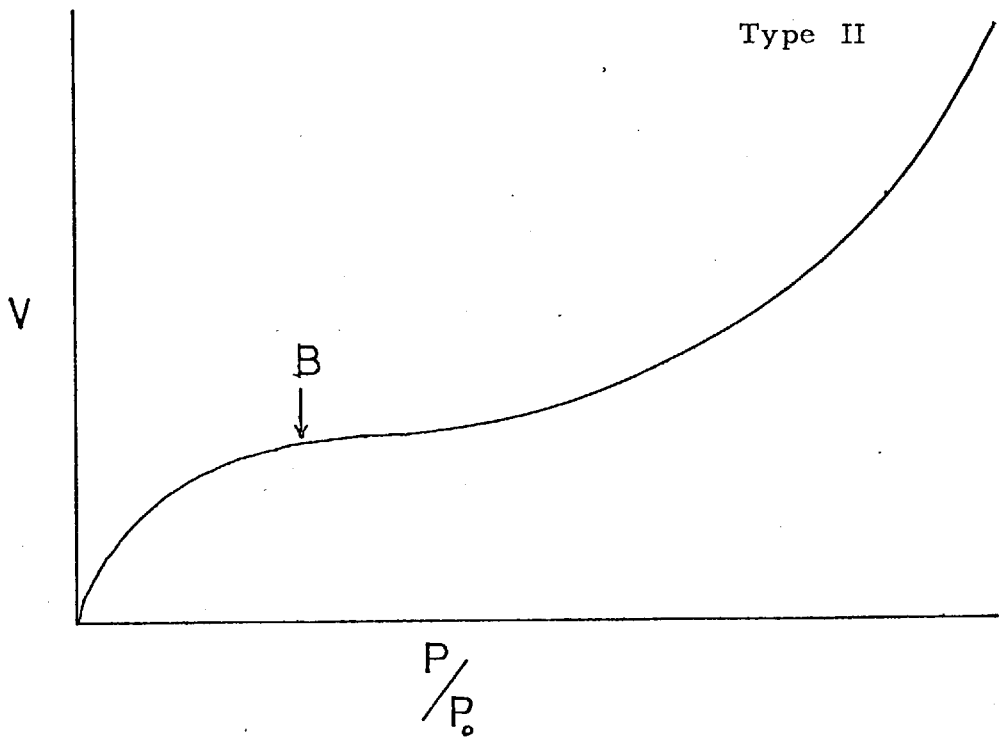
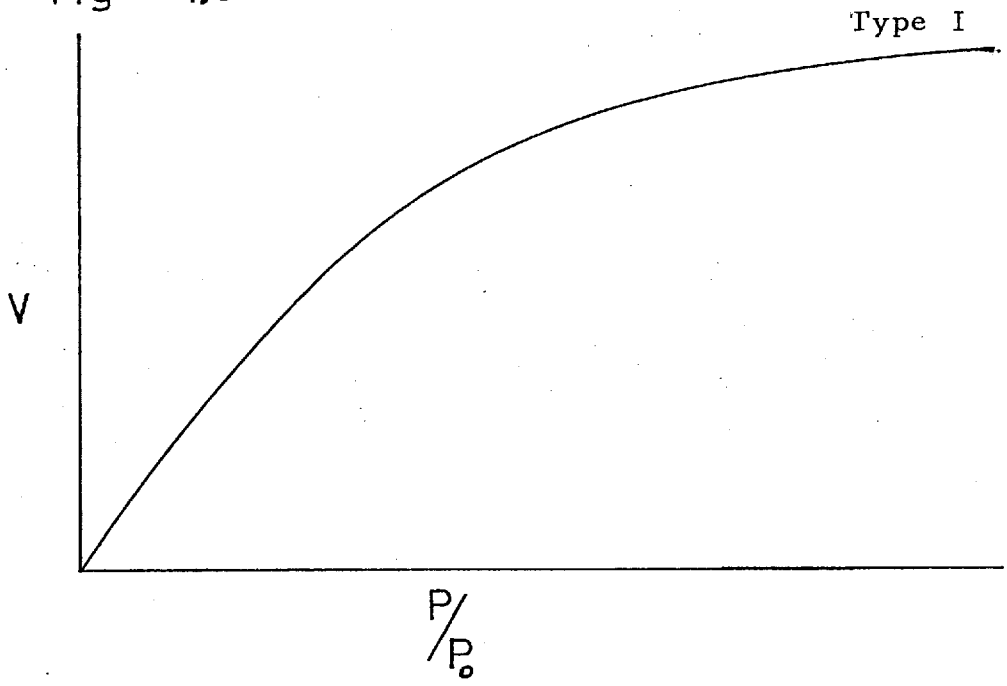
$$\frac{P}{\infty(P_0 - P)} = \frac{1}{\infty_m C} + \frac{C - 1}{\infty_m C} \frac{P}{P_0}$$

where, ∞_m is the monolayer capacity, P_0 is the saturation vapour pressure of the adsorbed gas at the temperature used and C can be represented by

$$C = \exp \left[\frac{(H_a - H_b)}{RT} \right]$$

where H_a is the heat of adsorption of the first layer and H_b is the heat of formation of remaining layers. Thus a plot of volume adsorbed against the ratio of pressure to saturation vapour pressure at a given temperature, gives rise to five types of isotherm, two of which are shown in figure 1.6. Type I is the Langmuir adsorption isotherm mentioned earlier, but Type II permits the monolayer capacity ∞_m

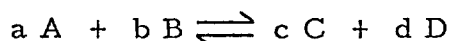
Fig 1.6



to be derived from 'point B' on the isotherm. Thus, with the monolayer capacity corresponding to $\Theta = 1$ established, a knowledge of the area of the surface occupied by each molecule gives

$$\text{total surface area} = \frac{\text{number of molecules}}{\text{area per molecule}} \times \text{collision diameter}^2$$

Besides surface coverage, another important factor in heterogeneous catalysis is the rate at which the reaction proceeds. This is decided by the height of an energy barrier the reactants must surmount before products can be formed. In the reaction



the reaction rate can be expressed as

$$r = k P_A^m P_B^n$$

where m and n are the orders of reaction with respect to A and B respectively and k is the rate coefficient.

The rate coefficient varies with absolute temperature according to the Arrhenius equation

$$k = A \exp. \left(\frac{-E}{RT} \right)$$

where A is the pre-exponential factor, E the activation energy and R the gas constant. The size of this activation energy represents the amount of energy the reacting molecules must have before reaction will occur.

This equation is similar to that obtained for a simple gas-phase reaction in which the exponential term is related to the Boltzmann distribution of kinetic energy, specifying the fraction of molecules with kinetic energy greater than E . Thus, the collision theory gives

$$k = Z_{AB} \exp. \left(\frac{-E}{RT} \right)$$

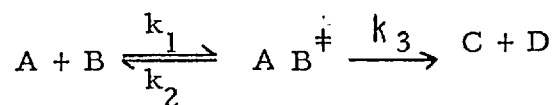
where Z_{AB} is the collision number for unlike molecules. Bimolecular reaction rates determined experimentally show that this formula does not give good agreement with experimental data and so an empirical steric factor P has been introduced.

$$k = P Z_{AB} \exp. \left(\frac{-E}{RT} \right)$$

Neither of these two approaches has been adequate to predict the rate of reaction of molecules adsorbed on surfaces. However, the 'transition state theory' or 'theory of absolute reaction rates' studies

the state of reactants at the top of an energy barrier. The activated complex is considered to be in equilibrium with the reactants and so chemical thermodynamics can be applied.

In the bimolecular reaction,



AB^\ddagger represents the transition state, which decomposes to products slowly, so that the equilibrium with reactants is not disturbed.

Therefore,

$$\frac{k_1}{k_2} = K_p^\ddagger = \frac{P_{AB^\ddagger}}{P_A P_B}$$

$$\text{or } P_{AB^\ddagger} = K_p^\ddagger P_A P_B$$

The rate of the forward reaction r_f is given by

$$r_f = k_3 P_{AB^\ddagger}$$

When the complex disintegrates, bond breakage occurs and a vibrational mode becomes two translational modes. Thus,

$$E_{\text{vib}} = h\gamma$$

$$E_{\text{trans}} = \frac{1}{2} kT + \frac{1}{2} kT = k_B T$$

where k_B is the Boltzmann constant.

$$\therefore h\gamma = k_B T$$

$$\gamma = \frac{k_B T}{h}$$

Hence,

$$\begin{aligned} r_f &= k P_A P_B \\ &= K_p^\ddagger \frac{k_B T}{h} P_A P_B \end{aligned}$$

$$\therefore k = K_p^\ddagger \frac{k_B T}{h} \left(\frac{k_B T}{h} = 6 \times 10^{12} \text{ s}^{-1} @ 300\text{K} \right)$$

Thermodynamic relationships can now be applied to the

equilibrium constant K_p^\ddagger . Hence, the free energy of activation is given by

$$-\Delta G^\ddagger = RT \ln K_p^\ddagger$$

$$\text{and } \Delta G^\ddagger = \Delta H^\ddagger - T\Delta S^\ddagger$$

in which ΔH^\ddagger and ΔS^\ddagger are the standard free enthalpy and standard entropy of activation respectively.

$$\therefore K_p^\ddagger = \exp(-\Delta G^\ddagger / RT)$$

$$\therefore K_p^\ddagger = \exp(-\Delta H^\ddagger / RT) \exp(\Delta S^\ddagger / R)$$

$$\text{but, } k = A e^{-\frac{E}{RT}}$$

$$= \frac{k_B T}{h} \exp(-\Delta H^\ddagger / RT) \exp(\Delta S^\ddagger / R)$$

$$\therefore E \approx \Delta H^\ddagger$$

$$\text{and } A = \frac{k_B T}{h} \exp(\Delta S^\ddagger / R)$$

Thus, in terms of the transition state theory,

$$K_p^\ddagger = \exp(-\Delta G^\ddagger / RT)$$

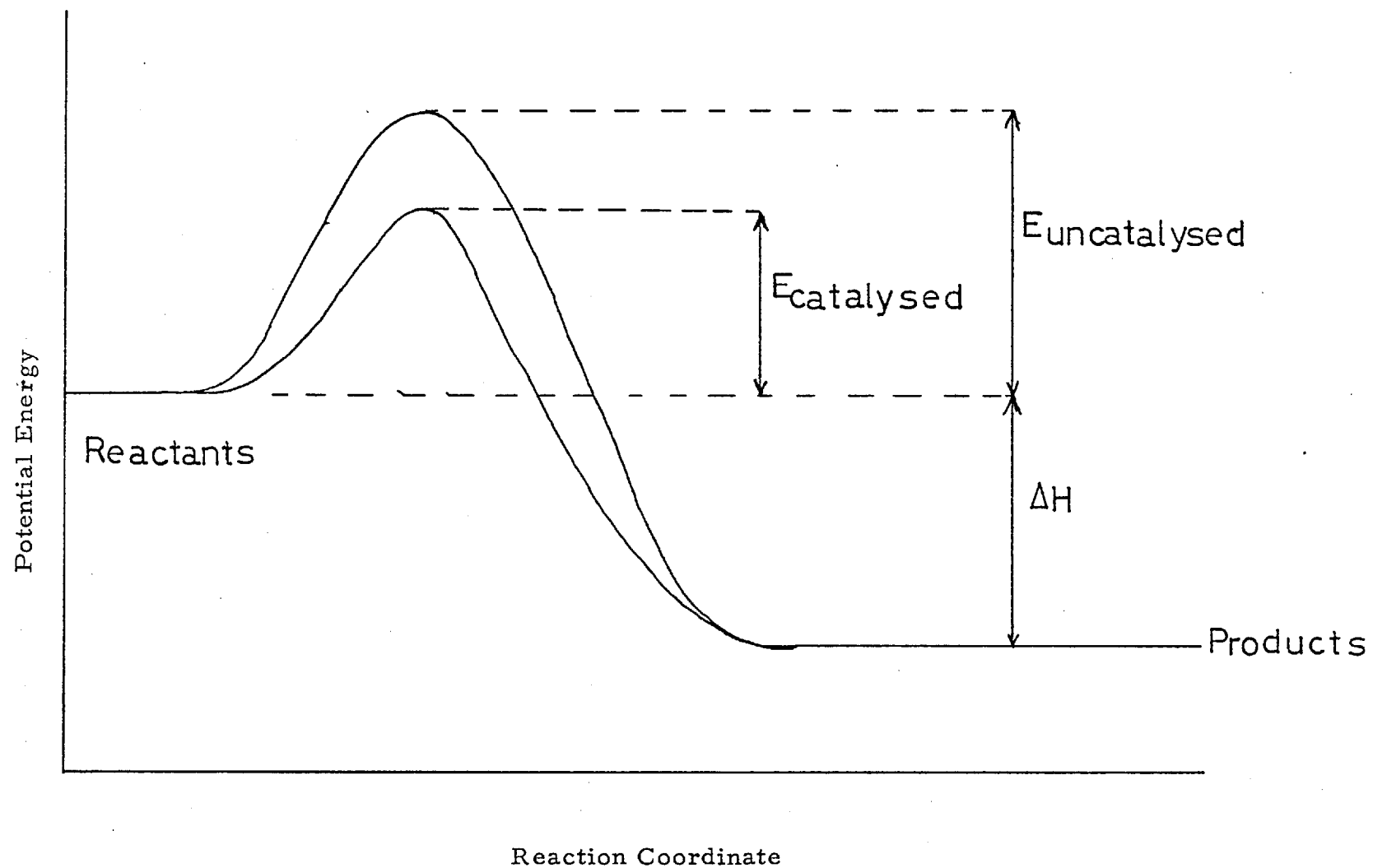
$$\text{and } k = K_p^\ddagger \frac{k_B T}{h}$$

$$\therefore k = \frac{k_B T}{h} \exp(-\Delta G^\ddagger / RT).$$

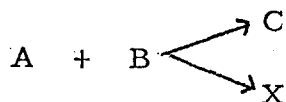
Thus, the effect of a catalyst must be to decrease the free energy of activation to give a corresponding increase in the rate. The free energy of activation is composed of the enthalpy of activation and the entropy of activation which usually decreases due to loss of translational degrees of freedom during adsorption. To compensate for this, there must also be a corresponding decrease in the enthalpy of activation as shown in figure 1.7.

Measurements of kinetic parameters of catalytic reactions can be shown to be important in the determination of a reaction mechanism.

Fig 1.7



Consider two reactions,



in which C is the desired product, and X an unwanted by-product which may remain on the catalyst surface strongly adsorbed as a poison. Using the Langmuir approach for the unimolecular conversion of molecule A, adsorbed without dissociation and producing molecule C which immediately diffuses away from the catalyst, then the rate of adsorption of A will depend on surface coverage, where k is the rate coefficient.

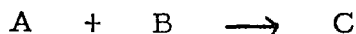
$$\frac{-dP_A}{dt} = k\Theta_A = \frac{kb_A P_A}{1+b_A P_A}$$

Having established a general rate equation, two limiting conditions may be applied, namely

(i) either b_A or P_A is small when $b_A P_A \ll 1$, then $\Theta_A \approx b_A P_A$ or first order in A. This occurs at low pressures with Θ_A low.

(ii) either b_A or P_A is large so that $b_A P_A \gg 1$. The reaction thus becomes zero order in A, independent of P_A and occurs at high pressures with $\Theta_A \approx 1$.

In bimolecular processes, assumptions have to be made which are very often inappropriate to actual conditions. These are that the molecules A and B in the reaction



are adsorbed on separate sites and do not dissociate. Also the slow step has to be the reaction between the two molecules themselves, and finally the product C must not be adsorbed. Thus the rate equation becomes

$$\frac{dP_C}{dt} = k\Theta_A \Theta_B = \frac{kb_A P_A b_B P_B}{(1+b_A P_A + b_B P_B)^2}$$

Now, if both A and B are weakly adsorbed then b_A and $b_B \ll 1$

and the rate expression reduces to

$$\frac{dP_c}{dt} = k' P_A P_B$$

giving first order in each reactant and second order overall. If

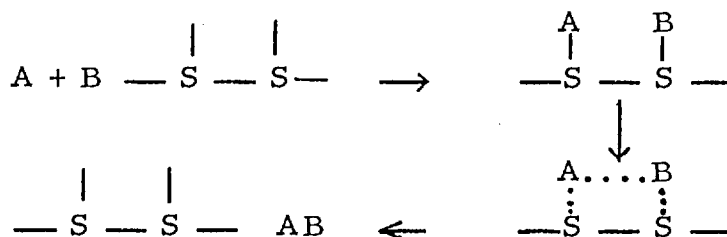
A is weakly adsorbed and B is strongly adsorbed then $b_A \ll 1 \ll b_B$ and the rate expression becomes,

$$\frac{dP_c}{dt} = \frac{k'' P_A}{P_B}$$

in which $k \ll \frac{b_A}{b_B}$ and the reaction is first order in A and minus first

order with respect to B.

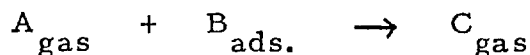
These reactions assume side by side simultaneous adsorption on the surface followed by reaction. This mechanism, the Langmuir - Hinshelwood mechanism is illustrated below and shows how the reaction occurs entirely



at the catalyst surface. In some cases however, only one molecule may be adsorbed on the surface, and the reaction occurs between this adsorbed molecule and molecules in the gas phase. This mechanism, the Rideal mechanism is indicated below.



Thus, in a general equation



the rate equation becomes

$$\frac{dP_c}{dt} = k P_A \theta_B = \frac{k P_A b_B P_B}{1 + b_B P_B}$$

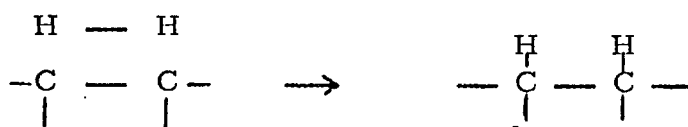
Thus with b_B or P_B large, the rate becomes first order in A and zero order in B. With A weakly adsorbed the reaction would be first order in A and minus first order in B.

We may now move on to consider some theoretical aspects of heterogeneous catalysis with particular reference to the oxidation of ammonia.

1.2.e The geometric factor in heterogeneous catalysis

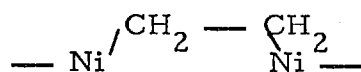
The role of the geometric factor in heterogeneous catalysis has received much attention since early work on the activation energy of adsorption of hydrogen on carbon. This early work led to the conclusion that lattice spacing plays a dominant role in determining the magnitude of a required activation energy.

In the adsorption shown below, a



minimum activation energy of $14 \text{ k cal mol}^{-1}$ was obtained at a C — C distance of 3.6 \AA . Low separation distances gave rise to high activation energies because the repulsion forces between adsorbate species retard adsorption. Large separation distances also give rise to high activation energies because the hydrogen bond has to be broken before adsorption can occur.

Heats of adsorption are also dependent on lattice spacing. In the intermediate below, if the nickel - carbon



bond length is taken to be 1.82 \AA (cf. $\text{Ni}(\text{CO})_4$) and the carbon - carbon bond length is taken to be 1.54 \AA , then the Ni - C - C angle can be shown to be 105° with a Ni - Ni distance of 2.48 \AA and 123° on a Ni - Ni distance of 3.51 \AA . The former angle varies little from the tetrahedral angle of $109^\circ 28'$ and any strain arising can be alleviated by twisting the molecule. Straining to a larger extent would occur on

the 3.51 \AA Ni - Ni spacing, and hence the heat of adsorption on 2.48 \AA would be expected to be larger than the latter case. However, low heats of adsorption give rise to high activity and thus the 3.51 \AA Ni - Ni distance might be expected to be more active catalytically.

Further evidence for this dependence was shown when it became possible to produce orientated evaporated metal films. Nickel films with preferentially exposed (110) planes were found to be five times as active in ethylene hydrogenation as non-orientated films. This arises because (110) lattice planes in nickel contain the optimal 3.51 \AA spacing discussed earlier.

Similar ideas to this had earlier been proposed by Balandin in his multiplet theory of catalysis. This theory postulates that the activity of a catalyst depends on the presence of correctly spaced groups of atoms in the catalyst. Balandin studied the reaction of benzene \rightleftharpoons cyclohexane and proposed that the benzene skeleton should lay flat on the surface, adsorbed to six metal - carbon bonds. Thus, the crystal face would have to display octahedral symmetry, in addition to the necessary surface metal atom interatomic distance. Thus platinum, palladium and nickel were good catalysts because they possessed the required spacings whilst iron was not a good catalyst due to incorrect lattice spacing.

A further classification of reactions involving the geometric factor has been devised by Boudart. Reactions which have been shown to be independent of the surface geometry of the catalyst he classified as facile. Those which were dependent on a geometric effect have been classed as demanding reactions.

It will be shown later (section 2.4. b) that evaporating gold onto the surface of a Pt/10%Rh catalyst deactivates the catalyst for ammonia oxidation. It is well known that gold will not adsorb oxygen and it does therefore seem that adsorption of oxygen is a prerequisite for ammonia oxidation. Much work has been undertaken by Somorjai in the field of adsorption of oxygen on different crystal faces of platinum using low energy electron diffraction.

In his book on the Principles of Surface Chemistry, Somorjai (118)

has devised an abbreviated notation system for surface structures. The arrangement of surface atoms that is identical with the bulk unit cell is called a 'substrate' structure denoted by (1×1) . Further, the notation takes into account the gases which may be adsorbed at this surface and the chemical symbol for the adsorbed species may be added e. g. Pt (111) - (1×1) - 0.

Somorjai and Szalkowski (119) have devised three simple rules to predict the structure of adsorbed gases on crystal surfaces.

The first of these, the rule of close packing, implies that adsorbed atoms or molecules tend to form surface structures characterised by the smallest unit cell permitted by the molecular dimensions and adsorbate - adsorbate and adsorbate - substrate interactions.

The second rule, that of rotational symmetry states that adsorbed atoms or molecules form ordered structures that have the same rotational symmetry as the substrate face.

Finally, the rule of similar unit cell vectors predicts that adsorbed atoms or molecules in monolayer thickness tend to form ordered surface structures characterised by unit cell vectors closely related to those of the substrate, not those of the bulk condensate.

Thus work carried out by Somorjai (118) and Morgan and Somorjai (120) has shown that platinum (100) surfaces undergo atomic rearrangement to a structure which can be designated Pt (100) - (5×1) , which is stable from 300K to the melting point of platinum (2042K). Nitrogen is not adsorbed on the Pt (100) face (121). Work undertaken by Lewis and Gomer (122) on the adsorption of oxygen on platinum has shown that adsorption occurs on (111) and (100) faces, with the formation of epitaxial overgrowths of platinum oxides at temperatures greater than 700K. This result is in line with work undertaken by Mclean and Mykura (123) who showed that platinum exposed to air at 1,400K preferentially adsorbs oxygen on the (100) and (110) terrace sites and also on ledges of (111) planes. Tucker (124) has shown that adsorption of oxygen on the (110) face of platinum leads to a rearrangement of the top layer of platinum atoms and Lyon and Somorjai (125)

have shown that whilst (111) and (100) substrates are stable, (110) showed faceting at temperatures below 873K. This work also showed two types of surface structure developing, an ordered and a disordered structure. Ordered structures appeared during annealing after ion bombardment at temperatures of the order of 1,200K. This ordering is believed to arise from arrays of vacancies in the substrate plane induced by bombarding. The disordered surface structure became apparent at higher temperatures up to the melting point of platinum and were characterised by 'ring like' diffraction features which developed gradually with increasing time and temperature. This work also showed that hexagonal structures appeared on all platinum surfaces and they conclude that this disordered close packed hexagonal structure seems to be the stable surface phase of platinum, a conclusion which Clarke et al (126) have also arrived at following his work on the structure of the Pt(100) surface. They also showed that the structure of the first layer of platinum is partly described by a hexagonal close packed structure which is a rearrangement from the bulk face centred cubic arrangement.

Thus it would seem that oxygen attack on platinum not only varies with different exposed planes, but also gives rise to a different surface structure.

The presence of impurities in the platinum surface may also give rise to effects in the adsorption of oxygen. Weinberg et al (84) have shown that the initial sticking probability of oxygen (7×10^{-7}) is considerably smaller on uncontaminated surfaces. This value must be compared with values of 0.14 obtained by Weber and Fusy (127) and Voelter, Procop and Berndt (128) for clean carbon free surfaces; the values are independent of temperature. Somorjai (118) has shown that whilst platinum metal surfaces undergo atomic rearrangement to Pt(100) - (5 x 1), the presence of impurity atoms, particularly carbon, stabilizes the (1 x 1) structure. This he states is due to the four unpaired valence electrons per atom on carbon whereas oxygen acting as an electron acceptor can stabilize a hexagonal surface structure (5 x 1).

Finally Gwathmey and Cunningham (129) have identified regions of high and low activity on catalyst surfaces. Those reactions which give rise to surface faceting produced rearrangements to expose facets parallel to certain crystal planes. Also, the rate of reaction varied with the face exposed, and the formation of a film of oxide on the surface not only affected the properties of the catalyst, but also gave rise to powder formation. They also noted that the addition of a very small amount of foreign solid, either an impurity or dopant, affected the rearrangement of the catalyst. Most significantly however, they conclude that because of the rearrangement process, the reaction can be said to be preparing its own surface. It is this point which has been shown to be important in ammonia oxidation (38).

The final section on the role of the geometric factor, the role of lattice imperfections, will now be introduced with reference to ammonia oxidation.

Baker, Thomas and Notton (85) have shown that attack on platinum/rhodium wires during ammonia oxidation predominates at grain boundaries, whilst the activity of a platinum catalyst towards ethylene hydrogenation has been increased tenfold by bombarding the surface with argon ions (130). This has been attributed to the production of lattice defects in the catalyst surface. Alfons (131) has scratched the surface of a platinum catalyst for formic acid oxidation and found that the activity has been increased considerably.

It will be shown later that the activation of platinum/rhodium catalysts in oxygen at $1,000^{\circ}\text{C}$ produces not only grain boundary grooving, but pitting. These phenomena have also been noted by Lacroix (47) and Domanski et al (132).

Schmidt and Luss (133) have compared the behaviour of platinum/rhodium gauze catalysts in ammonia oxidation and hydrogen cyanide synthesis. Activation of the gauze catalysts has been shown to increase the surface area and to form randomly oriented facets. Pan (134) has shown that the face-centred tetragonal structure gave a higher HCN yield than a face-centred orthorhombic structure.

The work of Schmidt and Luss (133) indicates that the wires have become roughened during use, giving rise to extensive faceting. The facets appear to be randomly oriented planes; regions of sixfold symmetry characteristic of (111) planes have been observed. The (111) planes are presumably those of minimum surface free energy. This faceting process could be due to the removal of platinum as its volatile oxide from around defects such as grain boundaries. This may be due to an increased rate of reaction at these defects giving rise to local heating.

McCabe, Pignet and Schmidt (135) have studied the catalytic etching of platinum in ammonia oxidation. Their results indicate that etching is much more extensive and rapid in mixtures of ammonia and oxygen than in either of the two gases individually. Their results show that flat facets, exposing crystal planes of low surface energy, are produced in excess oxygen. Heating to temperatures below $1,200^{\circ}\text{C}$ in excess ammonia gave facets with curved surfaces. Whilst they also identify V shaped valleys with rounded ridges, U shaped valleys with rounded ridges and U shaped valleys with sharp ridges they cannot unambiguously connect this phenomenon with temperature, but state that underlying crystal structure has a greater influence on the type of etching obtained.

Pit formation occurred in excess ammonia at temperatures greater than $1,000^{\circ}\text{C}$. These pits were square and hexagonal in shape and symmetry considerations imply that the walls of square pits are (100) planes whilst those of hexagonal pits are (111) planes. Pit formation leads to metal deposition at the pit mouth presumably by diffusion to the ledge when it is deposited.

Etching can result from faceting occurring due to the variation of reaction rate on different exposed crystal faces. They therefore diluted by half the ammonia/oxygen mixture with nitrogen examining the surface after two hours and compared this to a surface exposed after heating in an ammonia/air mixture for one hour. The surface morphologies appeared similar, thus showing that etching is a function of the total transport of ammonia and oxygen to the surface.

Thus, it can be seen that whilst the overall catalytic oxidation of ammonia may depend on other effects besides the geometric factor, it is clear that this factor plays a vital role in the activation process, an understanding of which is essential for efficient catalysis.

1.2.f The electronic factor in heterogeneous catalysis

Theory behind the electronic factor in heterogeneous catalysis is based on the fact that the electronic properties of metals, alloys or semiconductors are in some way related to the catalytic activity of the substances in heterogeneous gas phase reactions. Thus, the electronic approach seeks to relate the catalytic activity of a solid to its bulk electronic structure.

The electronic factor can be divided into a number of rival theories. The band theory, developed by Mott and Jones supposes that the electrons in a metal retain much of the character they possess in isolated atoms, with the valency electrons moving freely through the metal lattice. In an isolated atom, the s, p and d electrons have discrete single energy levels. In a solid, these states have 'bands' of permitted values. These bands may contain a different number of electrons to those associated with single atoms, e.g. Fe, $3d^6 4s^2$ in the atomic state becomes $3d^{7.8} 4s^{0.2}$ in the metallic state. Thus it becomes possible to talk of 'holes' in the d band, and generally transition metals possess incomplete d bands, which affects their ability to catalyse reactions.

The second electronic theory ascribed to Pauling envisages metal crystals being held together by covalent bonds between adjacent atoms. He postulates three types of orbitals associated with each atom these being, bonding d orbitals to participate in dsp hybrid bonds, metallic d orbitals for electrical conduction and non-bonding atomic d orbitals into which electrons can be placed. Transition metals, having vacant atomic d orbitals, can easily be involved in bond formation between gas phase species and the metal surface. Thus, the percentage d character, δ , represents the extent to which d electrons participate in dsp orbitals. The higher

the value of ξ , the fewer are the number of atomic d orbitals available for bonding purposes.

Whilst these ideas simplify the situation, they do represent possible electronic effects arising from electrons present in metals. The situation arising with alloys however is more complicated and chemisorption on platinum/rhodium alloys has been studied by Rand and Woods (80). They propose two models, which differ in assumptions made regarding the involvement of neighbouring metal atoms on the bond between an adsorbate and the surface.

They postulate a rigid band model of Mott discussed earlier and compare this with a minimum polarity model ascribed to Lang and Ehrenreich. This theory, in complete opposition to the band theory, assumes complete lack of interaction between nearest neighbours, the adsorption and catalytic properties being a function of the localised properties of the individual surface atoms. Sachtler and Van der Plank (136) have studied the role of individual surface atoms in chemisorption and catalysis by nickel/copper alloys. They showed that for hydrogen chemisorption and its reaction in the hydrogenation of benzene, chemisorption and catalysis were not determined by collective properties of the catalyst but by the chemical properties of individual surface atoms.

In electrocatalysis it has been assumed that activity is a collective property of the bulk metal (80). A voltammogram which showed a single oxygen desorption peak rather than peaks at potentials characteristic of each element present in the alloy would be in agreement with a rigid band model. The localised model, which assumes the formation of a bond between adsorbate and a single surface metal atom, would show two peaks for a binary alloy, though their potentials would be shifted due to the influence of neighbouring atoms. In fact the experimental results obtained by Rand and Woods (80) is best explained by a model in which delocalised chemisorption orbitals arise, with adsorption involving several surface atoms. This could be explained by the fact that surfaces involved in chemisorption are only several monolayers thick and do not involve the bulk of the metal.

Therefore, results seem to indicate that a process somewhere between the two theories is taking place.

Thus it can be seen that attempts to correlate the bulk electronic factor with surface reaction have proved unsuccessful. Perhaps the largest flaw in the theory is that it does not explain the variation in activity occurring on different crystal faces of the same metal. Thomas and Thomas (107) quote Cox et al. who studied the decomposition of carbon monoxide over single crystal alloys of copper and nickel. Generally, a decrease in percentage d character of the nickel was accompanied by a decrease in activity. However, (100) planes in both pure nickel and alloy crystals remained inactive.

Whilst further work should include the effect of possible complex formation at the surface it is interesting to note the work of Dowden (137) who has postulated a crystal and ligand field model for solid catalysts. This work involved comparing the catalytic activity of transition metal oxide semiconductors over the first series of transition elements in the hydrogen-deuterium exchange reaction.

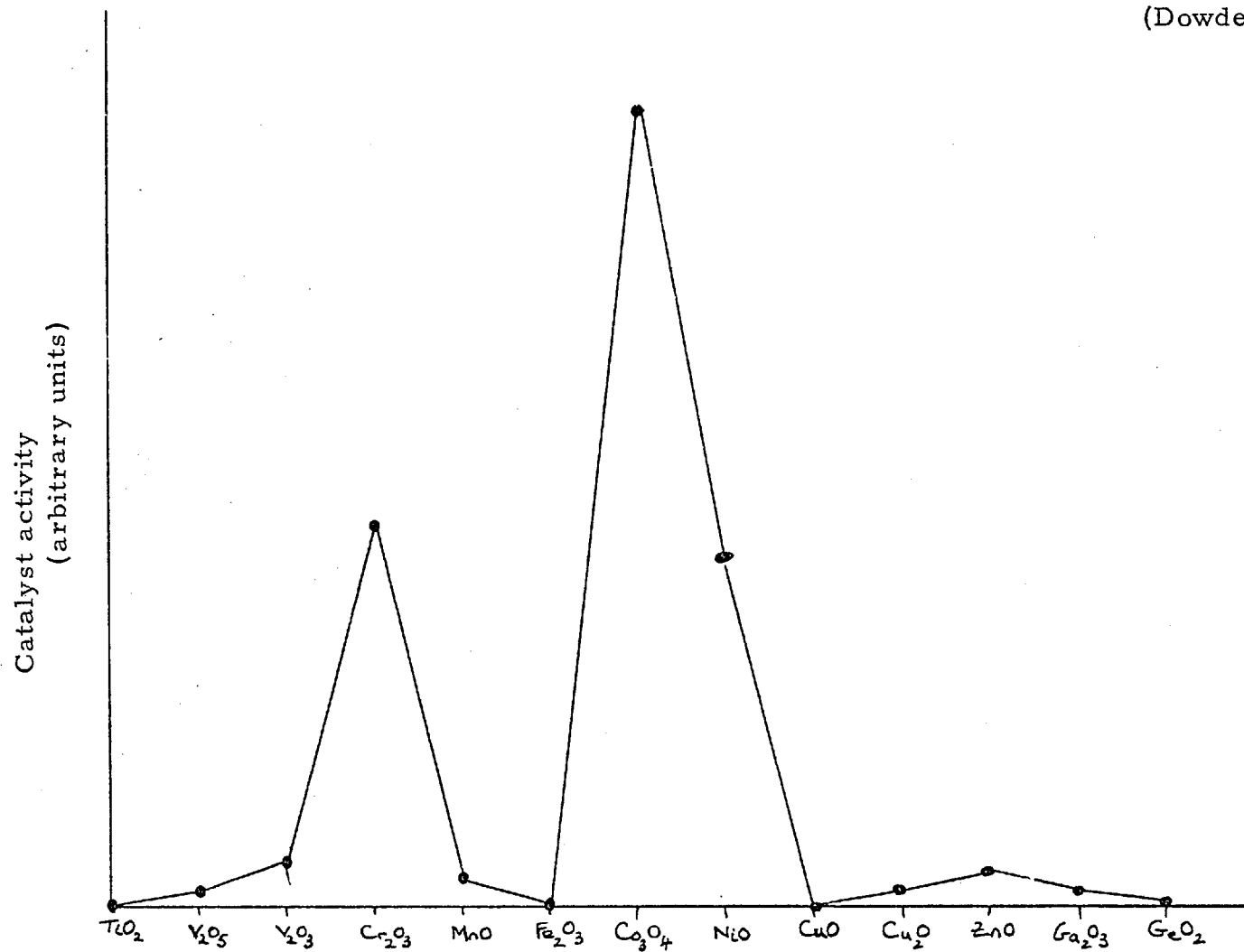


Crossing the series from TiO_2 to CuO , two peaks of activity were found at Cr_2O_3 and $\text{Co}_3\text{O}_4/\text{NiO}$ (Fig 1.8.). The ions with highest activity were found to be $3d^3$ (Cr^{3+}), $3d^6$ (Co^{3+}), $3d^7$ (Co^{2+}) and $3d^8$ (Ni^{2+}). Ions of lowest activity were either $3d^5$, $3d^0$ or $3d^{10}$ (Zn^{2+}). Thus, from the application of crystal field theory, a rate controlling step which involves the adsorption of a polarised specie resulting in the restoration of near octahedral symmetry contributes to higher energies of activation and lower activities of the cation electronic configuration d^0 , d^5 , d^{10} .

Bond (138)(139) has developed a theory involving the application of molecular orbital theory to the bonding of adsorbed species at catalyst surfaces. Bond (139) quotes Goodenough and Dowden and extends the theory to cover the f. c. c. metals of Group $\overline{\text{VIII}}_3$ (Ni, Pd, Pt).

Fig 1.8

The catalytic activity of the oxides of the first long period for H_2/D_2
exchange at $80^\circ C$
(Dowden 137).



In an f. c. c. metal each atom is in contact with twelve others, four in three planes at right angles, whilst the other six are octahedrally placed at a greater distance (Fig 1.9). When an atom is in an octahedral environment, crystal field theory predicts that the five d orbitals will be split into two higher energy levels $d_{x^2-y^2}$ and d_{z^2} lying along the axes, and three lower energy orbitals d_{xy} , d_{yz} and d_{zx} , lying between the axes. These orbitals are termed e_g and t_{2g} respectively.

Each of the t_{2g} orbitals has four lobes, which are used to bond to the twelve nearest neighbours, whilst the remaining six next nearest neighbours are bounded by e_g orbitals which do not overlap significantly because these next nearest neighbours are too far apart. Thus, from Goodenough, who divides the 0.55 d electron holes between t_{2g} (0.41) and e_g band (0.14) it is possible to say that the e_g band is sufficiently unoccupied to take part in σ bond formation, and the t_{2g} band sufficiently filled to take part in π bonding.

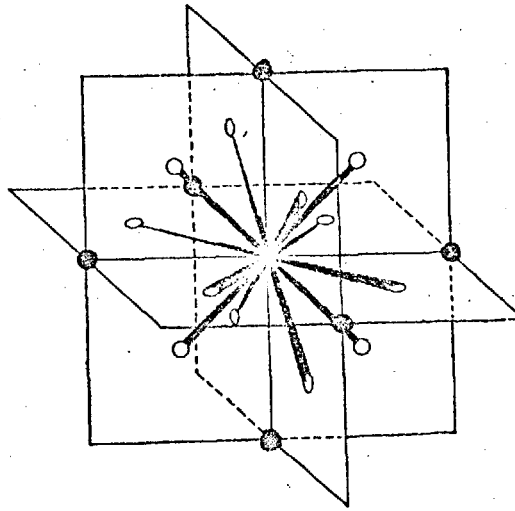
Bond then shows that for (100) planes, an e_g orbital emerges normally from the surface (Fig 1.10), whilst in the (110) case it is a t_{2g} orbital which emerges (Fig 1.11). This will result in variation in the strengths of bonding when ad atoms, such as hydrogen are adsorbed on the surface. This should result in a variation in activation energy and thus the catalytic reaction rate on different surfaces.

1.3. Modern analytical methods used in this work

1.3.a X-ray photoelectron spectroscopy.

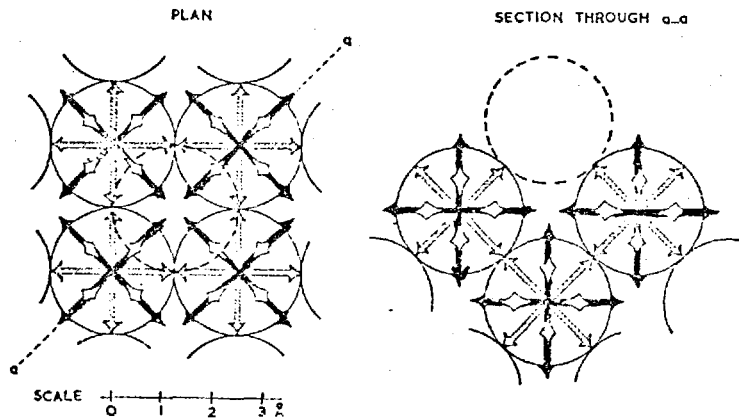
When atoms form molecules, the orbitals of the individual atoms are mixed and replaced by molecular orbitals. Thus, two types of orbitals are now present. The first involves the original inner atomic orbitals of the atom which remain unperturbed and have high binding energy, whilst the second type, the external orbitals, combine to form the valence bonds in the system which have a lower binding energy. It is these orbitals which form chemical bonds with other elements and which determine the chemical characteristics of the species in question.

Fig 1.9



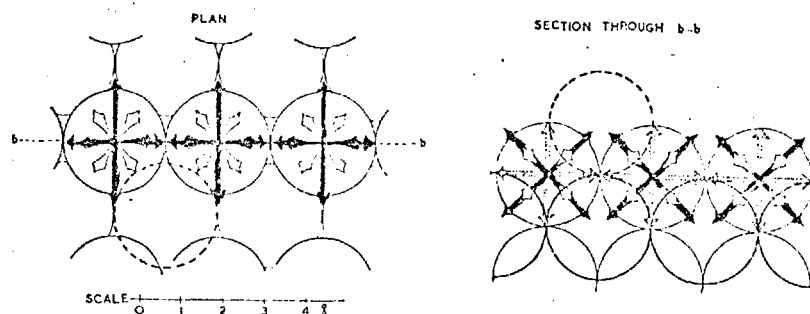
—The disposition of atoms about a central atom in a face-centred cubic metal. Near-neighbours (open circles) are bonded by overlap t_{2g} orbitals of (d_{xy} , etc.) and next-nearest neighbours (filled circles) by overlap with e_g orbitals ($d_{z^2-y^2}$ and d_{z^2}).

Fig 1.10



—Diagrammatic representation of the emergence of orbitals at the (100) face of a face-centred cubic metal. Filled arrows: e_g orbitals in plane of paper; hatched arrows: t_{2g} orbitals in plane of paper; open arrows: t_{2g} orbitals emerging at 45° to plane of paper. The broken circle shows the position of an atom in the next layer above the surface layer. In both the plan and section, an e_g orbital emerges normal to the plane of the paper from each atom. The scale applies to nickel.

Fig 1.11



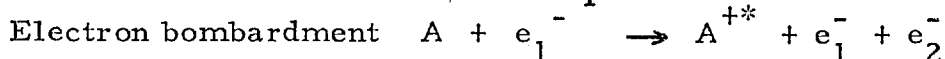
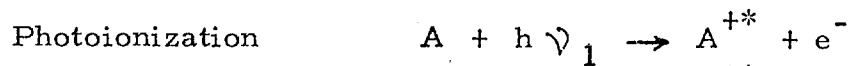
—Diagrammatic representation of the emergence of orbitals at the (110) face of face-centred cubic metal. Filled arrows: e_g orbitals in plane of paper or emerging at 45° ; hatched arrows: t_{2g} orbitals in plane of paper; open arrows: t_{2g} orbitals emerging at 30° to plane of paper. In the plan, a t_{2g} orbital emerges normal to the paper from each atom: in the section, it is an e_g orbital.

Chemical bond formation affects the distribution of charge around the atom. Thus an atom in a molecule can be regarded as a sphere with a potential. If a small unit of charge is removed from one atom to another, then the inner levels of the atom are shifted, each level being shifted by an equal amount. The levels in different atoms in a molecule are shifted by different amounts, and by measuring the position and size of this chemical shift, the element and its oxidation state can be determined. Thus, this is an ideal technique for the study of surface chemical effects occurring on catalyst surfaces.

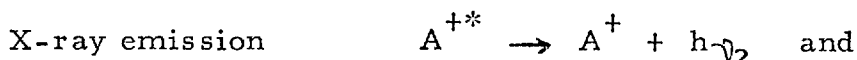
The technique of electron spectroscopy was developed by Siegbahn (140). The method is based on a high resolution study of the energy distribution of electrons expelled from their orbitals by exciting radiation. X-ray radiation reaches not only the valence electrons, but also core levels of the atom. As each element in the periodic table has its own characteristic core level binding energies, an element can be positively identified. Information concerning chemical bonds and molecular orbitals can be obtained by using ultraviolet radiation. Overall, E.S.C.A. is applicable to all elements in the periodic system in both solid and gaseous form with the exception of hydrogen. However it is essentially a surface method the analysis being performed on a layer less than 50 \AA thick.

The theory of electron spectroscopy in its relation to chemical applications has been covered by Hercules (141). Two types of processes are responsible for the emission of electrons from atoms. These are electron ejection and electronic relaxation.

Electron ejection can be obtained by two processes namely:



Electronic relaxation by



Excitation can be induced by either photoionization or electron

bombardment and electron relaxation is produced by the two competing processes of X-ray emission (fluorescence) and Auger electron emission.

Figure 1.12 shows the photoionization processes occurring during the excitation of an electrical insulator. Photoionization processes are shown for 1s, 2s and 2p electron levels. Photoionization gives rise to a positive hole in the atom, and the nature of this hole is indicated by the term symbols on the right hand side of the diagram. Thus, photoejection of a 1s electron leaves a $2S_{\frac{1}{2}}$ state or K hole. The electron is promoted to the free electron level, where it has become free of its binding atomic and molecular forces.

Photoexcitation is not equally probable for all electrons in a given atom or for the same electron in different atoms. Excitation of an electron is inversely proportional to the square of the orbital radius. Thus, the probability of excitation of a 1s electron will be approximately twenty times greater than that for a 2s electron.

Figure 1.13 shows the electronic relaxation process. Assuming a primary vacancy occurs in the K shell, the normal K_{α} and K_{β} emission lines are shown as transitions from the 2p and 3d orbitals to the 1s orbital respectively. These represent X-ray fluorescence if photoionization by X-rays had been used or X-ray emission if photoionization was induced by electron excitation.

The second major electronic relaxation process is Auger emission which is a radiationless process. An electron from a higher orbital undergoes a transition to fill the hole in the lower orbital, and simultaneously a second electron is ejected from the atom. In Figure 1.13, the KLL Auger emission is shown by the primary vacancy occurring in the K shell being filled by an electron from the L shell and simultaneously an L electron is ejected. These lines can be used as standard, because they are independent of excitation energy and are particularly valuable for the study of light atoms (142).

Fig 1.12

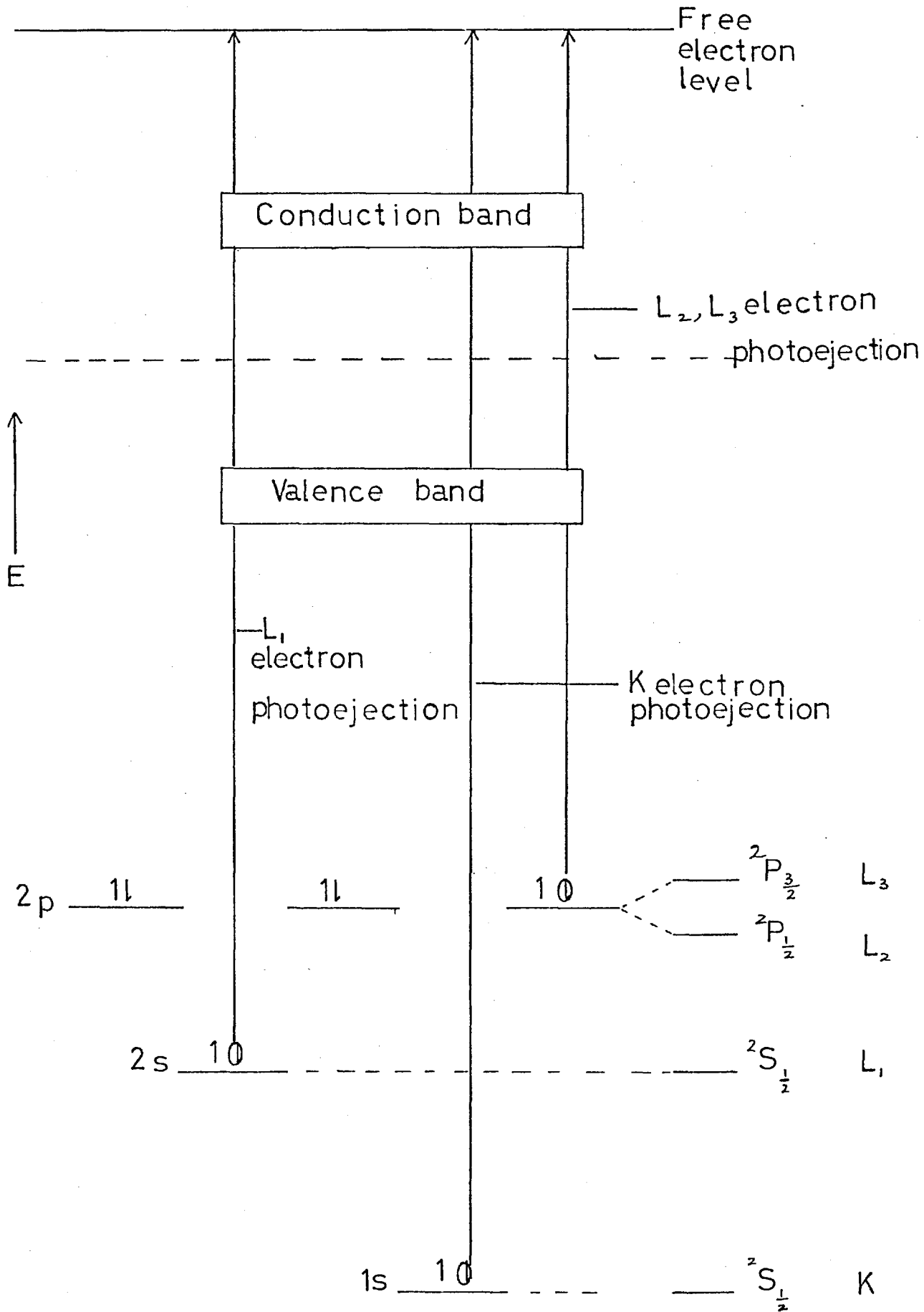
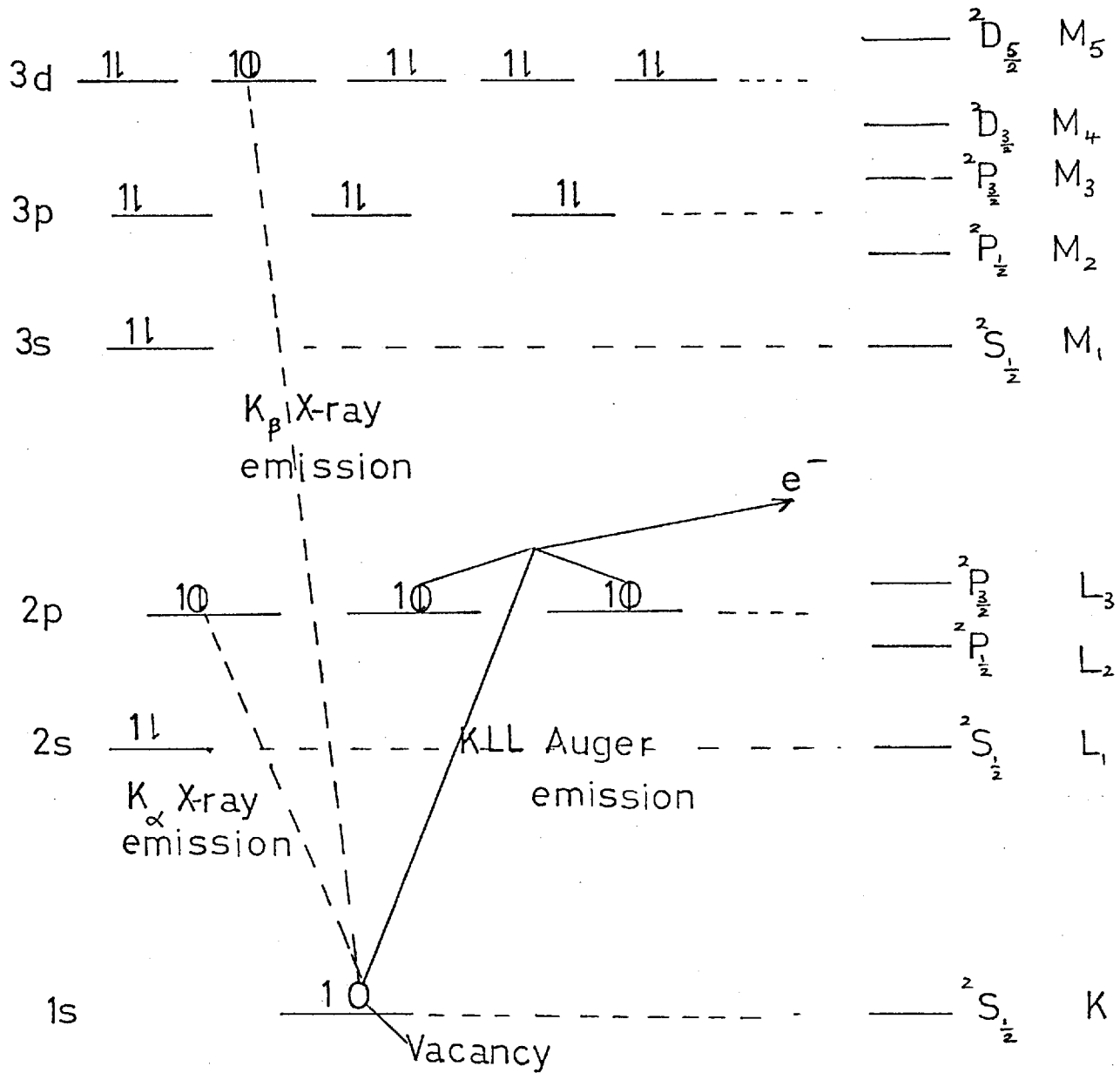


Fig 1.13



Instrumentation

A simple block diagram of an E.S.C.A. spectrometer is shown in figure 1.14. The source must produce intense ionising radiation and is some form of electron gun giving X-rays, typically of Al K α (1487 eV). As the radiation strikes the sample, the photoejected electrons are analysed in a monochromator which can be magnetic or electrostatic and finally the relative intensity detected by either a Geiger Muller tube or an electron multiplier.

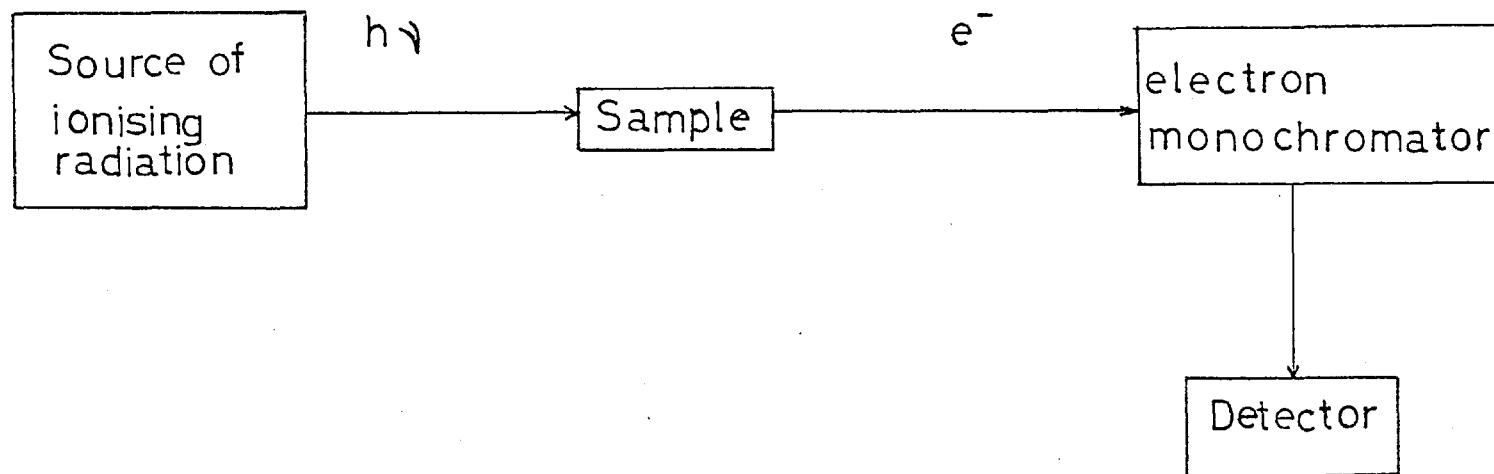
The measurement of absolute binding energies is one important use to which the technique has been applied. Figure 1.15 shows the sample being studied as an insulator, with the spectrometer assumed to be metallic.

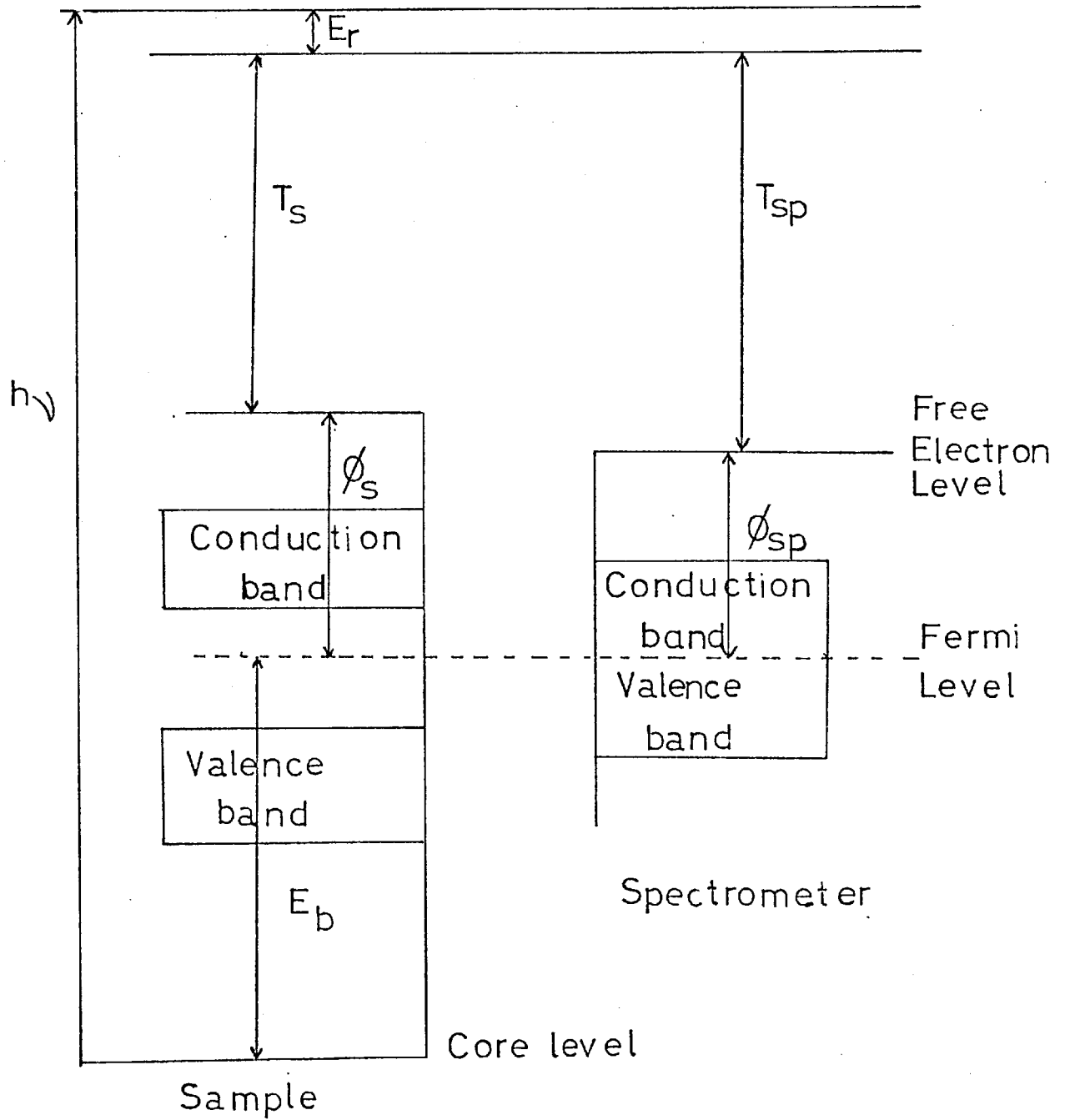
As photoejection of a core electron occurs, the energy is dissipated among four processes, the binding energy E_b of the core electron relative to the fermi level, the work function ϕ_s of the material, which is the energy necessary to raise the electron from the fermi level to the free electron level, the recoil energy E_r resulting from the conservation of momentum in the photoejection process, and finally the kinetic energy T_s of the electron in space after it has left the sample. Use of Al K α radiation makes recoil unimportant in atoms heavier than lithium. Thus, the free electron, with kinetic energy T_s , traverses the space between the sample and the spectrometer where it encounters a potential gradient due to the difference in work function between the sample and the spectrometer. The electron will therefore change velocity to kinetic energy T_{Sp} as it reaches the free electron level of the spectrometer material. Finally, adding the work function of the spectrometer ϕ_{Sp} brings the electron to the fermi level of the spectrometer. Thus, E_b , the binding energy of the electron in the sample is shown to be

$$E_b = h\nu - \phi_{Sp} - T_{Sp} - E_r$$

Thus, to measure the absolute binding energy of an electron, it is essential to know the work function of the spectrometer. This is usually calibrated against gold. Relative measurements can be

Fig 1.14





- $h\nu$ Energy of exciting photon
- E_b Binding energy of ejected electron
- ϕ_s Work function of sample
- ϕ_{sp} Work function of spectrometer
- T_s K. E. of photoejected electron at sample
- T_{sp} K. E. of photoejected electron at spectrometer
- E_r Recoil energy

obtained by assuming the work function of the spectrometer remains constant. If this is the case, and the recoil energy is negligible, the uncertainty in the measured binding energy will arise from either the uncertainty in the measured photon energy or from the binding energy of the core electron itself.

The use of E.S.C.A. in surface studies has been reviewed by Brundle (143). One of the great advantages of E.S.C.A. over other surface techniques such as Low Energy Electron Diffraction (L.E.E.D.) is that a surface can be studied even though it is covered by more than one layer of material. The sensitivity of X.P.S. in comparison with the other two main electron spectroscopy techniques, U.P.S. and Auger, has to be considered in the following ways.

In terms of escape depth, only those electrons ejected which do not lose energy by inelastic scattering will appear in the spectrum at their characteristic positions. Thus, X.P.S., with escape depths of up to 100 \AA will produce a backscattering effect at least twice as great as that associated with A.E.S. or U.P.S.

In terms of signal strength, another difference is significant. X.P.S. has been developed primarily as a tool for measuring chemical shift and therefore the electron analyzers designed for X.P.S. sacrifice signal strength for high resolution, whereas with A.E.S. the analyzers are set for high sensitivity but low resolution.

Quantitative analysis is theoretically possible by all three techniques, by following the variation in signal intensity with number of scans or the photon energy $h\nu$. However, U.P.S. can be discounted because there is no direct identification of elements, and the spectra produce broad peaks superimposed on a back scattered electron signal.

Core level ionizations however are atomic in nature and X.P.S. and U.P.S. give rise to sharp signals which vary very slightly with compound formation. Thus there is very little line broadening, giving rise to errors no greater than those associated with the experimental errors of the technique.

The chemical bonding information available has mostly come

from X. P. S. and A. E. S. data. X. P. S. shifts are more easily compared since only one core level is involved in each photoelectron process. Resolution is the most important factor here. In X. P. S. , resolution is poor compared with other spectroscopic standards. This is due to peak widths being normally 1eV or greater, since they are limited by the width of the X-ray line. Monochromators can reduce errors to the order of ~ 0.3 eV, but claims of shifts smaller than this may not be significant. Some surface work carried out with X. P. S. refers to thick ill-defined surface phases. It is possible that core level binding energies are lower in the surface layer owing to reduced coordination. Thus, for clean metal surfaces, broadening of the signal should be observed. No such phenomena has been reported, and it can therefore be taken that the reduced coordination theory is incorrect. Thus the effective electronic environment through the first few monolayers varies very little, indicating small coordination effects. Therefore it can be expected that chemisorption at metal surfaces will only give rise to small changes in binding energies of surface metal atoms. As a result, chemical shift resolution at best in X. P. S. is poor, whilst that in A. E. S. is even worse due to line widths not being source limited, since the Auger process is independent of whatever produces the original hole in the core level. Also, line widths are usually considerably broader than those associated with X. P. S. because auger is a three electron process.

Thus it can be seen that X. P. S. compares favourably with both U. P. S. and A. E. S. as an analytical technique for surface study. Work on the X-ray photoelectron spectroscopy of platinum compounds has been undertaken by Riggs (144). The results showed that platinum electron binding energies are a measure of the oxidation state of the platinum. Riggs reports Pt $4f_{7/2}$ binding energies from 76.1 eV for Pt (IV) to 71.6 eV for Pt(0). Similar work by Kim et al (145) reports the Pt $4f_{5/2}$ electrons for Pt (IV) to have a binding energy of 77.5 eV. The very close proximity of these two signals shows the care which must be taken in determining oxidation states from chemical shift data.

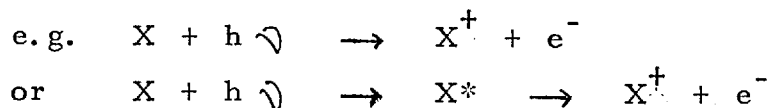
1.3.b Ultraviolet photoelectron spectroscopy

Prior to the development of U. P. S. the electronic structure of matter was studied by the emission or absorption of electromagnetic radiation. Photoelectron spectroscopy reviewed by Bahr (146) enables the electrons themselves to be observed. The photoionization process occurring can be represented by the Einstein Law

$$E_1 + E_c = h\nu - E_B$$

E_1 is the kinetic energy of the ion (for a free atom or molecule), E_c is the kinetic energy of the ejected electron, ν is the frequency of the incident radiation, h is Plank's constant and E_B is the minimum energy required to remove the electron from its binding state. As E_1 can be neglected, because momentum must be conserved, an accurate measurement of E_c can determine E_B the binding energy of the electron.

U. P. S. is concerned only with photo-absorption processes liberating electrons.



The second interaction, which is an example of autoionisation leads to the formation of an excited state of a neutral atom or molecule and eventually gives an ion plus an electron. The former interaction, which is the most common, gives an ion plus an electron directly.

U. P. S. is concerned solely with the valence orbital region in which the loosely bound electrons are not localised to any one particular atom, but distributed over the whole molecule. Vacuum ultra-violet photons (10 - 50 eV) are used to study this region, the most common sources being the He I (21.22 eV) and He II (40.81 eV) photons. Vacuum U. V. photons have inherent half widths of 10^{-3} eV (cf E. S. C. A. 1 eV), allowing vibrational structure of the molecule to be resolved, though the energy range is limited to ~ 500 eV.

The basic instrumental design is similar to that of the E. S. C. A. spectrometer outlined in figure 1.14, and these two techniques are often included together in commercial machines.

The information which can be obtained from U. P. S. spectra is similar to that from the E. S. C. A. spectrum. Kinetic energies of electrons ejected from the molecular state (and hence molecular binding energies) can be obtained together with relative intensities of each electron energy group. However, U. P. S. has been used to greatest effect in determining ionisation potentials of molecular orbitals, and provides direct confirmation of the Mulliken molecular orbital theory.

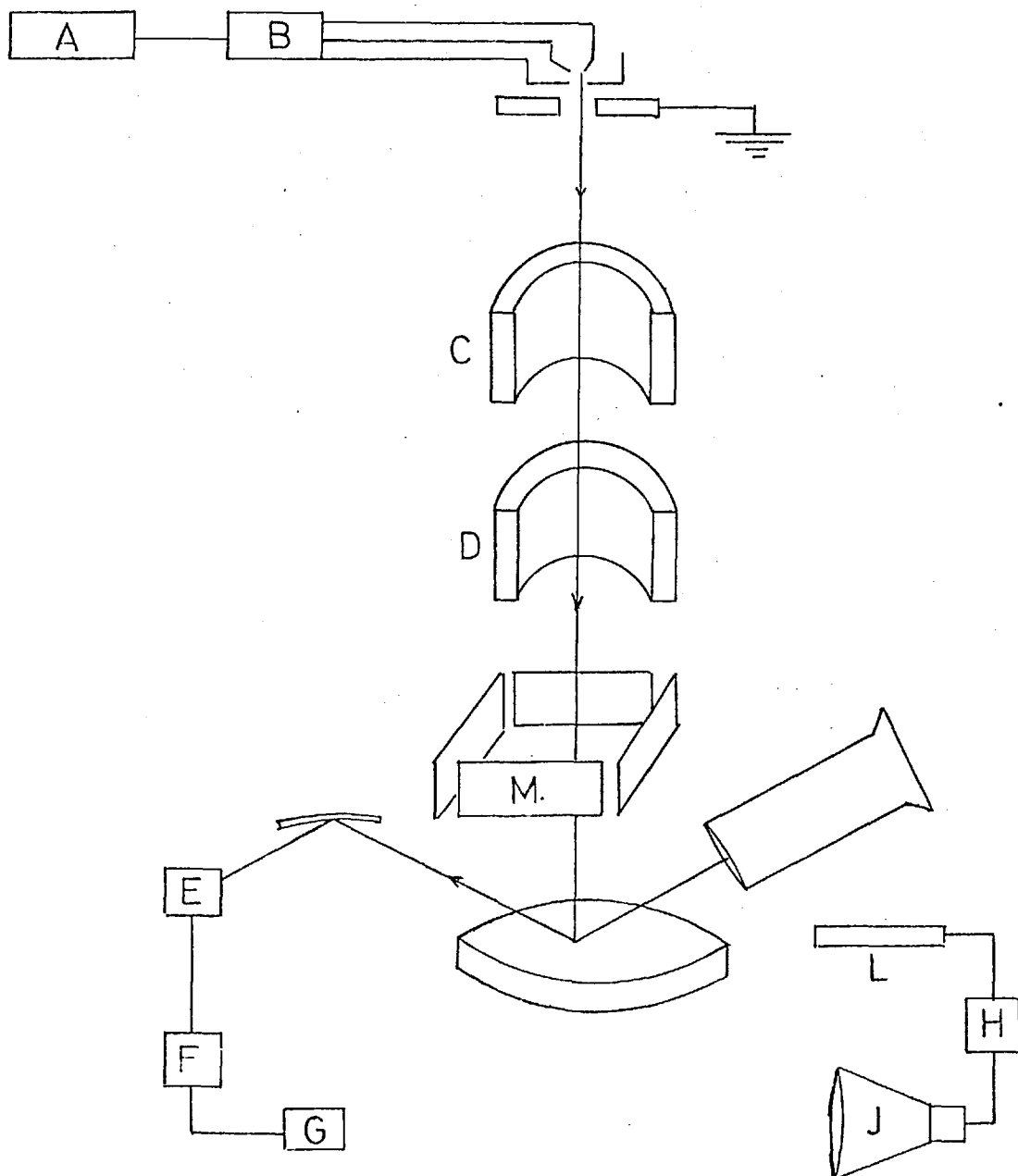
1. 3. c Electronprobe Microanalysis

The impact of electrons on solid materials gives rise to the production of X-rays. These X-rays consist of a 'white' background or continuum (Bremstrahlen), caused by random deceleration of electrons, and superimposed on this, the characteristic X-rays due to expulsion from and refilling of the K. L. M. shells of the atoms.

In 1959, Castaing described the first electron microprobe in which a narrow pencil of electrons is directed onto the surface of a specimen causing X-ray production from a localised area. These X-rays can then be examined to determine the nature of the sample. Electron probe analysers can be used to quantitatively analyse micron-sized areas in samples for boron and all heavier elements. Metallurgical problems of diffusion, corrosion, oxidation and particularly segregation and precipitation in micron-sized particles can be investigated. The instrumentation associated with electronprobe microanalysis has been described by McCall and Strabel (147), Wittry (148) and Birks (149). A diagram of the basic parts of an E. P. M. A. instrument is shown in figure 1.16. The electron column, the main part of the microprobe is similar to an electron microscope.

The electron gun consists of a heated tungsten filament operating at a high negative potential. Electrons are emitted from the filament and accelerated to the anode plate at ground potential. Electrons pass through the aperture in the anode plate and on down the microprobe. Below the anode plate, two magnetic lenses are used to demagnify and focus the electron stream from the aperture,

Fig 1.16 The Electronprobe Microanalyser



- A High voltage power supply
- B Filament and bias
- C Condenser lens
- D Objective lens
- E Detector
- F Preamplifier
- G Recorder
- H Video amplifier
- J Cathode ray tube
- L Photomultiplier tube
- M Deflection plates

so that the size of the electron beam striking the sample can be made as small as 1 micron diameter. By varying the strength of the lenses, it is possible to increase the size of the beam area up to 300 microns in diameter.

When the electrons strike the sample, a portion of their energy is converted into X-radiation having wavelengths characteristic of the elements present in the sample. The wavelengths of these X-rays are analysed by crystal-dispersive spectrometers, of which two may be incorporated to either analyse two elements simultaneously, or analyse X-rays from both sides of a sample. The wavelength of radiation from each element is peculiar to that element, and measurement of each X-ray wavelength emitted will be sufficient to identify all the components of the sample. By noting the position of diffraction, the wavelength of the radiation can be calculated from the measured position using the Bragg Equation.

$$n \lambda = 2d \sin \theta \quad (\theta \text{ Bragg angle})$$

The X-ray radiation diffracted from the crystals is detected using a gas-flow proportional counter, consisting of a thin wire fixed axially along a tube, with a suitable thin window. Argon is used, containing 10% methane, and a potential of 1,500 V is applied between the wire and the tube. In this way, the pulses produced by X-ray photons entering the window are amplified and counted.

Finally, the instrument uses a microscope and a precision mechanical stage to view and position the sample directly below the electron beam. Recent advances in electron probe instrumentation include work by Long (150) in which an electron microscope with facilities for selected area diffraction has been combined with an electron probe microanalyzer, thus further increasing the usefulness of this technique; a comprehensive review is given by McKinley, Heinrich and Wittry (151).

Besides the X-rays produced when the electron beam strikes the sample, backscattered electrons are also obtained. The proportion of the electrons backscattered depends on the atomic number of the atoms in the sample. The higher the atomic number, then the

greater will be the extent of backscattering. Hence using a photomultiplier tube coupled to a cathode ray tube, the backscattered fraction of the incident electron beam can also be studied.

A quantitative assessment of each element present in the sample can be determined by monitoring the intensity of the X-ray radiation emitted for each wavelength. X-ray intensity increases with concentration in an approximately linear manner, and so direct ratioing of the intensity of a particular element in an unknown sample with the intensity produced by a known standard, should give an accurate quantitative assessment of the concentration of the element present in the unknown sample. This however will depend on the state of the sample.

Common sources of error in quantitative E. P. M. A. work have been studied by Heinrich (152). Careful sample preparation is essential and the sample should be flat and free from surface disturbance. Further problems are caused by non-conducting samples, which give rise to charging during exposure in the electron beam. To avoid this electrical conductivity must be maintained between the specimen and the specimen stage, usually by means of a conducting 'paint bridge'. Metallic samples give no charging problems. Heinrich (152) highlights the problems of poor sample characterisation and measurement together with omission of characteristic fluorescence corrections. These corrections are necessary because combinations can occur in which higher energy X-rays produced by one element can cause production of X-rays of lower energy from another element. Errors in quantitative determinations also arise from absorption of X-rays on the way out of the specimen and atomic number effects, in which the 'stopping power' and the backscatter effects are involved. These can be substantial owing to the depth of penetration of the beam (2 microns) which is much greater than the other analytical techniques outlined previously. Problems associated with the detector system give rise to inaccuracies through 'dead time' or paralysis time which is the time during which the detector does not count after the arrival of the X-ray photon.

Finally, beam scanning analysis can be carried out using the deflection plates shown in figure 1.16. Alternately energising these deflection plates moves the electron beam back and forth across the sample, and an image can be displayed on a cathode ray tube.

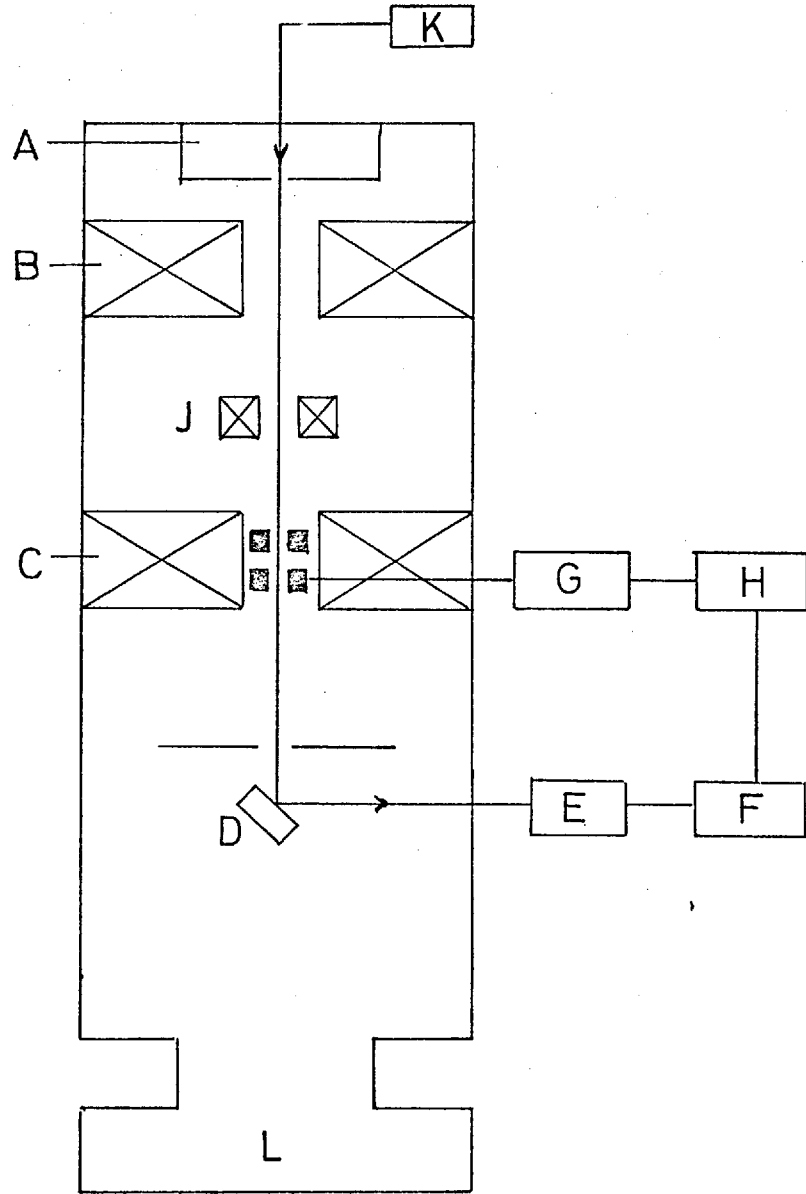
1.3.d Energy dispersion analysis of X-rays (E.D.A.X.)

The E.D.A.X. technique has developed as an analytical tool associated with scanning electron microscopy. A block diagram of a scanning electron microscope is shown in figure 1.17. Reviews of the technique and instrumentation and X-ray microanalysis have been given by Russ (153) and Yakowitz (154).

The instrument is basically similar to the electronprobe microanalyzer described earlier. Electromagnetic lenses are used to produce a fine beam of electrons of energy 30 - 50 kV and to focus it onto the specimen surface. The beam is scanned over the specimen in synchronisation with a display cathode ray tube.

The technique is best compared with that of E.P.M.A. although the intended use may be different. The surface penetration depth is 0.5 micron compared with 2 microns in E.P.M.A. Scanning electron microscopy is an imaging microscope technique, for examination of surfaces at higher magnification than those obtainable with optical microscopes. As the surface topography of the specimen is under investigation, then samples may be rough, so the secondary electrons emitted from the surface are collected and amplified for imaging. The increased depth of field associated with S.E.M. (several hundred times that of an optical microscope) is a distinct advantage when studying uneven surface topography. E.P.M.A. however is not suitable for rough surfaces and requires flat polished specimens. The maximum magnification associated with a scanning electron microscope can be up to X 50,000, which is much higher than that associated with E.P.M.A. (X400 to X500).

The beam diameter in S.E.M. is smaller, of the order of 100 \AA , which is lower than that of E.P.M.A. ($1 \mu\text{m}$). This reduction in beam diameter is accompanied by a reduction in beam current from



- A Electron gun
- B Condenser lens
- C Objective lens
- D Specimen
- E Amplifier
- F Display unit
- G Magnification unit
- H Scanning circuit
- J Stigmator
- K Electron gun supply
- L Vacuum system

10^{-8} A with E. P. M. A. to 10^{-12} A with S. E. M. This lower beam current causes a proportionate reduction in all the signals generated, including the characteristic X-rays.

Energy dispersion analysis is used because it is better suited to the low X-ray fluxes associated with S. E. M. Electronprobe microanalysis uses wavelength dispersion (W. D.) spectrometry to analyse the emitted X-ray lines. Wavelength dispersion spectrometers use collimators to restrict the analysed X-ray beam to a very small angle, giving counts of the order of 10^5 s^{-1} , for a 10^{-7} A beam on a pure element. The low beam currents associated with S. E. M. mean that W. D. spectrometers would need to count 1 s^{-1} , which is clearly not practical.

Energy Dispersion (E. D.) spectrometers require very little collimation, only sufficient to stop X-rays excited by back-scattered electrons which strike other parts of the specimen from reaching the detector. Hence the detector can be placed closer to the specimen which automatically increases the count rate 100 times.

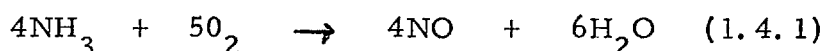
In contrast to W. D. analysis, in which the diffraction of X-rays by a crystal of known d spacing is the determining factor for wavelength determination, E. D. does not require crystals which reduce overall efficiency by 80% in W. D. spectrometers.

Limitations do arise with energy dispersion however, when it is used to detect light elements. This is due to the use of beryllium windows 0.025 mm thick over the detector. This will detect 15% of incident sodium X-rays (1.04 KeV). Thinner windows are more porous and lack film strength.

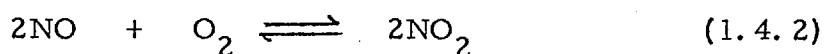
Qualitative analysis by energy dispersion involves the detector collecting the entire X-ray spectrum entering it and a multichannel analyser is used to divide the spectrum into energy packets, corresponding to a convenient energy such as 25 or 50 eV. Moseley's Law is used to relate the characteristic energy of an X-ray peak to the atomic number of the element responsible for that signal. Thus by determining channel numbers, or the energy of peaks in the spectrum, appropriate atomic numbers can be assigned to these signals.

1.4. The mechanism of catalytic ammonia oxidation

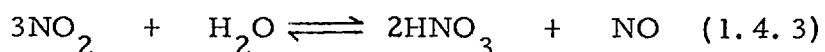
The availability of synthetic ammonia led directly to a process for the preparation of nitrogen oxides by reaction of ammonia with air:-



Nitric oxide is further oxidised to nitrogen dioxide by excess oxygen

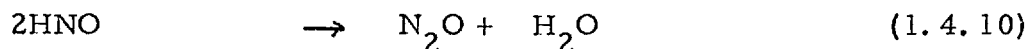
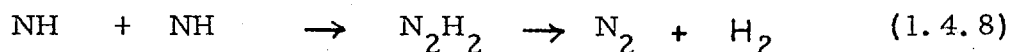
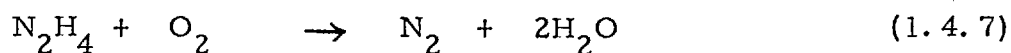
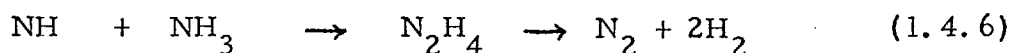
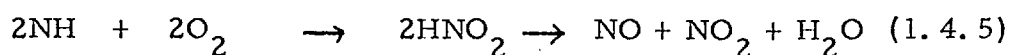
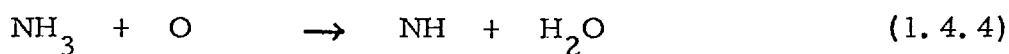


The nitrogen dioxide may then be absorbed by water in scrubbing towers, forming nitric acid and more nitric oxide which is further reacted with excess air.

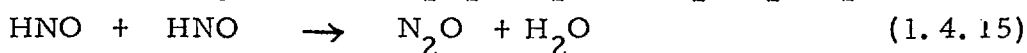
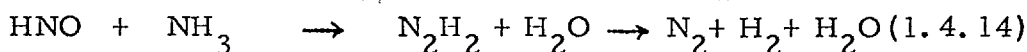
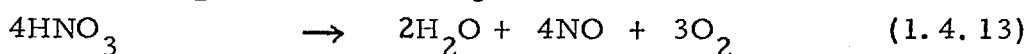
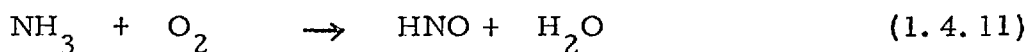


Many workers have studied the formation of nitric oxide as in equation (1.4.1). Dixon and Longfield (110), Bond (108) and Zawadzki (155) have reviewed the earlier mechanisms.

The 'imide' theory, attributed to Raschig, may be summarised as follows.

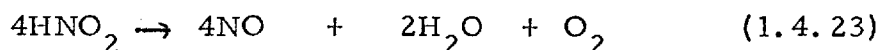
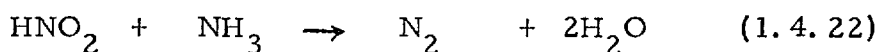
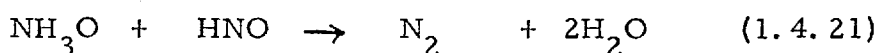
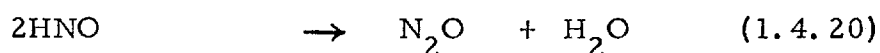
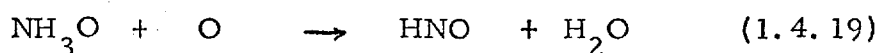
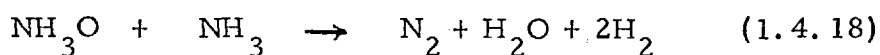
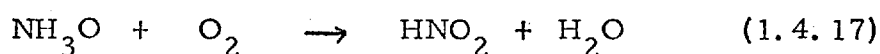
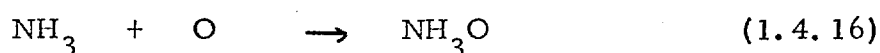


The rival 'nitroxyl' theory of Bodenstein can be represented as follows



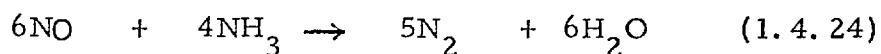
Bodenstein followed this theory by studying the oxidation of ammonia on a platinum wire at low pressure and freezing out the products at liquid air temperature. Nitrous acid, hydroxylamine (NH_2OH or NH_3O) and nitrogen were the main products of the reaction. Further reactions in the gas phase produced nitrous acid from the hydroxylamine. He also noticed that little if any hydrazine was obtained either in the presence or absence of oxygen.

The results of these experiments led Bodenstein to modify his nitroxyl theory as follows.

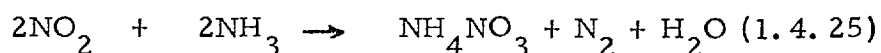


This theory does give rise to some highly improbable reactions, such as (1.4.23) in which four molecules must react together simultaneously or (1.4.18) in which two molecules react to give four product molecules.

Zawadzki (155) has critically reviewed both mechanisms and suggested modifications. Basically, any postulated mechanism must differentiate between reactions at the catalyst surface, and in the gas phase. Thus, at low flow rates, counter current diffusion is possible leading to reaction between nitric oxide and ammonia.

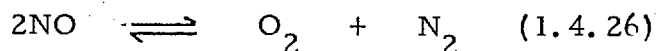


or nitrogen dioxide and ammonia



With packs of thirty plus gauzes it is possible that this reaction could take place on the gauzes lower in the pack. However, this reaction

does not lower the yield appreciably and the yield is similar if the reaction is carried out on three gauzes. This indicates that the reaction,

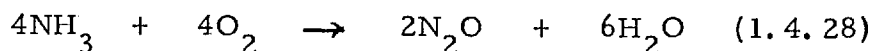


is not important under the reaction conditions. Falk and Pease (156) have shown that ammonia and nitrogen dioxide react together to give ammonium nitrate, nitrogen and water as shown in equation (1.4.25). Thus it is essential that a high gas velocity be maintained.

Whilst there is no optimum temperature for the catalyst to work, the higher the temperature of operation, then the greater the gas velocity if the maximum yield of nitric oxide is to be maintained, and undesirable side reactions avoided, such as (1.4.26) and

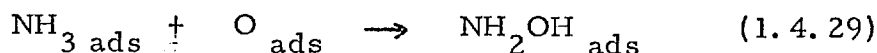


At temperatures below 500°C , the formation of nitrous oxide is favoured.



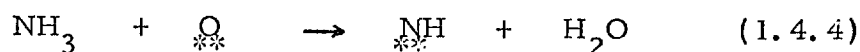
The nitrous oxide formed is at the expense of nitric oxide. Nitrous oxide will decompose readily into nitrogen and oxygen, and the higher the temperature, and the greater the contact time, then the greater the decomposition of nitrous oxide.

Zawadzki concludes that the formation of HNO in the nitroxyl theory (1.4.19) is not an intermediate but a side reaction, giving rise to nitrous oxide in the product stream (1.4.20). Also, the nitroxyl theory assumes that both molecular oxygen and ammonia are adsorbed on the catalyst surface. Zawadzki quotes Langmuir, to the effect that adsorption of atomic oxygen occurs, but not ammonia. Work carried out in this thesis (section 5.1.5) also shows that no ammonia is adsorbed at the catalyst surface. Hence the reaction

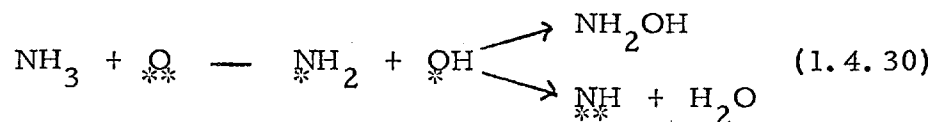


is unlikely to occur.

Following this, Zawadzki has developed the 'imide' theory of Raschig. He argues that the initial reaction step must be exothermic to account for its high efficiency, and describes this as



the asterisks indicating an adsorption site on the catalyst. A transition state is produced which gives rise to hydroxylamine.



Thus, nitrous acid could then be formed by



which may decompose according to (1.4.5). Nitrous oxide is formed at low temperatures due to the reaction between surface adsorbed species as follows.

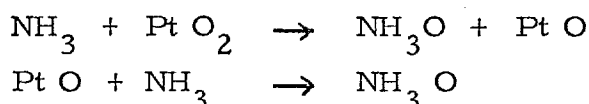


followed by (1.4.10).

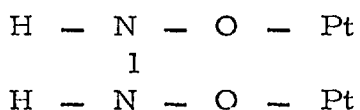
The hydrazine intermediate has been positively identified by Raschig.

These processes do not necessarily reflect the actual mechanism under industrial conditions. Very often work has been carried out at lower temperatures or pressures than those of commercial processes, and these elementary step reaction systems must be viewed with caution. With the advent of more highly sophisticated spectroscopic techniques it is possible that more light will be thrown on the actual mechanism occurring at the surface. These techniques suffer from the disadvantage of working at pressures considerably below that pertaining to the commercial process.

Dixon and Longfield (110) have concluded that reaction occurs between ammonia in the gas phase and adsorbed oxygen atoms as follows.



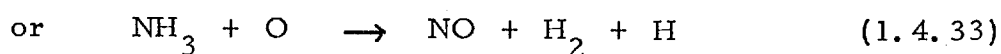
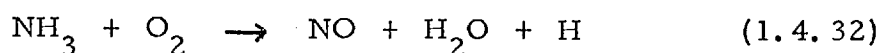
Ashmore (157) however favours the formation of a surface complex at lower temperatures



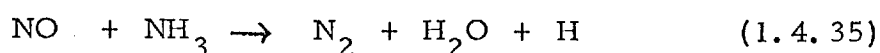
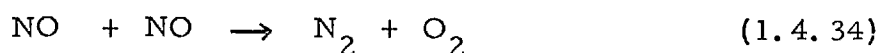
which breaks down to give hydrogen, nitrous oxide, and a surface which can be readily oxidised by the excess oxygen. He then speculates that temperature effects the lifetime of the chemisorbed HNO intermediate. Low temperatures seem to favour longer life and increase the chances of N - N bond formation. Finally, he states that high temperature infra-red spectroscopy ought to be able to determine the true mechanism of the effects.

Fogel and his coworkers (158) (102) (103) (159) (160) (161) (162) have used secondary ion emission to study the catalytic oxidation of ammonia on platinum, the reaction between ammonia and nitrous oxide and the decomposition of nitrous oxide on platinum. Mass spectra of secondary and gas phase ions were obtained for temperatures varying from 20 - 1200°C at pressures of 10^{-4} mm Hg. They obtained results which showed that the reaction commenced at 200°C under these conditions, producing ions of mass 18(H_2O^+), 28(N_2^+ and CO^+) and 30(NO^+). Thus they conclude that under these conditions, the reaction is purely heterogeneous. No ions with masses 31(HNO^+), 33(NH_2OH^+), 47(HNO_2^+) or 79(HNO_4^+) were present. Thus they conclude that intermediate compounds such as HNO or NH_2OH are not formed in quantity.

The authors concluded that the principal final products of ammonia oxidation may arise by direct reaction of ammonia with oxygen. By studying mass lines 32(O_2^+) and 16(O^+) they conclude that both atomic and molecular oxygen are present on the catalyst surface. These two species can be used to oxidise ammonia as follows.



No intermediates are involved in their reaction mechanism, so nitrogen formation may arise by

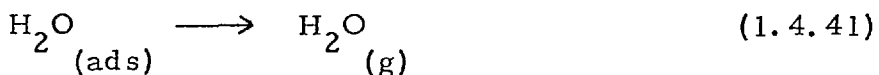
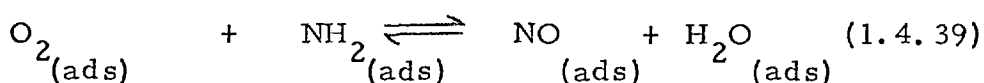
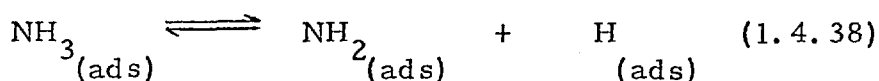
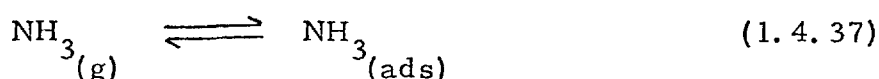
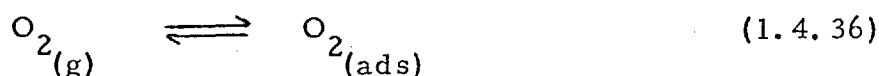


It is unlikely that (1.4.34) is the cause of nitrogen production. In a high pressure ammonia oxidation plant the product mixture has to

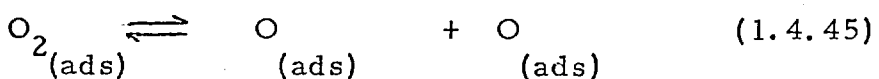
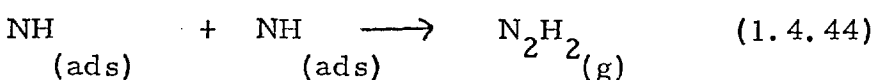
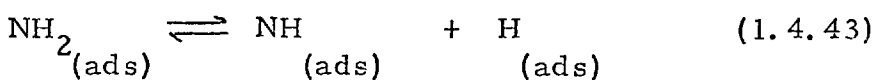
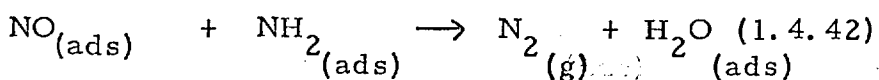
pass through a further 20 - 30 gauzes before absorption in water, yet no appreciable quantities of nitrogen are obtained. Hence (1.4.35) is probably the correct mechanism for nitrogen formation.

Perhaps their most significant suggestion is that ammonia and oxygen adsorb on the catalyst surface giving rise to a Langmuir Hinshelwood mechanism for the formation of nitric oxide. They show that oxygen penetrates an adsorbed ammonia layer, but does not completely replace it. Whilst this may be true for the conditions of the study, it does show that great care must be taken in extrapolating these results to atmospheric conditions.

Nutt and Kapur (101) (33) have used molecular beam techniques to sample the species from the catalyst surface in collision free conditions. They estimate their reactant concentrations to be equal to an ambient pressure of 10^{-2} mm Hg, to ensure that the reaction products were not back-reflected onto the catalyst surface. They predict the main oxidation route to occur as follows

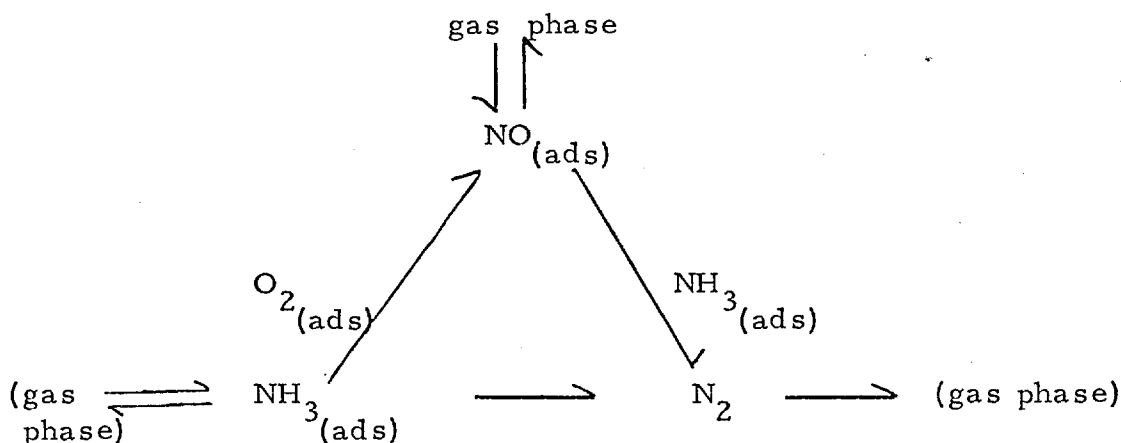


They also predict low (1.4.42) and high (1.4.43 - 45) temperatures side reactions occurring as outlined below.

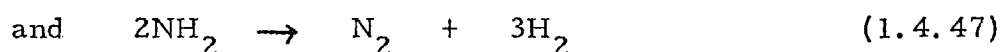
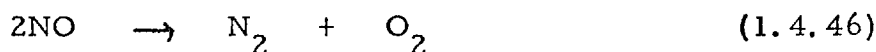


It can be seen from (1.4.39) that Nutt and Kapur are agreeing with Fogel et al that the Langmuir Hinshelwood mechanism is operative. Once again however, this work was not carried out at atmospheric pressure and direct comparison between this mechanism and the commercial process may not be applicable.

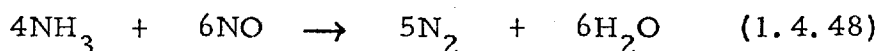
Recent work by Pignet and Schmidt (163) has resulted in the following series - parallel scheme



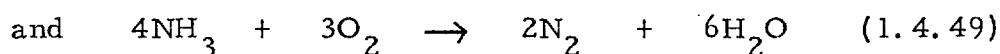
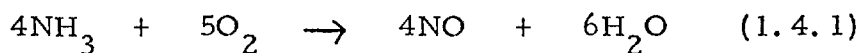
They divided their experiments into three stages, the first being the unimolecular decomposition of nitric oxide and ammonia on platinum.



Secondly, the reaction of nitric oxide with ammonia on platinum.



Finally, they considered the reaction of ammonia and oxygen on platinum.

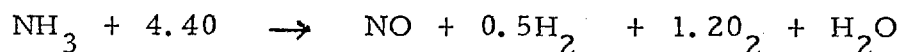


From their results they conclude that three surface reactions appear to be in competition, these being nitric oxide formation from oxygen and ammonia, nitrogen formation from nitric oxide and ammonia, and decomposition. They also observe a smooth transition from nitrogen production to nitric oxide formation, which eventually reverts to nitrogen production again. This they explain, in the low temperature region, by rapid formation of nitric oxide from ammonia and oxygen at low temperature,

but the nitric oxide formed is bound strongly to the catalyst, possibly reacting with more ammonia, to form nitrogen. As the temperature increases, more nitric oxide escapes the catalyst surface, and the selectivity moves towards nitric oxide production. At approximately 800°C, virtually all the nitric oxide formed escapes, but beyond this temperature, the formation of nitric oxide becomes adsorption limited, thus resulting in the overall decay of nitric oxide formation to ammonia decomposition. It is one of the features of the Langmuir Hinshelwood mechanism that decreasing surface coverage of reactant produces a decreased surface reaction rate, and the treatment relies on the fact that the adsorption process is much faster than the surface reaction, which may not be the case in commercial atmospheric pressure conditions. Finally, Pignet and Schmidt surmise that surface oxygen inhibits the ammonia decomposition process, whilst favouring the bimolecular NO - NH₃ reaction at low temperatures. They conclude that its role may be to maintain the catalyst surface free of contaminants.

Work has been carried out by Molinari et al (104) (164) into the influence of gaseous oxygen atoms on the catalytic oxidation of ammonia on cobalt oxide. This work showed oxygen atoms present in the gas phase not only lowered the activation energy of the catalytic process, but increased the yield of nitric oxide, to the point that nitric oxide and water were the only reaction products. This effect they ascribe to an increased coverage of the surface with oxygen atoms.

Wong and Potter (165) have studied the gas phase reaction of oxygen atoms with ammonia, with no molecular oxygen present, at temperatures between 350 - 600 K. They obtain an overall stoichiometric equation



This is in contrast to work carried out by Branch and Sawyer (166), who studied the gas phase oxidation of ammonia in oxygen in an arc heated flow reactor between 1,100 - 1,377 K. Their results show that nitrogen and water are the major stable products of the reaction with no detectable production of nitrogen oxides.

Finally, reference must be made to the Russian work on a heterogeneous - homogeneous reaction mechanism for ammonia oxidation. Bretsznajder (167) (168) has found that the rate of oxidation of ammonia to nitric oxide at atmospheric pressure shows a 20% increase on the rate which would have been obtained if all the reacting molecules had to come into contact with the catalyst.

Early studies by Vladov (169) and Vainstein and Polyakov (170) have shown that ammonia oxidation commences on the surface of the catalyst and moves into the gas phase, providing a mixed heterogeneous - homogeneous mechanism. The studies indicated that activated particles were produced on the catalyst, though they could not prove that these particles were the cause of the reaction process.

Later work by Vladov (171) established the presence of this heterogeneous-homogeneous mechanism by comparing the temperatures of the ammonia/oxygen gas stream. In a gas stream of 1 - 20% ammonia, the temperature behind the catalyst was higher than in the oxygen stream, whereas with 80 - 99% ammonia the temperature behind the catalyst was lower than in the ammonia stream. He concludes that the degradation of ammonia is a heterogeneous/homogeneous reaction, involving an exothermic reaction in a reaction area away from the catalyst, liberating a quantity of heat greater than that of the ammonia oxidation.

Further work by Vladov (172) (173) (174) suggests that only a small fraction of the ammonia is oxidised by direct contact with the catalyst surface, whilst a chain reaction proceeds into the space adjacent to the catalyst. Approximately half of the total heat is evolved in the reaction space after the catalyst.

Finally, Vladov (175) has measured the activation energy of this process and found it to be $3,450 \pm 450 \text{ cal mol}^{-1}$. He also concludes that a homogeneous reaction zone is present around the catalyst which decreases with rise in temperature.

1.5. The kinetics of catalytic ammonia oxidation

The determination of the kinetics and mechanism of the ammonia

oxidation reaction can produce varying results if mass-transport considerations are not taken into account. If mass-transport to the catalyst is adequate, then a heterogeneous reaction will be possible. Inadequate mass transport could produce a heterogeneous/homogeneous mechanism (section 1.4). Thus when calculating activation energies for the ammonia oxidation reaction, it is essential to specify exactly the nature of the catalyst and the experimental conditions involved. Many authors have produced activation energies for the ammonia oxidation reaction and these are summarised in table 1.4.

Atroschenko (184) has studied the oxidation of ammonia on two wire mesh grids, 26 cm. apart. He found that a considerable proportion of the ammonia passed the first grid unreacted, and deduced that the reaction is taking place on the surface of the catalyst only. Further, he deduced that the unreacted ammonia was reacting with nitric oxide after the gauze according to equation (1.4.48).

Very recently Atroschenko (177) has developed an empirical equation for the reaction rate constant k , which allows for not only the oxidation of ammonia to nitric oxide but also to nitrogen and the reaction of nitric oxide with ammonia.

$$k = \frac{1}{t \left\{ \alpha_{\max} \ln \left[\frac{\alpha_{\max}}{\alpha_{\max} - \alpha} \right] - \alpha \right\}}$$

where t is the time and α is the yield of nitric oxide, where

$$\alpha_{\max} = 3.9 T^{0.46} - P^{-0.02}$$

is the maximum obtainable yield at a given temperature T (K) and pressure P (atm). This equation gives results which deviate from experimental values by 0.3 - 0.6%, and gives an activation energy of $33.5 \text{ kJ. mol}^{-1}$.

1.6. Present work

The literature review in the previous sections shows that little

Table 1.4

Reference	Catalyst Temperature	Order in [NH ₃]	Activation Energy
Atroschenko (176) (177)	Pt. 1123 - 1283°C		33.5 k J mole ⁻¹
Zasorin (178)	Pt grid	1	6.1 - 6.4 kcal mole ⁻¹
(179)	Combination Catalyst Fe-Cr oxide + Pt	1	1.45 - 2.5 kcal mole ⁻¹
Zasorin (180) (181)	Pt + H ₂ O vapour	1	26.5 k J mole ⁻¹
Vladov (175)	Pt/Rh wire 630 - 1015°C		3.45 ± 0.45 k cal mole ⁻¹ (homogeneous reaction zone)
Pan (134)	Pt/Rh gauze 1050 - 1250°C	1	(HCN synthesis)
Williamson (182)	Cu II NaY Zeolites 175°C	1	36.7 ± 2.6 k cal mole ⁻¹
Bradley (183)	Non Catalytic NH ₃ + O ₂		60 k cal mole ⁻¹
Alkhazov (7)	Bi - Mo 1.2	1.5	11 k cal mole ⁻¹
Molinari (164)	Co O Co O + oxygen atoms		30 k cal mole ⁻¹ 9 k cal mole ⁻¹

work has been undertaken on the activation and deactivation of platinum/rhodium catalysts during the oxidation of ammonia. The work described in the following sections was undertaken to rectify this omission.

The following effects were investigated with reference to catalyst activation.

- (a) Do surface contaminants influence light-off temperature and activity?
- (b) Are geometric and electronic factors important in the activity of the catalyst?
- (c) The nature of adsorption at the catalyst sites.
- (d) Is alloy composition important in its relation to activity?

Deactivation was then studied by doping the catalyst with metal oxides. Induced geometric effects and electronic effects have been considered in their relation to catalyst activity.

Finally a method of calculating catalyst weight loss occurring during reaction has been improved and its application extended to high pressure ammonia oxidation processes.

CHAPTER 2

EXPERIMENTAL

		Page.
2. 1.	<u>Reagents</u>	93
2. 2.	<u>Apparatus</u>	
2. 2. a.	Gas - mixing system	93
2. 2. b.	Furnace	94
2. 2. c.	Reactors	94
2. 2. d.	Thermocouples	99
2. 3.	<u>Analysis</u>	
2. 3. a.	Wet method	100
2. 3. b.	Gas chromatography	101
2. 3. c.	Microscopy and photographs	104
2. 3. d.	E. S. C. A. and U. P. S. investigations	108
2. 3. e.	E. P. M. A. investigations	109
2. 4.	<u>Catalytic Studies</u>	
2. 4. a.	<u>Activation studies</u>	
2. 4. a. (i)	Laboratory work	109
2. 4. a. (ii)	Surface diffusion experiments	111
2. 4. b.	<u>Doping studies</u>	
2. 4. b. (i)	Doping methods	111
2. 4. b. (ii)	Temperature effects	112
2. 4. b. (iii)	Variation in light-off temperature with surface coverage	113

2. Experimental

2.1. Reagents

The materials used in the experimental work are shown below.

Gases

<u>Gas</u>	<u>Supplier</u>	<u>Grade</u>	<u>% Purity</u>
Oxygen	B. O. C.	commercial	99.5
nitrogen	"	O ₂ free	99.9
hydrogen	"	commercial	99.9
ammonia	"	anhydrous	99.98
helium	"	A	99.998
nitric oxide	"	technical	99.0
carbon dioxide	"	"	99.0

Gauzes

Pt/10%Rh, 0.003" diameter, 80 meshes per linear inch.

Foils

Pt/10%Rh, 0.003" thickness

Pt/40%Rh, 0.003" thickness

Thermocouple wire

Pt/13%Rh, 0.003" diameter

2.2. Apparatus

2.2.a Gas-mixing system

The gases were piped to a flowboard, using $\frac{1}{4}$ " O.D. P. V. C. tubing. A glass tube, 1 foot in length was incorporated in each gas line. Each tube was packed with dried molecular sieve 13 X 30/60

mesh and glass wool. This ensured that the gases were dry and dust-free before mixing.

The rotameters were supplied uncalibrated by G. E. C. Elliot Ltd. Each rotameter had a flow capacity of between 100 and 1,200 $\text{cm}^3 \text{min}^{-1}$, except for the nitrogen line, which had a capacity of $1\text{-}5 \text{ dm}^3 \text{min}^{-1}$. The rotameters were calibrated using the soap-bubble flow meters for their respective gases at a pressure of 12 cm. mercury. After flowing into the main gas line, the gases were mixed in the flame trap which was constructed from 1" O.D. pyrex glass tubing, nine inches in length and filled with small pieces of glass rod.

2.2. b Furnace

To preheat the reactant gases, a furnace was constructed from $1/10$ " Pierrite in a Dexion frame to a size 8" x 8" x 8". An inner lining of Kao wool was provided and the space around the central furnace tube packed with Vermiculite to provide heat insulation. The furnace tube, of aluminous porcelain of $1\frac{1}{2}$ " I.D., was wrapped in Nichrome wire, which was held in place with alumina cement. Twelve yards of Nichrome wire, resistance $2.49 \Omega \text{yd}^{-1}$, were used giving a total resistance of 30Ω . The Nichrome wire was double wound around the lower end of the furnace to provide extra heating capacity. When the reactor was in place, both ends of the furnace were closed with Kao wool to prevent excessive heat loss.

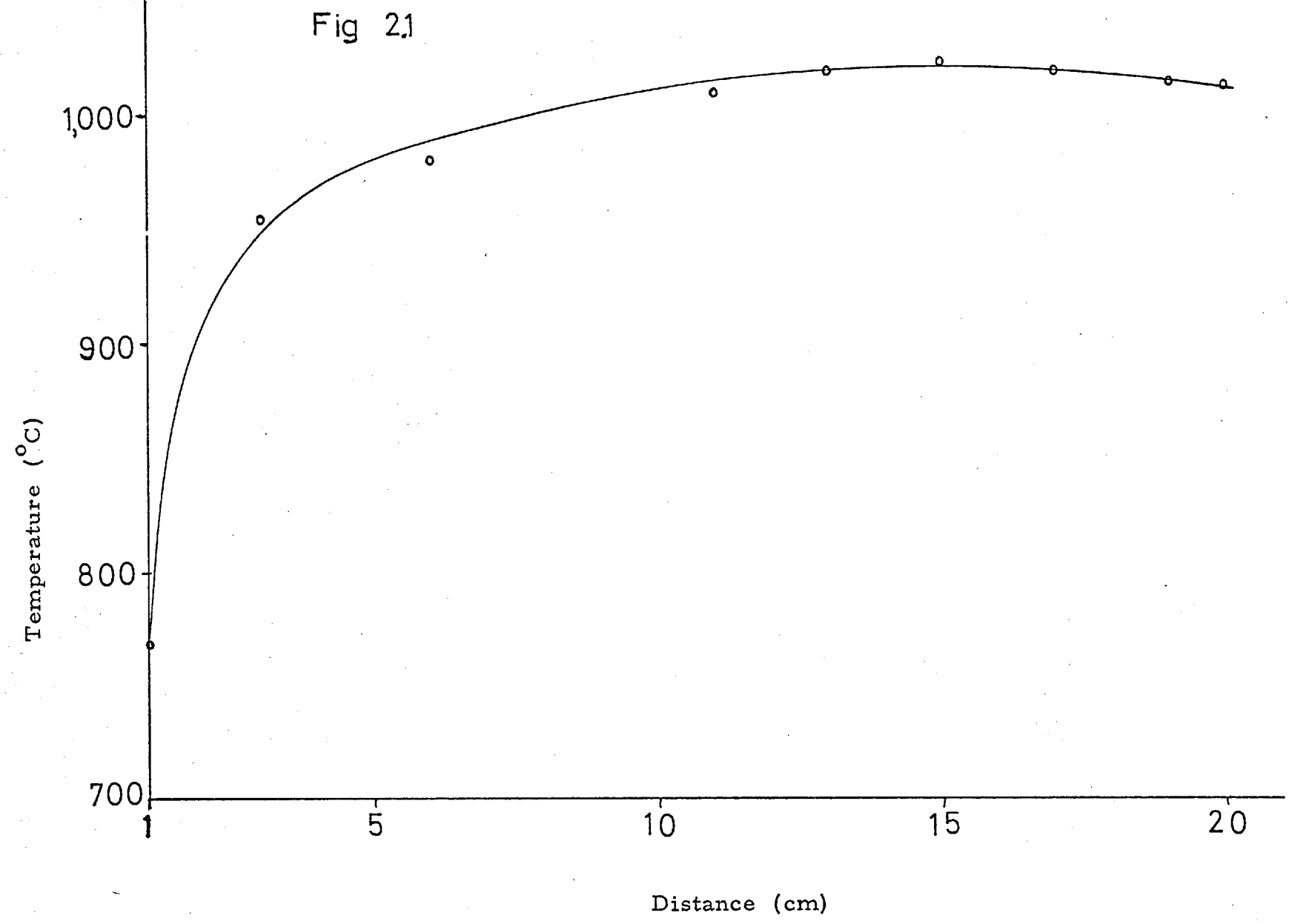
The furnace was powered by an A. E. I. 17.5 amp power regulator, coupled with an A. E. I. resistance thermometer controller.

The temperature distribution along the furnace is shown in Fig 2.1. The distance is measured from the top (inlet) end of the furnace to the lower end where the reaction takes place.

2.2. c Reactors

The industrial design of an ammonia oxidation burner is basically very simple (section 1.1.d). On a laboratory scale however, various modifications have been incorporated. These can be described as follows.

Fig 2.1



- (1) To obtain gas temperatures before and after the gauze pack, thermocouples have to be incorporated above and below the gauze pack.
- (2) The gauze pack must be accessible and easily removable for analysis.

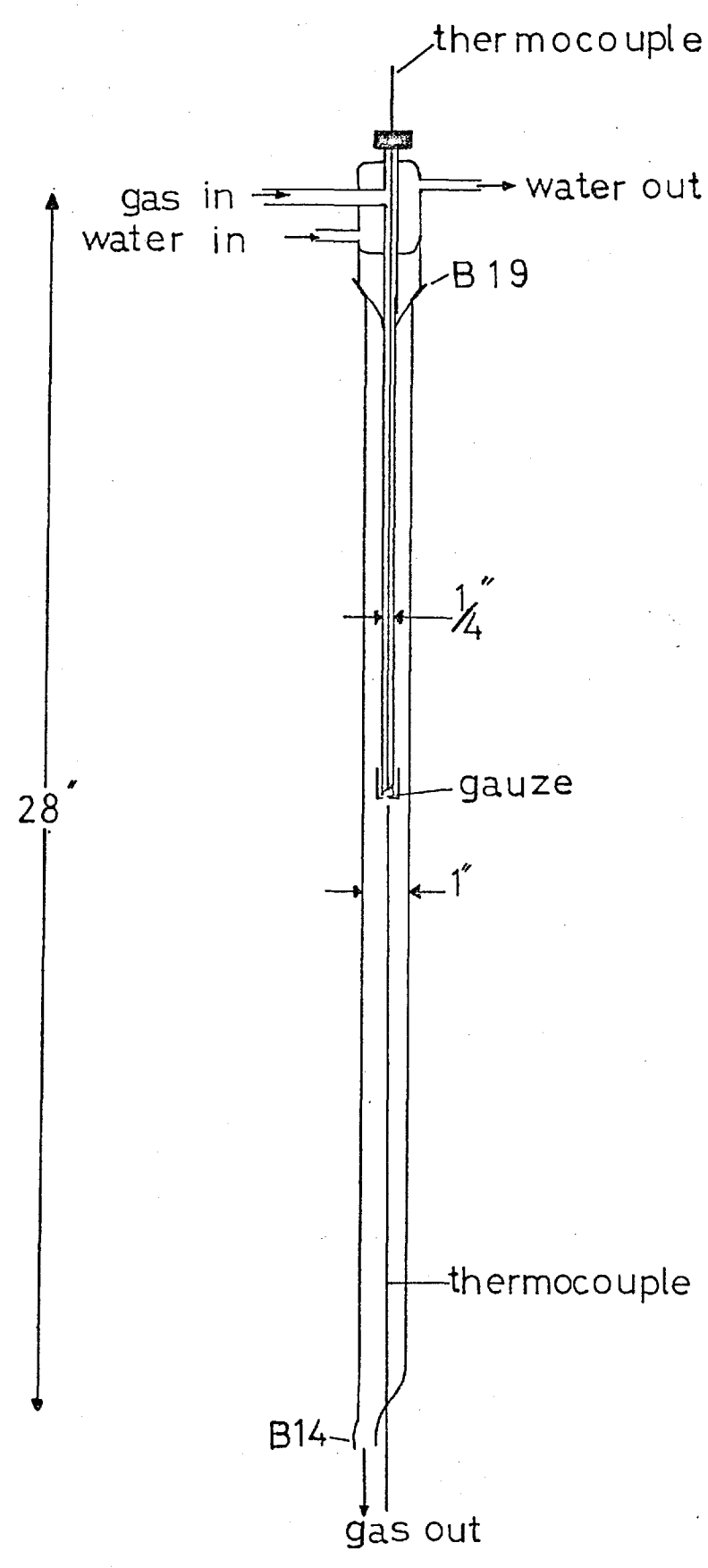
The first reactor designed was constructed in stainless steel. Experience with this reactor showed it had two major draw-backs.

- (1) It proved difficult to handle when hot i. e. it had to be cooled before it could be opened. This was a major draw-back when it became necessary to investigate the gauze whilst the reactor was hot.
- (2) It was difficult to obtain efficient sealing of the reactor whilst it was hot, thus giving rise to gas leaks. Industrial reactors are sealed with gold gaskets between steel-steel faces. This was impractical for laboratory use.

To avoid these difficulties, the Mark I reactor shown in Fig 2. 2. was constructed. The pack of three gauzes was mounted in a 'bayonet' cap and could be withdrawn easily. The problems of sealing were overcome by using quartz cones and sockets, and the complete reactor was made of silica for easy handling. Silica proved to be completely inert towards ammonia oxidation as opposed to stainless steel on which the ammonia oxidation reaction can occur at high temperatures. The wet method of analysis (section 2. 3. a) was used with this reactor. This method however proved inadequate and following the failure of the on-line technique (section 2. 3. b) this reactor was abandoned in favour of the Mark II reactor shown in Fig 2. 3.

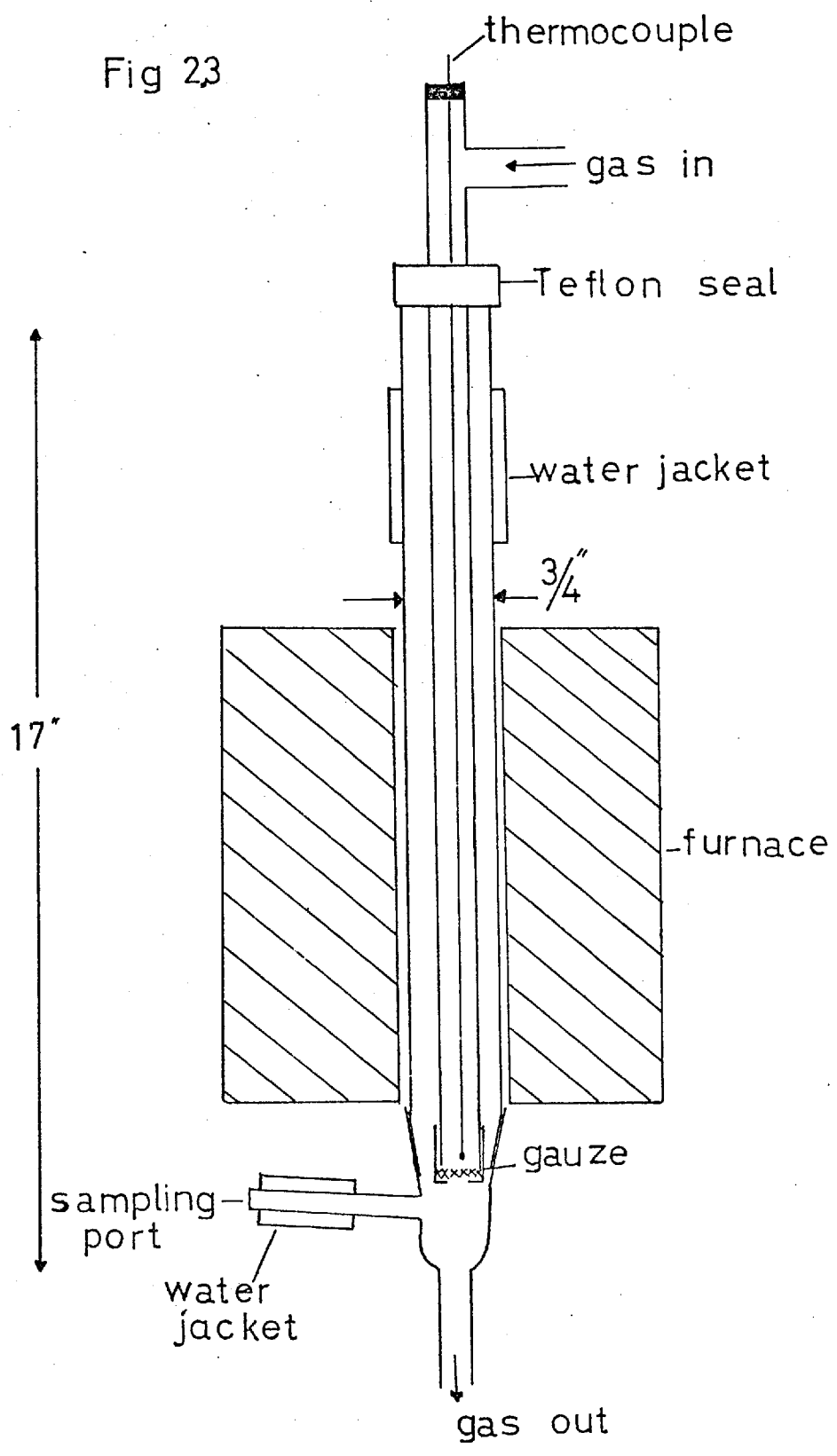
This reactor incorporates several improvements over the Mark I reactor. The most important of these is the ability to activate in any gas, and then run in a 10% NH_3 /air mixture without admitting laboratory air into the reactor and without waiting for the reactor to cool from the activating temperature. This is achieved by constructing

Fig 2.2.



Ammonia Oxidation Reactor Mk I

Fig 23



Ammonia Oxidation Reactor Mk II

the reactor with the central tube movable. Hence, in the activating mode, the gauze is raised to the centre of the furnace. After activation, the gauze can be lowered into the running mode as shown in Fig 2. 3. Water jackets conduct the heat away from the Teflon seals and the sampling port. Analysis is carried out by the injection method (section 2. 3. b).

2. 2. d Thermocouples

The thermocouples utilized in the Mark I and II reactors had to satisfy three important conditions.

Firstly that they could have to be of the same composition as the catalyst gauze, to enable thermocouples to be attached directly to the gauze in order to measure gauze temperature. Pt/13%Rh thermocouples have therefore been used throughout.

Secondly, the sheathing would have to be resistant to high concentrations of nitric oxide and ammonia at temperatures in excess of $1,000^{\circ}\text{C}$. Hence silica sheathing has been used for thermocouple construction.

Thirdly, the thermocouple would have to register large changes of temperature very rapidly i. e. have a short response time.

To fulfil these three important criteria Pt/13%Rh thermocouples were constructed using silica sheathing.

The outer tube was first formed by pulling down a piece of $\frac{1}{4}$ " O.D. silica tube. This tube was cut to the required length and one end sealed. A small bubble was then blown at the closed end, the diameter of this bubble being not greater than $\frac{1}{16}$ ". A silica tube of smaller bore was then pulled down, so that it could slide inside the larger bore tube. A piece of .0.003" dia. platinum wire was then inserted into the inner silica tube. A similar length of Pt/13%Rh wire, also 0.003" dia. , was welded to the platinum wire and the whole assembly inserted into the outer silica sheath. Finally, the open end was sealed with 'Autostic' high temperature adhesive, taking care that the thermocouple did not touch the outer silica wall.

The thermocouples were then incorporated into the apparatus as shown in figures 2.2 and 2.3. The reference thermocouple was immersed in an ice/water mixture and copper compensating leads were used throughout.

The thermocouples were calibrated against a standard chromel/alumel thermocouple supplied by Spemby Technical Products Ltd., used in conjunction with a Cropico P6 thermocouple potentiometer.

Two serious problems relating to thermocouple construction were encountered. The first was due to the fact that the gas temperature immediately after the gauze was approximately that of the melting point of silica. This resulted in the gas mixture gaining access to the surface of the thermocouple, giving a catalytic reaction on the thermocouple tip and consequent high temperature readings. This problem was overcome by using an outer sheath of EN 58B stainless steel tubing. This modification then gave rise to the second problem, that of a chemical reaction occurring on the thermocouple sheathing. Above 800°C , it was found that ammonia was oxidised on the thermocouple sheath, and that the thermocouple placed immediately after the gauze gave rise to back-reflection of the product gases into the gauze, thus resulting in incomplete oxidation and inaccurate analysis of gas products. Hence to obtain an accurate product analysis, the reactors were run with the lower thermocouple removed.

These thermocouples gave measurement errors of the order of $\pm 1.5\%$ and though this is high, corrections were applied to all temperature measurements.

2.3. Analysis

2.3.a Wet method

A titrimetric method, as devised by Gaillard (106), was used at first to analyse the products of the ammonia oxidation. Briefly, the method involved weighing an evacuated glass bulb (capacity 600 cm^3), introducing as rapidly as possible a sample of either inlet or product gas mixture and then titrating.

In the case of the reacting gases, ammonia and air, after collecting a sample, the bulb was immersed in distilled water and the tap opened. Due to the partial vacuum in the globe resulting from the cooling of the gas and the high solubility of the ammonia, water was drawn into the bulb. After all the ammonia had been absorbed, the tap was again opened and air blown into the bulb. The solution was then decanted into 25 cm³ of 0.2 M H₂SO₄ and the excess acid back-titrated with 0.1 M NaOH solution using methyl red indicator.

The procedure for the product gases was similar, though oxygen was used instead of air, and the solution transferred into sodium hydroxide solution. The resulting mixture was then back-titrated with the sulphuric acid solution using methyl red indicator.

This method is still used in pilot plants to determine conversions in ammonia oxidation reactions. In his paper Gaillard (106) states that an average precision of $\pm \frac{3}{4}\%$ can be obtained with this method.

This method did not prove suitable for this work, due to the fact that to operate the method successfully, a sample of at least 600 cm³ is required. This is necessary to give appreciable weight changes and sufficient sample volume to give meaningful titration results. On a pilot plant or commercial plant scale, in which flow rates are high and gauze areas much greater, a 600 cm³ gas sample can be obtained in approximately 5-10 seconds at the outside. However with the small gauzes and lower flow rates used in this apparatus, the time taken to collect 600 cm³ of sample was over 30 seconds. This caused moisture to condense in the neck of the sample bulb, and the gas cooled substantially before a complete sample could be collected. This rendered the method virtually useless, because neither air nor oxygen could then be admitted into the sample bulb without displacing the gas sample. These drawbacks resulted in gas chromatography techniques being developed.

2.3.b Gas Chromatography

One major advantage of gas chromatography is the decrease in time needed for analysis. The disadvantages for this particular

analysis, rest with the corrosive nature of the gases and with the fact that an on-line sampling valve created major pressure build-up. An on-line chromatograph was constructed but proved impossible to operate. As a result, a separate gas chromatograph was built, and samples of gas were injected with the aid of a syringe.

The method involves withdrawing a 1 cm^3 sample of gas from directly below the gauze. This is only possible using the Mk II reactor described previously. The sample is then injected into the gas chromatograph.

Hydrogen carrier gas passes into a microkatharometer, which is kept at a temperature of 40°C , and into a 3-way valve. The gas sample can be directed through a 2 metre Porapak Q column of $1/8''$ diameter at a temperature of 40°C or a 3 metre molecular sieve 13X column of $1/8''$ diameter, kept at room temperature. Injection ports were provided to inject the gas samples into the system. The Micro Katharometer (model Mk. 158) was supplied by Taylor Servomex and connected to a G. C. 197 Katharometer Bridge Control Unit. The signals were transferred to a Vitatron UR 402 M linear integrating recorder.

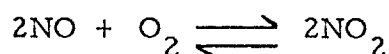
Prior to installation of the katharometer, the platinum resistances of the bridge were checked and found to be 30 ohms each which is within the manufacturers specification of 15-35 ohms each. The two columns were then activated by heating them to 200°C for 48 hours under flowing nitrogen. Following this, the columns were installed and calibration graphs obtained for the major components. The instrument conditions and retention times are listed below.

<u>Voltage</u>	5 volts
<u>Katharometer temperature</u>	40°C
<u>Column temperatures</u>	
Porapak Q	40°C
Molecular sieve	20°C
<u>Carrier gas</u> Hydrogen,	$13.5 \text{ cm}^3 \text{ min}^{-1}$, 10 p. s. i.

Retention times

<u>Gas</u>	<u>Molecular Sieve</u> <u>13X</u>	<u>Porapak Q</u> <u>40-60 mesh</u>
Nitrogen	2 min 15 sec	50 sec
Oxygen	1 min 30 sec	50 sec
Nitric oxide	3 min 40 sec	50 sec
Nitrous oxide		4 min
Nitrogen dioxide		5 min
Ammonia		9 min

There are several disadvantages with the G. C. system in its present form. Ammonia oxidation using gas mixtures of 10% ammonia/air contains oxygen in excess. This oxygen is then free to combine with the nitric oxide formed to give nitrogen dioxide.



This reaction is termolecular and it is possible that a reaction on the column may affect the position of the equilibrium. Therefore, activities quoted as a percentage of free nitric oxide in the mixture are only relative to that obtained from an active gauze, and no absolute values can be derived.

Water and any unreacted ammonia will irreversibly adsorb on the molecular sieve column eventually poisoning it, giving rise to irreproducibility. The molecular sieve column was therefore activated frequently and the calibrations and retention times checked before any experimental work was undertaken. Further, during each experiment, the calibration of the molecular sieve column was checked by frequently injecting volumes of air and monitoring retention times and integration values.

It has been noticed that errors arise from the recorder integrator and the fact that nitric oxide and ammonia give long tailing signals. To rectify this, the columns were heated, but with the molecular sieve, this proved impractical due to the oxygen and nitrogen signals coinciding. Overlap also occurred between the nitric

oxide and nitrogen signals at 40°C. The Porapak Q column and the katharometer were heated to 40°C, whilst the molecular sieve column was kept at room temperature, by surrounding it with Kao wool to act as an insulator.

Thus it would seem that there are several important regions in which errors can arise. The doping studies (see later) were carried out using a mixture of 14% NH₃/air, to eliminate the excess oxygen. This prevented any further reaction on the column and yields have been reported up to 92%.

The accuracy of the method was found to be $\pm 3.5\%$ for nitric oxide, which is considerably less than that normally encountered with gas chromatography determinations. However, the method gives rapid results (10 minutes) in contrast to the wet method described earlier, which takes 1 hour for each determination. The calibrations for nitrogen and oxygen show a greater accuracy of $\pm 0.6\%$.

Finally, to establish the suitability of the method for analysis of the ammonia oxidation reaction, it was tested with a 10% NH₃/air mixture using a gauze supplied by Johnson, Matthey Ltd. This gauze had previously been used in a high pressure ammonia oxidation pilot plant, and had developed full activity. The analysis is shown in figure 2.4. Following this, the method was checked using a gauze activated in oxygen (see later). The analysis is shown in figure 2.5. Finally the effect of varying the ammonia/air ratio over the active gauze supplied by Johnson Matthey Ltd. is shown in figure 2.6. The analytical method predicts 97.5% conversion to nitric oxide at 14.1% ammonia, whereas the volume of ammonia in the stoichiometric equation



is in fact 14.2% ammonia by volume.

2.3.c Microscopy and Photographs

Changes in surface topography were examined using an optical microscope. For this work an Olympus compound optical

Fig 2.4.

- N₂
- O₂
- NH₃
- NO

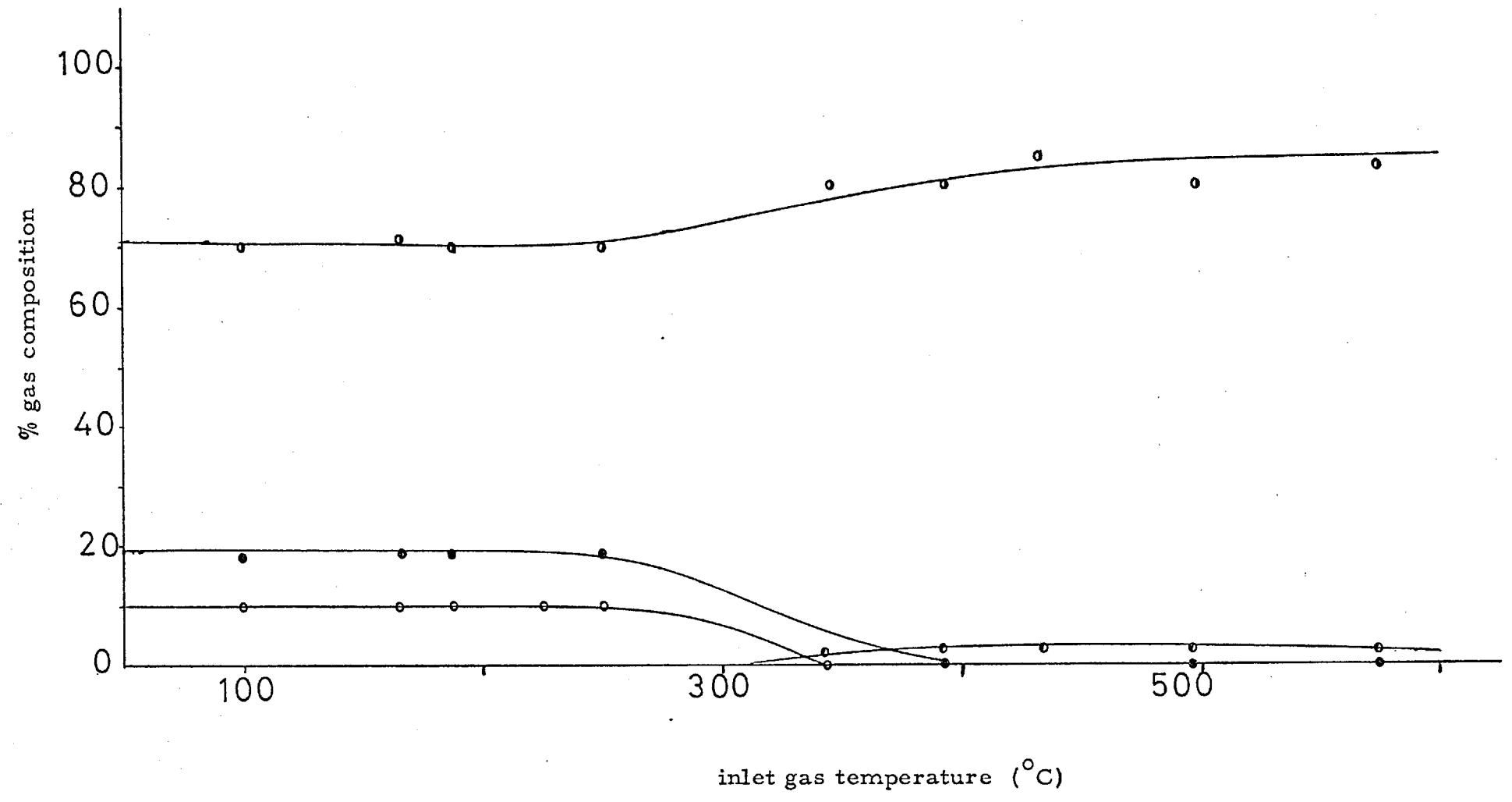


Fig 2.5.

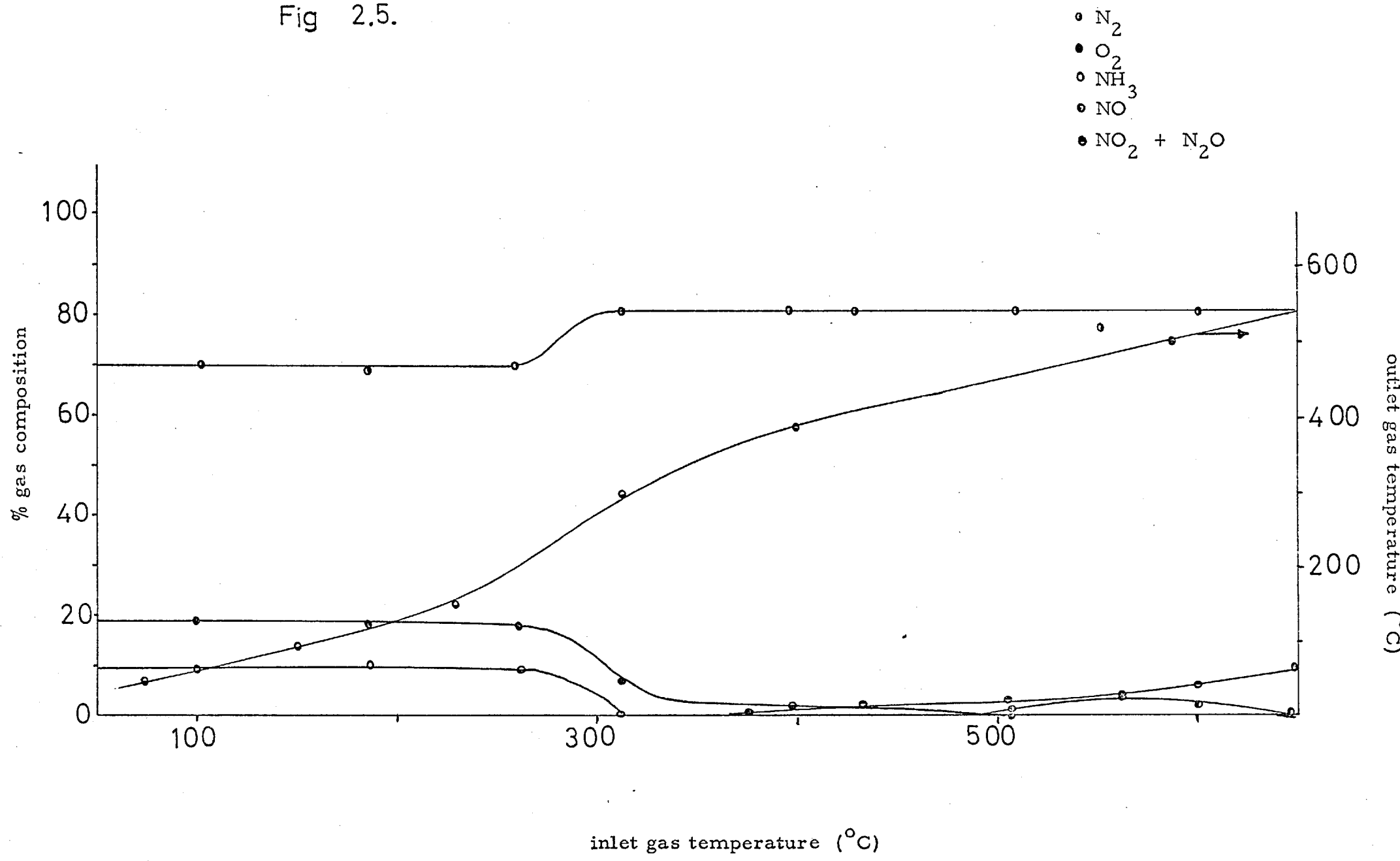
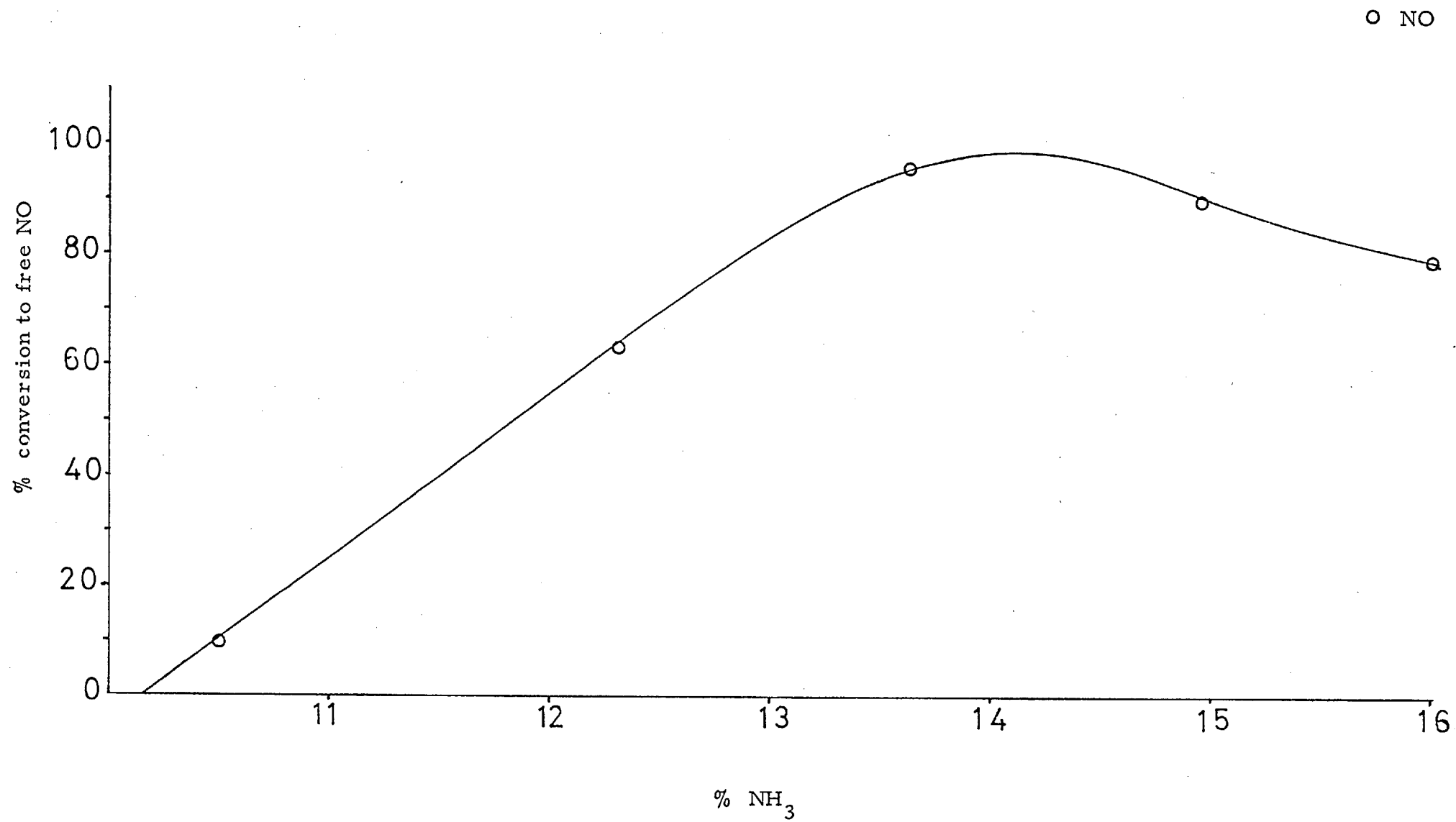


Fig 2.6.



microscope was used, enabling a maximum magnification of 600 times to be obtained. This microscope was used in conjunction with a microscope camera attachment. Photographs were taken from the central area of the gauzes and enlarged to give a greater magnification. This magnification was obtained by photographing a graticule with known line spacings. After developing and enlarging the negative, the inter-line spacing was measured, giving a magnification of 2,000 times.

When fine detail is required on a photograph, it is essential to use fine grain, slow speed film. In this work, Recordak Microfile film, type 566a was used, rated at 3ASA and developed for 3 minutes in Kodak D76 developer. After washing for 1 minute, the film was fixed in Amfix high speed fixer for 1 minute. The negatives were then printed on Kodak single weight, soft glossy paper, to give a high contrast print.

2.3.d E.S.C.A. / U.P.S. Investigations

The electron spectroscopy work was carried out using a Vacuum Generators E.S.C.A. 3 machine. Samples of platinum/rhodium foil and Pt/10%Rh gauzes were solvent washed and treated externally before insertion in the spectrometer. Three layers of Pt/10%Rh gauze produced signals of intensity equal to those obtained from a Pt/10%Rh foil.

The samples were mounted on a tungsten support ring, using either silver 'dag' or bending the sample around the mount. In either case, care was taken to ensure that none of the sample mount was exposed to the incident X-ray beam.

A general X-ray spectrum was obtained using the following instrument conditions.

Source	Al $K\alpha$, 15Kv, 20 μ A
Analysing energy	100v
Analyser pressure	10^{-8} Torr
Display	40 eV cm^{-1} .
No. of scans	100 ₈

After this, the peaks were assigned, and their height in centimetres measured to obtain relative intensities.

Argon bombarding was carried out at a current of $10\mu\text{A}$ for 30 seconds, which was sufficient to remove approximately 600\AA of the surface.

For the U. P. S. investigations, the foils were spot-welded to the tungsten support ring and treated 'in situ' in the spectrometer before analysis.

2.3. e E. P. M. A. Investigations

Platinum / 10% Rhodium gauzes were examined for Pt/Rh surface composition and for the detection of surface impurities. The gauzes were fixed to the sample holder with sellotape, no paint bridge being necessary, because the samples were conducting. The investigations were carried out on a JEOL JXA - 3A machine and for the estimation of Pt/Rh composition, the Pt and Rh $L\alpha$ lines were used. The measurements were made by counting simultaneously for platinum and rhodium at the highest point of the mesh crossover. The results were compared with pure platinum and rhodium samples.

Errors arose owing to the curvature of the samples. Normally, samples are polished prior to investigation. However, in this case, as surface concentrations were being determined, polishing was not applied. As a result, errors of $\pm 5\%$ could be expected.

2.4. Catalytic Studies

2.4. a Activation

2.4. a (i) Laboratory work

The activation studies were carried using Pt/10%Rh gauze catalysts. The gauzes were cut to a hexagonal shape to a weight of approximately 24.0 mg, representing a surface area of 0.635 cm^2 (Gauze surface area is $26.5\text{ cm}^2\text{ g}^{-1}$). An attempt was made to produce a die for cutting the gauze. However owing to the nature of the fine wire this proved impossible. Therefore samples were cut

with scissors to an overall accuracy of 0.5 mg.

Where appropriate, the gauzes were solvent treated prior to insertion in the reactor. This solvent treatment involved two initial soakings for fifteen minutes in 1,1,2-trichloroethylene followed by soaking twice for similar periods in acetone. Finally the gauzes were washed several times in distilled water and dried in air. To avoid any contamination, the samples were handled with tweezers at all times.

Hydrogen flame activation

The gauzes were activated by holding them in the hottest region of a hydrogen flame ($T = 2,223\text{K}$) produced by burning pure hydrogen from a narrow silica tube.

Activation by various gases

Prior to activation, the gauzes were solvent treated to remove surface contaminants. The gauzes were then placed in the reactor and the reacting gases allowed to flow through for sufficient time to change the atmosphere in the reactor ten times (dead volume of reactor + tubing 180 cm^3). The gauzes were then raised into the centre of the furnace for activation at a specified temperature.

After activation, the gauzes were lowered into the running position shown in figure 2.3. Nitrogen and oxygen were mixed and passed through the reactor, followed by the required amount of ammonia. After running for a specified time the reaction was stopped by turning off the ammonia gas.

Initial experiments were carried out using a 10% NH_3 /air mixture flowing at $1,000\text{ cm}^3\text{ min}^{-1}$ over one gauze, giving a gauze loading of $4.2\text{ tons ammonia m}^{-2}\text{ catalyst day}^{-1}$.

Later experiments used three gauzes with a 10% NH_3 /air mixture flowing at $4,300\text{ cm}^3\text{ min}^{-1}$ (equivalent to 6 tons ammonia $\text{m}^{-2}\text{ catalyst day}^{-1}$).

Finally, in the doping experiments, 14% NH_3 /air mixtures were used with three gauzes giving a gauze loading equivalent to $8.4\text{ tons ammonia m}^{-2}\text{ catalyst day}^{-1}$.

2.4. a (ii) Surface diffusion experiments

A piece of Pt/10%Rh foil was solvent washed and activated using a hydrogen flame. Two parallel scratches were scored in the surface using a new razor-blade. The foil was then run in the reactor along with 3 Pt/10%Rh gauzes for up to 30 minutes, using a 10% NH₃/air stream flowing at 4,300 cm³ min⁻¹. Photographs were taken at various time intervals, of the distance between the scratches and the ends of the scratch channel.

2.4. b Doping studies

Following the activation studies using E. P. M. A. it was noticed that surface impurities such as calcium compounds were giving increased light-off temperatures and low activities. It was therefore decided to study the deactivation of Pt/10%Rh gauze catalysts after they had been doped with various compounds.

Ideally, the dopants should either increase the catalytic activity of the Pt/10%Rh gauze or not significantly decrease it. Dopants, if possible, should reduce the weight loss of the platinum/rhodium catalyst, possibly by lowering the gauze running temperature. Finally, the dopant should not volatilize off the surface of the gauze during the reaction.

Initial experiments were therefore carried out to find a suitable dopant which would fulfil all these requirements.

2.4. b (i) Doping methods

Initial efforts were directed towards obtaining a reproducible method of doping the gauzes. Three methods of doping were investigated.

(a) Vacuum evaporation

Three Pt/10%Rh gauzes were solvent treated to remove surface impurities. Gold was then deposited by heating 3 cm. of 0.003" diameter Au wire at a pressure of 10⁻⁴ Torr using a Balzers machine. Both sides of the gauze were coated to a thickness of approximately 4Å. The experiment was repeated with iron.

(b) Solution deposition

Three Pt/10%Rh gauzes were solvent treated and activated by heating in oxygen, flowing at a rate of $200 \text{ cm}^3 \text{ min}^{-1}$, for two hours at $1,000^\circ\text{C}$. The gauzes were then immersed in saturated aqueous solutions of the dopant for 10 minutes. Following this, the gauzes were placed on a watch-glass and the water evaporated off. The gauzes were then shaken to remove the excess dopant.

(c) Melt deposition

Three Pt/10%Rh gauzes were solvent washed and heated in a hydrogen flame. Whilst still red-hot, the gauzes were dipped into the powdered dopant. Of the three methods (a) proved impractical for dopants other than elements in wire form, whilst (c) was not reproducible. Method (b) was adopted, and was found to be reasonably reproducible. The amount of dopant deposited on the surface could be altered by altering the concentration of dopant solution.

After doping, the gauzes were run in a 14% ammonia/air mixture flowing at $4,300 \text{ cm}^3 \text{ min}^{-1}$. This kept the superficial contact time similar to that used in the activation studies (10^{-5} sec) even though a higher ammonia rate was used ($8.4 \text{ tons ammonia m}^{-2} \text{ catalyst day}^{-1}$). This ammonia concentration eliminated the excess oxygen, and an accurate determination of free nitric oxide was possible.

2.4. b (ii) Temperature effects

Gauze running temperatures were determined by placing an exposed thermocouple onto the top surface of the top gauze.

Light-off temperatures were obtained by both the exposed and shielded thermocouples, and no significant difference was found between light-off temperatures below 500°C . At temperatures in excess of this however, the thermocouple itself lit-off, giving a temperature rise of approximately 50°C .

An attempt was made to determine gauze temperatures using a pyrometer. Temperature changes were found to be too rapid for monitoring by this method and therefore the exposed thermocouple was connected to a potentiometric recorder.

This method gave temperatures accurate to approximately $\pm 15^{\circ}\text{C}$.

2.4. b (III) Variation in light-off temperature with surface coverage

Following the investigation of light-off and gauze running temperatures, a study was undertaken to investigate the variation in light-off temperature with surface dopant concentration. The gauzes were solvent cleaned, activated in oxygen, and weighed in a C.I. Electronics Mk. 2B microbalance. The gauzes were then doped and weighed again. The amount of dopant applied was obtained by difference, and the surface dopant coverage obtained. The light-off temperature of the gauzes was then measured as before.

CHAPTER 3

RESULTS

	Page.
3. 1. <u>Activation studies</u>	
3. 1. a. Activation by hydrogen flame	116
3. 1. b. Oxygen treatment	117
3. 1. c. Activation by various gases	117
3. 1. d. Comparison of activation by oxygen and nitrogen	117
3. 1. e. (i) Activities of gauzes vs. temperature of oxygen treatment	124
3. 1. e. (ii) Electronprobe microanalysis of gauzes activated at various temperatures in oxygen	124
3. 1. f. Activity produced by heating in oxidising, inert and reducing gases	124
3. 1. g. Surface rearrangement occurring during activation with various gases	131
3. 1. h. Development of surface rearrangement with time under ammonia oxidation conditions	131
3. 1. i. Activation with oxygen, followed by deactivation with CO ₂ , SO ₂ and water	131
3. 1. i. (a) Carbon dioxide deactivation	136
3. 1. i. (b) Water deactivation	136
3. 1. i. (c) Steam deactivation	139
3. 1. i. (d) Sulphur dioxide deactivation	139
3. 1. j. Electronprobe microanalysis of inactive gauzes	139
3. 1. k. Effect of heating in the activation process	140

3.2.	<u>E.S.C.A. studies of Pt/Rh foils and gauzes</u>	
3.2. a.	Pt/10% Rh foils	140
3.2. b.	Pt/40% Rh foils	154
3.2. c.	Pt/10% Rh gauzes	154
3.2. d.	Pt/10% Rh foil deactivated by water	154
3.2. e.	Shift of the $\text{Rh}_{\text{M III}}$ signal during oxidation	168
3.3.	<u>U. P. S. studies</u>	
3.3. a.	Pt/40% Rh foil heated in situ	168
3.4.	<u>Surface diffusion</u>	
3.5.	<u>Deactivation studies</u>	
3.5. a.	Iron oxide dopant	177
3.5. b.	Gold dopant	177
3.5. c.	Metal oxide dopants	177
3.5. d.	Variation in light-off temperature with dopant loading	182
3.5. e.	Weight loss from doped gauzes	182
3.6.	<u>Heterogeneous - homogeneous mechanism studies</u>	182

3. Results

The activation of a Pt/10%Rh gauze for ammonia oxidation has received little or no attention from research workers in the past. Industrial methods of activating include inserting the gauzes into the reactor and heating them electrically to red heat, when the reaction starts, or heating the gauze in an hydrogen flame, either after insertion in the reactor or in the air before insertion in the reactor. The reproducibility of both of these activation techniques is open to question, and attention was focussed on factors important in the activation, with the objective of developing reproducibility in the process.

Before activation treatment, the gauze had to be cleaned to remove dirt and oil deposited on the gauze during its production. This was carried out as follows.

The gauze was first immersed in 1,1,2 -trichloroethylene for fifteen minutes to remove any oil film. This was repeated for a further fifteen minutes, after which the gauze was soaked twice in acetone, again for fifteen minute periods. The acetone was then decanted and the gauzes washed in distilled water for ten minutes. After this solvent treatment, the gauzes could then be activated.

3. 1. a. Activation by hydrogen flame

A piece of Pt/10%Rh wire of 0.003" dia. was heated for one second intervals in an hydrogen flame. With the wire held horizontally, very little rearrangement occurred at the centre of the wire, although grain boundary grooving was extensive after 20 seconds (Photo. 1).

However, when the wire was held vertically in the flame, large globular aggregations of the alloy were found at the lower end of the wire. In this case rearrangement was extensive, and after heating for only one second, extensive grain boundary grooving was apparent (Photo. 2). Thus it was immediately apparent that this activation process was not reproducible due to lack of temperature control causing the formation of molten metal and of non-reproducible grain boundary grooving effects.

3. 1. b. Oxygen treatment

Consideration of hydrogen flame treatment led to the conclusion that activation resulted either from oxidising or reducing conditions or to the high temperature of the flame. These were tested in turn, starting with activation in oxygen. Initial experiments involved a gauze pre-activated in an hydrogen flame. Following activation as in 3. 1. a, a piece of Pt/10%Rh wire was heated in oxygen flowing at a rate of $900 \text{ cm}^3 \text{ min}^{-1}$ for two hours at 800°C . The results are shown in photographs 3 - 10. From these it can be seen that oxygen causes extensive pitting of the surface of the platinum. The oxygen treatment is shown superimposed on a hydrogen activation. This enabled one individual grain to be studied throughout the reaction, rather than taking any random grain on the wire. Thus, this experiment showed that oxygen caused extensive pitting of the surface, and that a simple optical microscope coupled with a camera, could give photographs of suitable clarity for defects to be followed, thus eliminating the need for scanning electron microscope investigations.

3. 1. c. Activation by various gases

Pt/10%Rh gauzes were solvent treated to remove any oil film and then treated in a static atmosphere of oxygen, hydrogen, nitrogen, ammonia and hydrogen. Comparisons of an hydrogen flame activated gauze and an untreated gauze were also made. The results are shown in table 3. 1. 1. and graphs 3. 1. 1. to 3. 1. 7.

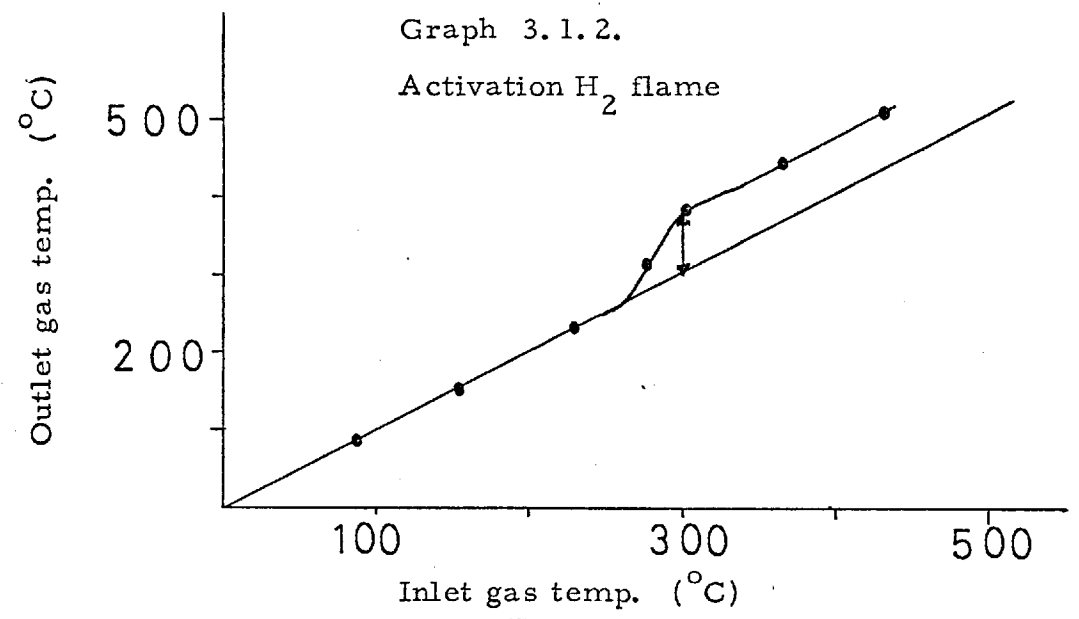
3. 1. d. Comparison of activation by oxygen and nitrogen

A Pt/10%Rh gauze was heated in an atmosphere of static oxygen for two hours at 350°C . The gauze was allowed to cool in oxygen and then its activity was measured. Two pieces of gauze were similarly treated using nitrogen at 800°C . The activity of one of these gauzes was found immediately after this treatment, but the other was again given an oxygen treatment before reaction. Pt/10%Rh foils were similarly treated and E. S. C. A. spectra obtained (Fig. 3. 2. 13). The results are shown in table 3. 1. 2. and graphs 3. 1. 8. to 3. 1. 10.

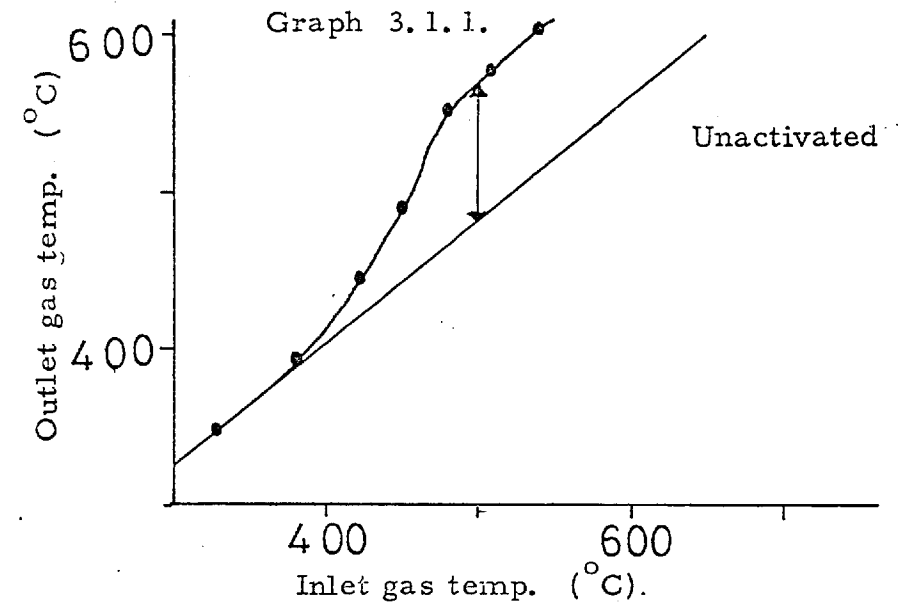
Table 3. 1. 1.

Gauze treatment	Unactivated	H ₂ flame	H ₂ 1,000°C	O ₂ 1,000°C	N ₂ 1,000°C	He 1,000°C	NH ₃ 1,000°C
Light-off temperature (°C)	380	360	270	270	340	345	300
Inlet gas temperature rise	70°C At 500°C	70°C At 300°C	180°C At 380°C	150°C At 380°C	100°C At 450°C	100°C At 450°C	100°C At 480°C
Graph No.	3. 1. 1.	3. 1. 2.	3. 1. 3.	3. 1. 4.	3. 1. 5.	3. 1. 6.	3. 1. 7.
Photo No.	11	11	12	13	14	15	16

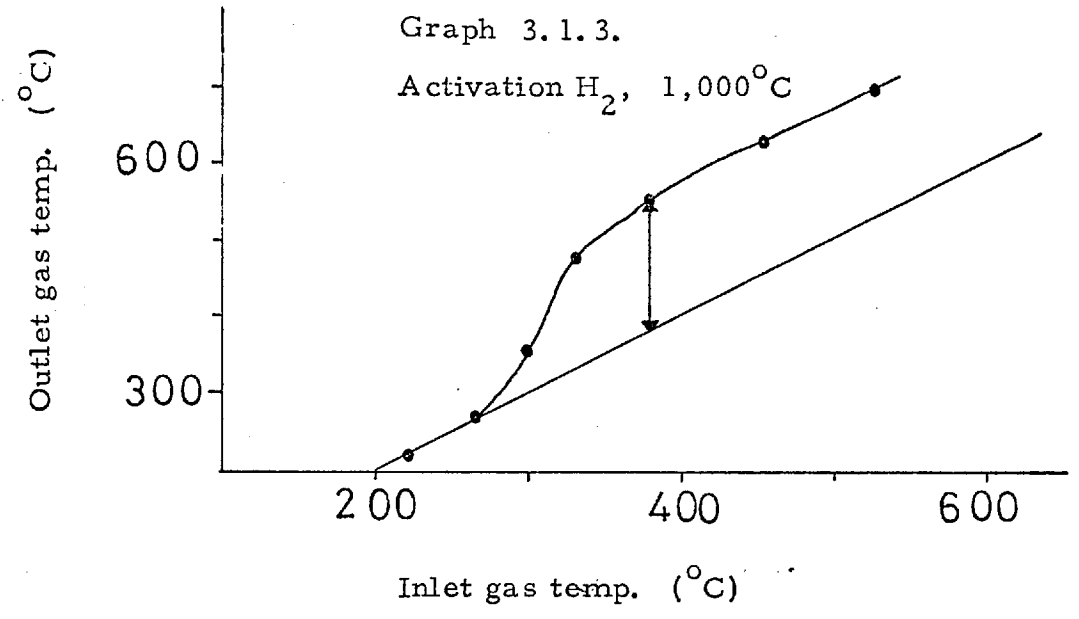
Graph 3.1.2.
Activation H₂ flame



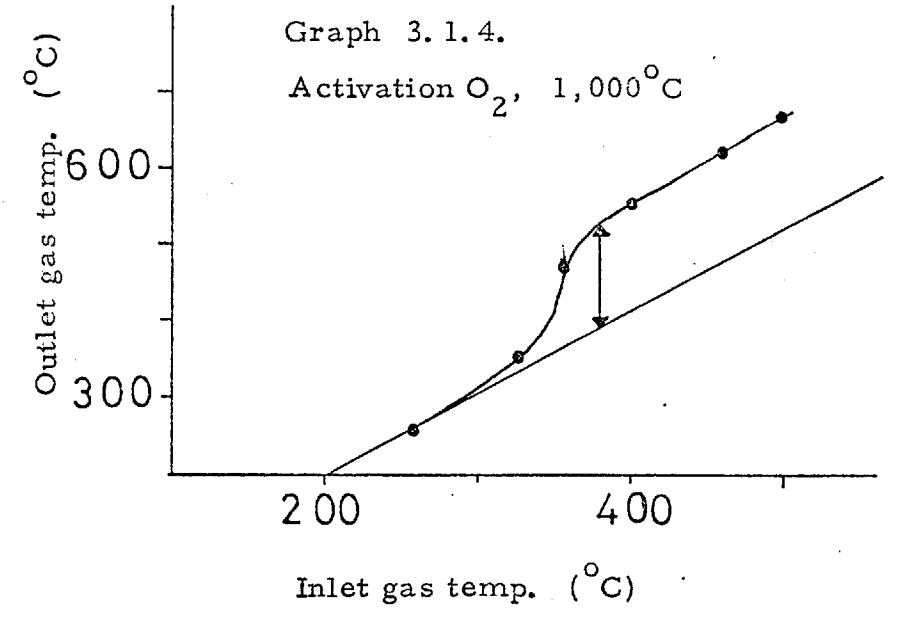
Graph 3.1.1.



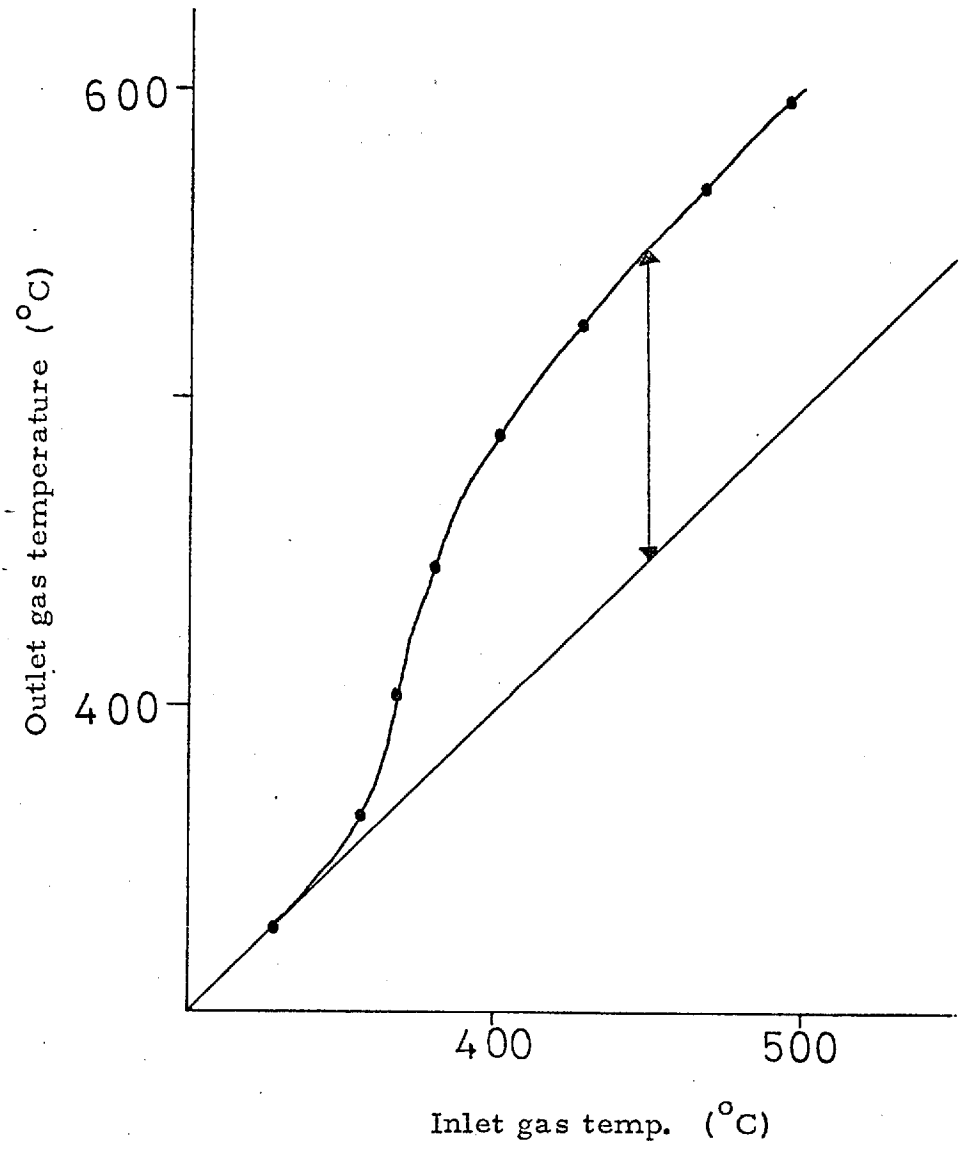
Graph 3.1.3.
Activation H₂, 1,000°C



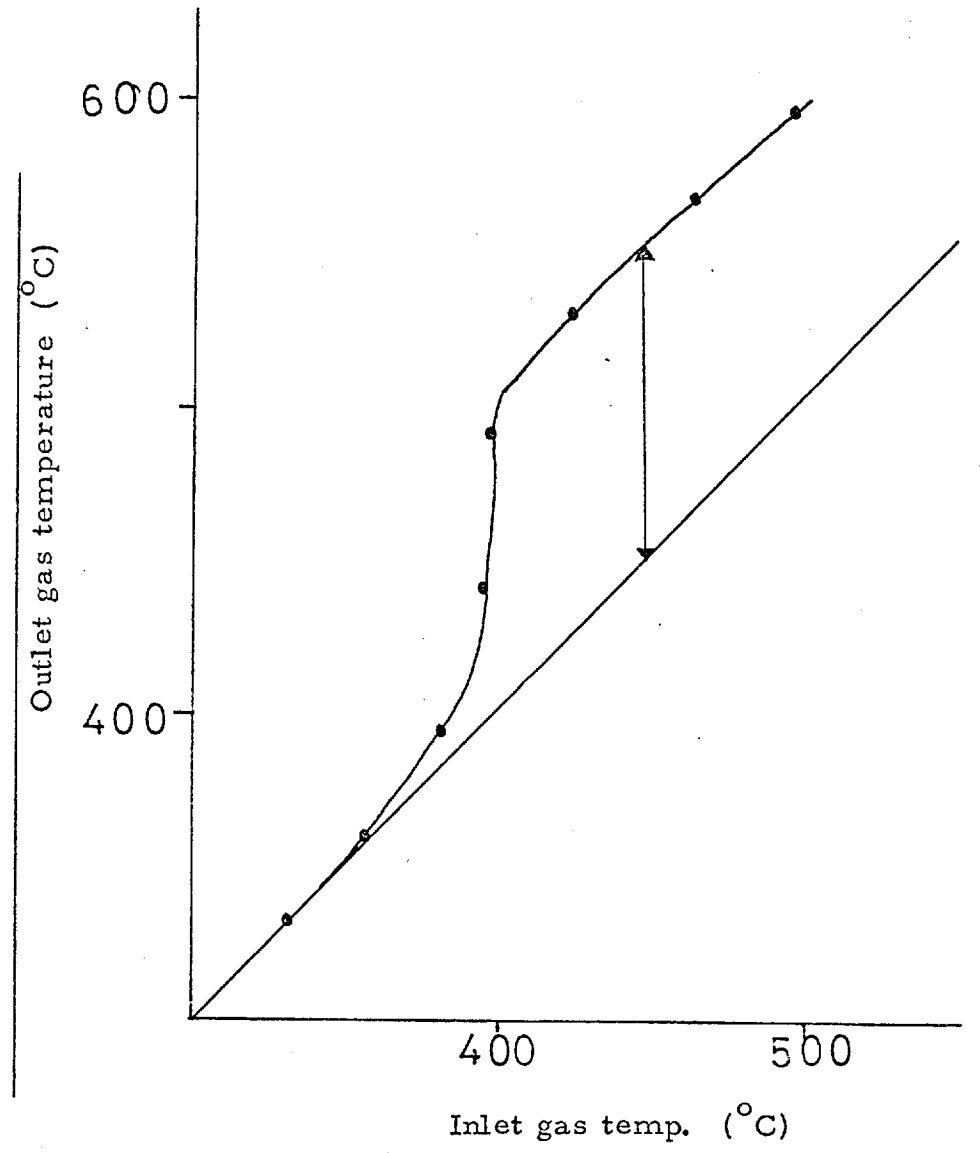
Graph 3.1.4.
Activation O₂, 1,000°C



Graph 3.1.5.
Activation N₂ 1,000°C



Graph 3.1.6.
Activation He 1,000°C



Graph 3.1.7.

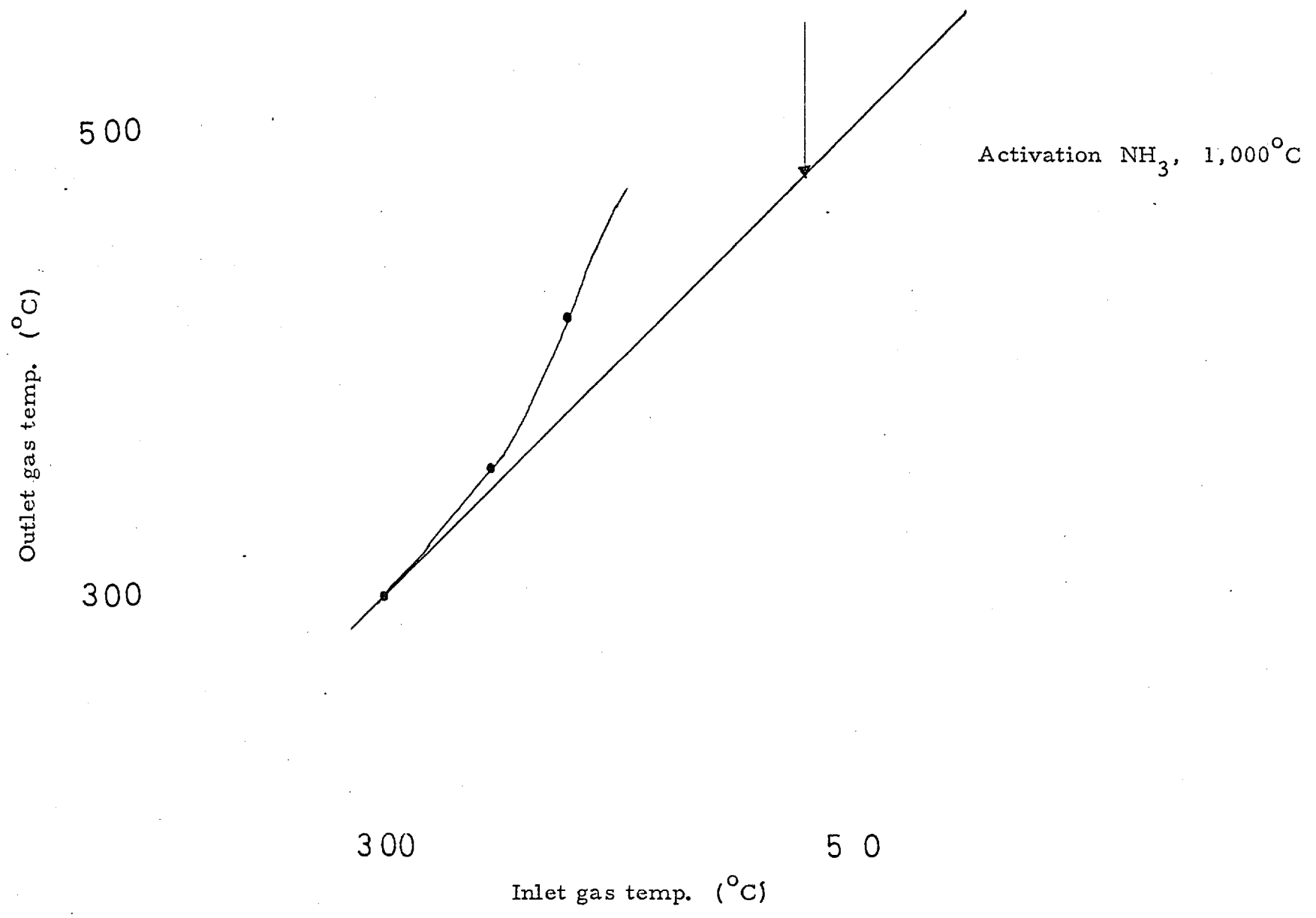
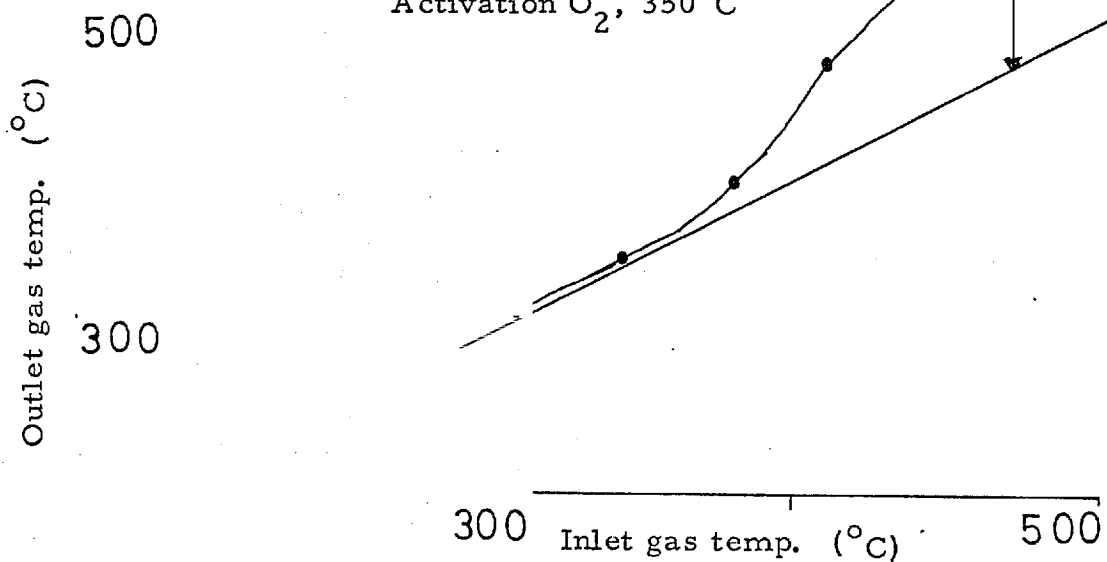


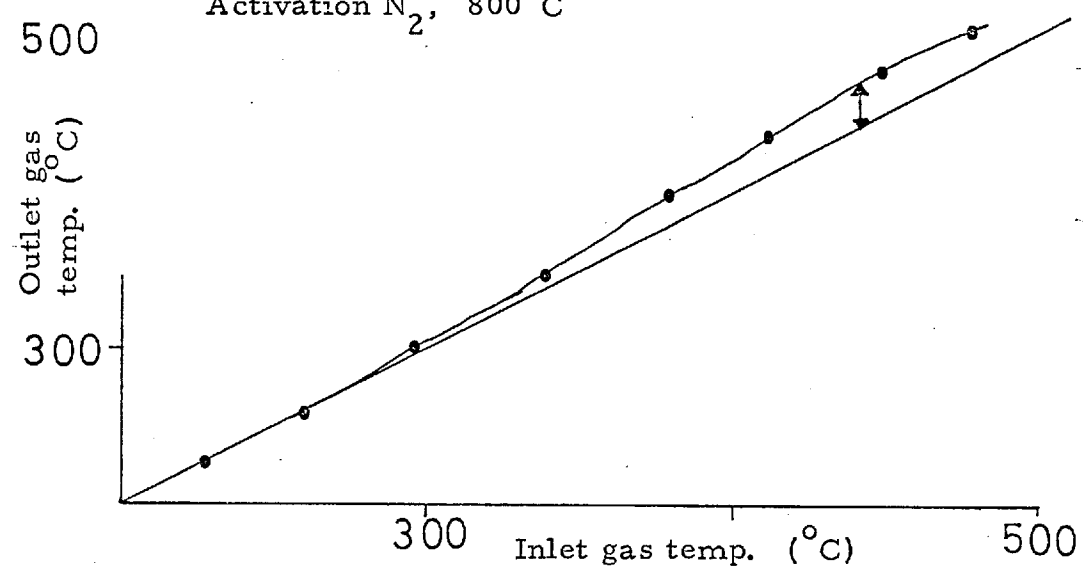
Table 3.1 2

Gauze treatment	O ₂ 350°C	N ₂ 800°C	N ₂ 800°C + O ₂ 350°C
Light-off temperature (°C)	275	270	270
Inlet gas temperature rise	95°C At 470°C	35°C At 430°C	30°C At 430°C
Graph No.	3.1.8.	3.1.9	3.1.10.
Photo No.	17 - 19	20 - 22	23 - 25
Pt _{N VII} / C _{Is}	4.2.	3.6.	7.6.
Pt _{N VII} / O _{Is}	3.1	1.7	1.5
C _{Is} / O _{Is}	0.74	0.47	0.19
Pt _{N VII} / Rh _{M III}	10.0	7.6	8.7

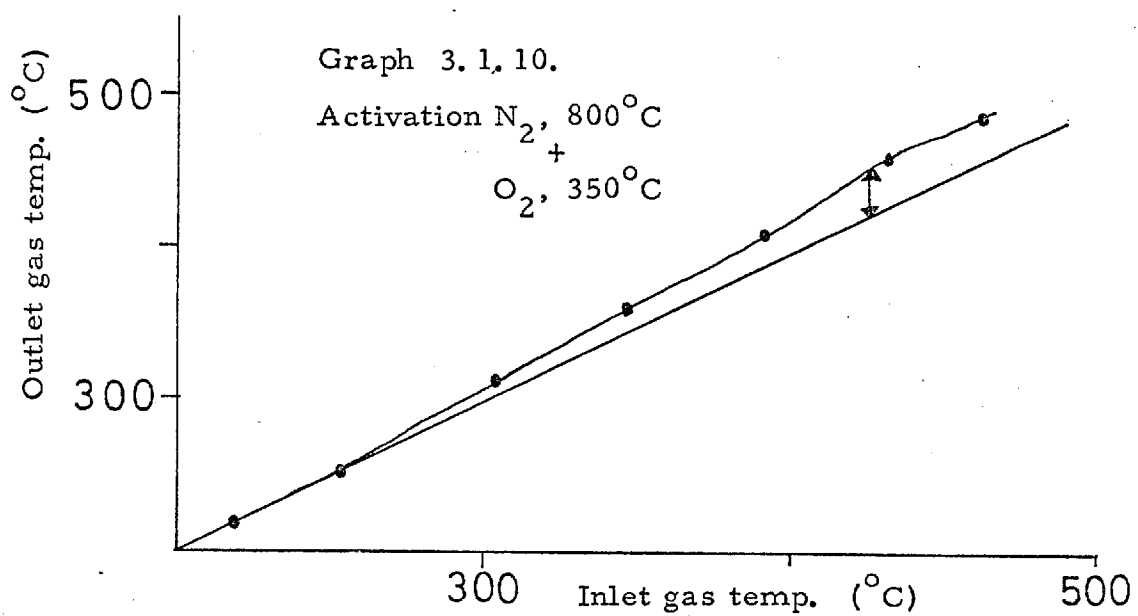
Graph 3.1.8.
Activation O_2 , $350^\circ C$



Graph 3.1.9.
Activation N_2 , $800^\circ C$



Graph 3.1.10.
Activation N_2 , $800^\circ C$
+
 O_2 , $350^\circ C$



3. 1. e. (i) Activities of gauzes vs. temperature of oxygen treatment

Pt/10%Rh gauzes were treated in atmospheres of static oxygen for two hours at temperatures between 100°C and 1,000°C. They were then tested for activity and the results shown in table 3. 1. 3 and graphs 3. 1. 11 - 3. 1. 17. The results were combined and shown in graphs 3. 1. 18 - 3. 1. 20.

3. 1. e. (ii) Electron probe microanalysis of gauzes activated at various temperatures in oxygen

Five Pt/10%Rh gauzes were activated by treating at 200°C, 400°C, 600°C, 800°C and 1,000°C in oxygen. Following these treatments, they were analysed for surface rhodium concentration using E. P. M. A. An untreated gauze was examined as a blank.

The samples were mounted with sellotape and were not pre-treated before examination. The beam was focussed onto the top surface of both the 'horizontal' and 'vertical' wires in the gauzes, resulting in errors of the order of $\pm 5\%$. Clearly this is a large error, though as table 3. 1. 4 shows, the value obtained for the rhodium concentration at 800°C is outside these expected errors, and clearly shows a large increase in surface rhodium concentration. The analysis was repeated on a further series of gauzes and the average values tabulated against temperature treatment. The results are shown in table 3. 1. 4 and graph 3. 1. 21.

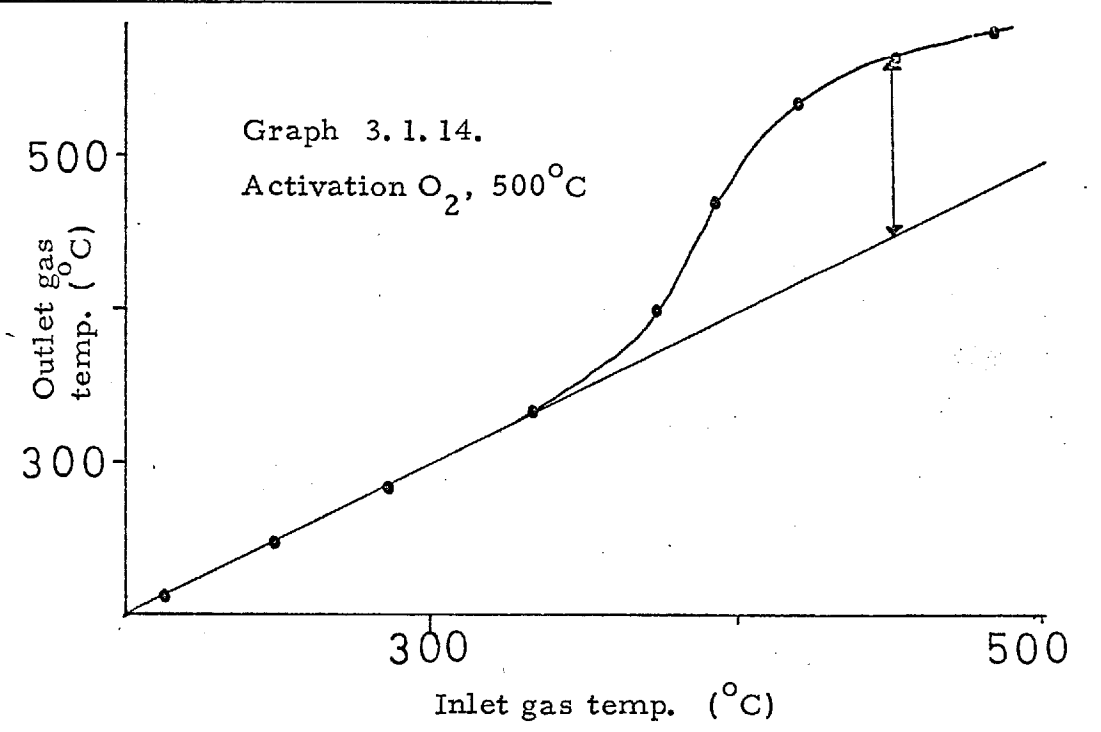
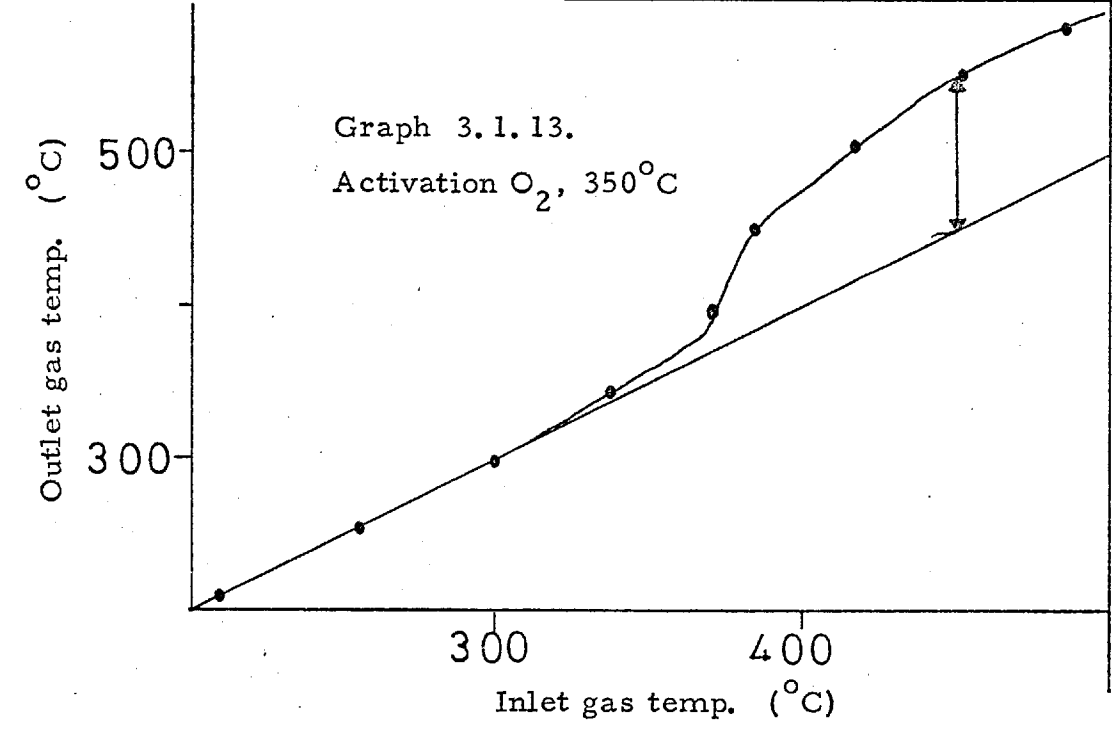
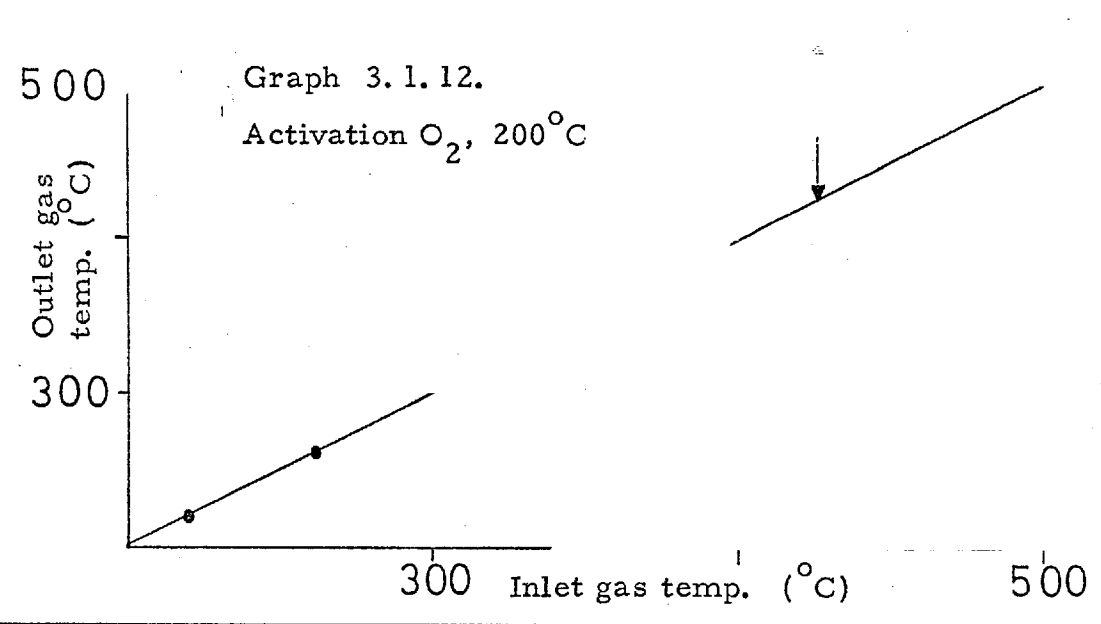
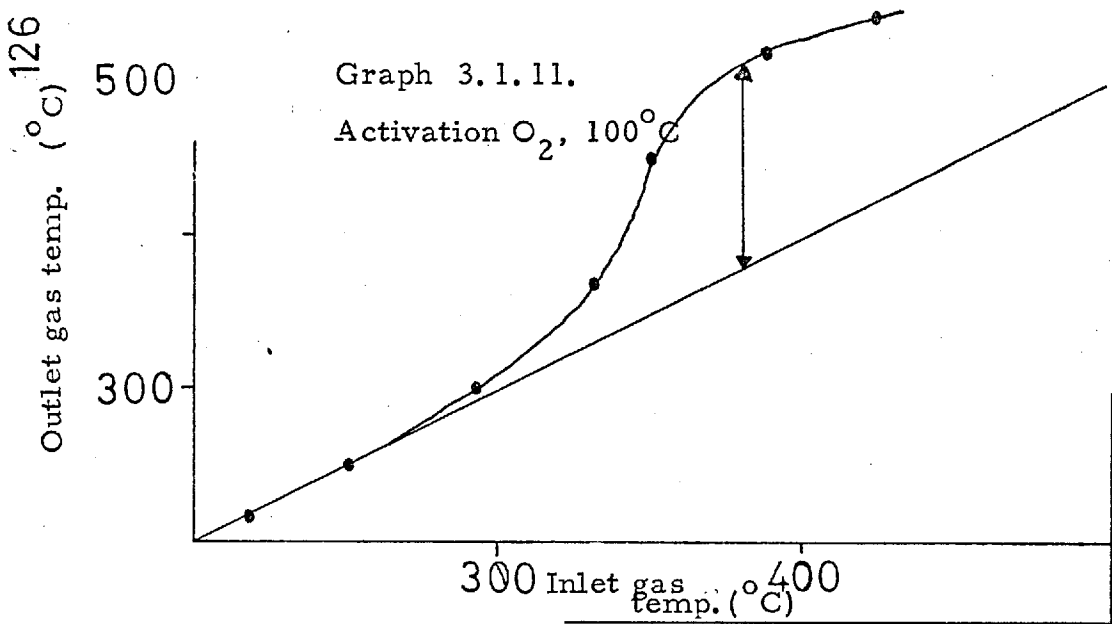
3. 1. f. Activity produced by heating in oxidising, inert and reducing gases

Experiments carried out in 3. 1. c have clearly shown that activation with different gases produces different light-off temperatures with some variation in the temperature at which the maximum occurs.

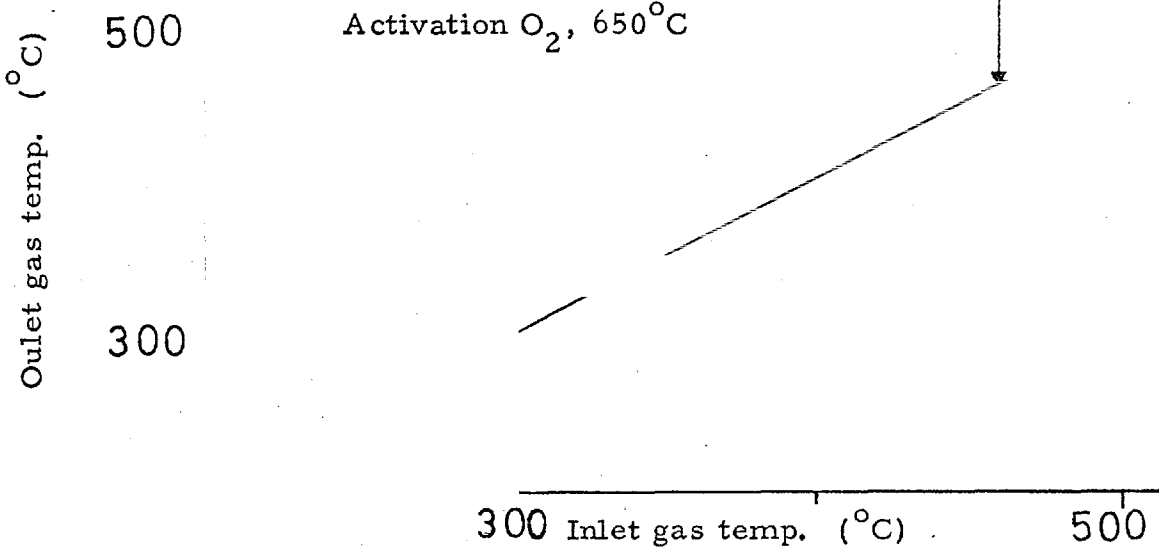
To study these effects, the Mark II reactor was used, involving 3 Pt/10%Rh gauzes, and product gas analysis was carried out using the gas chromatograph system described in chapter 2. Light-off temperatures were monitored, although as the gas flow rate has been increased

Table 3.1.3.

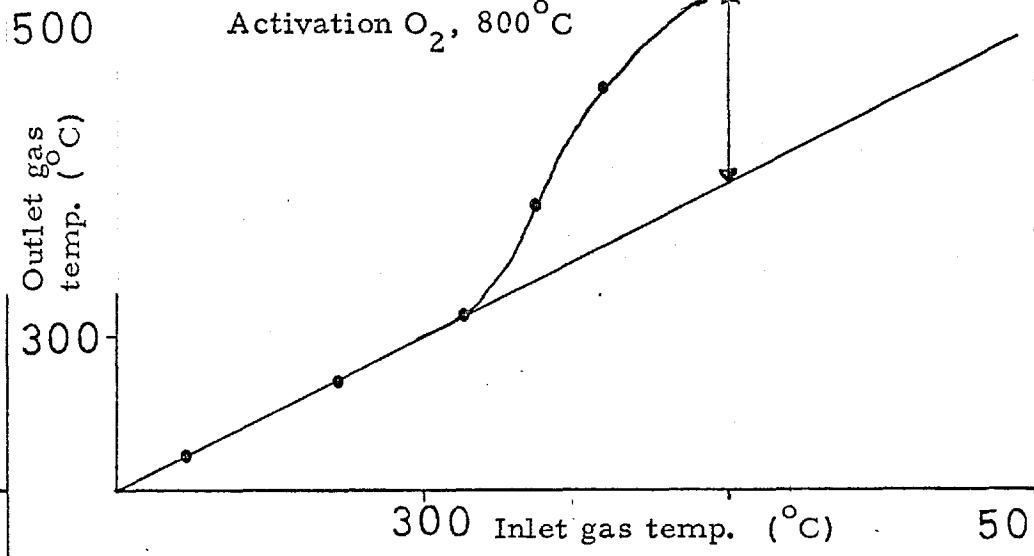
Temperature of oxygen treatment ($^{\circ}\text{C}$)	100	200	350	500	650	800	1,000
Light-off temperature ($^{\circ}\text{C}$)	275	295	345	340	350	370	340
Inlet gas temperature rise ($^{\circ}\text{C}$)	125 At 380	100 At 425	95 At 455	115 At 455	90 At 450	70 At 480	125 At 425
Graph No.	3.1.11	3.1.12	3.1.13	3.1.14	3.1.15	3.1.16	3.1.17
Photo No.	26	26	27	28	29	30	31



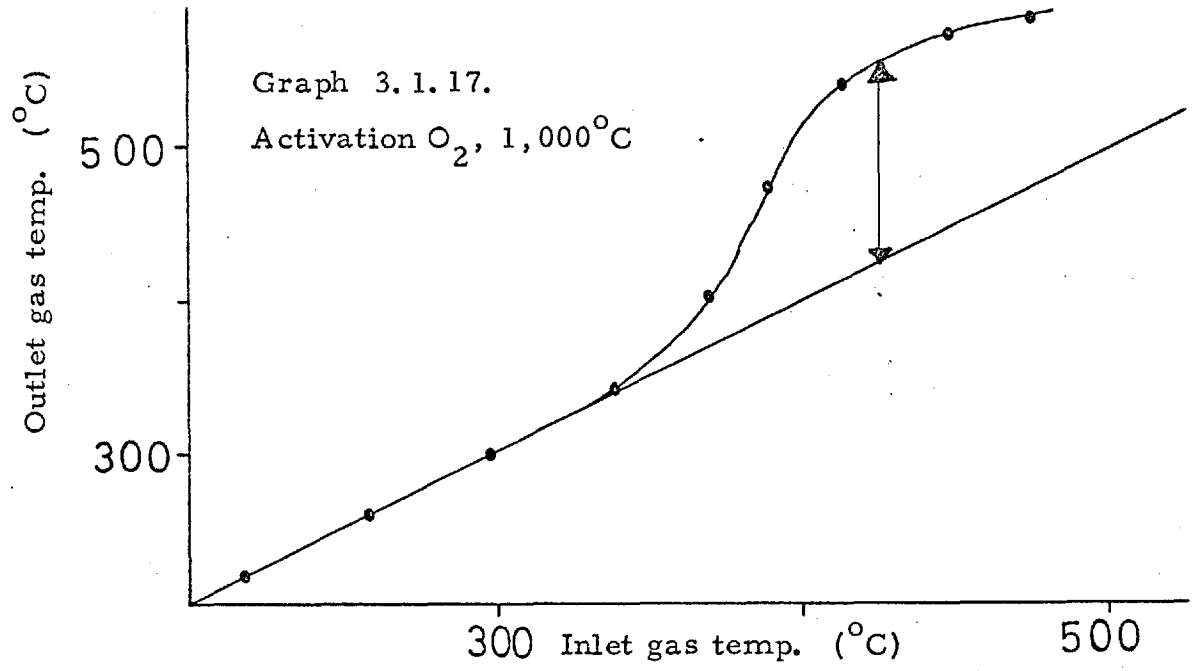
Graph 3.1.15.
Activation O₂, 650°C



Graph 3.1.16.
Activation O₂, 800°C



Graph 3.1.17.
Activation O₂, 1,000°C



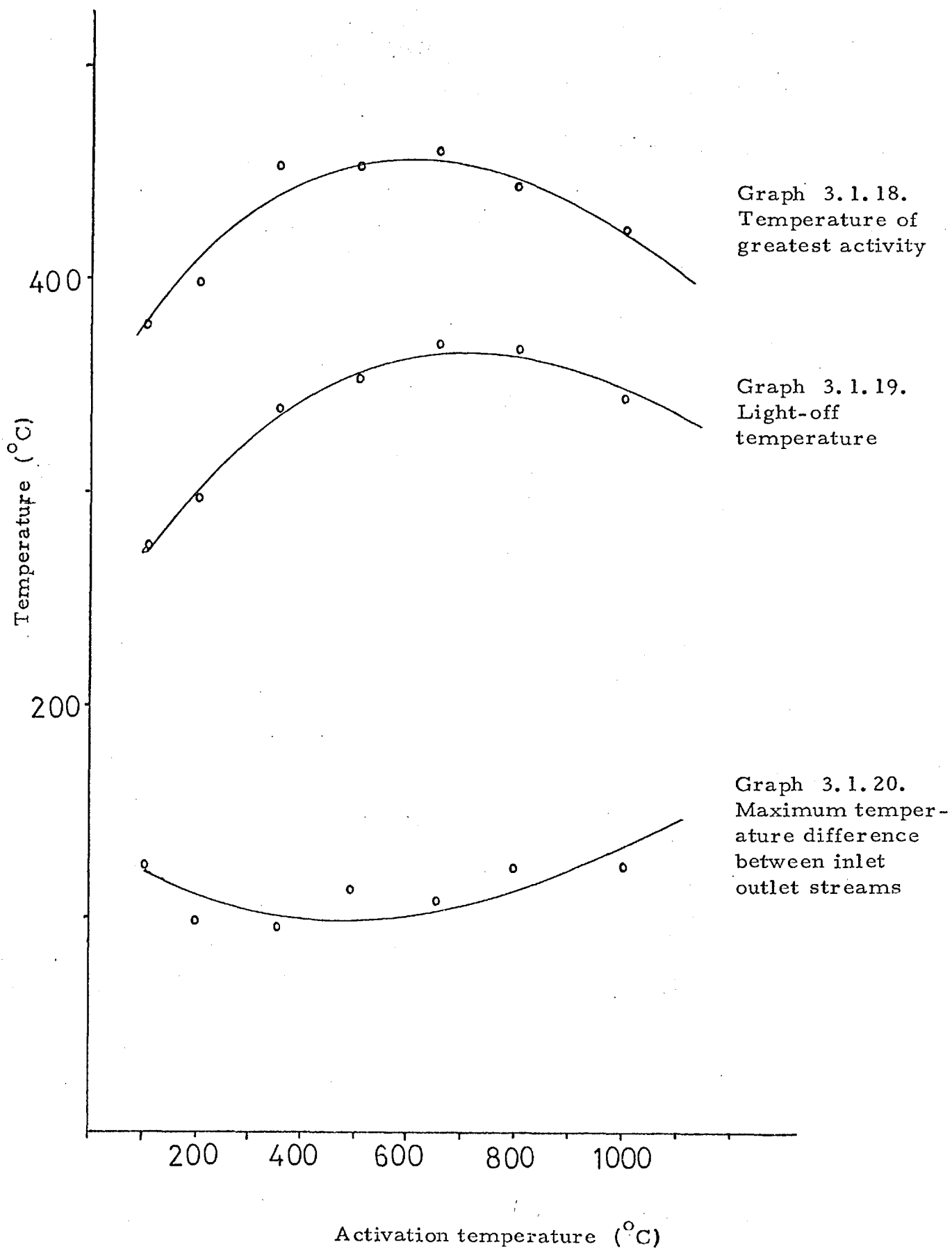
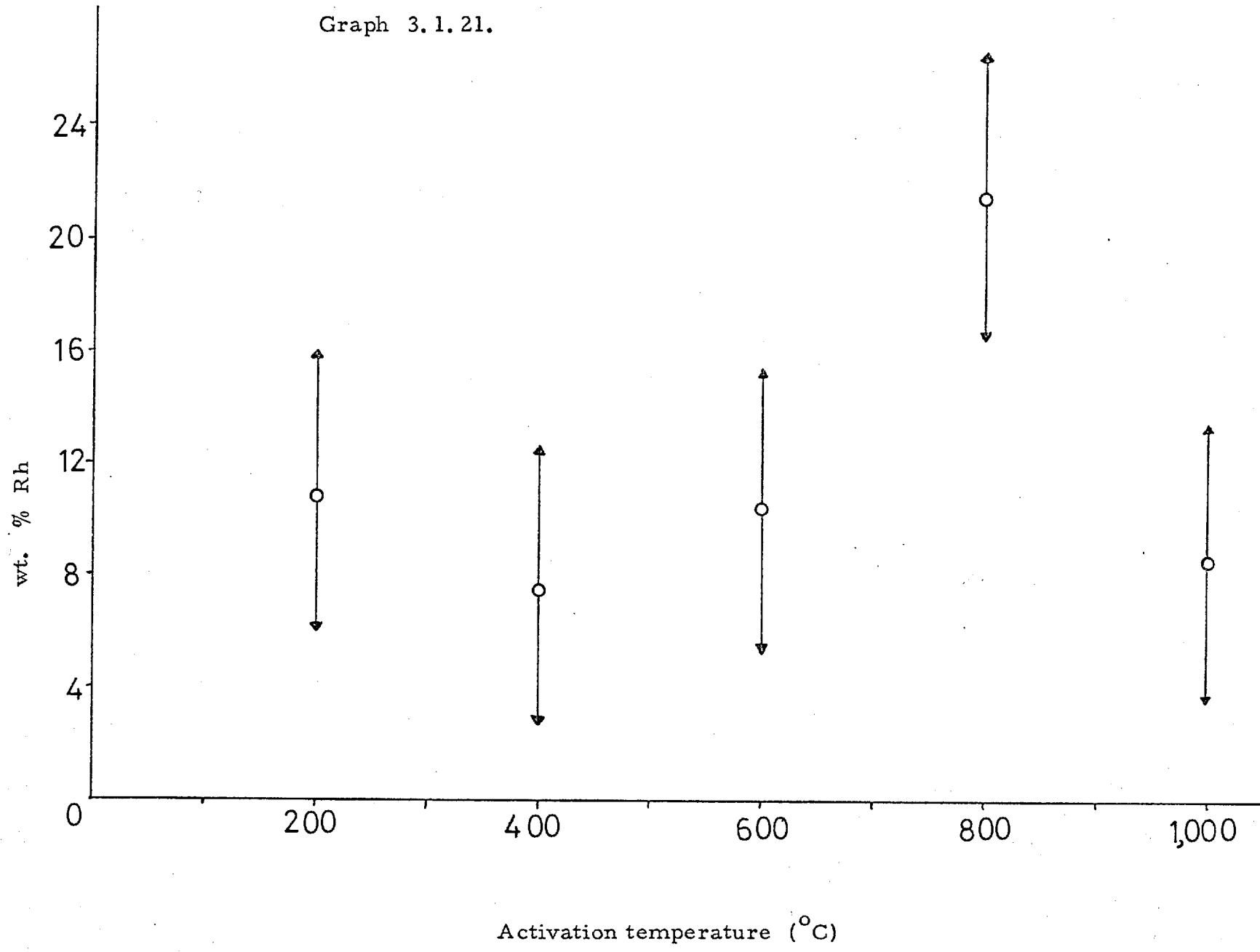


Table 3.1.4.

Surface concentrations of gauzes in which the bulk concentration is nominally 10%Rh.

Oxygen treatment temperature ($^{\circ}\text{C}$)	Wt % Rh	Wt % Pt
'blank'	8.3	91.7
200	9.7	90.3
400	5.3	94.7
600	7.0	93.0
800	21.9	78.1
1,000	7.7	92.3

Graph 3.1.21.



(from $1,000 \text{ cm}^3 \text{ min}^{-1}$ to $4,300 \text{ cm}^3 \text{ min}^{-1}$) direct comparisons between these and earlier experiments are impossible.

The experiment was divided into seven parts, designed to study the effect of each individual operation in the activation process. A two hour heat treatment was used with the activating gases flowing at $200 \text{ cm}^3 \text{ min}^{-1}$, and cooling in the same gases also flowing at $200 \text{ cm}^3 \text{ min}^{-1}$.

These results were compared with gauzes which had undergone no previous treatment, a solvent wash only, and a solvent wash with hydrogen flame treatment. The results are shown in table 3.1.5 and graphs 3.1.22 and 3.1.23.

3.1.g. Surface rearrangement occurring during activation with various gases

The gauzes were first solvent washed and then heated at $1,000^\circ\text{C}$ for 2 hours in the gases shown in table 3.1.6.

From the photographs, it can be seen that oxygen induces most surface rearrangement. Oxygen treatment produces extensive pitting, whilst the reducing gases tend to produce smoother metal surfaces and larger grain sizes.

3.1.h. Development of surface rearrangement with time under ammonia oxidation conditions

A Pt/10%Rh gauze was activated by solvent washing and treating at $1,000^\circ\text{C}$ for 2 hours in oxygen. The gauze was then inserted in the ammonia oxidation reactor and run in 10% NH_3 /air mixture at a rate of $4,300 \text{ cm}^3 \text{ min}^{-1}$ (equivalent to 6 tons ammonia m^{-2} catalyst day $^{-1}$). The gauze was withdrawn and photographed after the reaction times shown in table 3.1.7.

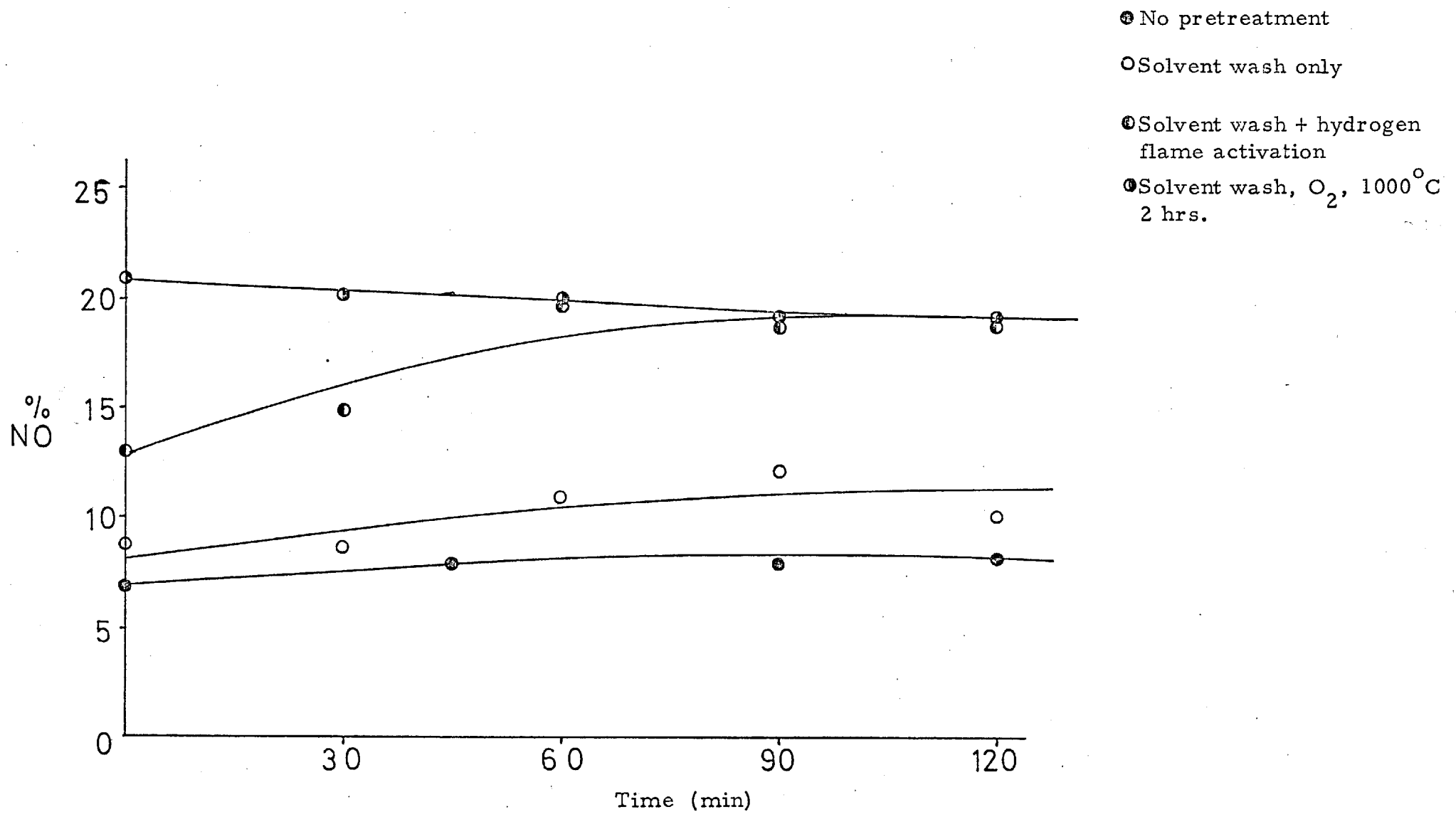
3.1.i. Activation with oxygen followed by deactivation with CO_2 , SO_2 , and water

Three Pt/10%Rh gauzes were activated by solvent washing and treating with oxygen at $1,000^\circ\text{C}$ for 2 hours at $200 \text{ cm}^3 \text{ min}^{-1}$. The

Table 3.1.5

Activation treatment	Light-off temperature ($^{\circ}\text{C}$)	Activity after 2 hrs as a % NO	Graph No.
No pretreatment	410	8	3.1.22
Solvent wash	310	11	3.1.22
Solvent wash + hydrogen flame	310	19	3.1.22
Solvent wash O_2 $1,000^{\circ}\text{C}$	310	19	3.1.22
Solvent wash He $1,000^{\circ}\text{C}$	380	16	3.1.23
Solvent wash H_2 $1,000^{\circ}\text{C}$	270	18	3.1.23
O_2 $1,000^{\circ}\text{C}$	332	16	3.1.23

Graph 3.1.22.



Graph 3.1.23.

- Solvent wash H₂,
1,000°C, 2 hrs.
- Solvent wash He
1,000°C, 2 hrs.
- ⊙ O₂, 1000°C, 2 hrs.
(No solvent wash)

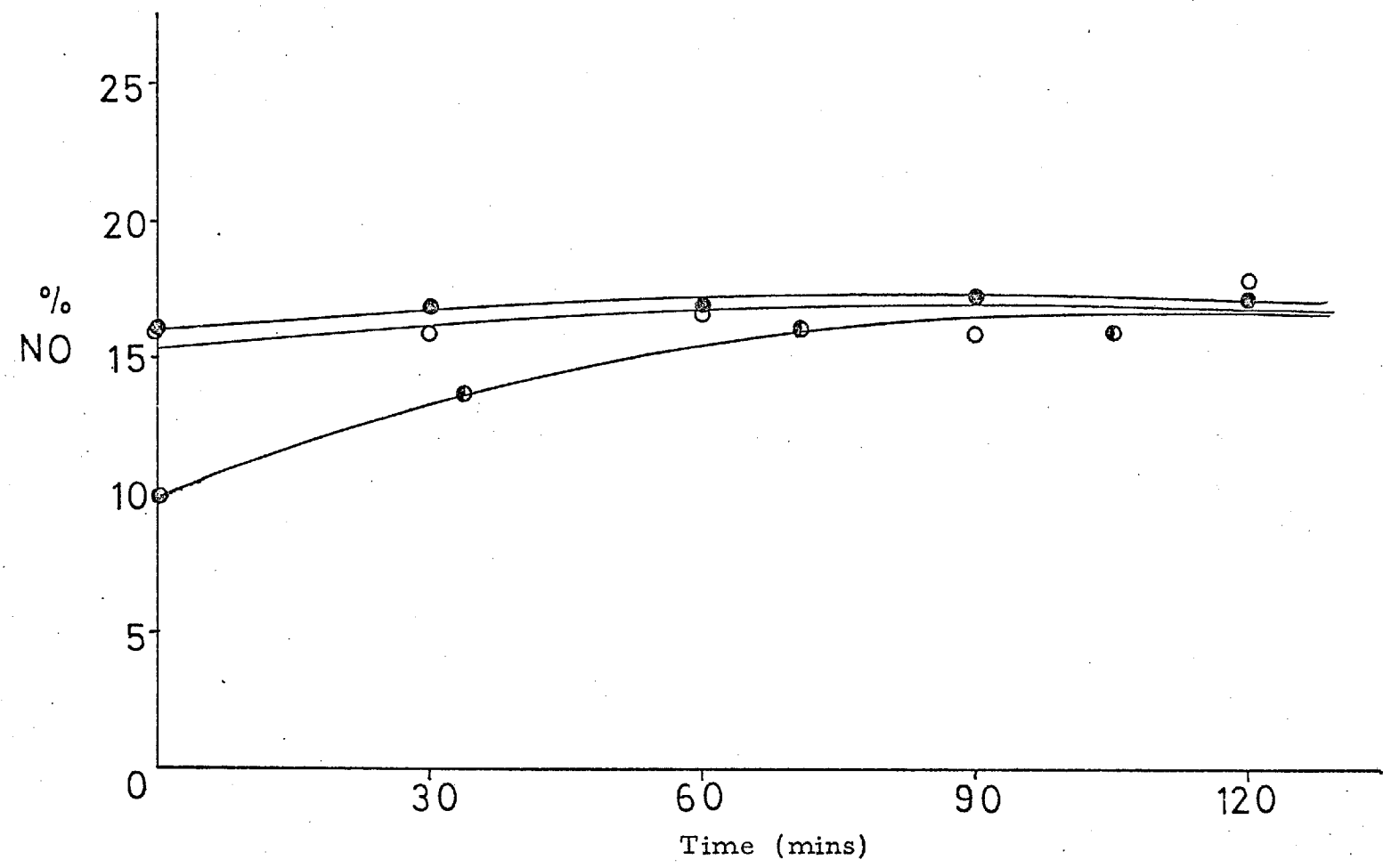


Table 3.1.6

Treatment	Photo. No.
oxygen	32
nitrogen	33
helium	34
hydrogen	35
ammonia	36

Table 3.1.7

Time	Photo. No.
30 seconds	37
60 seconds	38
3 minutes	39
9 minutes	40
22 minutes	41
41 minutes	42
60 minutes	43
120 minutes	44

gauzes were cooled in air from the gas mixing rig (80% N₂, 20% O₂). The gauzes were then tested for light-off temperature.

A further three gauzes were prepared under identical conditions, except that they were allowed to cool in the air of the laboratory overnight. These gauzes were tested for light-off temperature. The results are shown in table 3.1.8.

The results of this experiment show that cooling in air causes substantial loss of activity. This could be due to carbon from carbon dioxide, or sulphur from sulphur dioxide, or moisture recondensing on the gauze surface to cause loss of activity.

Following these results, a series of experiments were performed to study this deactivation caused by exposure to laboratory air.

3.1.i (a) Carbon dioxide deactivation

Three Pt/10%Rh gauzes were activated by solvent wash/oxygen treatment outlined above. The gauzes were allowed to cool overnight in dry flowing oxygen to prevent moisture contamination. The gauzes were then treated with carbon dioxide flowing at a rate of 100 cm³ min⁻¹. for two hours at room temperature. If deposition of carbon on the surface of the gauze was going to occur, then this treatment would have been sufficient to cause the resulting deactivation to take place. The result is shown in table 3.1.9 and graph 3.1.24. As a further check, three Pt/10%Rh gauzes were similarly treated but left in a static atmosphere of carbon dioxide overnight. The result is shown in table 3.1.9.

3.1.i (b) Water deactivation

Three Pt/10%Rh gauzes were activated by the solvent/oxygen treatment outlined previously. They were then cooled in oxygen overnight, removed from the reactor and immersed in distilled water for 2 hours, after which the light-off temperature and activity were determined. The result is shown in table 3.1.9 and graph 3.1.24.

Table 3.1.8

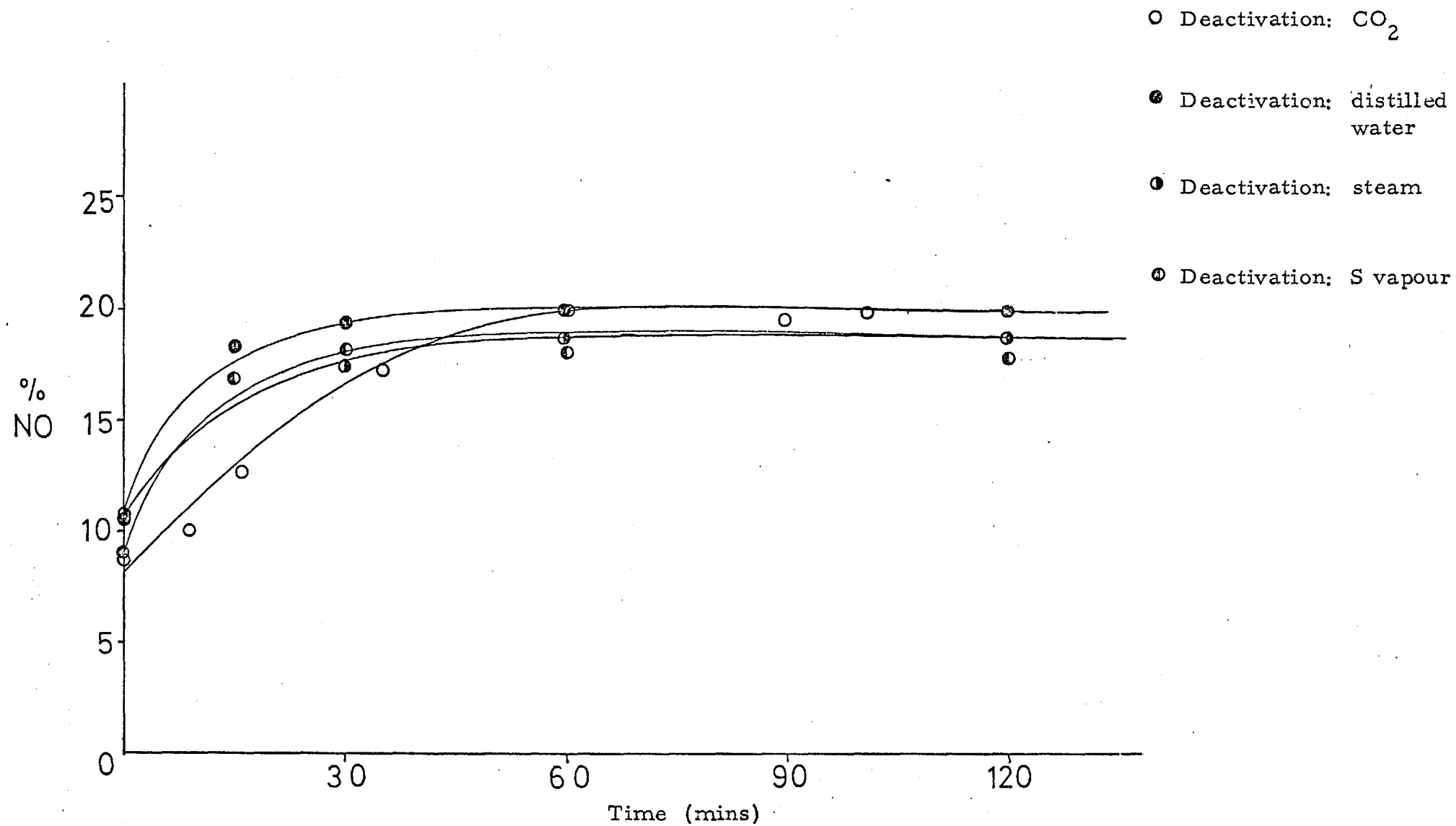
Treatment	Light-off °C
Activation + cooling in rig air	310
Activation + cooling in lab. air	345

Table 3.1.9

Deactivation treatment	Light-off temperature (°C)	Activity after 2 hours as a % of free NO	Graph No.
Flowing CO ₂	320	19	3.1.24
Static CO ₂	310		
Immersion in water	400	20	3.1.24
Steam	362	18	3.1.24
Sulphur	295	18	3.1.24

Graph 3.1.24.

Activation Solvent wash, O_2 , $1,000^\circ C$, $200\text{ cm}^3\text{ min}^{-1}$ 2 hrs.



3. 1. i. (c) Steam deactivation

Three Pt/10%Rh gauzes were activated using the solvent/oxygen treatment outlined previously. The gauzes were then allowed to cool overnight in flowing oxygen and held in steam vapour for 5 minutes, after which they were tested for light-off temperature and activity. The results are shown in table 3. 1. 9 and graph 3. 1. 24.

3. 1. i. (d) Sulphur dioxide deactivation

Three Pt/10%Rh gauzes were activated using the solvent/oxygen treatment. After cooling in oxygen overnight, the gauzes were held in an atmosphere of burning sulphur for 10 minutes. This resulted in a sulphur deposit on the gauze which was clearly discernible in the microscope. The gauzes were then tested for light-off temperature and activity and the results are shown in table 3. 1. 9 and graph 3. 1. 24.

3. 1. j. Electron probe microanalysis of inactive gauzes

It has been shown previously (3. 1. f.) that a substantial difference exists between the activities of gauzes which had undergone different methods of activation. Therefore, to obtain more information on the surface changes occurring during these treatments, an E. P. M. A. analysis was undertaken.

This involved using gauzes which had undergone the following pretreatments.

- (i) An unactivated gauze which had been run in a 10% ammonia/air mixture at $4,300 \text{ cm}^3 \text{ min}^{-1}$. (equivalent to 6 tons $\text{NH}_3 \text{ m}^{-2} \text{ catalyst day}^{-1}$). The total reaction time was two hours and the gauze showed low activity (3. 1. f.).
- (ii) A gauze which had been solvent cleaned, heated to $1,000^\circ\text{C}$ for 2 hours in oxygen flowing at $200 \text{ cm}^3 \text{ min}^{-1}$. The gauze was then used to catalyse the oxidation of ammonia as in (i) above. This gauze showed higher activity (3. 1. f.).
- (iii) An untreated unreacted gauze to act as a standard for (i) and (ii). The results of the elemental analysis are shown

in table 3.1.10. Investigation of the variation in Pt/Rh ratio across the grain boundaries was also undertaken.

This showed that there was no apparent rhodium enrichment occurring across the grain boundaries.

3.1.k. The effect of heating in the activation process

From earlier determinations (3.1.f.), it was apparent that samples which had been activated by heating gave a light-off temperature considerably below that of an untreated gauze.

To study the effect of heating, three unactivated, untreated gauzes were run for four hours, to ascertain the time at which these gauzes showed the activity equivalent to that of an untreated gauze. As was expected, the gauze had a high light-off temperature of 540°C . The development of activity of the gauzes is shown in graph 3.1.25, together with that of gauzes which had been activated in oxygen at $1,000^{\circ}\text{C}$ for 2 hours and then cooled in oxygen overnight.

3.2. E.S.C.A. studies of Pt/Rh foils and gauzes

Electron spectroscopy for chemical analysis has been used to study the changes in Pt/Rh ratio occurring during the activation of Pt/Rh foils and gauzes for ammonia oxidation. The catalysts have also been studied after reaction.

It was necessary to investigate the quantitative aspect of E.S.C.A. as a preliminary to the study. For these experiments, foils were used, containing different concentrations of rhodium and platinum, namely Pt/10% Rh and Pt/40%Rh. For comparison, a Pt/10%Rh gauze was investigated.

3.2.a. Platinum / 10% Rhodium foils

A piece of Pt/10%Rh foil was solvent treated to remove surface grease. An E.S.C.A. spectrum was then obtained, using the instrument conditions outlined in chapter 2. The spectrum is shown in Fig. 3.2.1. The signals have been assigned as shown in Fig. 3.2.1 particular attention being paid to the $\text{Pt}_{\text{N VII}}$, $\text{Pt}_{\text{N VI}}$, C_{Is} , O_{Is} and $\text{Rh}_{\text{M III}}$ signals.

Table 3.1.10

Treatment	Photo No.	Elemental Analysis	Wt % Rh	Wt % Pt
(i) Unactivated reacted	45	Si, Fe, Ti, Ca (high) Ca in pits + grooves	8.5	91.5
(ii) Activated + reacted	46	Low Ca in grooves None in pits	10.3	89.7
(iii) No treatment	47	Ca present as specks of dirt on gauze	8.7	91.3

Graph 3.1.25

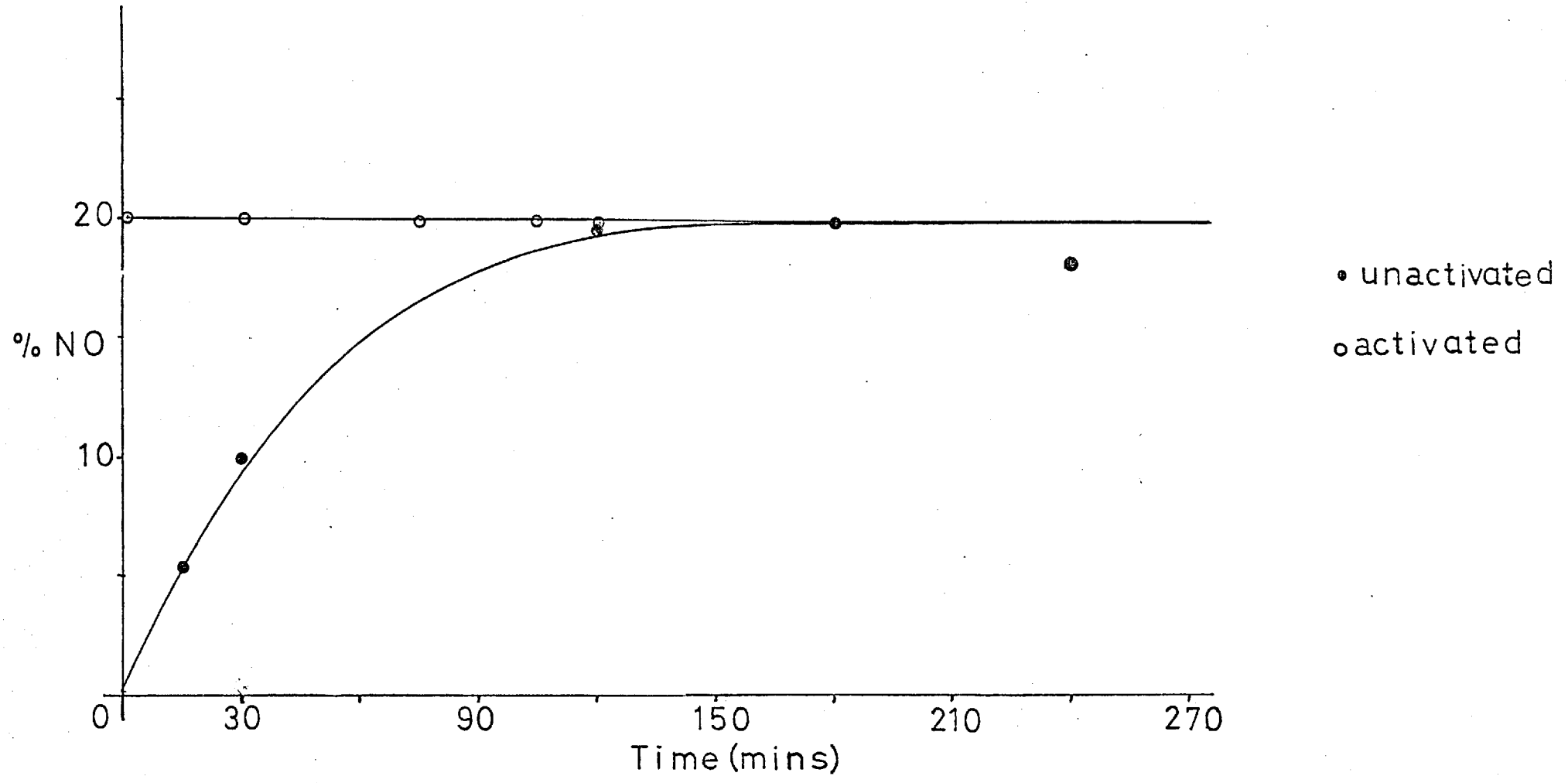
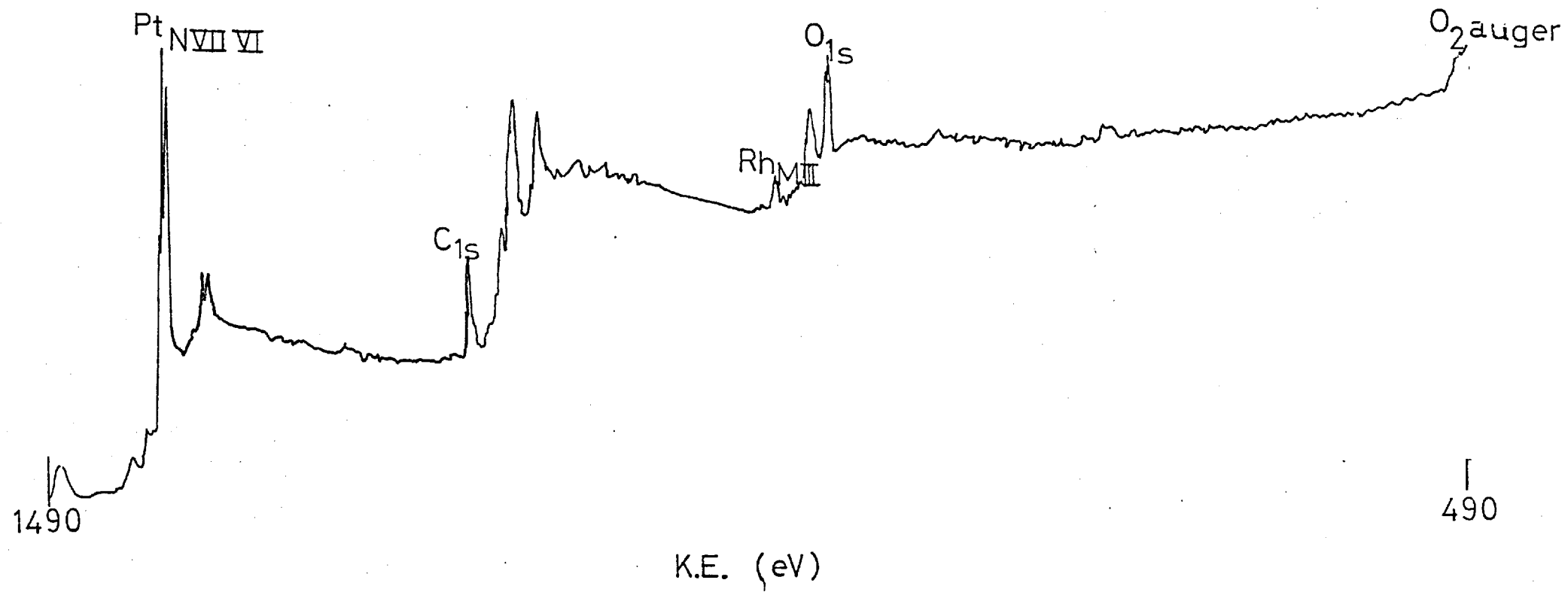


Fig 3.2.1



These are the signals which have been chosen for observation due to them being sharp, and well removed from any adjacent signals arising from other elements. After the general spectrum had been obtained, the instrument was set to scan the individual signals for further analysis. Hence, in Fig. 3.2.2, the $\text{Pt}_{\text{N VII}}$, $\text{Pt}_{\text{N VI}}$ signals are recorded, and in Fig. 3.2.3, the $\text{Rh}_{\text{M III}}$ and O_{Is} signals are shown.

To estimate the platinum and rhodium surface concentrations, the $\text{Pt}_{\text{N VII}}$, $\text{Pt}_{\text{N VI}}$ signals and $\text{Rh}_{\text{M III}}$ signals were scanned as shown in Figs. 3.2.4 and 3.2.5 respectively. The peak heights were measured, as shown, to provide a value for the surface concentrations of the platinum and rhodium present. The peak positions were also recorded relative to the fermi level at 1490 eV. The O_{Is} signal was then monitored for position and intensity as shown in Fig. 3.2.6.

The foil was then bombarded with argon ions for 30 seconds, to remove the top surface layers to a depth of 600 \AA . A general spectrum was obtained, Fig. 3.2.7, before repeating the determinations for the platinum and rhodium signal intensities and positions.

A second foil was inserted, which had undergone a solvent cleaning treatment followed by activation in an hydrogen flame. The general spectrum was obtained as shown in Fig. 3.2.8, and then the above experiment repeated.

A reacted foil was then investigated. This foil had been solvent treated, activated with an hydrogen flame and then reacted for two hours in a 10% ammonia/air mixture at a rate of $1,000 \text{ cm}^3 \text{ min}^{-1}$ (catalyst gauze loading $1.4 \text{ tons NH}_3 \text{ m}^{-2} \text{ catalyst day}^{-1}$). The positions and intensities of the platinum, rhodium, carbon and oxygen signals before and after bombarding were obtained. The results of these experiments are shown in table 3.2.1 and 3.2.2.

The activation by oxygen was then studied. This method of activation has been shown to produce reproducible light-off temperatures and a heavily pitted gauze surface. The foil was first solvent washed and activated for two hours at $1,000^\circ \text{C}$ in oxygen flowing at a rate of $200 \text{ cm}^3 \text{ min}^{-1}$. A second foil was similarly treated and then reacted in a 10% ammonia/air mixture flowing at a rate of $4,300 \text{ cm}^3 \text{ min}^{-1}$

Fig 32.2

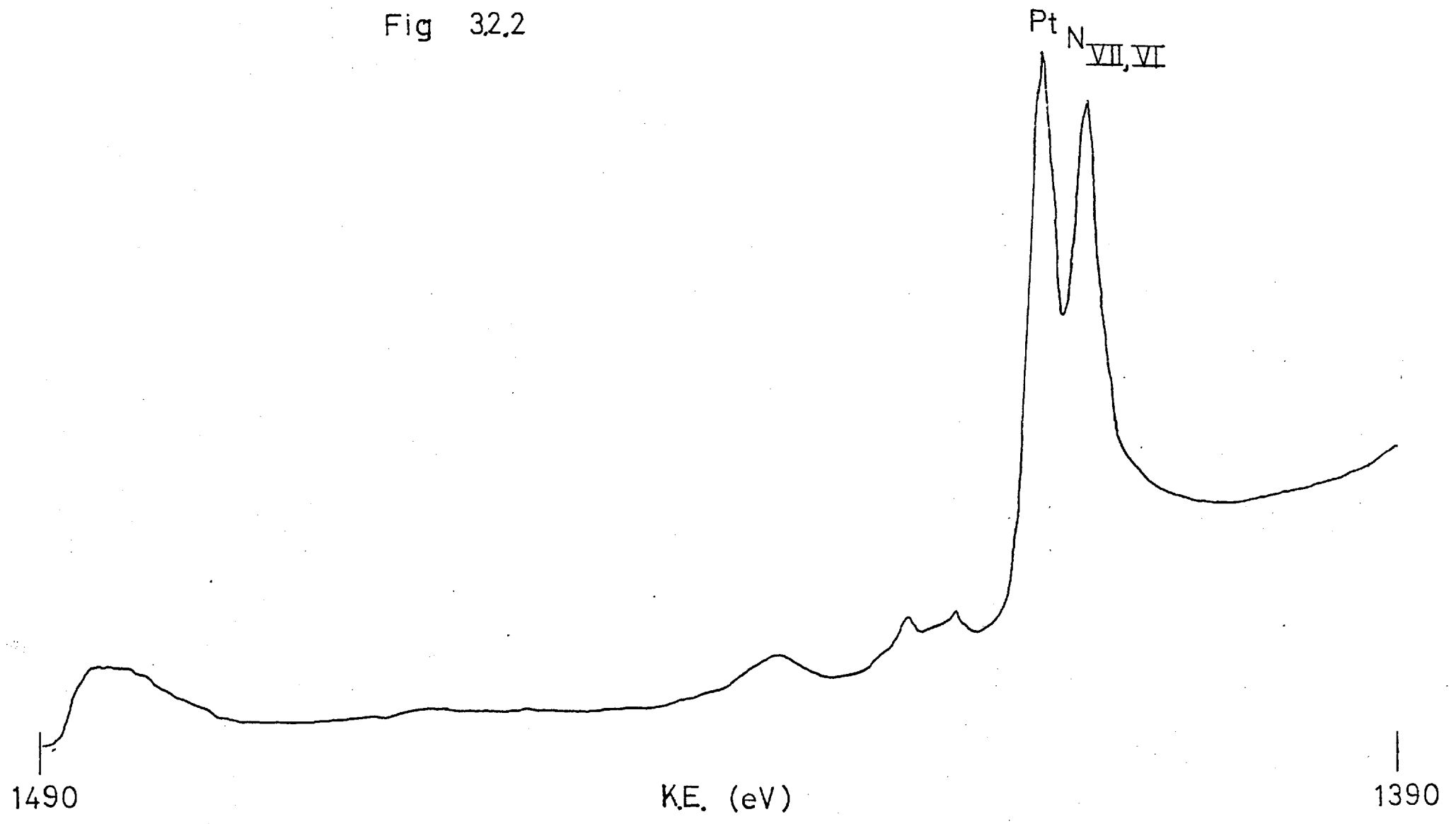


Fig 3.2.3

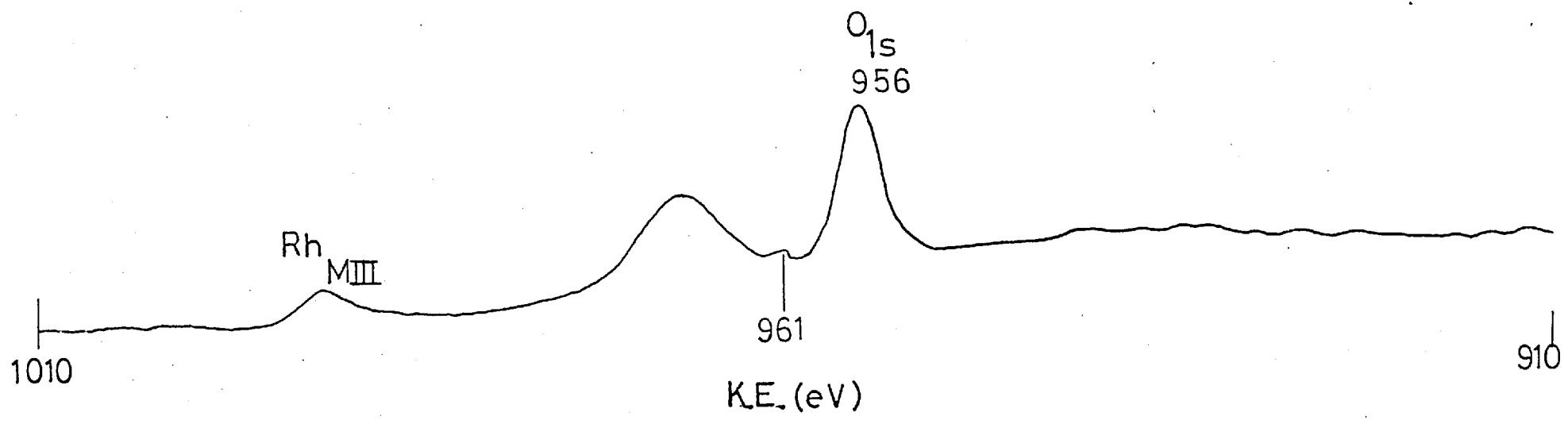


Fig 3.24

Pt
N_{VII} VI

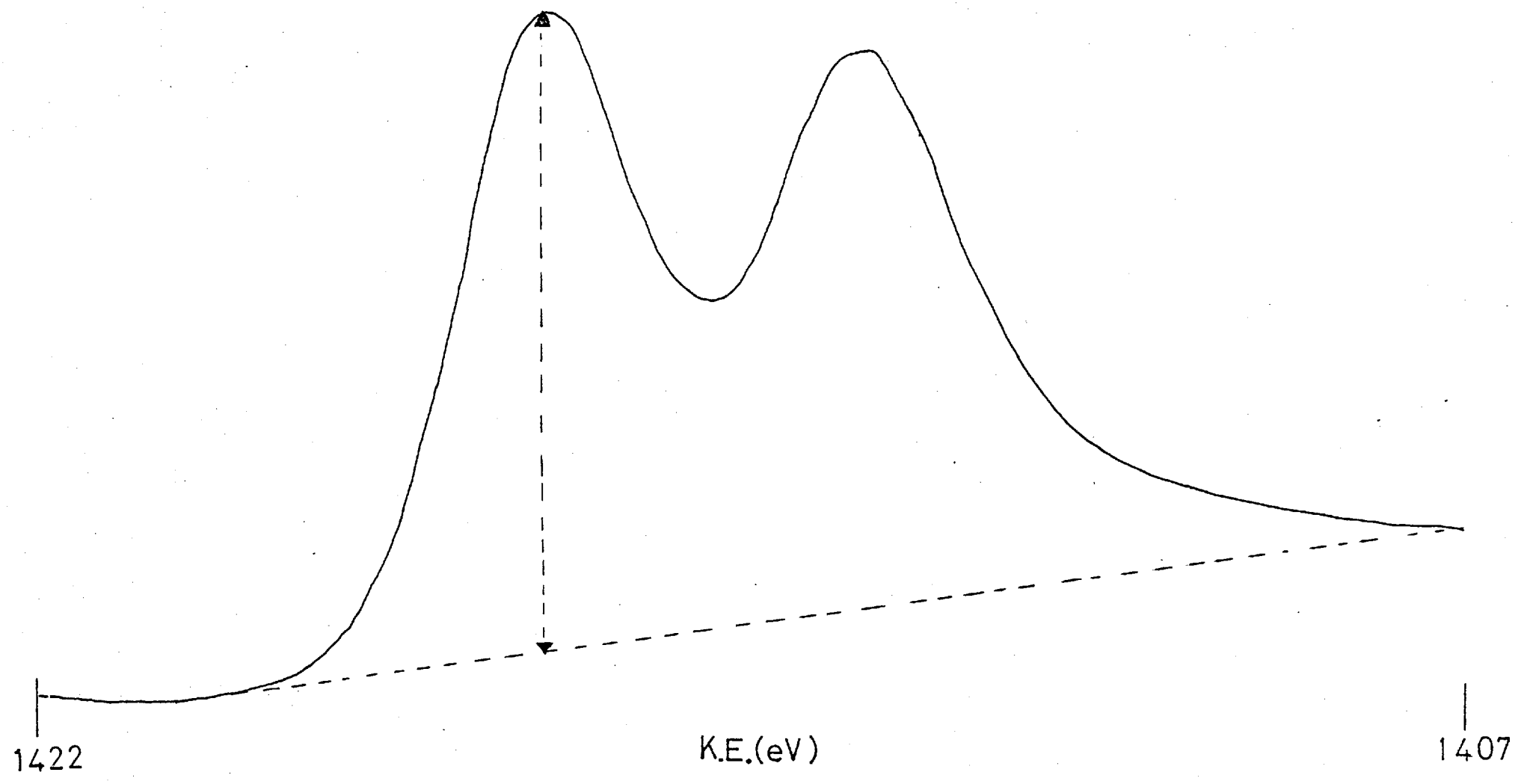


Fig 3.2.5 Rh_{MIII}

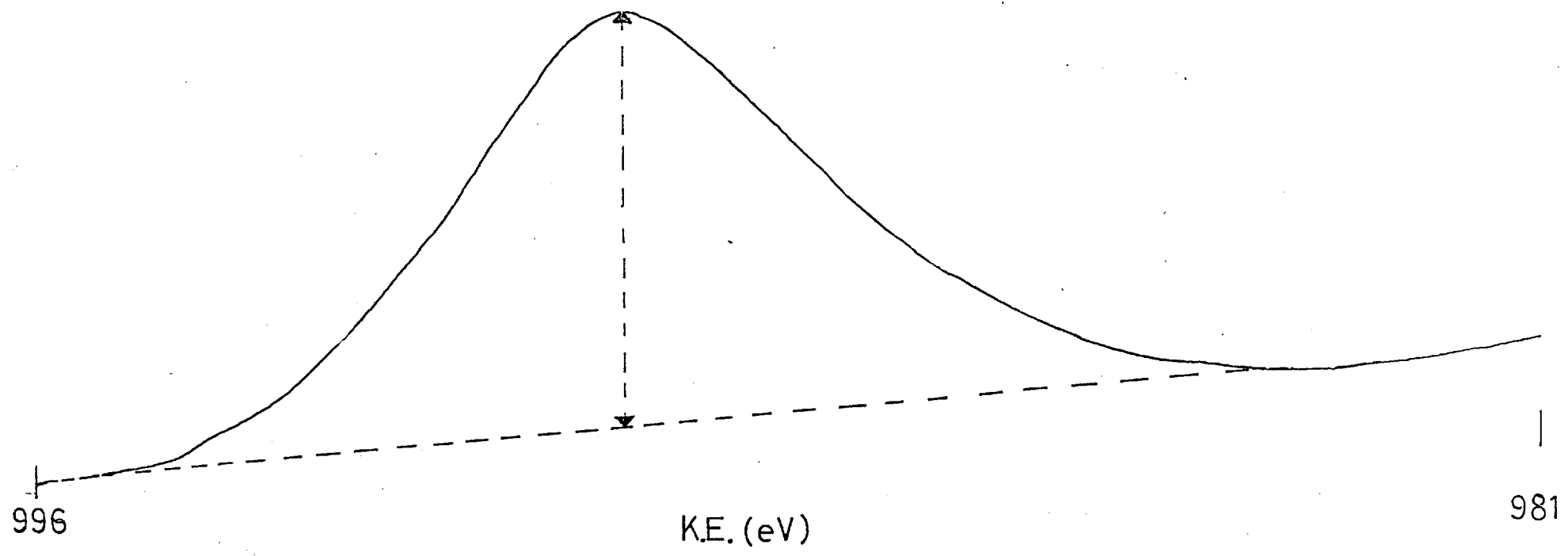


Fig. 3.2.6

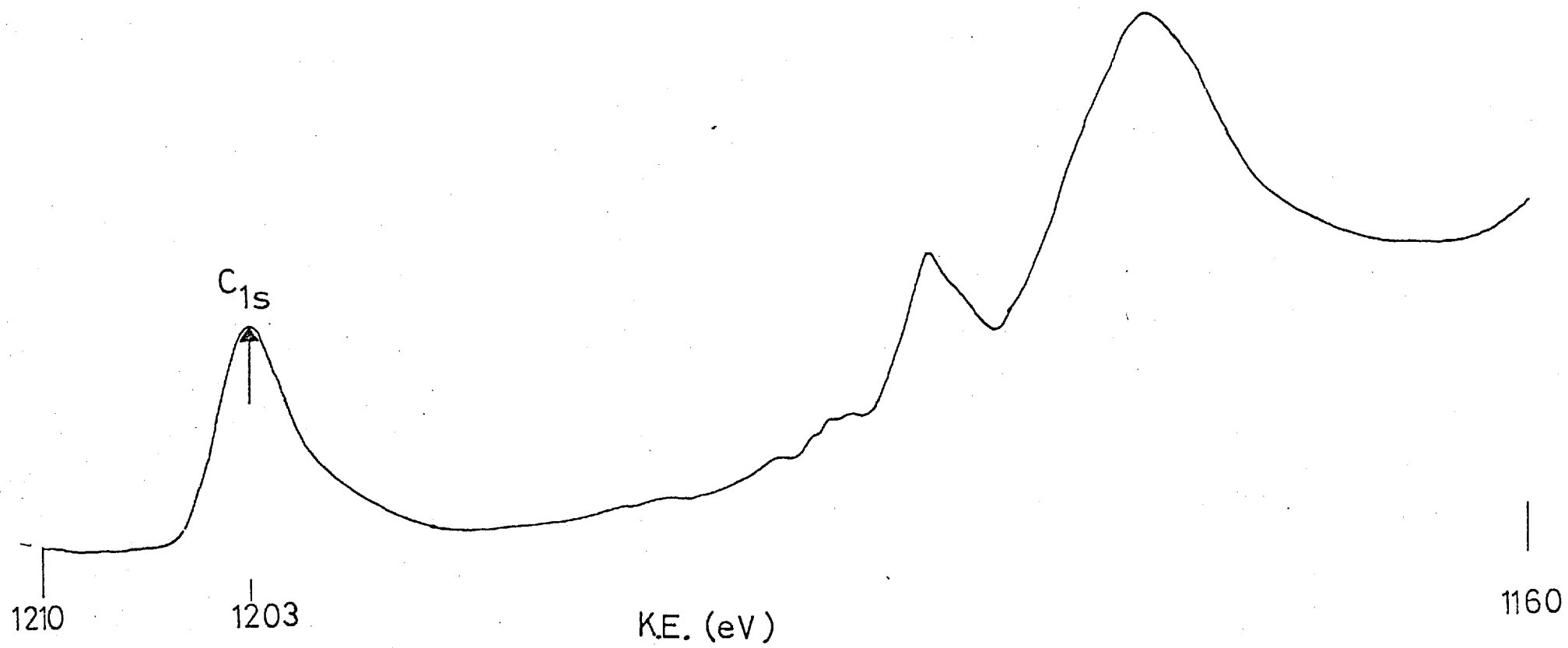


Fig 3.2.7

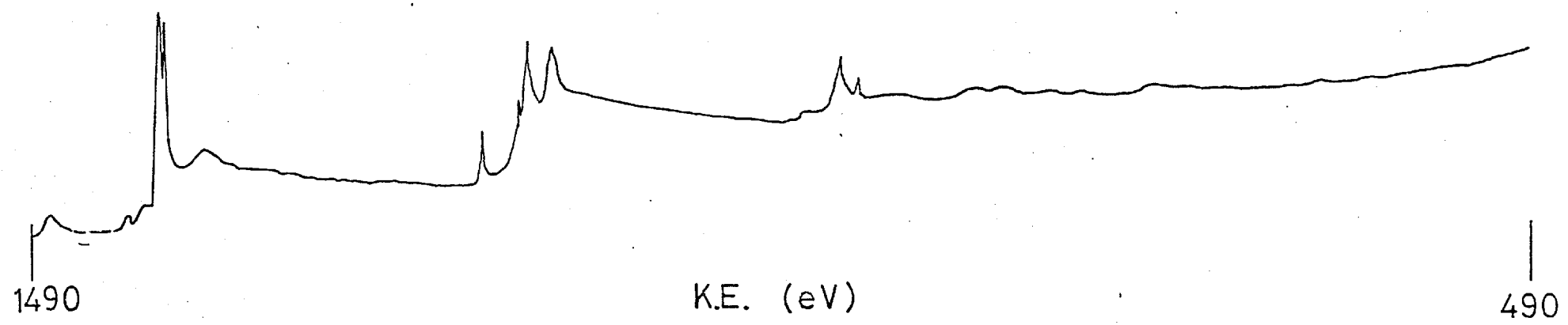


Fig 3.2.8

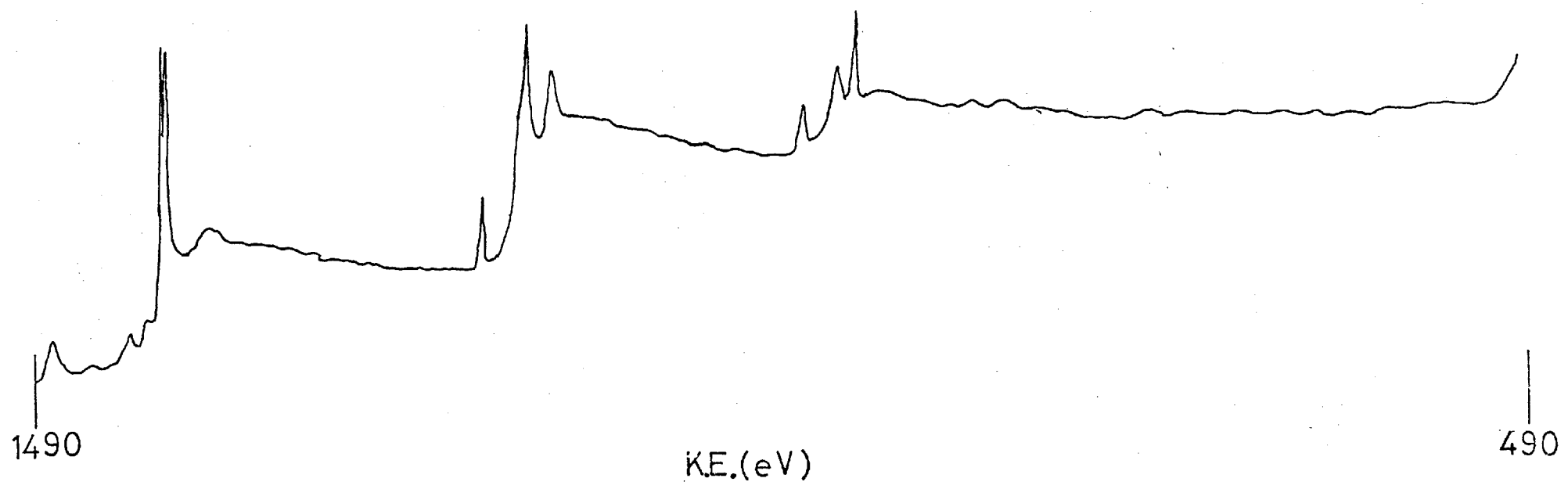


Table 3.2.1

Pt/10%Rh foil	Platinum				Rhodium			
	Initial		After bombardment		Initial		After bombardment	
	Intensity (cm)	Position (eV)	Intensity (cm)	Position (eV)	Intensity (cm)	Position (eV)	Intensity (cm)	Position (eV)
As supplied	22.2	71.8	20.0	71.6	1.45	497	1.25	497
Activated	21.2	71.8	27.2	72.1	3.5	498.5	1.9	497.3
Activated + Reacted	15.4	71.6	24.8	71.6	1.55	497.5	1.65	496.9

Table 3.2.2.

Pt/10% Rh foils	$Pt_{N \overline{VII}}/C_{Is}$	$Pt_{N \overline{VII}}/O_{Is}$	C_{Is}/O_{Is}
As supplied	3.13	3.13	1
" " + bombard.	3.75	10.00	3.67
Activated	3.42	2.74	0.8
" + bombard.	6.1	1.4	2.3
Activated	4.0	3.64	0.91
" + bombard.	9.5	2.85	3.00

(equivalent to a catalyst gauze loading of 6 tons $\text{NH}_3 \text{ m}^{-2}$ catalyst day^{-1}). Total reaction time was 2 hours at a running temperature of 580°C . The results are shown in tables 3.2.3 and 3.2.4.

3.2.b. Pt/40%Rh foils

Three Pt/40% foils were treated as shown in 3.2.a. E.S.C.A. spectra were obtained, showing positions and intensities of the $\text{Pt}_{\text{N VII}}$, $\text{Pt}_{\text{N VI}}$, $\text{Rh}_{\text{M III}}$, C_{Is} and O_{Is} signals. The results are shown in tables 3.2.5 and 3.2.6.

3.2.c. Pt/10%Rh gauze catalysts

Three layers of Pt/10%Rh gauze catalyst were spot-welded to the tungsten support mount of the E.S.C.A. spectrometer. The sample was inserted and the investigation carried out using the conditions outlined previously. Three gauzes were needed to produce a signal of sufficient intensity to be comparable to that obtained with a Pt/10% Rh foil. These gauzes, as supplied, were then treated 'in situ' in the E.S.C.A. spectrometer. This was necessary because the area of the gauze required for the E.S.C.A. analyser could not be accommodated in the ammonia oxidation reactor. (The largest piece which could be prepared in the reactor has a diameter of approximately 1 cm : a gauze 2 cm in diameter was needed for an E.S.C.A. analysis). The results are shown in table 3.2.7 and a complete summary of the Pt/Rh ratios for this and previous experiments is shown in table 3.2.8.

3.2.d. Pt/10%Rh foil deactivated by water

It has been shown previously (3.1.i), that water treatment substantially increases the light-off temperature of the catalyst. Two pieces of Pt/10%Rh foil were solvent washed and activated for 2 hours at $1,000^\circ\text{C}$ in oxygen flowing at $200 \text{ cm}^3 \text{ min}^{-1}$. A spectrum of one of these foils was obtained and used as a reference. The second foil was soaked in distilled water for two hours, dried in air, and its spectrum obtained. The results are shown in table 3.2.9.

Table 3.2.3.

Pt/10%Rh foil	Platinum				Rhodium			
	Initial		After bombardment		Initial		After bombardment	
	Intensity (cm)	Position (eV)	Intensity (cm)	Position (eV)	Intensity (cm)	Position (eV)	Intensity (cm)	Position (eV)
Activation O ₂ , 1,000°C 2 hrs.	11.6	71.6	24.0	72.2	3.05	498.2	2.7	497.3
Activation † Reaction	15.6	71.9	18.4	71.9	2.15	498.2	1.35	497.0

Table 3.2.4.

Pt/10% Rh foils	$Pt_{N \overline{VII}}/C_{Is}$	$Pt_{N \overline{VII}}/O_{Is}$	C_{Is}/O_{Is}
Activated, O_2 , $1000^\circ C$, 2 hrs.	2.79	1.3	0.5
" + Ar^\oplus bombard	6.4	6.4	1.0
Activated + reacted	5.1	2.18	0.34
" + Ar^\oplus bombard	5.5	8.34	1.5

Table 3.2.6.

Pt/40% Rh foils	$Pt_{N \overline{VII}}/C_{Is}$	$Pt_{N \overline{VII}}/O_{Is}$	C_{Is}/O_{Is}
As supplied	1.25	3.4	2.74
Activated-hydrogen flame	4.0	4.0	1
Activated + reacted	3.67	2.2	0.6

Table 3.2.5.

Pt/40% Rh foils	Platinum		Rhodium	
	Position (eV)	Intensity (cm)	Position (eV)	Intensity (cm)
As supplied	72.2	34.4	497.6	4
Activated, hydrogen flame	72.1	44.0	497.9	11.2
Activated + reacted	71.9	6.6	497.7	2.35

Table 3.2.7.

Pt/10% Rh gauze	Platinum		Rhodium
	Position (eV)		Position (eV)
	Initial	After bombarding	Initial
As supplied	72.1	72.3	498.2
Activated	72.2	72.0	498.1
Reacted (in situ)	71.9		497.3

Table 3.2.8.

Treatment	Pt/10% Rh gauze		Pt/10% Rh foil		Pt/40% Rh foil
	Pt/Rh		Pt/Rh		Pt/Rh
	initial	after bombardment	initial	after bombardment	initial
As supplied	7:1	11:1	15:1	16:1	8.6:1
Activated - hydrogen flame	5:1	14:1	6:1	14.3:1	4:1
Activated oxygen, 1,000°C, 2 hours			4:1	9:1	
Activated + Reacted	18:1*		10:1	15:1	2.8:1

* in situ

Table 3.2.9.

Pt/10% Rh foil	Pt				Rh				Pt/Rh	
	Initial		After bombarding		Initial		After bombarding		initial	After bombarding
	position (eV)	intensity (cm)	position (eV)	intensity (cm)	position (eV)	intensity (cm)	position (eV)	intensity (cm)		
Activation, O ₂ 1,000°C, 2 hrs.	72.3	34.4	72.2	75.1	499.1	5.4	497.7	9.0	6.4:1	8.4:1
Activation + soak 2 hrs, distilled water	72.1	12.8	72.2	49.6	498.9	6	497.7	4.8	2.1:1	10.3:1

Fig 3.2.9

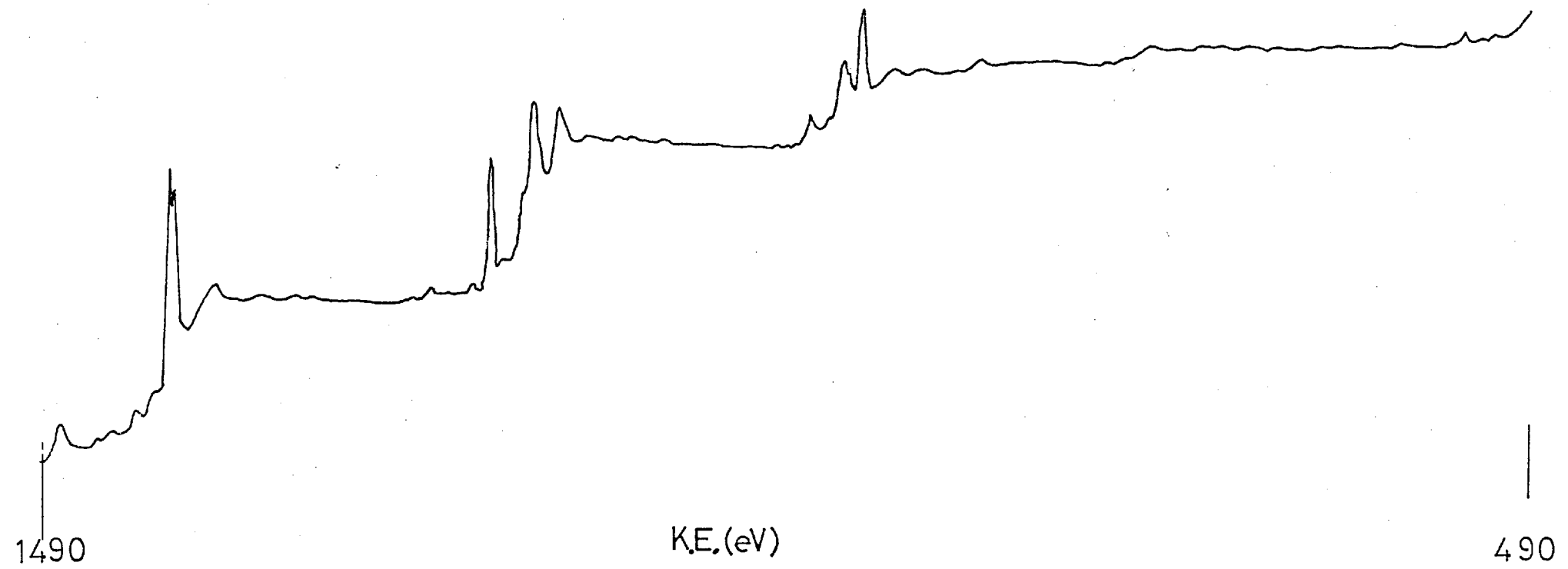


Fig 3.2.10

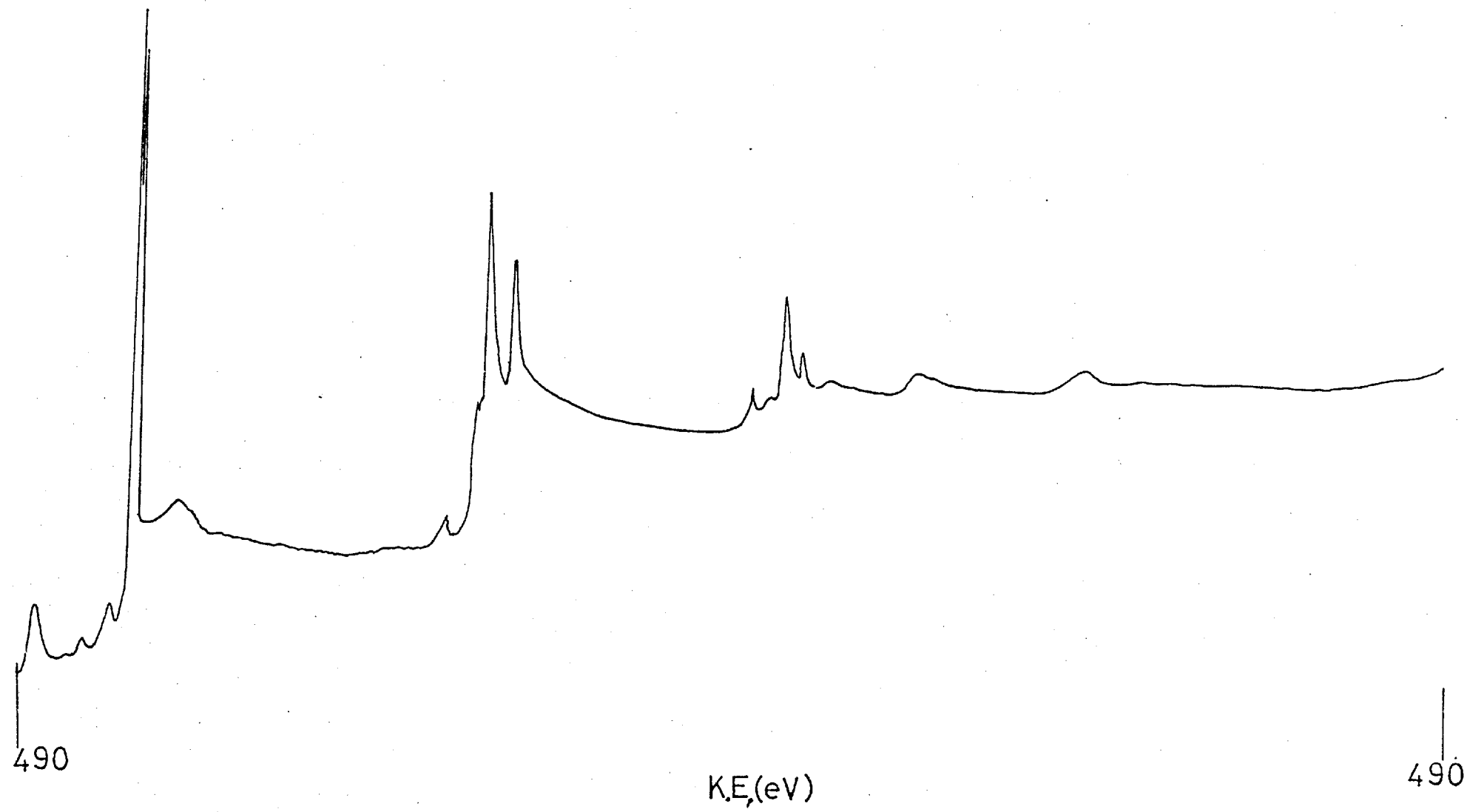


Fig 3.2.11

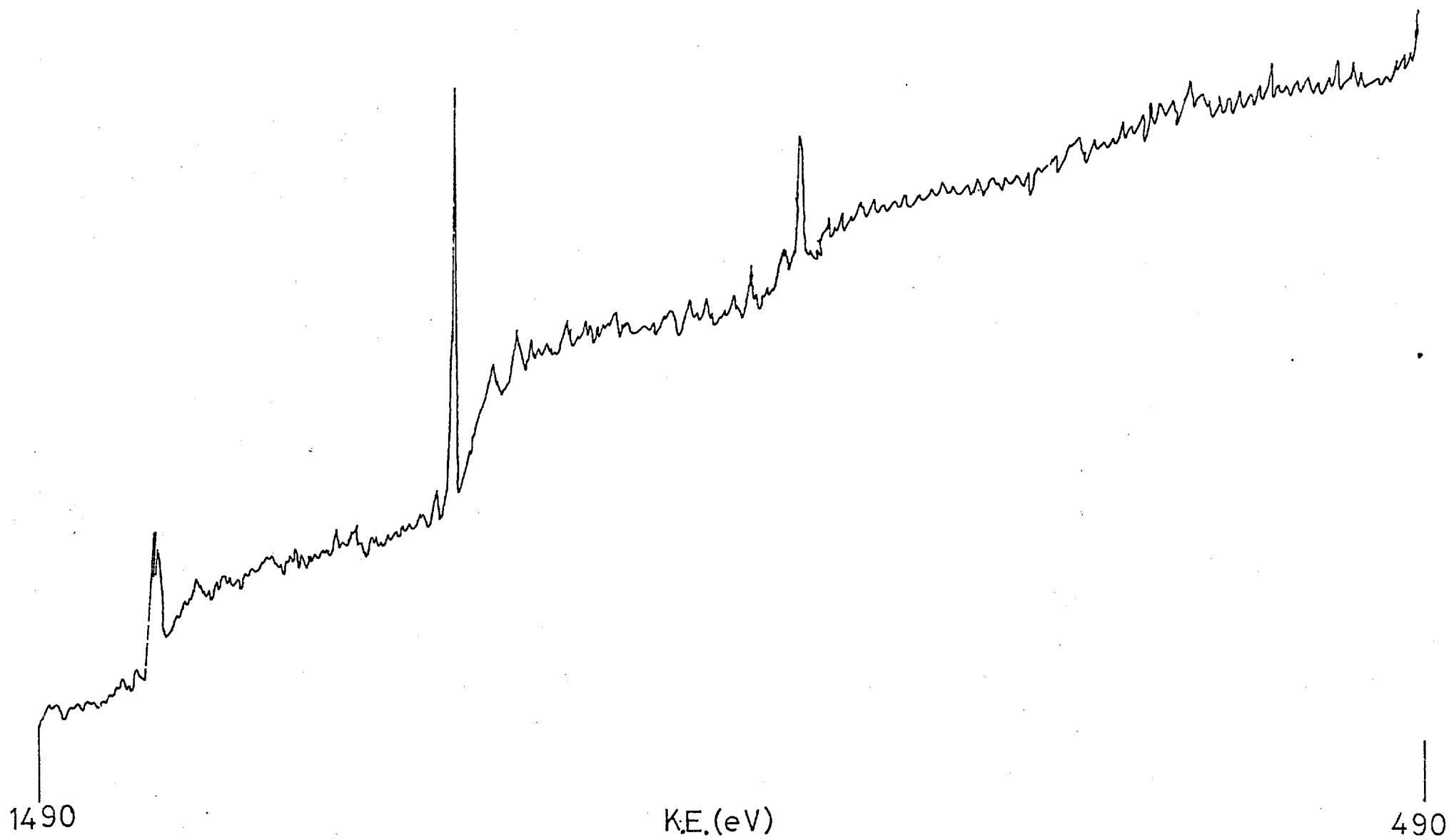


Fig 3.2.12

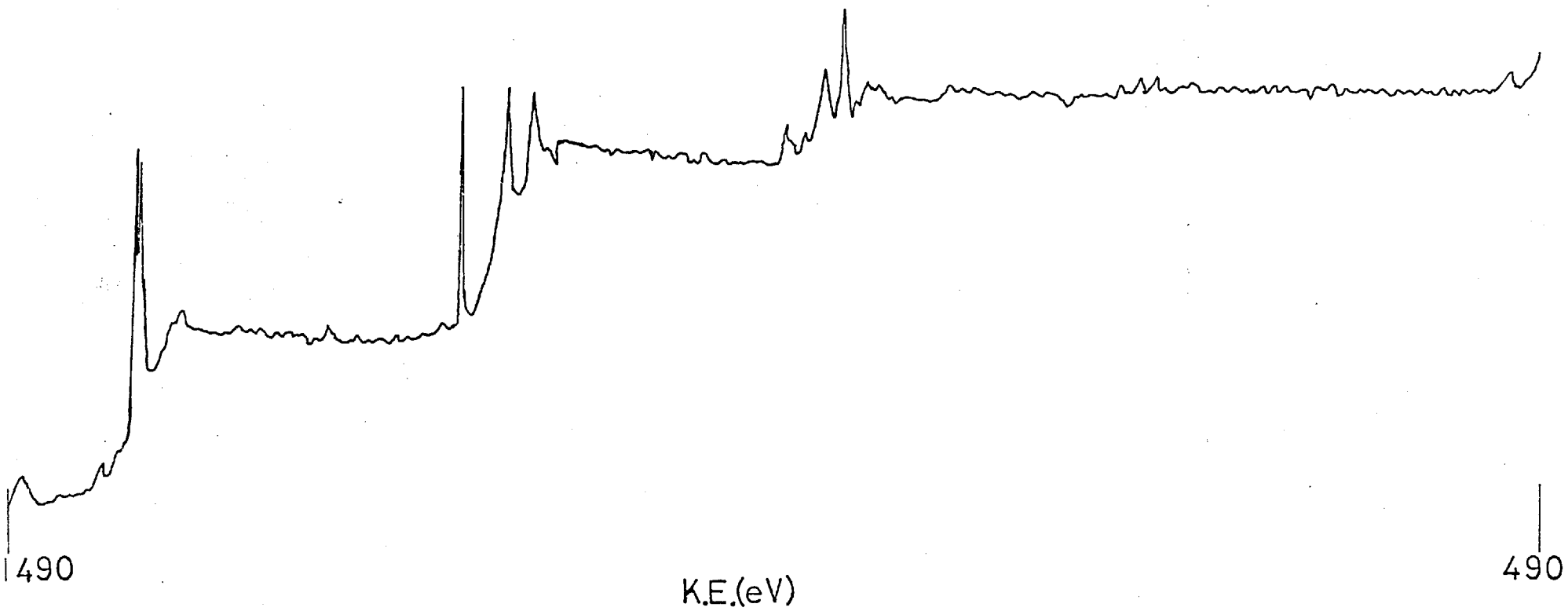
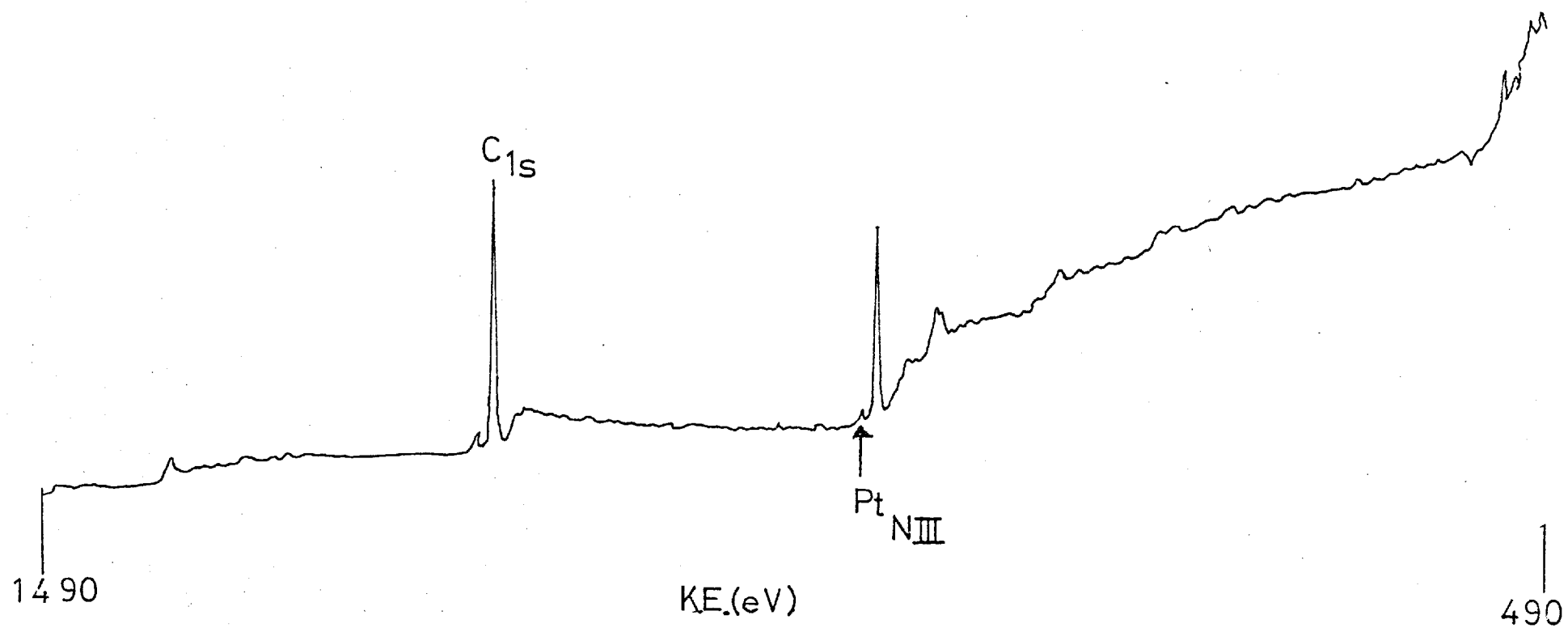
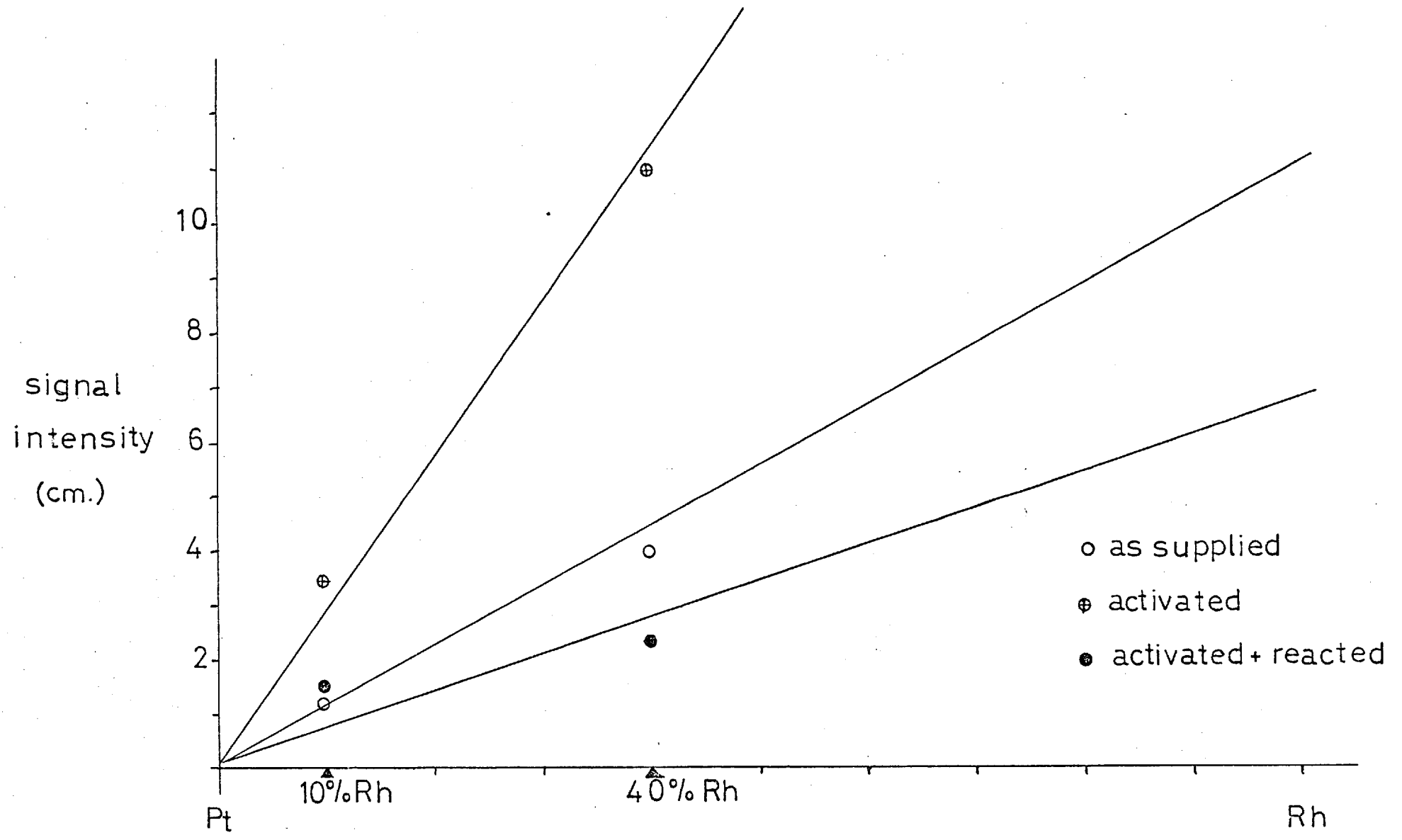


Fig 3.2.13

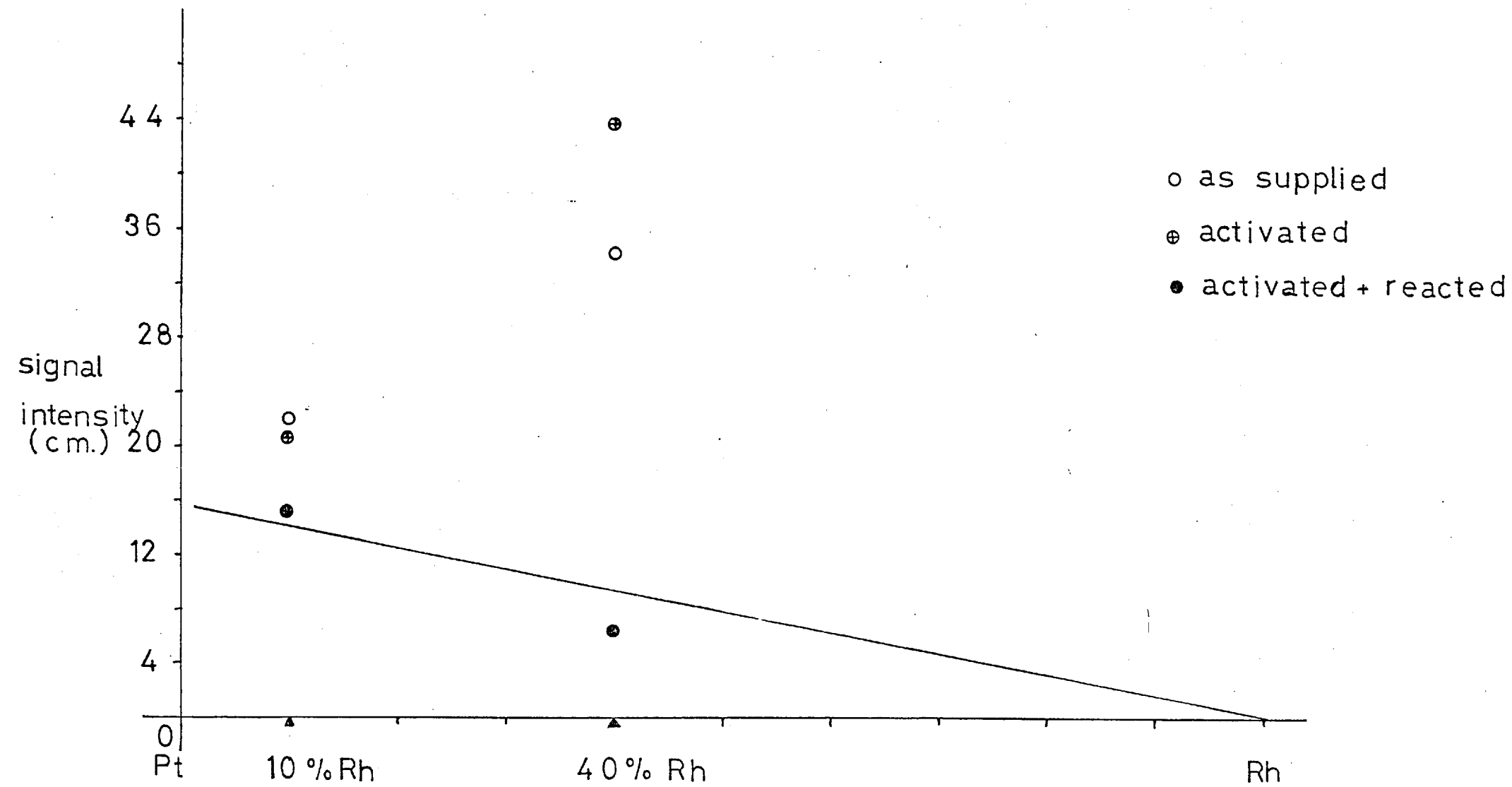


Graph 3.2.1 Rh calibration



Graph 3.2.2

Pt calibration



3. 2. e. Shift of the Rh_{M III} signal during oxidation

A piece of Pt/10%Rh foil was solvent cleaned and heated in air for 3 days at 750°C. An E. S. C. A. spectrum was then obtained using Mg K α radiation, at 12 Kv and a current of 40 μ A. The positions of the Rh_{M III} signals are listed in table 3. 2. 10.

3. 3. Ultra violet Photoelectron Spectroscopy (U. P. S.)

3. 3. a. Pt/40%Rh foil heated in situ

A piece of Pt/40%Rh foil was activated by washing in solvent and heating in an hydrogen flame. It was then spot-welded to a tungsten support ring and placed in the spectrometer. The foil was then heated to 800°C in vacuo and argon bombarded for 30 minutes using 500 eV ions at a current of $1/5$ μ A. A U. P. S. spectrum of the sample was then obtained using He_{II, III} radiation (Fig. 3. 3. 1). The foil was then treated in situ as shown in table 3. 3. 1.

3. 4. Surface Diffusion

Photographs 79 - 82 and 83 - 86 show the results obtained when scratches were drawn in a Pt/10%Rh foil and the foil then reacted. Photographs 79 - 82 show that no accurate results of scratch widths can be obtained due to the reaction proceeding at varying rates on different grains.

Photographs 83 - 86 do show that no 'hump' is formed at the edges of the scratches.

Table 3.2.10.

Pt/10% Rh foil	$Rh_{M \text{ III}}$	Photo No.
Treatment	position (eV)	
Activation, air 3 days, 750°C	498.5	48
Activation + reaction	497.6	49

Table 3.3.1

Pt/40% Rh foil	
Treatment	Fig No.
5×10^{-6} Torr NH_3 , room temp. 5 min.	3.3.2.
5×10^{-6} Torr NH_2 , at 500°C	3.3.3.
5×10^{-6} Torr O_2 , room temp. 10 min.	3.3.4.
10^{-6} Torr O_2 , at 800°C 5 min.	3.3.5.
10^{-5} Torr H_2 , at 800°C 10 min.	3.3.6.
5×10^{-5} Torr H_2 , at 1,000°C 30 min.	3.3.7.

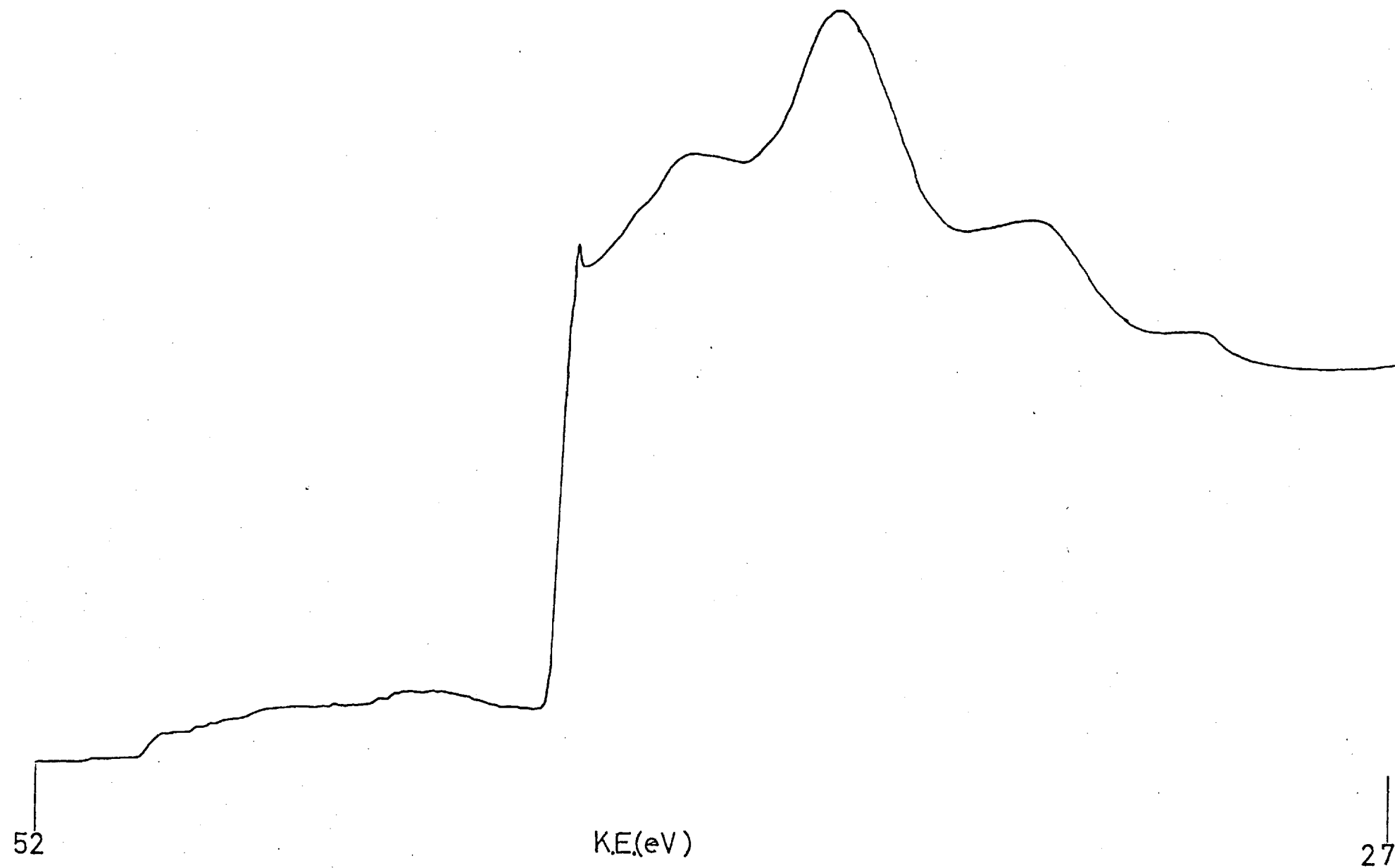


Fig 3.3.2

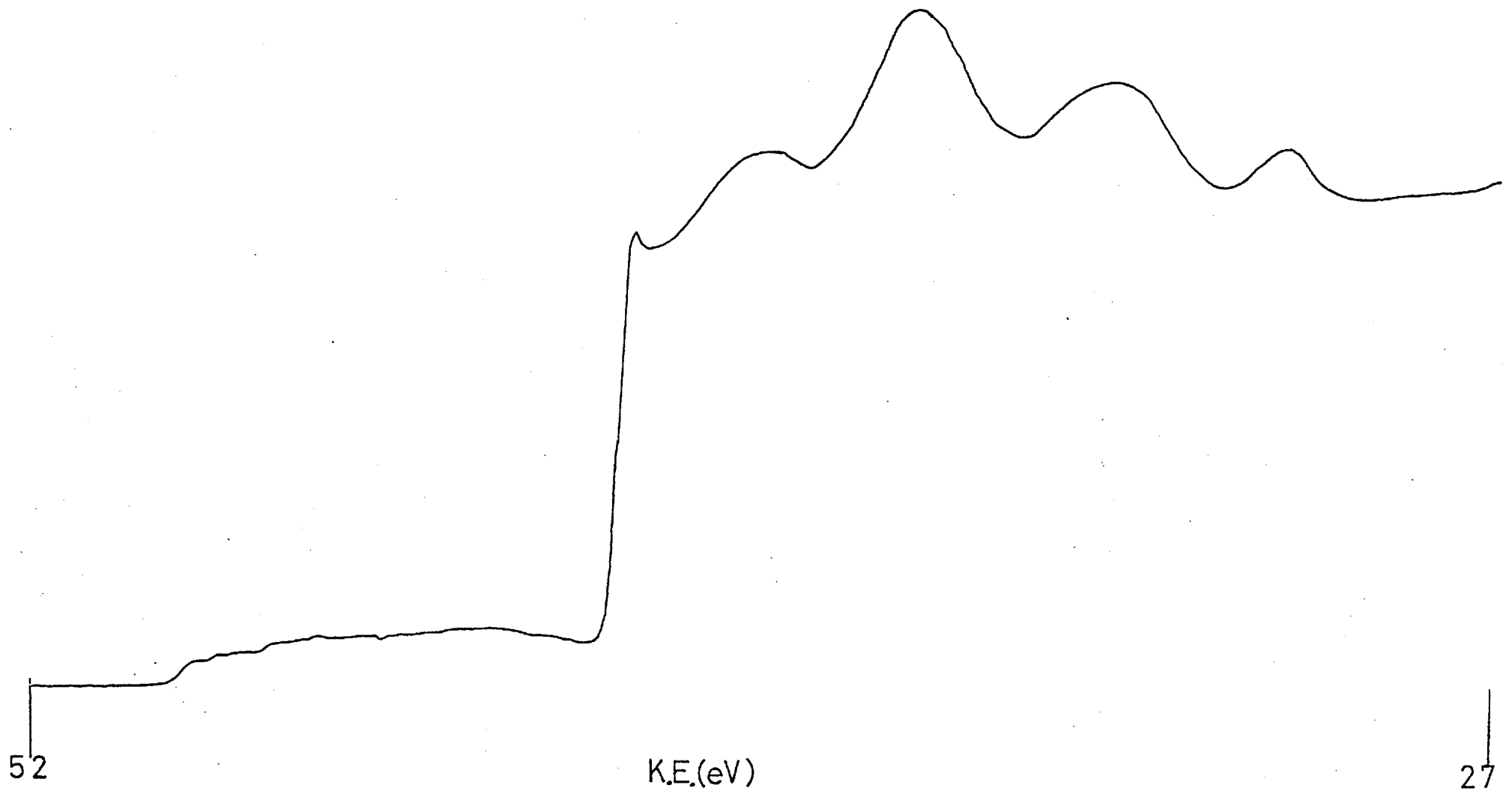


Fig 3.3.3

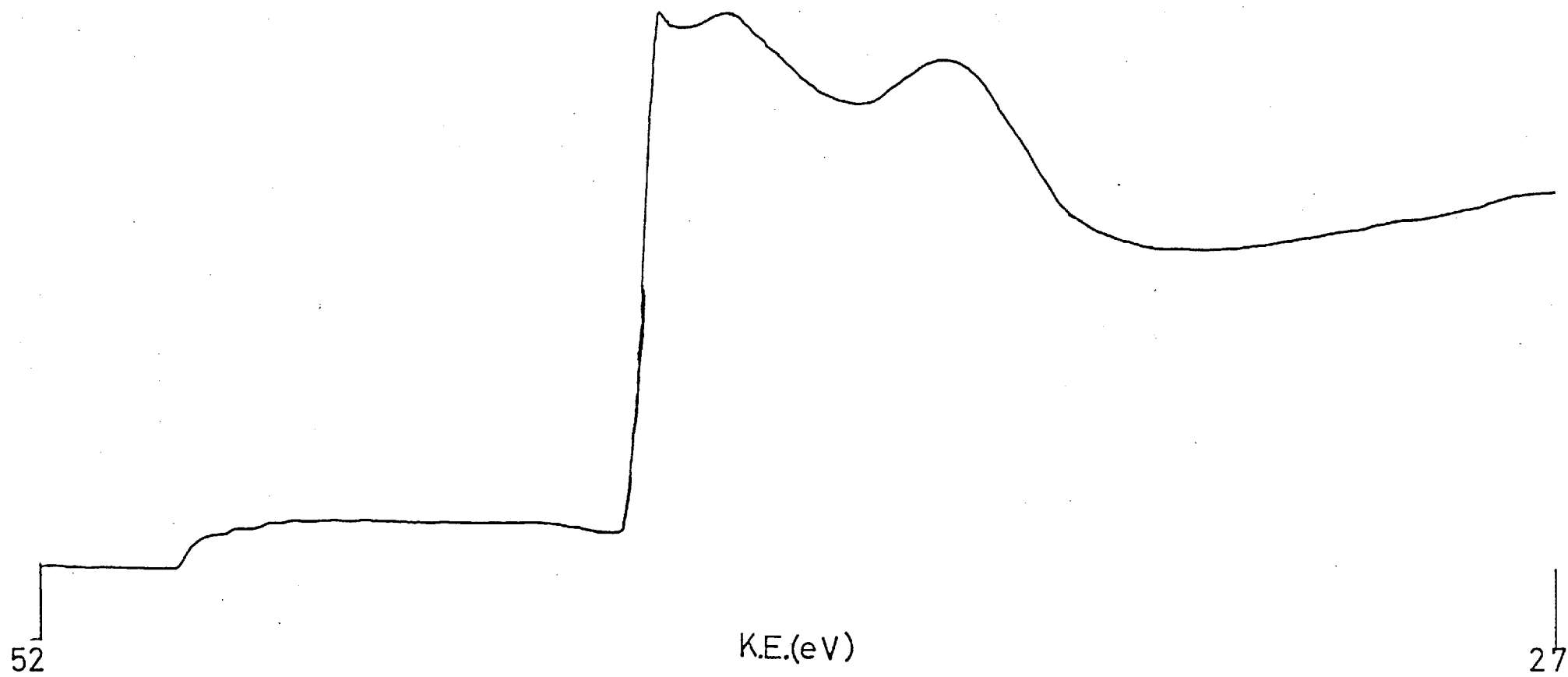


Fig 3.3.4

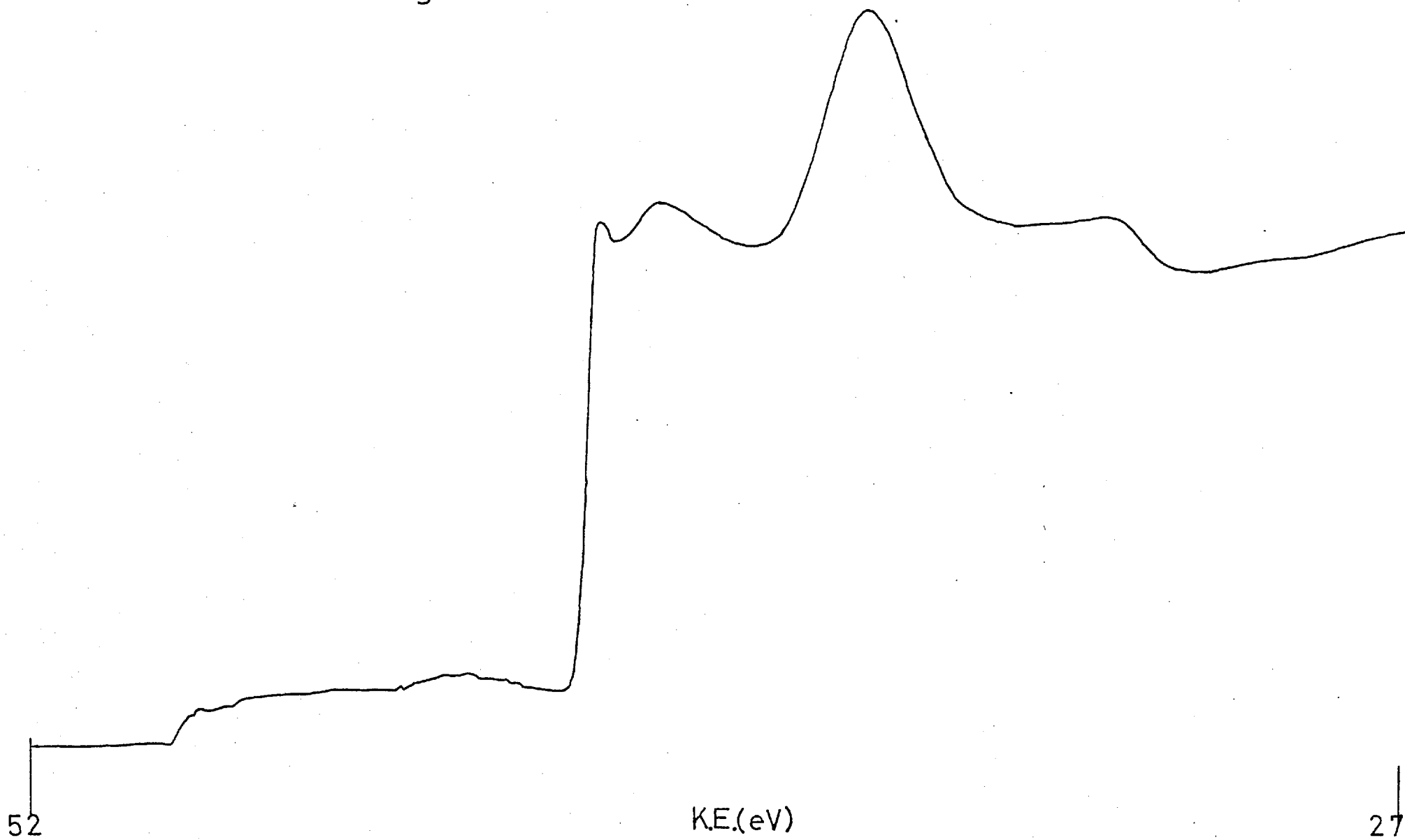


Fig 3.3.5

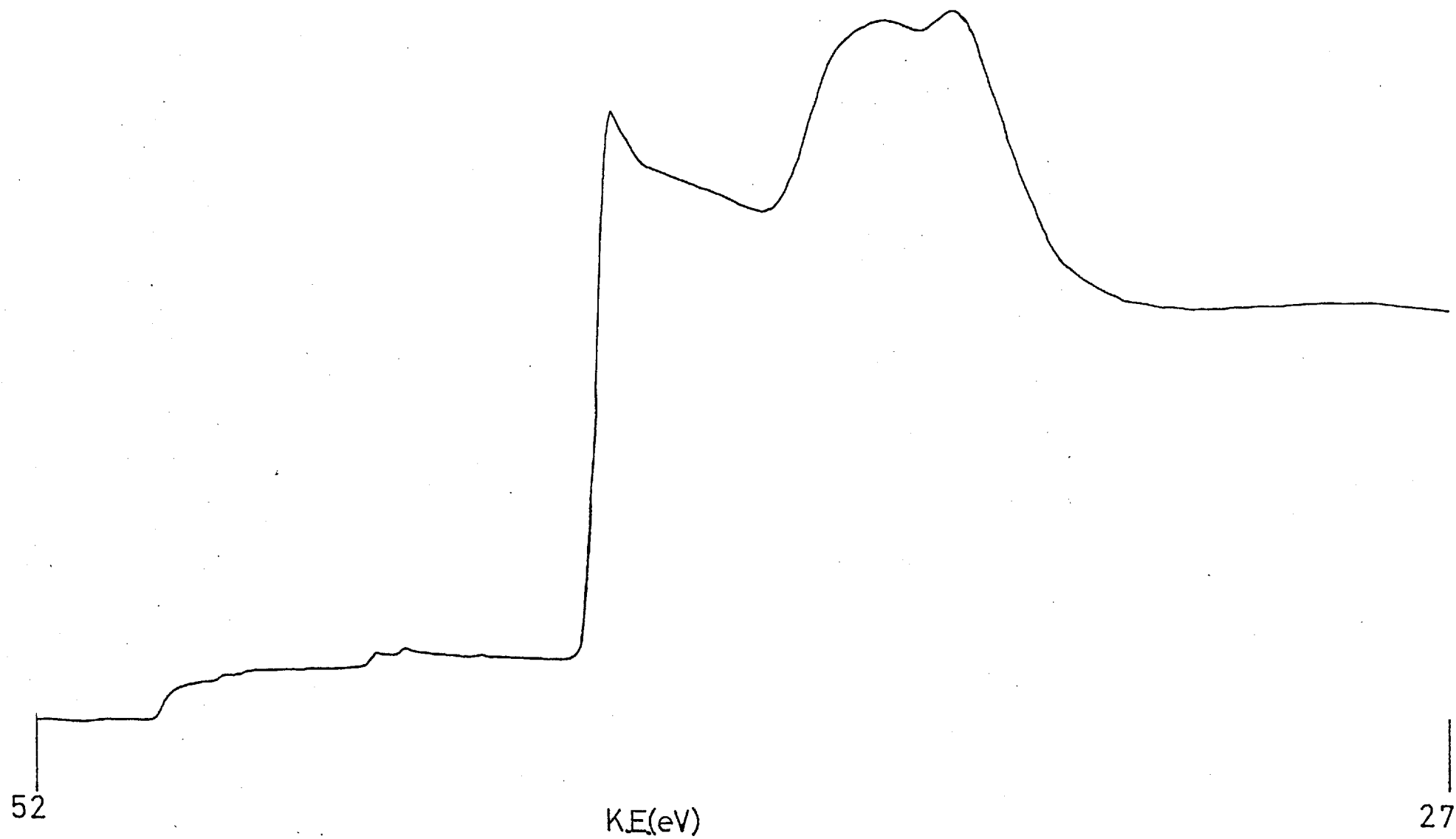


Fig 3.3.6

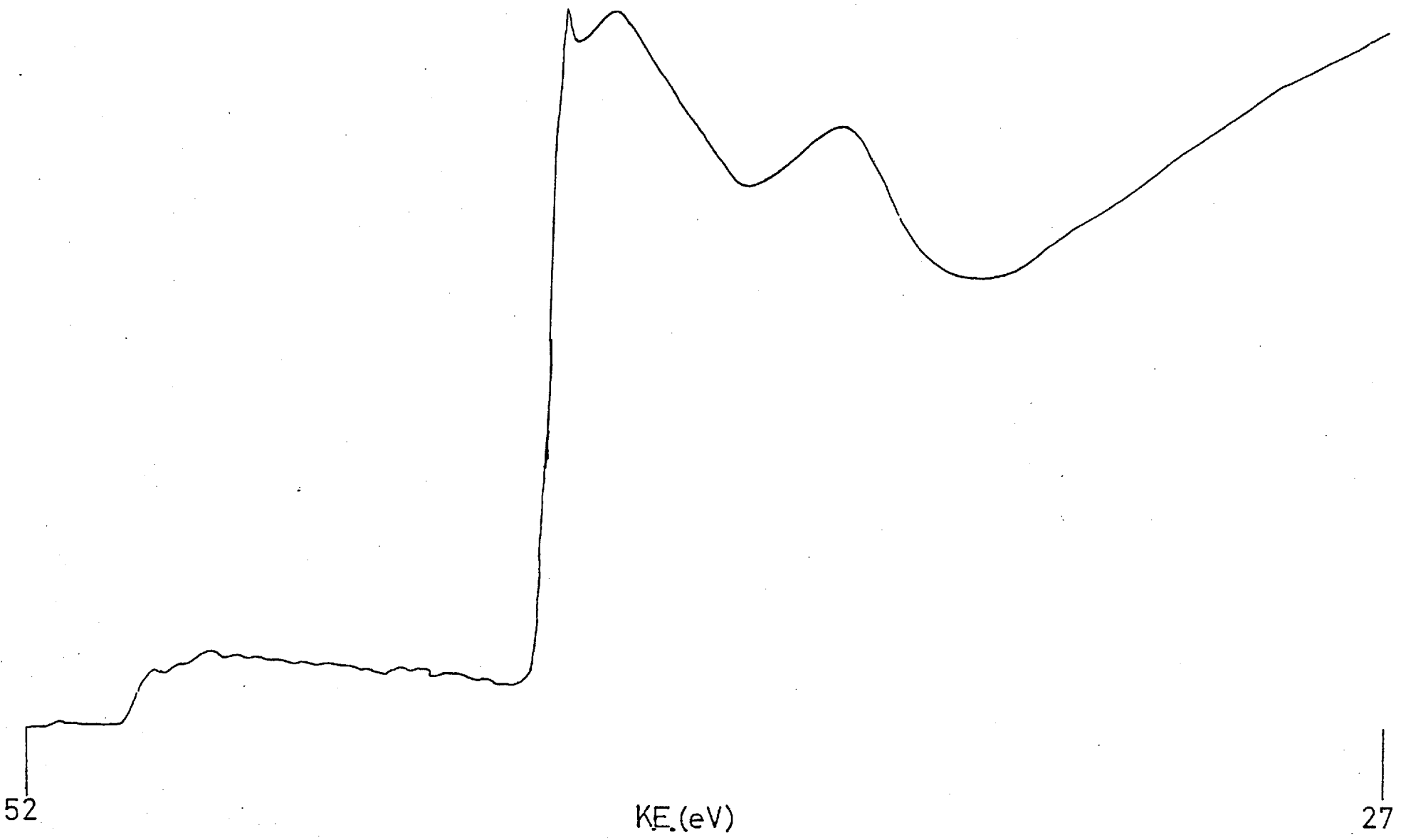
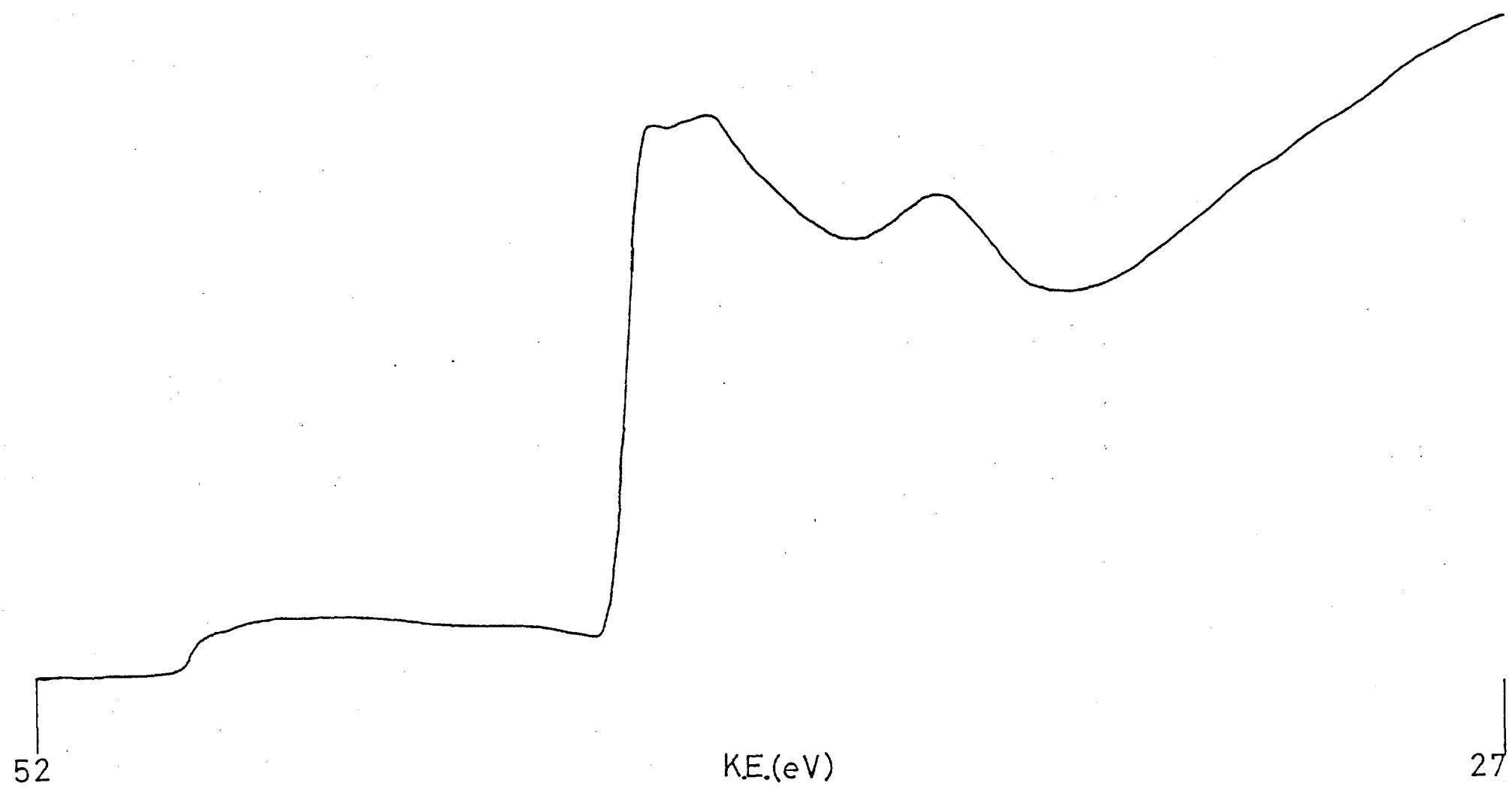


Fig. 3.3.7



3. 5. Deactivation Studies

It has been noted previously (38) that iron oxides are poisons for ammonia oxidation catalysts. Iron oxide was therefore used as a dopant to find the most suitable method of deactivating the Pt/Rh catalyst.

3. 5. a Iron oxide (Fe_2O_3) dopant

A comparison was drawn between gauzes which had first been activated prior to doping, and those which had been solvent washed prior to doping. Graph 3. 5. 1 and table 3. 5. 1 show that the former was deactivated more than the latter, giving both a higher light-off temperature and a lower conversion rate after 1 hour of running.

This can be explained by the fact that activation in oxygen causes pitting. These pits allow more iron oxide to be retained on the gauze surface, thus giving greater deactivation.

As a direct comparison, iron oxide was deposited on the catalyst by vacuum evaporation of iron wire. The result is shown in table 3. 5. 1 and graph 3. 5. 1. The gauze temperature profiles are shown in graph 3. 5. 2.

3. 5. b Gold dopant

Both sides of three Pt/10% Rh gauzes were coated with gold using the vacuum evaporation technique. The results are shown in table 3. 5. 1 and graph 3. 5. 1, with the temperature profiles in graph 3. 5. 2.

3. 5. c Metal oxide dopants

Suspensions of the metal oxides shown in table 3. 5. 2 were prepared and used in the doping of three Pt/10% Rh gauzes as outlined previously.

Graph 3.51.

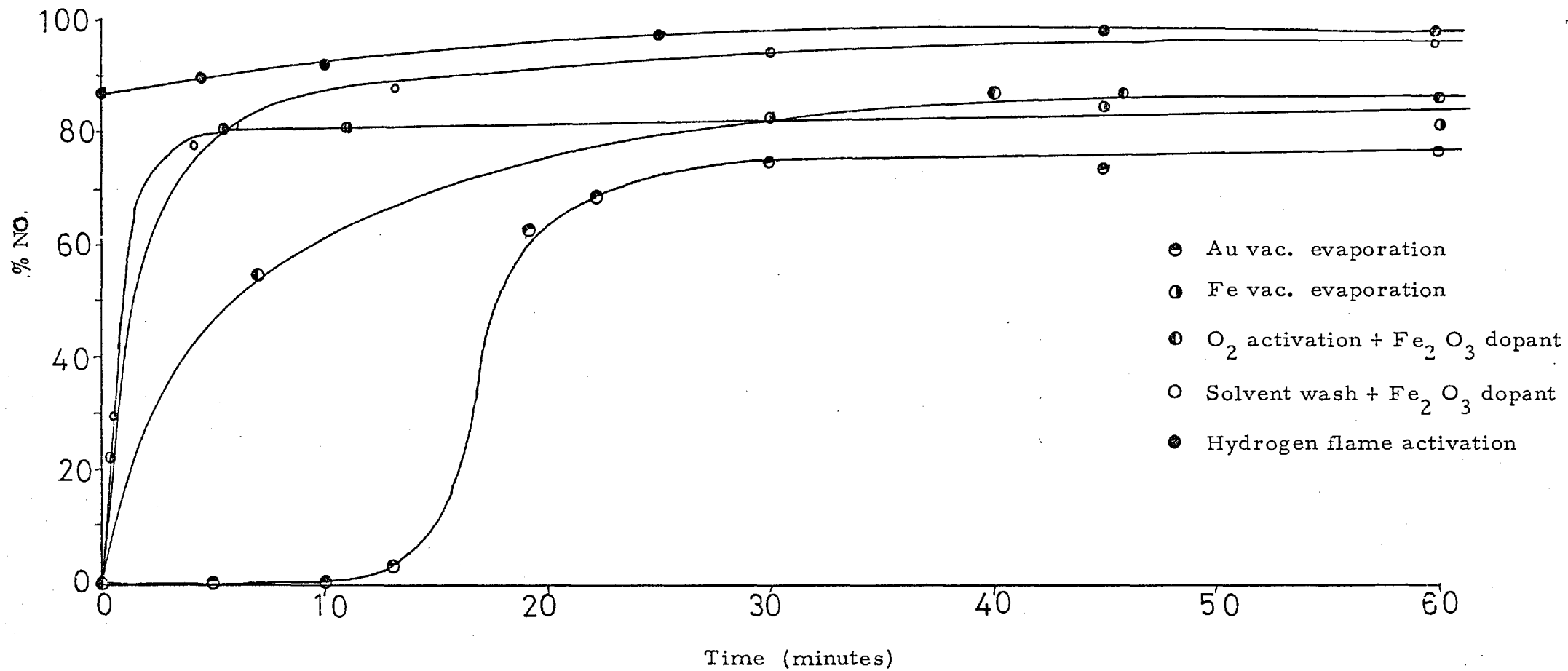


Table 3.5.1

Dopant	Light-off (°C)	Conversion efficiency % (after 1 hour)	Photo
Hydrogen flame (no dopant)	320	98	
Oxygen activation + Fe ₂ O ₃ solution	370	88	53,54
Solvent wash + Fe ₂ O ₃ solution	350	96	55,56
Solvent wash + Fe Vac. evap.	280	86	59,60 61
Solvent wash + Au vac. evap.	645	79	57,58

Graph.3.5.2.

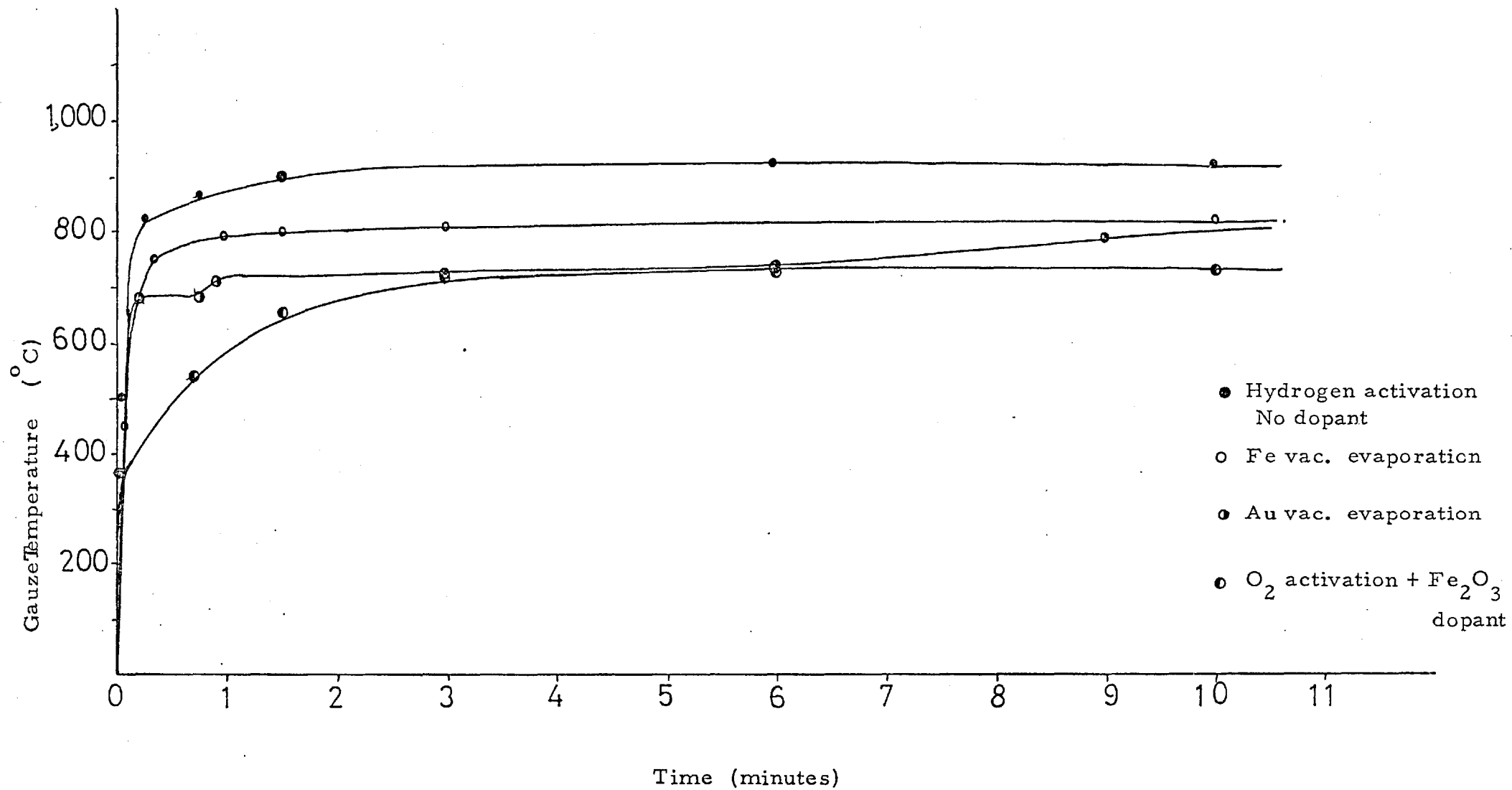


Table 3.5.2

Dopant	Light-off (°C)	Gauze temperature (°C) after 10mins	Conversion efficiency % NO.	Photo. No.
MgO	355	885		62
CaO	485	835	82	63
BaO	No light off	-	-	64
TiO ₂	355	930	-	65
ZrO ₂	370	810	95	66
V ₂ O ₅	385	650	10	67,68
Cr ₂ O ₃	415	840	95	69
MnO ₂	300	890		70
Fe ₂ O ₃	440	815	88	53,54
Co ₃ O ₄	570	795	-	71
NiO	352	802	90	72
CuO	460	860	-	
ZnO	310	755	-	
CeO ₂	355	815	-	73
ThO ₂	290	810	-	74
La(NO ₃) ₃	480	920	-	75
SiO ₂	395	845	90	76
Al ₂ O ₃	360	885	93	77
NaOH	No light off	-	-	
KOH	620	860	-	78
No dopant	320	910	98	

3.5.d Variation in light-off temperature with dopant loading

Table 3.5.2 shows that zirconia maintains conversion (95%) but lowers the gauze running temperature by 100°C , whilst Co_3O_4 has produced a high light-off temperature with a low running temperature indicating low activity. Therefore, these two oxides were studied for variation in light-off temperature with gauze dopant loading.

One Pt/10% Rh gauze was activated by solvent washing and then heating in oxygen flowing at $200\text{ cm}^3\text{ min}^{-1}$ for two hours. This gauze was then weighed and doped using a saturated solution of the oxide. To maintain a pressure drop similar to that occurring in other experiments, two gauzes were also included which had been doped, but not activated. Thus, light-off occurred on the top gauze only. The results are plotted on graphs 3.5.3 and 3.5.4.

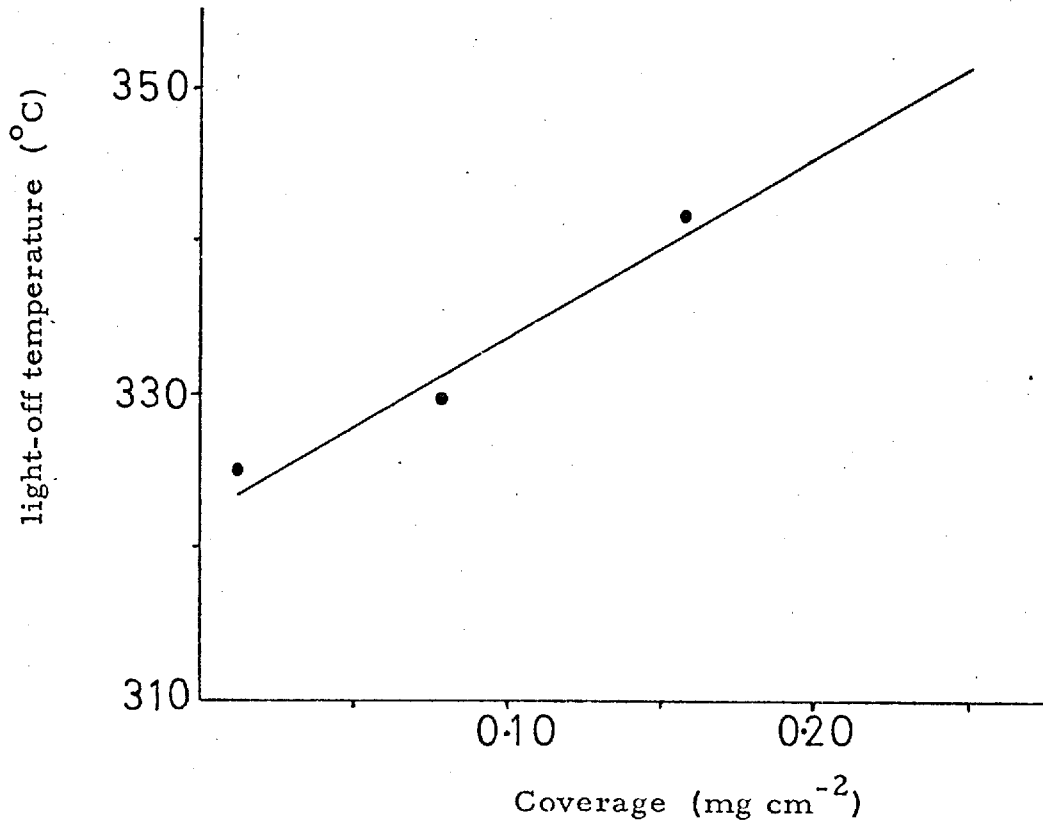
3.5.e Weight loss from doped gauzes

Following earlier experiments using 14% NH_3 /air, several of the dopants were tested using 10% NH_3 /air mixtures flowing at $4,300\text{ cm}^3\text{ min}^{-1}$. Three Pt/10% Rh gauzes were activated by solvent washing and heating in oxygen at $1,000^{\circ}\text{C}$ for 2 hours. The top gauze of the pack was then weighed on the microbalance and doped using the solution deposition technique outlined earlier (section 2.4. b(i)). The gauze was weighed again and reacted, with two other similarly prepared gauzes, for 1 hour. The top gauze was then weighed again and dopant loss calculated by difference. Conversion efficiencies and light-off temperatures were also recorded. The results are shown in table 3.5.3 and graph 3.5.6.

3.6. Heterogeneous - homogeneous mechanism studies

Recent Russian work (169) (170) has led workers to postulate that a heterogeneous - homogeneous reaction can occur in the ammonia oxidation reaction.

Graph 3.5.3.



Graph 3.5.4.

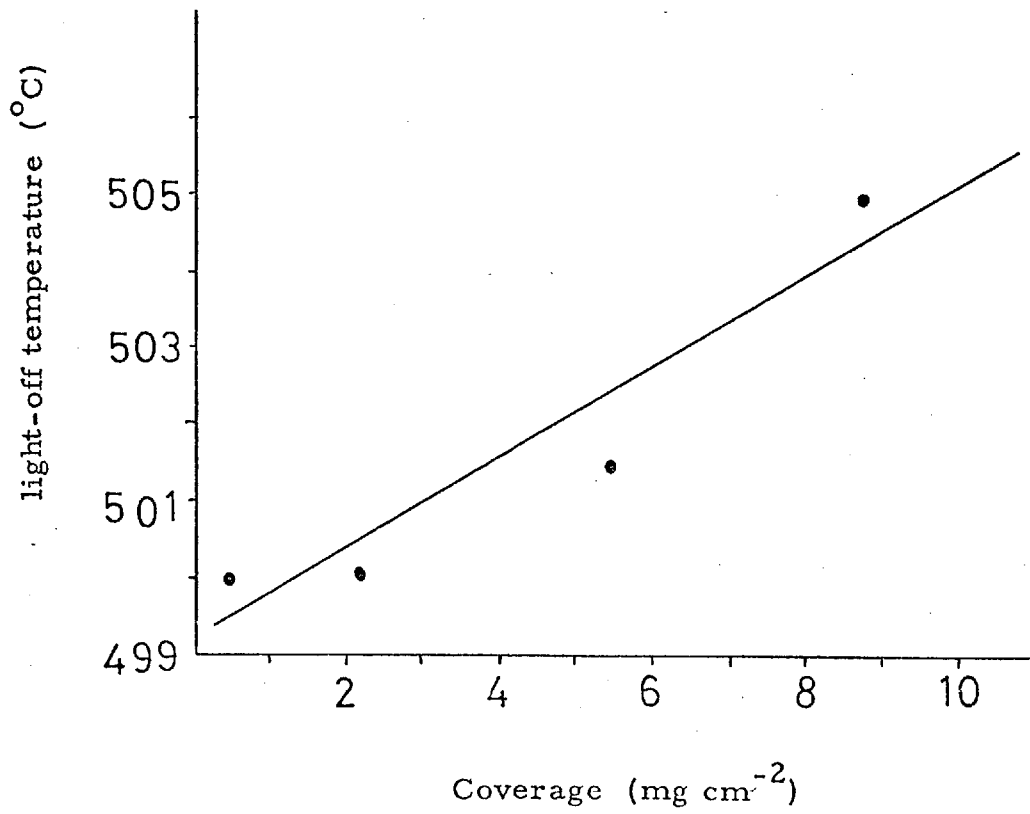
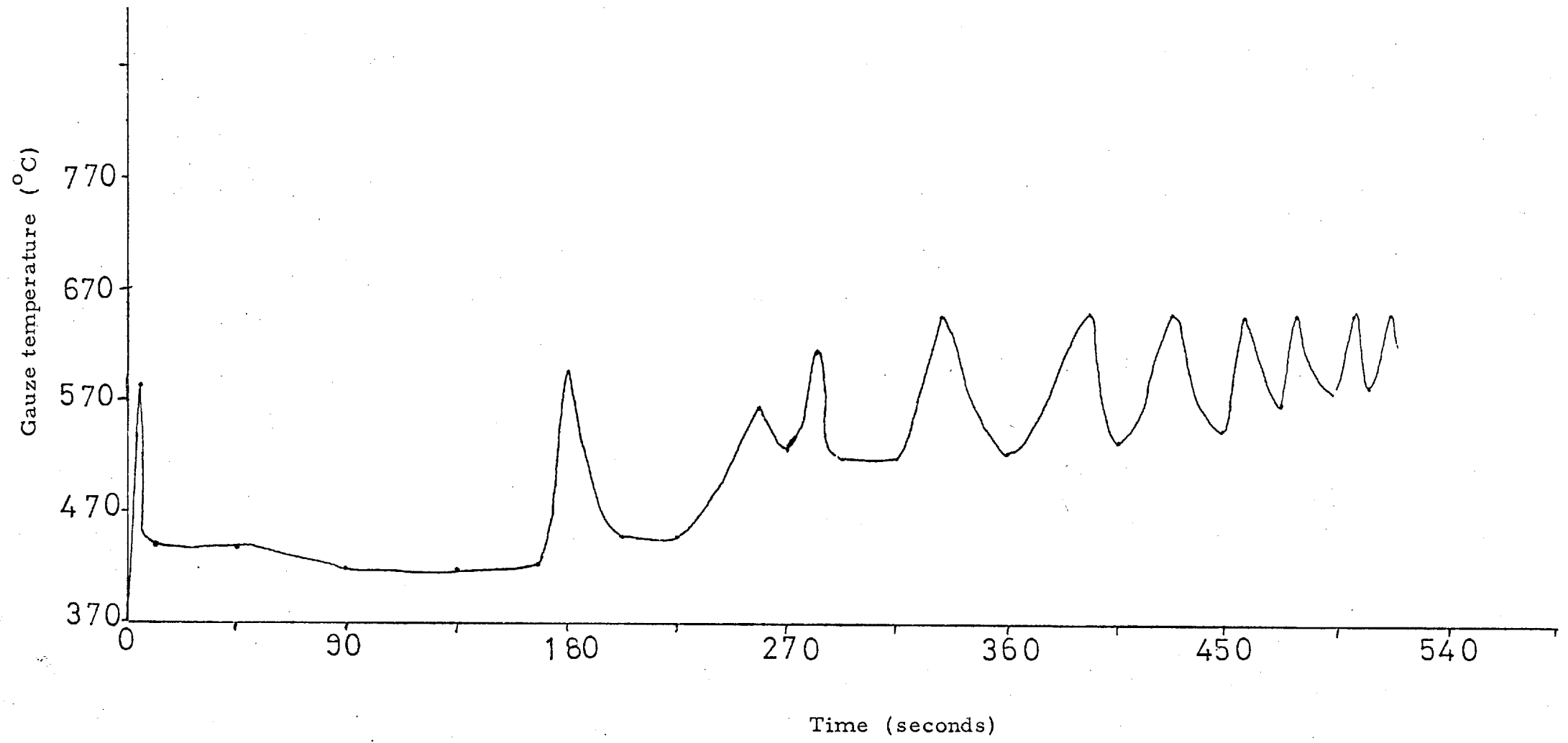


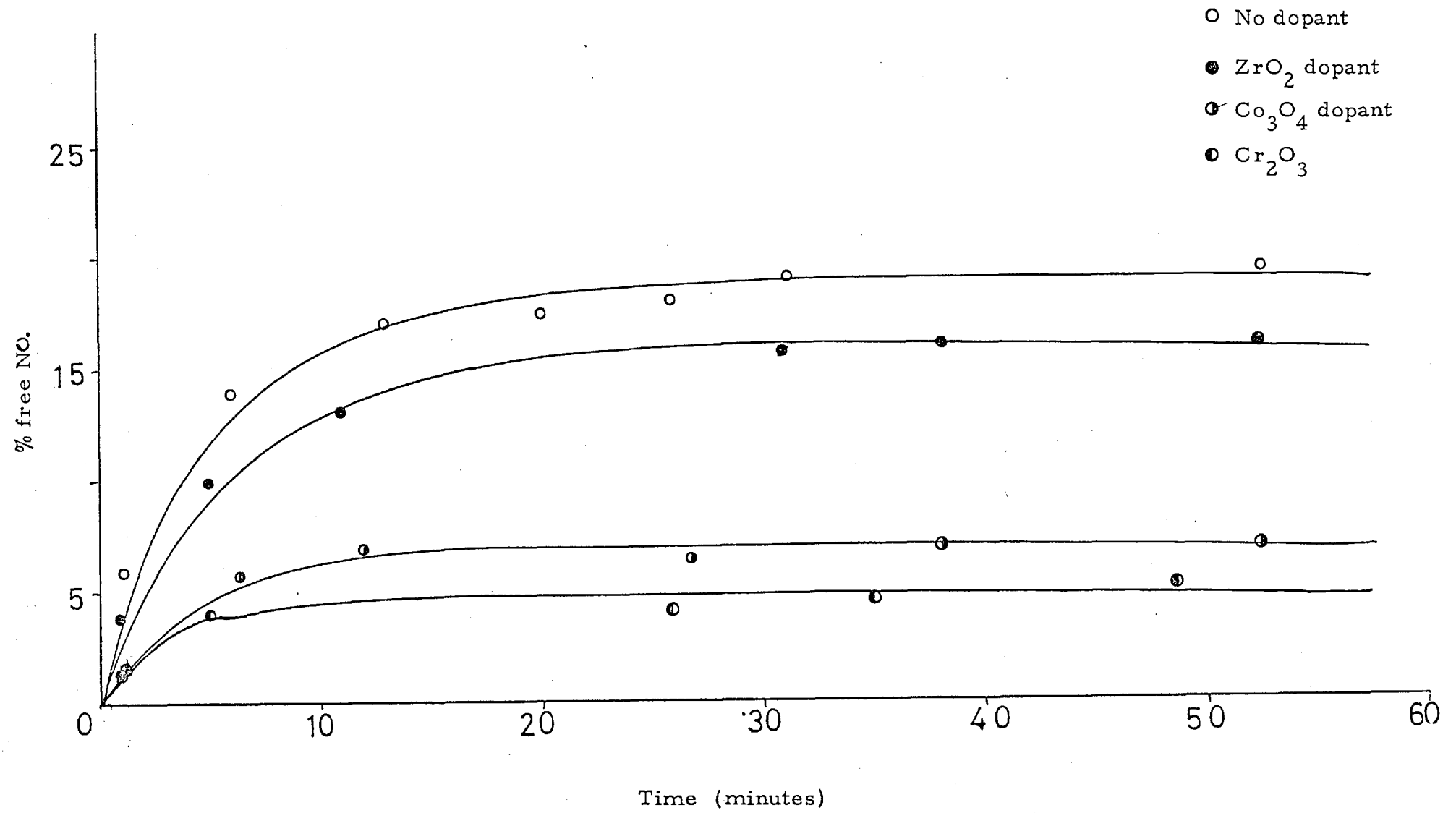
Table 3.5.3.

Dopant	Wt. before doping (mg)	Wt. after doping (mg)	Wt. after reaction (mg)	Loss of dopant (mg)	Conversion efficiency (% NO.)	Light off ($^{\circ}$ C)
No dopant	23.32		23.32	0.00	20.0	365
V_2O_5	25.37	25.60	← NO REACTION →			
ZrO_2	24.54	24.78	24.36	0.42	16.2	305
Co_3O_4	20.94	21.26	21.11	0.15	7.2	485
Cr_2O_3	21.81	22.60	22.13	0.47	5.0	475

Graph 3.55.

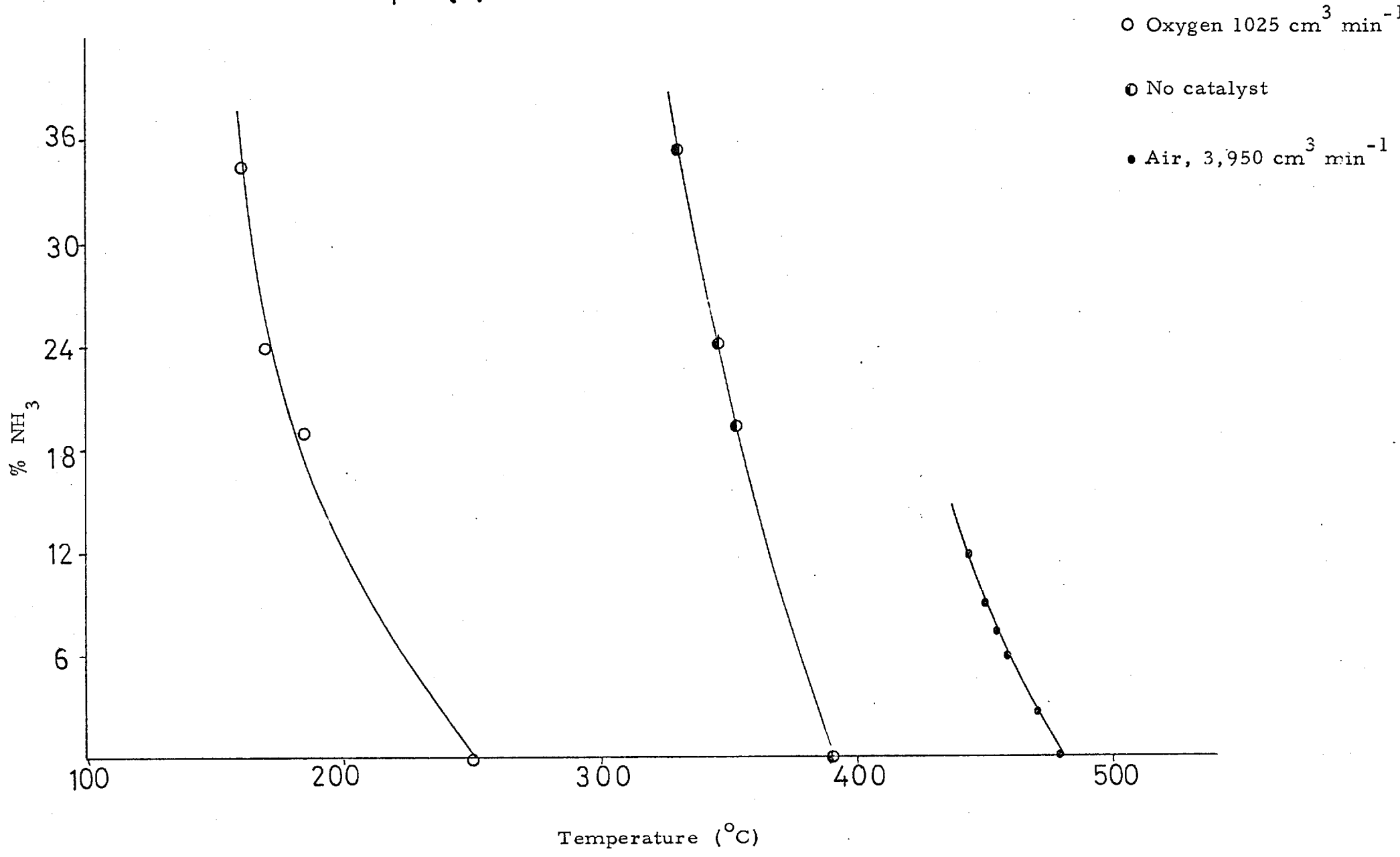


Graph 3.5.6.



The Mk II ammonia oxidation reactor (figure 2.3) was used in this work. The central heating tube was packed with 6 square inches of Pt/10% Rh gauze, which had been solvent treated. Oxygen was passed through the gauze at temperatures up to 1,000°C. Ammonia was admitted and the gas temperature was measured after the gauze. A thermocouple was also placed in the gauze to observe if a reaction was occurring due to back-diffusion of ammonia in the gas stream. The results are shown in graph 3.6.1.

Graph 3.6.1



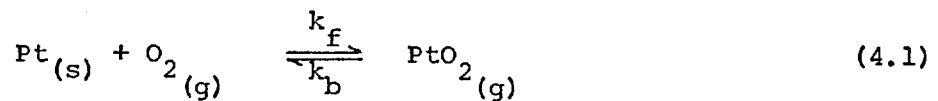
CHAPTER 4

Calculations of platinum weight loss occurring during
ammonia oxidation

4. Calculations of platinum weight loss occurring during ammonia oxidation

Nowak (43) (44) has extended work by Bartlett (45) using data from Handforth and Tilley (3) to cover the loss of platinum in ammonia oxidation reactions.

It has been shown previously (44) that a possible loss of platinum from gauze catalysts can occur by the reaction



Platinum dioxide is then transported away from the catalyst in the gaseous state, or may be back-reflected onto the catalyst surface where it decomposes to platinum and oxygen.

Nowak (44) has used the following rate equation to represent the rate of loss of platinum as platinum dioxide

$$\bar{R} = k_b \cdot \frac{K_{eq} \cdot P_{\text{O}_2}}{1 + \frac{k_b}{k_m}} \quad (4.2)$$

where, K_{eq} is the equilibrium constant for the reaction (4.1) expressed as $\frac{P_{\text{PtO}_2}}{P_{\text{O}_2}}$, k_b is the rate constant of the reverse reaction (4.1), equal to $10^3 \cdot (2\pi\text{MRT})^{-\frac{1}{2}}$. This has been used by Bartlett (45), with a decomposition probability of unity. k_m is a mass transfer coefficient calculated from

$$N_{\text{Nu}} = 0.45 + 0.33 (N_{\text{Re}})^{0.56} \quad (4.3)$$

Using this formula, Nowak (44) finds that platinum loss rates occurring in ammonia oxidation can be predicted and the theory predicts rates which vary from experimental rates (3) by a factor of four. Nowak suggests this discrepancy arises due to roughness of the wires or deviation

from low transport rate conditions.

It was whilst studying this discrepancy, that certain facts became apparent from Nowak's calculations. As a result it was decided to re-examine Nowak's calculations for any possible sources of error.

A preliminary investigation revealed that the Nusselt Numbers used by Nowak were probably incorrect.

Nowak (44) quotes

$$k_m = \frac{N_{Nu} P_t D}{L.R.Tg} \quad (4.4)$$

where k_m is the mass transfer coefficient ($\text{mol cm}^{-2} \text{sec}^{-1} \text{atm}^{-1}$), N_{Nu} is a dimensionless Nusselt Number, P_t is the partial pressure of oxygen (in this case 0.18 atm), D is the gaseous diffusion coefficient ($\text{cm}^2 \text{sec}^{-1}$), L is the diameter of the gauze wire (cm), R is the gas constant ($82 \text{ cm}^3 \text{ atm K}^{-1} \text{ mol}^{-1}$) and Tg is the average gas temperature (K). Examining the units of both sides of this equation gave,

$$\text{mol. cm}^{-2} \text{sec}^{-1} \text{atm}^{-1} = \frac{\text{atm cm}^2 \text{sec}^{-1}}{\text{cm cm}^3 \text{atm deg}^{-1} \text{mol}^{-1} \text{deg}}$$

which resolves to a dimensionless Nusselt number with units of atm^{-1} .

This could arise through confusion between the k_m values quoted by Nowak (44) and Bartlett (45) who quotes an expression

$$1 + \frac{(2\pi MRT)^{-\frac{1}{2}}}{k_m} \quad (4.5)$$

which should be dimensionless. It can be shown that

$$k_b = (2\pi MRT)^{-\frac{1}{2}}$$

should have units of $\text{mol. cm}^{-2} \text{sec}^{-1} \text{atm}^{-1}$.

Thus, $(2\pi MRT)P_t$ should have units of $\text{mol. cm}^{-2} \text{sec}^{-1}$. Therefore the k_m value quoted by Bartlett above (4.5) should also be independent of pressure. Thus, the k_m quoted by Bartlett has units of $\text{mol. cm}^{-2} \text{sec}^{-1}$, whilst that of Nowak has units $\text{mol. cm}^{-2} \text{sec}^{-1} \text{atm}^{-1}$

$$k_{m \text{ Bartlett}} = k_{m \text{ Nowak}} \times \text{pressure (atm)}.$$

However, as the total pressure is one atmosphere, the values should be equal, though the units will be different. It was therefore decided to recalculate all the data submitted by Nowak, a brief review of which is shown below.

Gaseous diffusion coefficients were calculated for oxygen at the required temperatures using the Chapman-Enskog equation as outlined by Bartlett (45)

$$D = \frac{1.86 \times 10^{-3} \sqrt{\frac{1}{M_{O_2}} + \frac{1}{M_{PtO_2}}}}{\sigma_{O_2}^2 \Omega_D} \left(\frac{T_g}{Pt}\right)^{3/2} \quad (4.6)$$

where M is the molecular weight, $\Omega_D = 0.78$ for oxygen (185) and the collision cross section $\sigma = 3.433$ at 1673 K. Values of D were obtained for the temperatures used by Nowak as shown in table 4.1.

Next, the viscosities of ammonia and air were determined for the temperatures used by Nowak, using the following formula

$$\mu = 2.6693 \times 10^{-5} \frac{\sqrt{MT}}{\sigma^2 \Omega_\mu} \quad (4.7)$$

Table 4.1

Temperature (K)	σ_{O_2} (Å)	$\frac{\epsilon}{K}$ (K)	KT/ ϵ	Ω_D	D cm ² sec ⁻¹
1673	3.433	113	14.805	0.69	2.755
1198	"	"	10.601	0.73	1.669
1173	"	"	10.380	0.73	1.617
1148	"	"	10.159	0.74	1.566
1123	"	"	9.938	0.74	1.515
1098			9.716	0.74	1.465
773			6.840	0.79	0.865

where μ is the gas viscosity in $\text{g cm}^{-1} \text{sec}^{-1}$. The viscosities were determined for air using $\sigma = 3.617 \text{ \AA}$, $\epsilon/K = 97$ and $M = 28.97$, and for ammonia using $\sigma = 2.902 \text{ \AA}$, $\epsilon/K = 692$ and $M = 17$. These values are shown in tables 4.2 and 4.3.

Having determined the viscosities of the individual components, the viscosity of a mixture of 10.5% NH_3/air (v/v) was determined using an extension of the Chapman-Enskog theory to cover multicomponent systems at low density by Curtiss and Hirschfelder (185). This shows that the viscosity μ_{mix} of a gaseous mixture can be predicted by

$$\mu_{\text{mix}} = \frac{\sum_{i=1}^n x_i \mu_i}{\sum_{j=1}^n x_j \phi_{ij}} \quad (4.8)$$

$$\text{where } \phi_{ij} = \frac{1}{\sqrt{8}} \left(1 + \frac{M_i}{M_j}\right)^{-\frac{1}{2}} \left[1 + \left(\frac{\mu_i}{\mu_j}\right)^{\frac{1}{2}} \left(\frac{M_j}{M_i}\right)^{\frac{1}{4}}\right]^2$$

where n = number of gases in the mixture

x_i and x_j = mole fraction of gases i and j

μ_i and μ_j = viscosities of components i and j at the system temperature and pressure

M_i and M_j = molecular weight of the components i and j

ϕ_{ij} dimensionless.

Typical values for the percentage of ammonia in mixtures used by Handforth and Tilley (3) was 10% NH_3/air . The viscosities of the mixtures of the temperatures used by Nowak are shown in table 4.4 and graph 4.1. Finally, to be able to estimate the modified Reynolds Number N_{Re} , the hydraulic radius r_H of the gauze was determined using

$$r_H = \frac{L A_{\text{flow}}}{A} \quad (4.9)$$

Table 4.2 Viscosities of air

Temperature (K)	σ_{air} (Å)	ϵ/K (K)	KT/ϵ	Ω_{μ}	μ $\text{g cm}^{-1} \text{sec}^{-1}$
1673	3.617	97	17.25	0.76	5.89×10^{-4}
1198			12.35	0.80	4.72×10^{-4}
1173			12.09	0.80	4.67×10^{-4}
1148			11.83	0.80	4.60×10^{-4}
1123			11.57	0.80	4.55×10^{-4}
1098			11.32	0.80	4.50×10^{-4}
773			7.96	0.85	3.57×10^{-4}

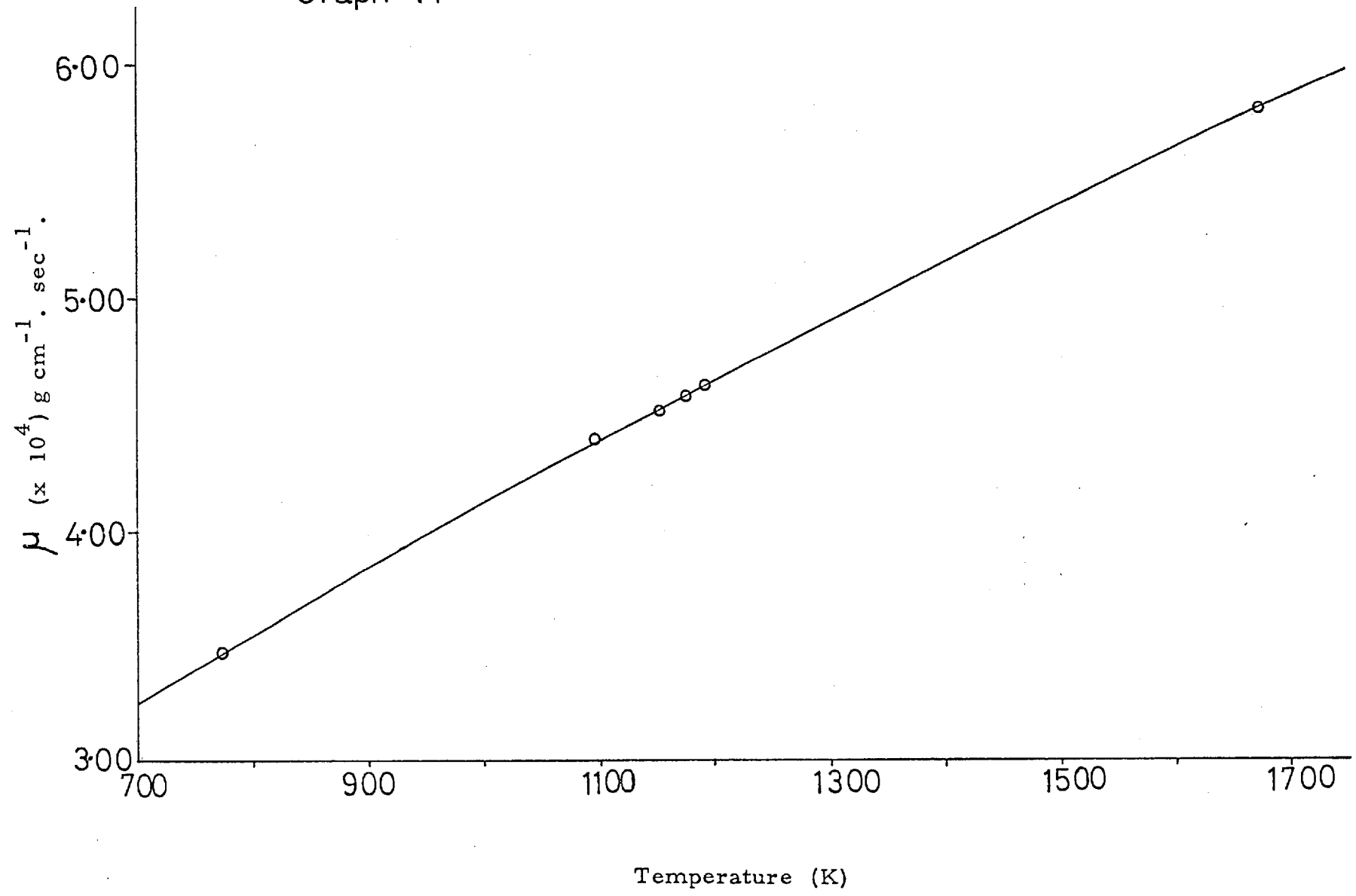
Table 4.3 Viscosities of ammonia

Temperature (K)	σ_{NH_3} O ₃ (Å)	ϵ/K (K)	KT/ϵ	Ω_{μ}	$\text{g cm}^{-1} \mu \text{sec}^{-1}$
1673	2.902	692	2.41	1.10	4.64×10^{-4}
1198			1.73	1.24	3.63×10^{-4}
1173			1.69	1.26	3.55×10^{-4}
1148			1.65	1.27	3.48×10^{-4}
1123			1.62	1.28	3.42×10^{-4}
1098			1.58	1.29	3.35×10^{-4}
773			1.11	1.48	2.45×10^{-4}

Table 4.4

Temperature (K)	μ_{mixture} g cm ⁻¹ sec ⁻¹	N_{Re}	N_{Nu}
1673	5.799×10^{-4}	0.4419	0.6589
1198	4.628×10^{-4}	0.5538	0.6870
1173	4.585×10^{-4}	0.5590	0.6883
1148	4.520×10^{-4}	0.5670	0.6902
1123	4.425×10^{-4}	0.5759	0.6923
1098	4.412×10^{-4}	0.5808	0.6943
773	3.483×10^{-4}	0.7358	0.7279

Graph 4.1



in which L = length of screen matrix in direction of flow, A is the heat transfer area, and A_{flow} is the matrix average flow area represented by

$$A_{\text{flow}} = A_{\text{frontal}} \times p \quad (4.10)$$

where A_{frontal} is the matrix frontal area and p is the porosity given by

$$p = \frac{V_v}{V_v + V_m} \quad (4.11)$$

in which V_v is the void volume of the matrix and V_m is the volume of the matrix wires.

Using a 0.003" diameter wire gauze, 80 meshes per linear inch and size 4" x 5.5" (3), gave r_H equal to 2.373×10^{-3} cm.

Thus the modified Reynolds Number N_{Re} , could now be calculated using

$$N_{\text{Re}} = \frac{4 r_H G}{\mu} \quad (4.12)$$

where r_H = hydraulic radius (cm)

G = average mass velocity in matrix (2.7×10^{-2} g cm⁻² sec⁻¹
100 lb NH₃/Troy oz cat. day).

μ = viscosity of mixture (g cm⁻¹ sec⁻¹)

The numbers obtained are shown in table 4.4.

Hence, the corresponding Nusselt Numbers N_{Nu} were calculated using equation (4.3), giving the values shown in table 4.4.

Referring to equation (4.4), the mass transfer coefficients were calculated (table 4.5) and the chemical rate constant for the reverse reaction was calculated using

$$k_b = 10^3 (2\pi MRT)^{-\frac{1}{2}}$$

where $M = 227$ (PtO_2). The values are shown in table 4.5. After calculation of k_b/k_m , the rate of loss of platinum as PtO_2 was calculated in $\text{g. cm}^{-2} \text{ hr}^{-1}$ using equation 4.2. The results are shown in table 4.5 (graph 4.2) and comparing these values with those obtained by Nowak (44) (table 4.6) it can be seen that the corrected values are a factor of 1.6 in excess of the experimental values obtained by Handforth and Tilley (3). This represents a considerable improvement to the results of Nowak (44).

This can be traced to Nowak using a frontal surface area of the whole gauze front and rear, instead of the frontal area only. It can be seen, from photographs 50 and 51 that more of the reaction occurs on the top of the gauze surface than on the rear of the gauze. It is therefore possible to use this modification, and hence to obtain a better result.

Finally the method has been extended to use in high pressure plants, unlike those used by Handforth and Tilley (3) in which atmospheric pressure data is used.

The conditions for the high pressure operation are set out below.

<u>Pressure</u>	110 p.s.i.
<u>Temperature</u>	910 °C
<u>Catalyst loading</u>	100 tons $\text{NH}_3 \text{ m}^{-2}$ catalyst day ⁻¹
<u>Ammonia concentration</u>	10 vol %
<u>Number of gauzes</u>	40
<u>Gauze specifications</u>	80 mesh linear inch ⁻¹ . 0.003" diameter Pt/10% Rh Area 0.126 m ²
<u>Catalyst loss</u>	350 mg ton ⁻¹ acid produced.

Table 4.5

Temperature (K)	k_m	k_b	k_b/k_m	K_{eq}	\bar{R}
	mol. cm ⁻² sec ⁻¹ atm ⁻¹	mol. cm ⁻² sec ⁻¹ atm ⁻¹			g cm ⁻² hr ⁻¹
1673	3.126×10^{-4}	7.149×10^{-2}	228.7	1.3×10^{-5}	5.951×10^{-4}
1198	2.758×10^{-4}	8.448×10^{-2}	306.3	1.2×10^{-7}	4.854×10^{-6}
1173	2.734×10^{-4}	8.538×10^{-2}	312.3	8.5×10^{-8}	3.408×10^{-6}
1148	2.712×10^{-4}	8.630×10^{-2}	318.2	6.0×10^{-8}	2.386×10^{-6}
1123	2.691×10^{-4}	8.725×10^{-2}	324.1	4.0×10^{-8}	1.58×10^{-6}
1098	2.669×10^{-4}	8.824×10^{-2}	330.6	2.7×10^{-8}	1.057×10^{-6}
773	2.346×10^{-4}	1.052×10^{-1}	448.4	1.5×10^{-11}	5.166×10^{-10}

Graph 4.2

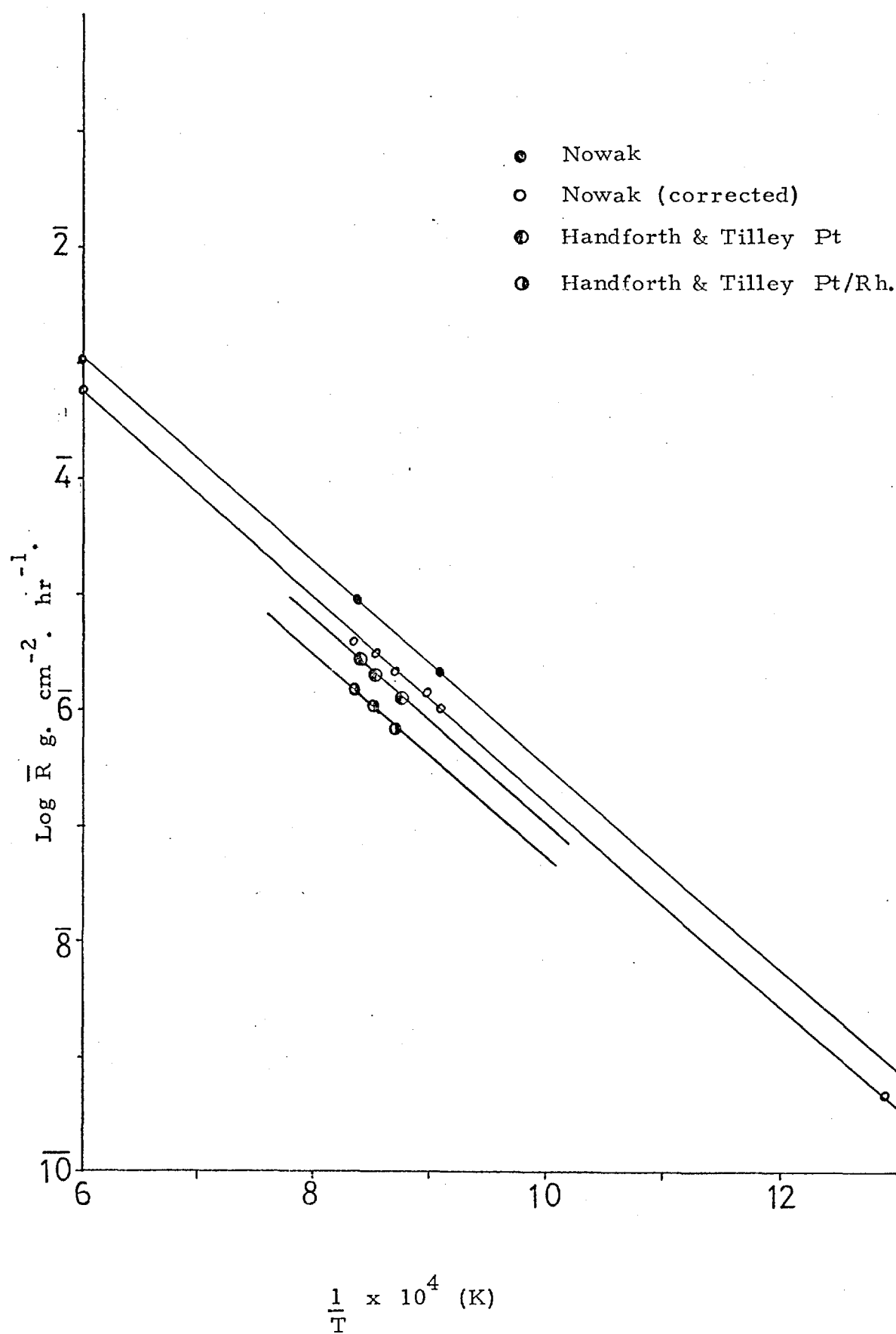


Table 4.6

$\frac{1}{T}$ ($\times 10^4$) (K)	\bar{R} $\text{g cm}^{-2} \text{ hr}^{-1}$	Reference (3) Pt $\text{g cm}^{-2} \text{ hr}^{-1}$	Reference (3) Pt/10% Rh $\text{g cm}^{-2} \text{ hr}^{-1}$
5.977	5.951×10^{-4}		
8.347	4.854×10^{-6}		1.682×10^{-6}
8.4		2.8×10^{-6}	
8.525	3.408×10^{-6}	2.1×10^{-6}	1.145×10^{-6}
8.7108	2.386×10^{-6}		6.87×10^{-7}
8.75		1.28×10^{-6}	
8.905	1.58×10^{-6}		
9.107	1.057×10^{-6}		
12.93	5.166×10^{-10}		

The method outlined previously gave a catalyst loss rate of 371 mg ton⁻¹ acid produced (100% acid). However, this assumes that the reaction and the weight loss occurs evenly and simultaneously from all the gauzes in the catalyst pack.

As a result it can be seen that the calculation gives a reasonable estimation of platinum weight loss at both low and high pressures and infers that essentially all of the weight loss involves volatilisation of platinum dioxide.

CHAPTER 5

DISCUSSION

	Page.
5. 1. <u>Activation</u>	
5. 1. 1. Surface contamination	206
5. 1. 1. a. The effect of solvent washing on surface contamination	207
5. 1. 1. b. The removal of carbon and sulphur in the activation process	208
5. 1. 1. c. Activity produced by heating in oxidising, inert and reducing atmospheres	210
5. 1. 1. d. Deactivation by air	211
5. 1. 2. Alloy composition	212
5. 1. 3. Electronic factor	220
5. 1. 4. Geometric factor	221
5. 1. 5. Adsorption	228
5. 2. <u>Deactivation</u>	
5. 2. 1. Induced geometric effects	235
5. 2. 2. Electronic effects	238
5. 2. 3. Dopant loss during reaction	245
5. 3. <u>The heterogeneous - homogeneous mechanism</u>	248

5. 1. Activation

Platinum/Rhodium gauze catalysts, used for the oxidation of ammonia to nitrogen oxides, are well known to require activation before use (1).

Despite the obvious importance of the activation process, comparatively little is known of the nature of the chemical processes involved. It can be expected that solvent washing removes organic and inorganic impurities, and it is known that at least one function of pickling is to remove impurities such as iron oxide from the surface of the gauze (38, 39). The role of the hydrogen flame treatment is open to some question. Gauzes are known to develop 'spongy' surfaces during reaction (1), and activity can be generated either by hydrogen flame treatment or by inserting a few active gauzes from another plant on top of a new gauze pack (38). Thus it could be expected that hydrogen flame treatment effectively involves either high temperature treatment alone or high temperature treatment in an oxidising or reducing atmosphere.

As a result of this uncertainty, attention was focused, in the first instance upon the factors that could influence activity, with particular attention to the following points.

1. Does the activation process result in the removal of a surface contaminant?
2. Is the surface composition of the alloy the same as the bulk composition, before and after activation?
3. Is the electronic factor, possibly involving transfer of electrons throughout the alloy or across the surface, important?
4. Is the geometric factor, as typified by the relative arrangement of platinum and rhodium atoms, or by a macroscopic rearrangement of the surface, important?
5. Is the relative ease of adsorption of reactants affected by activation?

These questions may now be considered in turn.

5. 1. 1. Surface contamination

5. 1. 1. (a) The effect of solvent washing on surface contamination

Experiments were undertaken to ascertain the effect of solvent washing on the activation process. (Table 3. 1. 5 Graphs 3. 1. 22/23). These experiments have shown that the solvent treatment lowers the light-off temperature substantially, from 410°C for an untreated gauze to 310°C for a gauze which had been solvent treated, and the activity of the solvent washed gauze is higher.

In order to investigate the effect of solvent washing, an electronprobe microanalysis study of the gauzes before and after washing was initiated (section 3. 1. j). From table 3. 1. 10 it can be seen that a substantial concentration of calcium was present on the unwashed gauze as specks of dirt on the surface. After reaction of the untreated gauze, unwashed gauzes were less active. Microscopic examination of the surface after reaction showed that pits developed during reaction (Photo. 45) but no calcium was found in the bottom of the pits. Calcium was present on the gauze as specks of dirt (section 3. 1. j).

Clearly, however, from table 3. 1. 10 it can be seen that washing the gauzes with the solvent mixture will result in the removal of this calcium, and produce a more active gauze as a result. It is not certain whether the large round pits are a cause or an effect or have no effect on the observed low activity (see later).

Following this solvent treatment the gauzes are then usually activated by treating with a hydrogen flame. Experimental work has been undertaken to ascertain the effect of this activation treatment and others involving heating in oxidising, inert and reducing gases on the removal of carbon, sulphur, moisture and other surface contaminants to produce active gauzes. These will now be dealt with in turn.

5.1.1.b The removal of carbon and sulphur in the activation process

In their work on the surface composition of platinum heated in oxygen, Pignet, Schmidt and Jarvis (34) have used Auger Electron Spectroscopy (A. E. S.) to show that heating the metal in oxygen to 300°C or above removes carbon and sulphur from the platinum surface, and more significantly, that the surface produced when platinum is heated in oxygen is not seriously contaminated by carbon or sulphur during exposure to the atmosphere for long periods. This was particularly interesting in that carbon contained in the platinum matrix has been found to greatly reduce the adsorption of oxygen (77).

Studies carried out in the present investigation using electron spectroscopy (section 3.2) tend to confirm, in general, that the carbon signal from platinum/rhodium foils used under ammonia oxidation conditions shows a considerable diminution as a result of both activation and reaction.

An X-ray spectrum was obtained of the gauze in the 'as supplied' state after solvent washing. It was then bombarded with 500 eV argon ions for 30 minutes at a current of $1/5 \mu\text{A}$. This treatment should have been sufficient to remove 600 Å of the surface, and hence to give an accurate estimate of bulk concentrations. The carbon signal was found to be substantially lowered (Figs. 3.2.1 and 3.2.7). Reaction of the gauze 'in situ' with an ammonia/oxygen mixture, lowered the carbon signal further (Fig 3.2.10) indicating that the carbon does not move into the bulk platinum/rhodium alloy during the reaction, and neither does oxygen. The oxygen signal was decreased however (Fig. 3.2.10), indicating that the oxide species present are only a few atomic layers thick.

Following these initial experiments with Pt/10% Rh gauzes, similar experiments were carried out using Pt/40% Rh foils. As expected, the carbon I_{S} signal was considerably reduced during the activation process, giving a correspondingly higher value for the Pt/ $C_{I_{\text{S}}}$ ratio (Table 3.2.6). The carbon/oxygen signal ratio also decreased during these treatments, though the platinum/oxygen ratio

is greater following activation.

As a comparison, a Pt/10% Rh foil was used in a similar series of experiments. Table 3.2.2 shows how the Pt/C, Pt/O and C/O ratios vary with treatment and argon ion bombardment. The Pt/C signal in the as supplied state shows little variation after argon bombardment. This indicates that there must be some diffusion of carbon into the platinum/rhodium alloy. However during activation and reaction, the Pt/C ratio still does not vary appreciably, but argon ion treatment approximately doubles these ratios. This shows that the carbon content is decreasing substantially, possibly due to movement of carbon atoms to the surface during reaction, following by oxidation to carbon dioxide. This would result in a lowering of the carbon in the bulk matrix as observed. Also, it would seem that removing the foils from the ammonia oxidation burner to the E. S. C. A. spectrometer has resulted in some deposition of carbon on the surface, a result which appears contrary to that of Pignet et al. mentioned earlier.

However, the Pt/O ratios shown in table 3.2.2 do not follow this trend. In the 'as supplied' state, there is a threefold increase in the Pt/O ratio after argon ion bombardment, due to a large decrease in the oxygen signal, and indicating that oxygen does not move through the metal matrix. After activation and reaction, this is reversed. In these cases, the Pt/O ratios are greater before bombarding, this being associated with an increase in intensity of the platinum signal. Further evidence of the difference in behaviour between carbon and oxygen in the platinum/rhodium matrix is shown with the C/O ratios. Before bombardment, the carbon/oxygen ratios are approximately constant, despite activation and reaction. Argon bombardment, in all cases, produces a ratio which is approximately three times that before bombardment. This shows the relative decrease in the oxygen content of the matrix, and that even in the reaction, oxide formation is confined to the surface of the catalyst, and does not penetrate the matrix to any depth.

Whilst hydrogen flame treatment is the industrial method of activation, for reasons of irreproducibility it was decided to investigate

the activity produced in platinum/rhodium alloys as a function of high temperature treatment in oxidising, inert and reducing atmospheres.

5. 1. 1. c Activity produced by heating in oxidising, inert and reducing atmospheres

Treatment with boiling concentrated hydrochloric acid (Fig 3. 2. 12) instead of the usual solvent treatment outlined earlier (section 2. 4. a (i)) has given a gauze with a cleaner surface and a lower carbon content, possibly due to the removal of oil deposits from the surface. Thus the removal of this oil deposit is of obvious importance prior to any high temperature treatment.

A Pt/10% Rh foil was heated in oxygen flowing at $200 \text{ cm}^3 \text{ min}^{-1}$ to $1,000^\circ \text{C}$ for two hours after a solvent treatment. This method of activation has been shown to result in a gauze with an activity equivalent to that produced by the hydrogen flame treatment (Section 3. 1. c), and it is a reproducible activation process. As could be expected with this method of activation, the Pt/O ratio is lower (cf. tables 3. 2. 4 and 3. 2. 2) due entirely to an increase in the intensity of the oxygen signal. The Pt/O and C/O ratios shown in table 3. 2. 4 all show increases after bombardment, again indicating that the oxide species is not present throughout the lattice.

However, despite solvent cleaning and oxygen activation, it has not been possible to completely remove carbon from the foil surface. This is almost certainly due to the fact that the foils are activated in an apparatus divorced from the spectrometer chamber. The foils are then temporarily exposed to the laboratory air for insertion in the spectrometer, and become carbon contaminated. In agreement with this 'in situ' treatment of Pt/10% Rh gauzes produces a much lower carbon content (Fig. 3. 2. 10). The exact amount of carbon present has not been ascertained, though in all the foils treated, the intensity of the carbon signal varies by only a small amount, even after bombardment, showing that carbon (unlike oxygen) does penetrate the alloy matrix.

A variation in activity and light-off temperature does result from the various treatments (section 3. 1. c). However, with helium, the gauze

should have been sufficiently clean, after a solvent wash, to light-off at 310°C , despite any further heat treatment. However, heat treatment in helium increased the light-off temperature to 380°C although the activity after two hours is not significantly below that obtained with other heated gauzes. This result could be explained by postulating that the carbon surface concentration is being increased by heat. Oxidising and reducing gases remove carbon and sulphur readily from the surface by the corresponding oxidation and reduction reactions. With helium however, this is not possible, and so the carbon and sulphur remain on the catalyst, blocking catalyst sites, thus preventing the light-off of the gauze. During reaction, these contaminants are removed by oxygen.

5. 1. 1. d Deactivation by air

Experiments were carried out to ascertain the relative importance of different components of air vis-a-vis deactivation (section 3. 1. i). A gauze was activated, cooled and left either in laboratory air or in oxygen overnight. The gauze that had been left in oxygen overnight lit-off at a lower temperature than that which had been cooled in laboratory air. To study the effect of the various possible constituents of laboratory air on the catalyst, experiments 3. 1. i (a) - 3. 1. i (d) were undertaken. Tables 3. 1. 8 and 3. 1. 9 and graph 3. 1. 24 shows that moisture in the laboratory air causes the increase in light-off temperature while the sulphur dioxide and carbon dioxide treatments have no effect.

The most extreme of the two moisture treatments, immersion in water, increases the light-off temperature considerably. Table 3. 2. 9 shows the results of an E. S. C. A. experiment using a foil which had been activated and then immersed in distilled water for 2 hours. As a comparison, a foil was activated by solvent washing and heating to $1,000^{\circ}\text{C}$ in oxygen. Table 3. 2. 9 clearly shows that before bombardment, the platinum/rhodium ratio is reduced by a factor of three in the water treated case. Following bombardment, the platinum/rhodium ratios

are approximately equal. Thus it appears that water treatment has removed the surface platinum, which is probably present in the form of an oxide, thus increasing the light-off temperature of the catalyst. This seems to indicate that platinum dioxide is the catalyst for ammonia oxidation. The position of the platinum and rhodium signals before bombardment give no indication of a chemical reaction such as the formation of the hydroxide. It must be concluded therefore that the platinum dioxide is being removed by dissolution.

To check this, the distilled water used in this experiment was evaporated to dryness over a copper foil, and an E. S. C. A. spectrum obtained of this foil. Figure 3.2.13 (section 3.1.d) shows a signal at 240 eV below the C_{1s} signal. This can be ascribed to $Pt_{N \text{ III}}$. No signal is observed for rhodium. It would seem that platinum has been deposited on the copper foil, but rhodium is absent. Water treatment must therefore remove platinum dioxide from the catalyst surface giving rhodium enrichment which causes an increase in light-off temperature.

To summarise then, carbon and sulphur can block catalyst sites preventing gauze light-off. Activation and reaction reduce the carbon surface contamination.

Solvent treatment removes calcium compounds present as specks of dirt and this results in a lower light-off temperature and higher activity.

Oxide formation is confined to the surface of the catalyst and does not penetrate the metal matrix to any appreciable extent.

Moisture in the atmosphere and immersion in water significantly increase the light-off temperature and lower the activity. In the latter case this is probably due to the removal of platinum dioxide by dissolution.

5.1.2. Alloy composition

Preliminary results obtained by Philpott (38) show that alloy composition differences can be observed between the surfaces of active and inactive

gauzes. Inactive gauzes showed a high concentration of rhodium on the surface, probably as Rh_2O_3 , and of iron, probably as Fe_2O_3 . The active gauze surfaces were homogeneous and showed no increases in the rhodium or iron surface concentration.

Possible changes in the surface composition of the catalyst were investigated in the present work by electron spectroscopic examination. This technique is particularly useful for qualitative analysis of the first few layers of the surface, but quantitative information is more difficult to establish.

In an attempt to obtain accurate quantitative assessments of surface concentrations, spectra were measured for alloys of different composition (Tables 3.2.1 and 3.2.5), and the data was plotted on graphs 3.2.1 and 3.2.2 (section 3.2.). These show that in the case of platinum, there appears to be no correlation between the intensity of the platinum signal and the surface concentration of platinum present in the 'activated' and 'as supplied' samples. However, for the 'activated and reacted' case, there is good agreement between these.

Good agreement was observed between the intensity of the signal for rhodium and the rhodium concentration. No attempt has been made to assess the errors arising from this method, and neither has a statistical experiment been performed to ascertain its overall accuracy. Nevertheless, it is significant that the rhodium signals produced for the activated sample are substantially increased, corresponding to an increased rhodium concentration at the surface of the catalyst. On reaction the rhodium moves back into the metal matrix. It cannot be assumed, without further experimentation, that there is any significant difference between the 'as supplied' and 'activated + reacted' states. Further experimentation is necessary to ascertain the exact nature and values of errors arising with this technique before accurate quantitative assessments can be carried out.

It is possible that in the activation process, not only is there a substantial increase in the surface rhodium concentration, but that there is also an increase in the surface area of the catalyst. This can be observed from the photographs of activated and reacted samples (Photos 48, 49). Thus, there will be more surface metal atoms

present in the 1 cm^2 sampling area of the spectrometer in these cases, than in the 'as supplied' state.

As a result of this, comparative measurements were carried out on the basis of peak height, and comparison experiments were completed with E. P. M. A. Although more quantitative, E. P. M. A. averages the signal from considerably deeper section of surface than electron spectroscopy (section 1.3.c). Where knowledge of the bulk concentration was required in the electron spectroscopy experiments, argon ion bombardment was used to remove this surface. Checks were made on the reproducibility of the samples after ion bombardment to ensure that the bulk concentration was accurately sampled.

A study of Pt/10% Rh gauzes (section 3.2.c) in the 'as supplied state' showed a relatively strong rhodium signal, with a strong oxide signal present. The platinum and rhodium signals were shifted 1 eV and 2 eV respectively from their listed positions of 71.1 eV and 496.2 eV, (Table 3.2.7) indicating the possibility of oxide formation at the surface. A relative ratio of Pt/Rh 7:1 (Table 3.2.8) was obtained from these signals which was higher in rhodium than would have been expected, assuming that the spectrometer is equally responsive to both platinum and rhodium. To ascertain the relative amount of rhodium in the bulk alloy, the gauze was then bombarded with 500 eV argon ions for 30 minutes at a current of $\frac{1}{5} \mu\text{A}$. This was sufficient to remove 600 \AA of the metal surface, and give an estimate of bulk concentration. The Pt/Rh ratio was altered from 7:1 to 11:1, nearer to that expected for a Pt/10% Rh alloy. Heating to $1,000^\circ\text{C}$ in oxygen at a pressure of 10^{-4} Torr did not restore the shift in the rhodium signal, indicating the inertness of rhodium towards oxidation. However, the Pt/Rh ratio was altered to 16:1.

Following the study of an 'as supplied' gauze, an activated gauze was examined (section 3.2.c). In this case, there was a substantial increase in the rhodium concentration at the gauze surface (table 3.2.8). Clearly, there has been an increase in oxide formation, together with an increase in the intensity of the rhodium signal relative to the platinum peak, to give a ratio of Pt/Rh of 5:1 (table 3.2.8). Argon bombardment

increased this ratio to 14:1 which once again approximates to that of the bulk concentration, and indicates the extensive rhodium enrichment which occurs during the activation process.

Whilst industry uses Pt/10% Rh gauzes, no gauzes were available with varying concentrations of rhodium. It therefore became necessary to resort to the use of platinum/rhodium foils for further experimentation. These have a disadvantage in that they do not have the same surface area (and hence activity) as gauzes. Therefore, a Pt/10% Rh gauze was included with the foils in experiments in which the oxidation reaction was needed.

Following the investigations of Pt/10% Rh gauzes, two foils with varying concentrations of rhodium were studied as a comparison. Reference to table 3.2.8 shows that initially a Pt/40% Rh foil had a surface Pt/Rh ratio of 8.6:1. Either the surface rhodium concentration was in no way indicative of the bulk alloy concentration, or the rhodium was not evenly distributed throughout the alloy. Despite this apparent discrepancy, table 3.2.8 shows how the surface rhodium concentration increases during activation, and increases again during reaction. This anomalous behaviour seems to be confined to the Pt/40% Rh foil only, though obviously on the basis of one result, no definite conclusions can be made. The rhodium and platinum signals do not show any variation in position, indicating the presence of both metal oxides at the alloy surface.

Table 3.2.5 shows the signal intensities measured as peak height, of the platinum and rhodium signals. In the activated + reacted sample, the intensity of the platinum signal is reduced five-fold, whilst that of the rhodium is reduced approximately twice. This is despite similar instrument conditions, sampling technique, and sample mounting. This result would seem to indicate an actual lowering of both the platinum and rhodium metal concentrations at the surface. The spectrum obtained showed no other new elements present, so it would appear that there is a large increase in oxide concentration.

To obtain a direct comparison between Pt/10% Rh gauzes and foils, a Pt/10% Rh foil was investigated. Reference to tables 3.2.1 and 3.2.8

shows that the intensity of the platinum and rhodium signals show only small decreases in the 'as supplied' sample. This indicates that the surface concentrations of platinum and rhodium in this sample are representative of the bulk composition. There is a substantial decrease in the intensity of the platinum signal in the 'activated + reacted' sample, but this is not accompanied by a corresponding increase in the rhodium signal intensity. However, the surface does have an increased rhodium content, arising from the activation process, though this appears to decrease back to the 'as supplied' state on reaction.

Accompanying the increase in rhodium content arising from activation, there is a corresponding shift in the signal position of over 1eV. This indicates a definite change in the atomic state of the rhodium atoms at the surface of the foil. Argon bombardment reduces this back to the 'as supplied' state. To further clarify this, a piece of Pt/10% Rh foil was heated in air and studied using Mg K α radiation. (Table 3.2.10). This confirmed that the binding energy of the Rh_{M III} signal has been reduced by 0.9 eV during reaction indicating a lowering of the oxidation state.

The preferred method of activation, that of treating in oxygen flowing at 200 cm³ min⁻¹ at 1,000°C for two hours, has been investigated using E.S.C.A. to note changes occurring in the alloy composition during this treatment. Table 3.2.3 shows that the intensity of the platinum signal in this case is approximately half that of the hydrogen flame activation shown in table 3.2.1. Bombardment with argon produces similar intensities (24.0 and 27.2). However, the rhodium concentrations are similar (3.5 and 3.05) but, after bombardment, the intensity of the rhodium signal in the oxygen activation is increased by approximately half, over that of the hydrogen flame activation. This indicates that an increased rhodium enrichment occurs in the oxygen activation.

The values for the 'activated + reacted' samples (table 3.2.3) show that, in comparison with those obtained by activation with the hydrogen flame and reaction (table 3.2.1), the initial surface

concentrations of platinum are similar (15.6 and 15.4). However, after bombardment, the signals are dissimilar, with the oxygen treated foil giving a lower platinum signal. This is once again consistent with a greater rhodium enrichment in the oxygen activation. The rhodium intensities in table 3.2.1 and 3.2.3 show that, even after reaction, the rhodium concentration had not decreased to that of the 'as supplied' state, as in previous examples. Clearly, this implies that a higher rhodium concentration is present in the oxygen activation than in the hydrogen flame treatment.

To summarise then, the E.S.C.A. experiments have shown that activation by an hydrogen flame or treatment with oxygen/air, give rise to increasing rhodium concentrations at the surface. When the catalysts were reacted, this increased surface rhodium concentration decreased, almost back to that of the unreacted catalysts.

Philpott (38) states that increased rhodium concentration may be due to some effect of the ammonia oxidation plant. The E.S.C.A. experiments show that this increased surface rhodium concentration arises as a result of the activation process, and is not a function of burner design or operation. Further, Philpott suggests that a prolonged period of operation at low temperature, encouraging separation and concentration of rhodium oxide on the surface (and retention of iron oxide from the feedstock) may be a cause of the rhodium enrichment. However, the Pt/10% Rh gauzes and foils used in the E.S.C.A. experiments were operated at temperatures below that quoted by Philpott, and did not show increased rhodium concentrations. In fact the rhodium concentration decreased as the activated gauze was reacted. Thus, it appears that Philpott's conclusion that increased rhodium concentration gives rise to inactivity is erroneous. The conclusion to be drawn from the E.S.C.A. studies must be that rhodium enrichment arises as a result of the activation process, but this then decreases on reaction. If the gauzes studied by Philpott as 'inactive' were not at sufficiently high temperature, then the high rhodium concentrations resulting after activation would not have had the opportunity to decrease during reaction, as has been shown with

active gauzes.

Ostermaier et al (78) have proposed that deactivation is due to formation of a surface platinum oxide different from oxygen chemisorbed on platinum.

However E.S.C.A. results in section 3.2 show that there is no change in the position of the platinum signal, indicating that the platinum is in the same oxidation state, both at the surface and in the bulk of the alloy.

An attempt was made to correlate changes in surface composition of the alloys with parameters which are important in the oxidation of ammonia. Gauzes were first activated in oxygen at varying temperatures, and the light-off point of the ammonia oxidation was measured (table 3.1.3). From graphs 3.1.18 - 20 it can be seen that the highest light-off temperatures occurred during activation between 600°C and 800°C .

E. P. M. A. analysis of gauzes treated in oxygen at temperatures between 200°C and $1,000^{\circ}\text{C}$ (section 3.1.e(ii)) was carried out to determine the variation in surface rhodium concentrations with temperature of oxygen treatment. Whilst the errors involved with this technique were large, it does show that substantial rhodium enrichment is occurring in the 600°C - 800°C region. From the data it can be seen that there is no apparent rhodium enrichment in the other treatments to parallel the uniform movement in light-off temperature shown in graph 3.1.19. This could be due to the inherent inaccuracies of the E. P. M. A. method (section 3.1.e(ii)), and more investigation is essential before a definite unambiguous correlation can be obtained.

One explanation of the rhodium enrichment could be advanced in terms of a paper by Darling (79), in which he reports that the vapour pressure for Pt O_2 is greater than that for Rh O_2 at temperatures below $1,200^{\circ}\text{C}$. Although the more rapid loss of platinum as Pt O_2 could account for the enrichment of the surface by rhodium, the explanation is not tenable above 800°C , where rhodium enrichment decreases (table 3.1.4). However, Darling (79) also quotes Muller and Roy who have constructed a phase diagram for the oxides of rhodium. They deduce from their work that none of the oxides of

rhodium are stable in air above $1,000^{\circ}\text{C}$. The oxide which is stable in air up to 700°C is Rh O_2 , which undergoes a phase change to Rh_2O_3 at these temperatures. A further change then occurs to a corundum structure, which decomposes to pure rhodium at approximately $1,100^{\circ}\text{C}$ at atmospheric pressure.

An explanation for this large rhodium enrichment occurring between 600°C and 800°C can then be advanced. Under the influence of increasing temperature, platinum volatilises off the catalyst (as Pt O_2) faster than Rh O_2 . This results in an increase in surface rhodium concentration. The rhodium oxide present becomes more stable as the temperature is increased, giving increased rhodium enrichment, present as Rh O_2 and Rh_2O_3 . However after treatment at $1,000^{\circ}\text{C}$ the rhodium oxide formed is no longer stable, and there is no driving force being applied to encourage rhodium enrichment by its reaction with oxygen. Thus it is possible that at $1,000^{\circ}\text{C}$, whilst rhodium enrichment may occur as an intermediate rhodium oxide, this will decompose at $1,000^{\circ}\text{C}$ giving no net oxidation, and the rhodium may move back into the matrix. This could also account for the fact that on reaction, the relative surface rhodium content decreases. The temperature of a gauze running in 14% NH_3 / air mixtures has been shown to be approximately $1,100^{\circ}\text{C}$, with inlet gas temperatures of 600°C . This would preclude the formation of rhodium oxide and stop rhodium enrichment. This explanation is also in agreement with the finding that the rhodium signals observed in the E.S.C.A. work show no large shift in position despite oxidation for 72 hours.

Hydrogen flame activation produces rhodium enrichment (tables 3.2.1 and 3.2.8) and a large shift in the rhodium oxidation state. Table 3.2.1 shows that this enrichment is lost on reaction, and the rhodium oxidation state returns to that in the 'as supplied' case.

The temperature of a hydrogen flame (2,223 K) is such that volatilisation rates of platinum and rhodium are approximately equal, whilst rhodium oxides are not stable in air above 1,323 K (79). These contradictory results can be explained by postulating that oxide formation and surface rhodium enrichment occur during cooling in air from the

white-heat temperatures of the hydrogen flame. This once again underlines the irreproducibility of the hydrogen flame treatment.

5. 1. 3. Electronic Factor

The nature of electronic effects and their relevance to catalysis by metals has been discussed earlier (section 1. 2.). It could be suggested that the catalytic activity of Pt/Rh gauzes resulted, at least in part, from electronic effects induced by alloying, despite the fact that rhodium was primarily added to the gauze to reduce platinum loss rather than to enhance activity (3).

The results which can be expected to be relevant as to the degree - if any - of electron exchange between the alloy components are the peak positions of the metal ions. Unfortunately these change in any case as a result of oxide formation (see above), and no specific conclusion emerges.

In the present work it was noticed that, with the foil catalysts, not only was there a substantial increase in surface rhodium concentration, but this was accompanied by a shift of approximately 1 eV. This is particularly noticeable with the oxygen activation treatment (Table 3. 2. 3) where this may indicate a definite change in the atomic state of the rhodium atoms at the surface of the foil. Argon bombarding reduces this back to the 'as supplied' state. This activation process clearly involves a change of state in the surface rhodium atoms.

To further clarify this, a piece of Pt/10% Rh foil was heated in air for 3 days at 750^oC and studied using Mg K α radiation to obtain an accurate value for the shift of the rhodium signal. The results shown in table 3. 2. 10, indicate that the signal from the surface rhodium atoms has shifted approximately 1. 0 eV during this oxidation process, possibly indicating the presence of a surface oxide. It is clear that activation produces a rhodium oxide at the surface, and that the rhodium present in the 'as supplied' state is not in as high an oxidation state. The listed values for Rh_{M III} and Pt_{N VII} binding energies are 496. 2 and 71. 1 eV respectively, and the spectrometer signals are accurate to \pm 0. 3 eV and \pm 0. 2 eV respectively. Thus, the data in table 3. 2. 1

shows no significant difference in any of the reported signal positions, with the exception of the activated rhodium signal. To definitely relate a shift to oxide formation, shifts of a least 1 eV and greater are essential. It therefore seems doubtful that this represents a transition from metal to metal oxide, but may indicate the formation of an oxide layer below one monolayer.

However, as both argon bombardment and reaction in ammonia oxidation conditions give signal positions which are similar to those in the 'as supplied' state, it can be concluded that this apparent rhodium oxide formation is not important in terms of the electronic state of the catalyst in relation to its activity towards ammonia oxidation.

As both platinum and rhodium are relatively inert to oxide formation, then it can be assumed that any oxide formation occurring will be confined to the surface layers of the metal matrix.

It is interesting to compare the catalytic oxidation of ammonia on platinum with platinum/rhodium alloys used in electrocatalysis. Work by Rand and Woods (80) has been described earlier in section 1.2. They do not observe two peaks in their voltammogram which could be ascribed to the individual components in a binary alloy. However work by Damjanovic et al. (81) has shown that nucleation of Pt/Rh alloys used in electrocatalysis gives pure oxides, not mixed oxides.

Whilst this nucleation process may occur in ammonia oxidation the present work cannot ascribe any result to variation in activity arising from electronic effects.

5.1.4. Geometric factor

It is well known that Pt/Rh gauzes undergo extensive rearrangement during activation and reaction, and that the catalytic activity increases during the time that this reorganisation occurs (1). It is useful to consider whether the increase in activity is caused by this rearrangement or by some other geometric effect.

Two geometric effects may be distinguished. The first of these is well described by Philpott (38) who studied the changes occurring in

active and inactive gauzes by scanning electron microscopy and by electronprobe microanalysis. Inactive gauzes were shown to have a uniform grain structure and to develop 'cauliflower' like growths under reaction conditions. Active gauzes showed a clearly developed octagonal crystal structure and developed 'nodules' under reaction conditions and particularly at cross-over points in the mesh. These effects may be described as macro-geometric.

The second geometric effect has been studied by Delaney and Manogue (9) and Ostermaier et al (78), who considered catalyst sintering and crystallite size effects in the low temperature ammonia oxidation over supported platinum. Ostermaier (78) has shown that the low temperature oxidation of ammonia is a demanding reaction, with smaller crystallites having a lower specific activity than larger ones. Initially, the specific catalytic activity was crystallite size dependent, though the catalyst underwent deactivation to a steady state. Though the work of Ostermaier et al. was carried out using supported catalysts, they concluded that there was no significant contribution from the alumina support, and the products, nitrogen and nitrous oxide, were those expected for the low temperature oxidation.

In their work on catalyst sintering in the low temperature ammonia oxidation over supported platinum, Delaney and Manogue (9) have cited Wilson (82), that platinum crystallite size may effect the amount of oxygen which can adsorb on the surface, and that this could be associated with a change in the ratios of exposed crystal faces.

As an appendix to their paper on the kinetics of the oxidation of platinum, Fryburg and Petrus (61) have studied the surface morphology of electrically heated ribbons at temperatures from 900°C to $1,500^{\circ}\text{C}$. Their investigation showed that ribbons heated above $1,400^{\circ}\text{C}$ had larger grain size than those heated below $1,250^{\circ}\text{C}$. Visual examination showed large, shiny areas interrupted by smaller etched areas, similar to those shown in photograph 52. X-ray back reflection measurements indicated that the smooth areas had a (111) plane parallel with the surface, whilst etched areas had a (311) parallel with the surface. These (311) areas appeared to be composed of steps.

Specimens annealed at $1,250^{\circ}\text{C}$ gave X-ray back reflection measurements indicating the entire surface oriented with a (111) plane parallel to the surface. This data compares well with the theory put forward by Somorjai (83). The Pt (111) surface has the highest atomic density and lowest free energy of the platinum low index planes and is stable close to the melting point of platinum. However, molecular oxygen has a sticking probability of only 10^{-6} on Pt (111) and Pt (100) planes (84), but on stepped surfaces, oxygen chemisorbs readily even at low temperatures (300 K) and low pressures.

Thus, it is probable that the surface rearrangement shown in photograph 52 could be explained by this, and if adsorption of oxygen at the catalyst surface is essential as a first step in the oxidation reaction, then the (311) stepped planes will be more reactive and hence produce more rearrangement than the (111) planes.

The present studies have been used to ascertain the importance of both types of geometric effect. Clear evidence of macro effects has been obtained both on activation and reaction, (Photos 1, 2, 48 and 49), and it has also been possible to show that reorganisation is very dependent on the particular grain in the wire (Photo 52).

Initial experiments were directed towards obtaining a reproducible method of activation. It is apparent from previous work (section 3.1.f) that solvent cleaning, to remove oil and surface impurities present as specks of dirt, is an essential part of the activation process. However, following this, it is essential to produce a gauze of uniform activity on which further experiments could be based. Several methods of activation were studied, beginning with the activation process adopted by industry.

The hydrogen flame activation, carried out in 3.1.a, clearly showed in photograph 1 and 2, that this method of activation was not reproducible. A molten metal surface was produced on the catalyst during treatment, resulting in extensive grain boundary formation, and movement of the molten metal to the ends of the wire, under the influence of gravity. In addition, the temperature variation over the gauze could be large, as a result of positioning of the gauze in the flame, giving another uncontrollable parameter.

A preliminary study of the surface rearrangement occurring with different gases was undertaken. The results shown in 3.1.g clearly indicate that oxygen induces the most surface rearrangement, in the form of extensive pitting. Reducing gases, however, tend to produce smoother metal surfaces and larger grain size. This is complemented by the U. P. S. work discussed later (section 5.1.5).

The activation process must produce a catalyst which can light-off at low temperatures and rapidly produce an active gauze, giving high selectivity. Experimental work in section 3.1.h has shown the very rapid surface development occurring under ammonia oxidation conditions. The photographs show that the surface rearrangement of the gauze begins immediately the reaction commences. Photographs 37 - 44 and 52 clearly show that different grains are showing varying degrees of rearrangement. After approximately three minutes, extensive pitting has occurred, and after nine minutes, the surface is almost completely covered with large pits. These pits rapidly agglomerate until, after twenty-two minutes, no clear grain structure is discernible. After two hours reaction time, the rearrangement has developed beyond the depth of field of the camera.

Platinum/10% Rhodium foils used in the E. S. C. A. experiments (photo 52) clearly shows that different grains on the metal surface are rearranging at varying rates during reaction. It may be that activation is producing a different grain structure, or, as discussed earlier, causing one particular set of crystal planes to predominate. If these planes preferentially adsorb one or both of the reactants, this would lead to preferred reaction on these grains, giving rise to extensive rearrangement. The exothermic nature of the reaction would also be sufficient to establish catalyst light-off, and the reaction would then spread rapidly from these areas to cover the whole of the catalyst. Attempts to ascertain the crystal structure prevalent in each individual grain have so far failed, and further experimentation is necessary before the reactivity of individual grains can be established.

To further study the effect of oxygen treatment at various temperatures (3.1.b), a piece of wire was first activated using a hydrogen

flame. This permitted a particular grain to be observed, and the wire was then exposed to oxygen at 800°C for times up to two hours. Photographs 3 - 10 clearly show the pitting of the surface to increase with time. As heat treating in oxygen represented a reproducible method of gauze preparation, this activation method was adopted for further work.

It was possible that activation could be produced by heating in gases other than hydrogen and oxygen. In section 3.1.c, a comparison has been drawn between oxidising, reducing and inert gases. The temperature of treatment ($1,000^{\circ}\text{C}$) and the time (two hours) were standardised, to enable a direct comparison to be drawn between light-off temperature and activities. Reference to table 3.1.1. shows that an inert gas (e. g. He) does influence the light-off temperature of the gauze, giving a 40°C lowering of light-off temperature, and a maximum activity at 450°C instead of 500°C in the unactivated case. The remaining treatments give substantially lower light-off temperatures. In the case of hydrogen flame, oxygen, and hydrogen treatments, a 100°C lowering of light-off temperatures was observed, and the maximum activity occurs at low temperatures (380°C , instead of 500°C). Reaction on the gauzes gave rise to a greater increase in temperature (between 150°C and 180°C , instead of 70°C with the unactivated gauze). Photographs of the gauzes also show marked difference in the extent of rearrangement. Inert gases (Photo 15) give grain boundary grooving but little pitting. Reducing gases (Photo 12) give a smoother catalyst surface, although extensive grain boundary grooving is observed. Oxygen treatment produces extensive pitting (Photo 31) while hydrogen flame treatment gives grain boundary grooving (Photo 3). At first sight, it would appear that pitting and grooving produce a more active gauze, but that massive rearrangements are not necessary. However, some pitting and grooving were observed on treatment with inert gas, while the gauzes were not as active as the oxygen treatment. As a result, it can be suggested that activation is not primarily connected with macrogeometric rearrangements on the surface. However, the results do show that oxygen activation at $1,000^{\circ}\text{C}$ produces a gauze with an activity

comparable to that of an hydrogen treated gauze, and for interests of reproducibility and safety, this treatment was adopted as a standard activation method.

The activities of gauzes treated in oxygen at varying temperatures was then studied (table 3.1.3). Reference to graphs 3.1.18 - 3.1.20 shows that the highest light-off temperatures occur when the oxygen treatment was carried out between 600°C and 800°C . Photographs 29 and 30 show that extensive pitting is occurring in this temperature range, but this appears to be confined to grain boundaries. However, at 500°C , and from 800°C to $1,000^{\circ}\text{C}$, the pitting has not occurred preferentially at grain boundaries, but completely covers the surface of the catalyst. This would seem to indicate that pitting definitely lowers light-off temperature and produces greater activity.

Experimental work carried out in section 3.1.j, has shown that calcium is present on the catalyst and must be removed by solvent washing. (table 3.1.10). The unwashed catalysts were inactive and characterised by large circular pits (Photo 45). These contrast with the smaller square pits obtained from an active gauze which had been solvent washed, activated and reacted (Photo 46). This could indicate that the surface impurities were directly responsible for the larger pits which could possibly be giving rise to low activity and high light-off temperature. It was possible to show however that calcium was not directly responsible for the pits. No calcium was present at the bottom of the larger pits, although calcium was present on the surface. No impurities were present in the smaller pits of the active gauzes. The E. P. M. A. investigation did show that there was no preferential concentration of rhodium at the grain boundaries or pits.

Baker, Thomas and Notton (85) have studied the behaviour of platinum catalysts in ammonia oxidation by controlled atmosphere microscopy. Their investigations show that attack on the wire surface predominates at grain boundaries, whilst Norris and Parravano (86) studying the reactive mass transport in platinum suggest that the formation of a volatile oxide of platinum is responsible for the extensive surface rearrangement which takes place in atmospheres containing

oxygen. They also report that surface diffusion played an important role. Experiments were carried out to couple these findings and estimate the rate of surface diffusion of platinum in the ammonia oxidation reaction.

Surface diffusion and thermal facetting have been reviewed by Blakely (87) and Moore (88) who both outline the interferometric method for following the development of grain boundary grooves. Use of this method on the platinum catalyst failed because the surface of the gauze was not flat and hence gave rise to interference patterns which obscured those arising from the grain boundary grooves.

The theory of thermal grooving and the kinetics of grain boundary grooving in copper have been reviewed by Mullins (89) (90) and Mullins and Shewmon (91). Theories predict that a groove profile will have a time independent shape whose linear width and depth will be proportional to $(\text{time})^{\frac{1}{2}}$ for an evaporation - condensation process, $(\text{time})^{\frac{1}{3}}$ for a volume diffusion process, and $(\text{time})^{\frac{1}{4}}$ for a surface diffusion process.

Attempts were therefore made to follow the variation in the width across a scratch made in the surface of a piece of Pt/10% Rh foil with time. This experiment used the multiple scratch method outlined by Blakely and Mykura (92). Two parallel scratches were made in the surface of the foil and reacted in the ammonia/air gas stream. Photographs 79 - 82 clearly show that the reorganisation occurring during the reaction was so extensive that no accurate measurements of groove width could be made. The ends of the grooves were also studied. Photographs 83 - 86 show that despite extensive reorganisation arising from the ammonia oxidation reaction it does appear that no 'humps' are formed at the edge of the groove, indicating an evaporation - condensation mechanism for groove formation in platinum/rhodium alloys during ammonia oxidation.

To complete the work associated with the geometric factor, the effect of pretreatment in oxygen at high temperature was also studied. Treating the catalyst at $1,000^{\circ}\text{C}$ in oxygen has been shown to give rise to extensive pitting, and the reaction lights-off at 310°C to give a high

activity. In comparison, an untreated gauze did not light-off until the inlet gas was preheated to 540°C . On running an untreated gauze for two hours, the activity increases to the level obtained from pretreatment in oxygen at $1,000^{\circ}\text{C}$ (graph 3. 1. 25). It is uncertain whether this increase in activity occurs as a result of the heat generated by the reaction at the gauze, or whether it is a combination of heat and oxygen included in the reactants. Certainly, extensive reorganisation occurred during the two hours whilst the catalyst was being used.

To summarise the work on the geometric factor, it can be stated that inert gas activation produces little pitting and that the gauze is inactive when compared with the hydrogen flame activation - which gives rise to extensive surface rearrangement, and the oxygen activation - which produces extensive pitting. For activation to occur, some surface rearrangement is needed, though this need not be as extensive as that associated with the hydrogen flame and oxygen treatments.

5. 1. 5. Adsorption

The extent and nature of adsorption on the surface of a catalyst is one of the most important factors in determining the activity and selectivity of a catalyst (section 1. 2. c). In an oxidation reaction on a noble metal the nature of any adsorbed oxygen and its subsequent diffusion through the metal is of obvious importance. The interaction of oxygen with platinum metal has been the subject of many investigations over recent years.

Fusy, Weber and Cassuto (93) have concluded that molecular oxygen is adsorbed at room temperature giving rise to Pt_2O formation, whilst Andeeva (94) has proposed that $\text{Pt}_3(\text{O}_2)_4$ is formed. Using oxygen at 800°C - $1,000^{\circ}\text{C}$, Asanov (95) has formed a Pt O phase by condensing a platinum film on a quartz plate. Vaneslow and Schmidt (96) have studied the field evaporation of platinum at high temperature with mass spectroscopy and have detected Pt^+ , Pt^{2+} , Pt^{3+} at $1,200^{\circ}\text{C}$

together with PtO^+ , PtO^{2+} , Pt_2O^+ , Pt_3O^{2+} , Pt_4O^{2+} , $\text{Pt}_3\text{O}_4^{2+}$, $\text{Pt}_2\text{O}_3^{2+}$, PtO_2^+ and PtO_3^+ in presence of oxygen between $600^\circ - 1150^\circ\text{C}$. Thus, whilst it would seem that many surface oxides can be formed, these do depend on ambient conditions of temperature and pressure, and platinum appears to only undergo surface oxidation (97) (98) (99), diffusion into the lattice not occurring (100) even at temperatures in excess of $1,400^\circ\text{C}$.

Techniques for the study of surface adsorbed species all use very low pressures, and many workers rely on the detection of intermediates in the gas phase. Thus Ostermaier (78) has detected nitrogen and nitrous oxide as the products of low temperature oxidation of ammonia at atmospheric pressure, whereas Nutt and Kapur (33) (101) and Fogel et al. (102) (103) and Molinari et al. (104) observed only nitric oxide and nitrogen as reaction products at sub-atmospheric pressures.

As a result of their work, Ostermaier et al. (78) have proposed that deactivation of the supported catalyst was due to the formation of a surface platinum oxide different from chemisorbed oxygen and they believe that the platinum surface below 460 K is intrinsically different from that above 460 K. However, the E. S. C. A. results from section 3.2 show that there is no significant change in the position of the platinum signal, indicating that platinum is in the same oxidation state, both at the surface and in the bulk of the metal.

The present studies show unambiguously that oxygen is the only gas adsorbed on the surface of the Pt/Rh catalyst during the oxidation of ammonia.

To study the nature of this probable oxide formation, a Pt/10% Rh gauze was studied in the 'as supplied state' using E. S. C. A. This showed a relatively strong rhodium signal, with a strong oxide signal present. The platinum and rhodium signals were shifted 1 eV and 2 eV respectively from their listed positions of 71.1 eV and 496.2 eV, indicating the possibility of oxide formation. Argon bombardment produced a shift in the rhodium signal indicating a lower oxidation state. Heating to $1,000^\circ\text{C}$ in oxygen at a pressure of 10^{-4} Torr did not restore the

shift in the rhodium signal, and neither did reaction 'in situ' of the gauze with an ammonia/oxygen mixture.

The absence of a shift back to the oxidised state for rhodium would seem to indicate one of two possibilities. Either, the rhodium does not exist in its oxidised state during the reaction, which seems unlikely, or the reaction 'in situ' was dissimilar from that obtained when the gauze was reacted in the ammonia burner. Investigations with Pt/10% Rh and Pt/40% Rh foils discussed earlier, seem to indicate that the latter of the two possibilities is correct. However, it must be noticed that in table 3.2.7, the shift of the rhodium signal in the 'as supplied' state is large, and is 1.2 eV higher than the corresponding figure obtained for Pt/10% Rh foils (table 3.2.1). This cannot be explained except by experimental error. Reference to figure 3.2.9, the spectrum of an untreated catalyst surface, with that of figure 3.2.10 which refers to a sample flashed to approximately $1,000^{\circ}\text{C}$ in 10^{-5} Torr ammonia, clearly shows the large reduction which occurs in the O_{1s} signal. This indicates that reaction with ammonia to produce nitric oxide removes oxygen from the surface of the catalyst. Hence adsorption of oxygen appears to be a precondition for ammonia oxidation.

Activation by oxygen at $1,000^{\circ}\text{C}$ was studied to observe the change in oxygen signal intensity, together with changes in the platinum and rhodium signal positions. Table 3.2.3 indicates that, as in the hydrogen flame activation procedure (table 3.2.1), there is no significant shift in the platinum signal, though the rhodium signal is once again shifted by 1.1 eV. There is, however, a marked difference in signal position after activation and reaction. With oxygen activation, reaction does not produce a shift back to the 'as supplied' state as was noticed with the previous treatments. The signal remains at 498.2 eV and does not return to 497.0 eV. This indicates that the rhodium oxide does not take part in the reaction and that the layer is thicker than in the previous treatments, but is still removed by argon ion bombardment. As expected, with the oxygen activation, the Pt/O ratio shown in table 3.2.4 is lower than that of the hydrogen flame

activation shown in table 3.2.2, due entirely to an increase in the intensity of the oxygen signal. No change was observed in the intensity of the platinum signal though, after argon ion bombardment, the oxygen signal was greatly reduced, whilst the intensity of the platinum signal more than doubled. This indicates that any oxide layer present on the gauze was not substantial and may be only a few monolayers thick, despite treatment in oxygen at $1,000^{\circ}\text{C}$ for two hours.

To further examine the effect of an oxide layer on the reaction, ultra-violet photoelectron spectroscopy (U. P. S.) was used. To study the nature of the oxide species present, the foil was first solvent washed and activated by heating in an hydrogen flame, after which it was treated 'in situ' at 800°C and argon ion bombarded to remove any surface deposit resulting from its exposure to laboratory air.

Recent work by Norton (105) has shown two states of adsorbed oxygen at 530.2 eV and 533 eV below the platinum fermi level. Figure 3.2.3 also shows these two levels, at 529 eV and 534 eV binding energies, corresponding to O 1s signals. Using P. E. S. Norton obtained a signal at 6.1 eV below the fermi level which he ascribes to a weakly adsorbed molecular state.

The general spectrum obtained in figure 3.3.1 clearly shows an oxygen signal at approximately 5 eV below the fermi level. This is reduced substantially on exposure to ammonia at room temperature and 5×10^{-6} Torr (Fig. 3.3.2). Figure 3.3.3 shows that flashing the foil briefly for approximately 10 seconds at 500°C reduces this oxide peak still further.

When oxygen is readmitted at 5×10^{-6} Torr at room temperature for 10 minutes, the signal increases, indicating that there is adsorption of oxygen at room temperature. Heating in this oxygen atmosphere for five minutes at 800°C caused the signal to split into a doublet. (Figs. 3.3.4/5).

Hydrogen was then admitted at 10^{-5} Torr at 800°C for 10 minutes, and the oxide signal was substantially decreased (Fig 3.3.6). Further treatment of twenty minutes hydrogen exposure at 5×10^{-5} Torr and $1,000^{\circ}\text{C}$ reduced but did not eliminate this oxygen signal (Fig. 3.3.7).

This U. P. S. work has shown that there is no obvious room temperature adsorption of ammonia, though there is definite evidence of room temperature adsorption of oxygen. Heating in oxygen gives strong oxide levels, though an X. P. S. spectrum of this foil showed the levels to be unshifted i. e. only a monolayer of oxide film is present.

The apparent lack of adsorption of ammonia would seem to rule out the Langmuir - Hinshelwood mechanism for the catalytic oxidation of ammonia. High temperature treatment of the catalyst in oxygen produces one or two monolayers of oxide, so it is unlikely that pure platinum or pure rhodium are the catalysts for the oxidation process.

Further evidence for oxide formation being a prerequisite for catalytic activity is shown by studying the activities produced by pretreating in nitrogen and oxygen. The comparison of the activation by oxygen and nitrogen in 3. 1. d has shown that oxygen treatment at 350°C produces an active gauze. Nitrogen activation at 800°C produces a catalyst with a lower activity and a higher light-off temperature (table 3. 1. 2). However, when the two treatments are combined, nitrogen at 800°C , followed -by oxygen at 350°C , this activity is not restored. This can also be seen from photos. 17 - 19, 20 - 22, and 23 - 25. The photographs of the nitrogen treatments 20 - 22 and 23 - 25 clearly show less surface rearrangement than those for the oxygen treatments. Whilst nitrogen treatment at 800°C produces a relatively inactive gauze, the oxygen treatment at 350°C proved inadequate to restore this activation.

To further investigate this effect, X. P. S. spectra of Pt/10% Rh foils heated in oxygen at 350°C , nitrogen at 800°C , and finally nitrogen at 800°C followed by oxygen at 350°C , were obtained. Table 3. 1. 2 shows the results obtained. No conclusions can be drawn from the Pt/C, Pt/O and C/O ratios. However, the platinum/rhodium ratios are significant. Treatment with oxygen at 350°C has produced a higher Pt/Rh ratio which, because of the relative increase in platinum concentration, produces higher activity. Treatment with nitrogen at 800°C has produced rhodium enrichment. The exact mechanism of this rhodium

enrichment is not clear but cannot be due to Pt O₂ evaporation. It is possible that decomposition of the oxides occurs in nitrogen at 800°C, but the fact that a further treatment in oxygen at 350°C did not restore the activity shows that the resulting deactivation was not due to lack of Pt O₂.

Heating at 800°C in nitrogen has produced rhodium enrichment which gives rise to lower activity and this is not due to the formation of a nitrogen containing compound at the catalyst surface.

5.2. The deactivation of platinum/rhodium gauzes in ammonia oxidation

During the work carried out on the activation of Pt/Rh gauzes, it was noticed that the presence of surface calcium compounds gave rise to low activity of the gauzes towards ammonia oxidation. Philpott (38) has also shown that iron oxides give rise to inactive gauzes. Work was undertaken to study the effect of various dopants on the activity of platinum/rhodium catalysts.

Early work by Scott (186) on catalysts for ammonia oxidation has shown that;

platinum > cobalt oxide > iron oxide
 chromium oxide > nickel oxide > manganese dioxide >
 copper oxide.

Thus Scott had first noticed that other oxides besides platinum could catalyse the ammonia oxidation reaction. None of these oxides were as efficient as platinum and though much research work has been carried out on oxide catalysts for ammonia oxidation, they have not become popular due to their poor conversion efficiency. (86.3% at $70 \text{ dm}^3 \text{ hr}^{-1} \text{ cm}^{-2}$ catalyst (187)).

Much research work has been concentrated on iron/chromium oxides. Dobrovolskaya (5) (188) and Ivanov and Petrova (189) have outlined the production of iron/chromium oxides for ammonia oxidation uses. The methods usually involve mixing and calcining iron/chromium nitrates, followed by a subsequent grinding and tableting process.

The object of work on two stage ammonia oxidation catalysts has been to maintain overall conversion efficiency whilst reducing the amount of expensive platinum/rhodium catalyst in use. Thus work by Mazgaj (190), Miniovich et al. (191) and Zasorin (192) has shown that when dual catalysts (such as a layer of platinum followed by a layer of iron/chromium oxides) are used, degrees of conversion up to 95% are possible.

Engineering problems arise however, because as fewer platinum gauzes are used, the mechanical strength of the gauze pad decreases.

Kubik (193) has overcome this problem using ceramic supports, whilst Hunter (194) has constructed his platinum catalyst support from an open mesh chromium/nickel sieve.

Work by Kurin (195) has shown that an increase in alumina concentration decreases the yield of nitric oxide from cobalt oxide/alumina catalysts. Optimum conditions for ammonia oxidation on these catalysts were shown to be 800°C preheat, on a 5% Al₂O₃ catalyst giving 83% conversion.

Other additions have been made to platinum alloy catalysts. Kenson et al. (196) have developed a catalyst containing 48.5% Pt, 35% Pd, 6.5% Rh and 10% Au. This they claim gave 96% ammonia conversion over 240 hours, as against 93.5% conversion for a 90% Pt/10% Rh catalyst over 388 hours.

Thus it can be seen that the addition of oxides and precious metals to platinum/rhodium alloy catalysts can improve the selectivity and reduce the weight loss of platinum.

The work carried out in this section has been undertaken to study two effects which will be dealt with in turn. These two effects, 'induced geometric effects' and 'electronic effects' are important in the surface doping of platinum/rhodium catalysts.

5.2.1. Induced geometric effects.

Doping of Pt/10% Rh gauze catalysts has been undertaken with the object of lowering the weight loss of platinum during the reaction. Any dopant which lowers gauze running temperature, but maintains or improves efficiency will be advantageous. Table 3.5.1 shows the effect of iron oxide on activated and unactivated gauzes. The activated gauzes showed extensive pitting arising from treatment with oxygen before doping. When doped, these pits - which may be a cause or an effect of the activation process - possibly act as centres for iron oxide deposition, giving rise to increased iron oxide concentration on the gauze surface.

Gauzes which had been activated and doped gave a higher light-off

temperature than those which had not been activated before doping, and the conversion efficiency of the activated gauzes was lower.

Hence it follows that whilst the pits arising from activation may be a cause or an effect of activation, blocking these pits with iron oxide does lower the activity of the catalysts.

Photographs 53 and 54 show that many small pits arise as a result of iron oxide doping. Photograph 54 shows that these pits are not present in every grain, but appear to be concentrated only in certain grains. This effect was also noticed with vanadium pentoxide dopant. Photographs 55 and 56 show normal rearrangement occurring on the top surface of the top gauze, but some pitting is apparent on the lower gauze. It does seem therefore that activation, followed by doping allows greater surface dopant concentration, and the fact that this dopant fills the pits produced in activation is associated with low conversion.

Vacuum evaporation of iron, shown in Photographs 59 - 61 produces the lowest light-off temperature (280°C) but also the lowest activity. Pitting is once again present on the bottom surface of the top gauze (photo. 60) though little reaction seems to have occurred on the bottom gauze. Finally, gold was used as a dopant to ascertain whether adsorption of oxygen was an essential prerequisite to ammonia oxidation. As gold does not adsorb oxygen, a high light-off temperature ought to have been realised. This in fact was the case, giving a light-off of 645°C , and a low activity (79%). Photographs 57 and 58 show that whilst the reaction occurred primarily on the top gauze, large irregular pits were formed, which did not give high activity. Graph 3.5.1 shows that nitric oxide was not produced until 10 minutes after light-off of the gauze. Thus, this indicates that adsorption of oxygen must occur if the catalyst is to oxidise ammonia.

Besides lowering the gauze running temperature without impairing efficiency, dopants must be stable at the high temperatures occurring in the catalytic reaction ($800 - 1,000^{\circ}\text{C}$) and should not readily volatilize off the catalyst under the conditions of operation. Table 3.5.2 shows the oxides which have been used to dope the surface

of the platinum catalysts; volatilization occurred with the following; MgO , TiO_2 , MnO_2 , Co_3O_4 , $\text{La}(\text{NO}_3)_3$, SiO_2 , Al_2O_3 and KOH . Conversion efficiencies were determined for those dopants which were not removed from the gauze.

Photograph 63 shows that doping with calcium oxide gave rise to small pits and to low activity (Table 3.5.2). This was accompanied by a high light-off temperature (485°C) and a low conversion efficiency (82%). Nickel oxide dopant also shows similar behaviour (photo 72). Chromium oxide (photo 69) does not readily volatilize at these temperatures, but does show a high light-off temperature. Barium oxide (photo 64) and sodium hydroxide completely deactivated the platinum/rhodium catalyst; barium oxide chemically reacted in the gas stream, undergoing a colour change from white to green.

The two most interesting results however are provided by zirconium dioxide and vanadium pentoxide. Zirconia is stable at the high temperatures occurring on the gauze, and lowers running temperature by 100°C without significantly lowering overall efficiency (95%). Vanadium pentoxide produced results totally incompatible with those of the other dopant oxides. The temperature profile is shown in graph 3.5.5. The profile shows a light-off temperature of 370°C followed by extinction of the gauze. This was accompanied by the dopant changing colour from orange to black. Thereafter alternate ignition/extinction cycles occurred until a steady temperature of 650°C was obtained after 5 minutes. At this low running temperature the yield of nitric oxide was found to be 10%, with 85 - 90% of the ammonia passing through the gauzes unchanged. Thus the initial ignition possibly produces V_2O_3 which acts as a poison. It can be seen from photographs 67 and 68 that the black dopant has concentrated in areas below which the platinum catalyst has rearranged. No dopant is present on the smooth platinum areas. This seems to indicate that the reaction is occurring on only certain grains in the gauze wire. Further work must be carried out to determine the exact chemical nature of the dopant after reaction before a satisfactory explanation can be offered for the cycling phenomenon. In terms of mass transfer effects it is possible that the

initial light-off produces a fast reaction which becomes diffusion limited giving extinction. As the gauze cools, diffusion limitation becomes unimportant and light-off occurs again. Final extinction is obtained owing to the formation of V_2O_3 , possibly by reducing conditions arising using a 14% NH_3 /air gas stream.

This effect could show up most markedly with the V_2O_5 system as opposed to other dopants if V_2O_3 is a particularly effective poison for the reaction.

5. 2. 2. Electronic effects

As shown in table 3. 5. 2, various dopants are seen to have a marked effect on catalytic activity. The most obvious suggestion was that these oxides had a catalytic activity of their own - as is known to be the case, for example, with Co_3O_4 - and the same dopants were deposited on a copper mesh. No similar pattern of activity was obtained, although this result is not unambiguous proof, in that the copper mesh could not be obtained in exactly the same dimension as the platinum/rhodium gauze.

It was then postulated that some kind of electron sharing could be affecting activity. As a result, attempts were made to correlate activity with electronic effects noted in other systems.

One such correlation has been developed by Dowden (137). As summarised earlier, crystal and ligand field models have been used to show that catalytic activity can be related to the number of d electrons.

A good example of this effect has been shown by Dowden (197) who reviewed hydrogen reactions on ionic compounds with unfilled d orbitals. In the H_2/D_2 exchange reaction at $80^\circ C$, Dowden et al. (197) have outlined a simple correlation between catalytic activity and electronic configuration of a metal ion. The results obtained by Dowden are shown in figure 5. 2. 1. From this it can be seen that high activity is obtained with $3d^3$ (Cr_2O_3), $3d^6$ or $3d^7$ (Co_3O_4) and $3d^8$ (NiO). These are believed to contain a 'fair' number of unpaired d electrons. With very few or no unpaired d electrons e.g. TiO_2 , V_2O_5 , V_2O_3 , CuO ,

Fig 5.2.1.

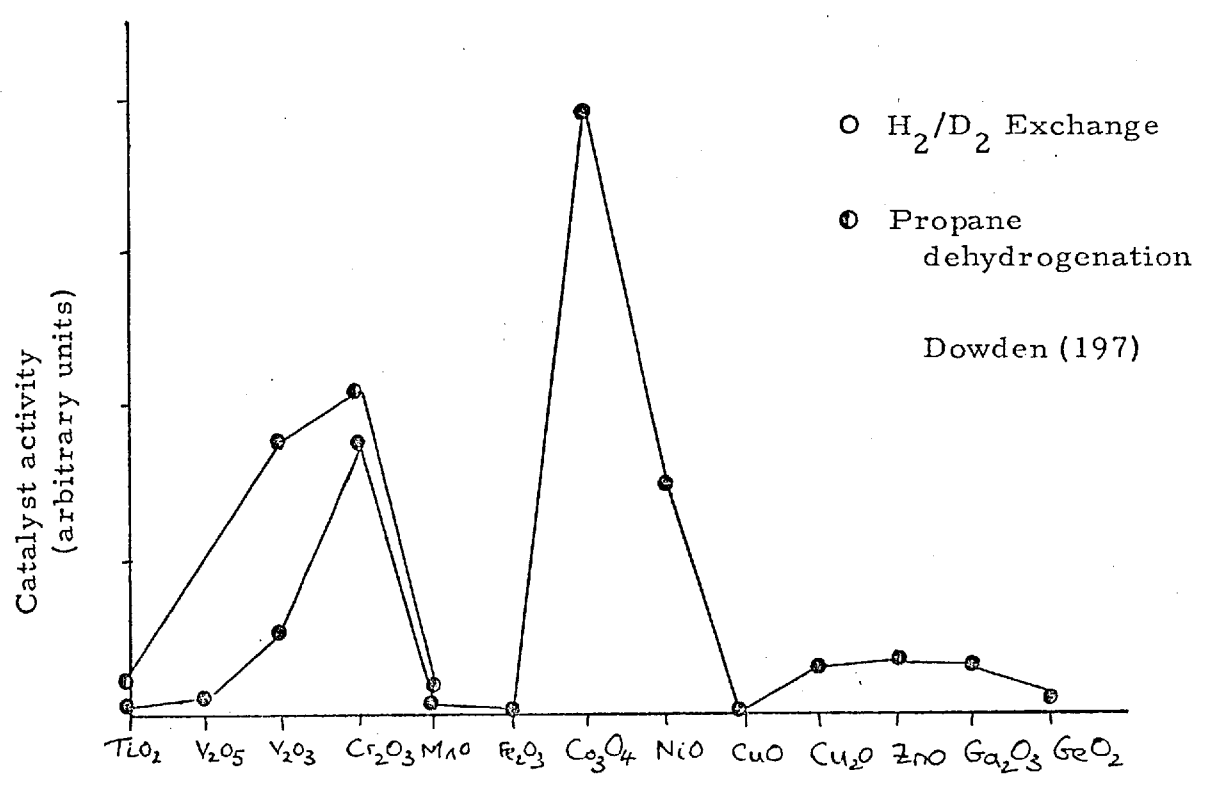
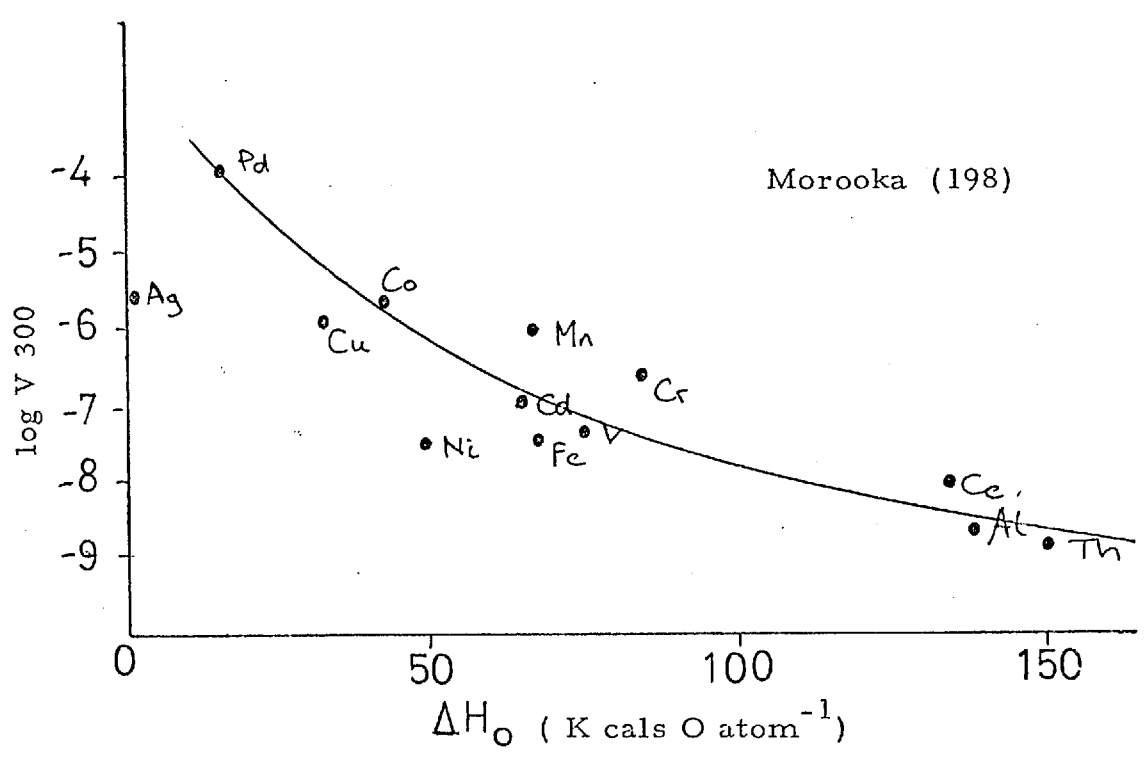


Fig 5.2.1.a.



Cu_2O , ZnO , Ga_2O_3 and GeO_2 , then low activity results. This is also the case for a metal ion containing a high number of unpaired d electrons e. g. MnO and Fe_2O_3 .

If the results in table 3.5.2 are plotted against d electron configuration in a similar manner to that of Dowden, then a similar reactivity pattern is obtained (Fig. 5.2.2). In fact a triplet peak pattern is obtained, similar to the twin peak pattern of Dowden, with an extra maxima at CuO . These maxima indicate positions of low activity, rather than high activity observed by Dowden for H_2/D_2 exchange. Nevertheless, the similarity is striking and indicates minimal poisoning at $\text{Mn}(\text{d}^5)$ and $\text{Zn}(\text{d}^{10})$. Activity minima occur at $(\text{Cr}^{3+})\text{d}^3$, $\text{Co}^{3+}(\text{d}^7)$ and $\text{Cu}^{2+}(\text{d}^9)$.

Apart from this correlation with the d electrons, this activity pattern is somewhat surprising. First it is seen that where Dowden has high activity, high light-off temperatures have been obtained, i. e. initial catalytic activity is low.

Secondly, several unexpected features of the pattern arise. Cobalt oxide (Co_3O_4), which is the best metal oxide for ammonia oxidation after platinum gives the highest light-off temperature when supported on a platinum catalyst.

Again compounds such as zinc oxide and manganese oxide which are not normally considered good catalysts have hardly any effect on the light-off temperature.

Another correlation has been developed by Morooka and Ozaki (198) for the catalytic properties of metal oxides in propylene oxidation. They found that reaction rates could be correlated with the heat of formation of catalyst oxides divided by the number of oxygen atoms in the oxide molecule. This correlation is shown in Figure 5.2.1.a.

When the light-off temperatures are plotted against ΔH_o (198), then figure 5.2.3 shows that a pattern similar to that obtained by Morooka for propylene oxidation is obtained. Thus, it can be seen that activity can be related to metal-oxygen bond strength, the exceptions being nickel and manganese.

Fig 5.2.2

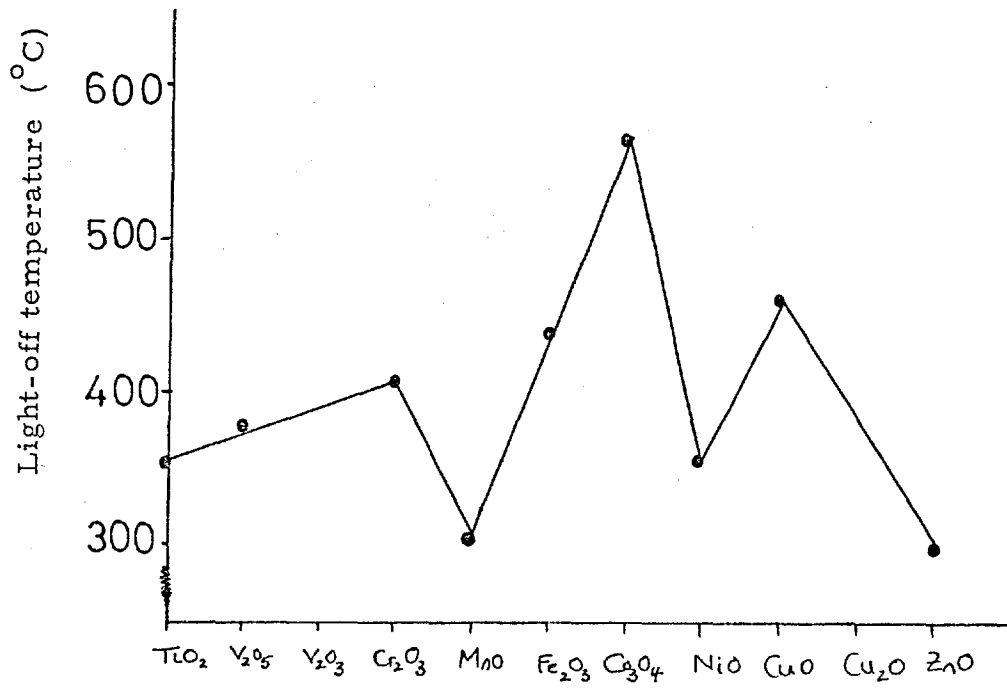
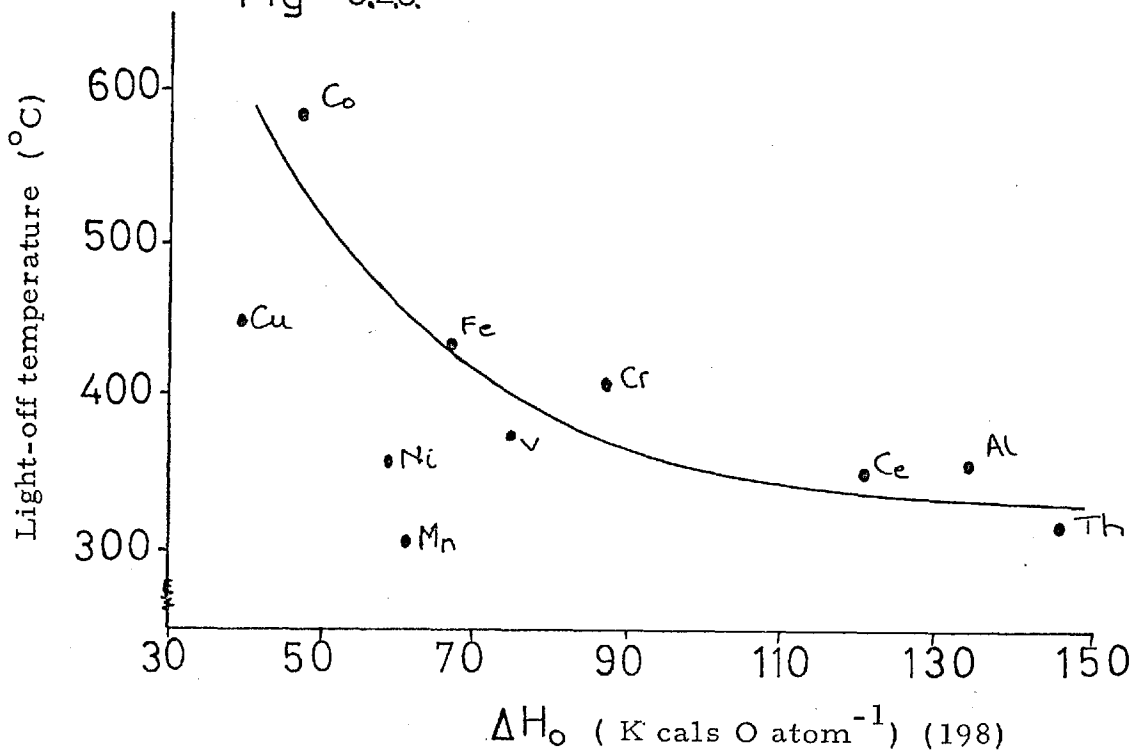


Fig 5.2.3



It would seem that to successfully explain the variation in light-off temperature with dopant species, the theories of Morooka (198) and Dowden (137) should be combined. Their respective experimental parameters are shown in figure 5.2.4. The results from Morooka (198) have been superimposed on the twin-peak pattern of Dowden (137). The similarity is striking, and a plot of the data from Morooka (198) with that of the work carried out section 3.5 (Fig. 5.2.5) shows good agreement.

That a correlation exists is fairly obvious, but the explanation of this correlation is much less obvious. Several postulates can be advanced.

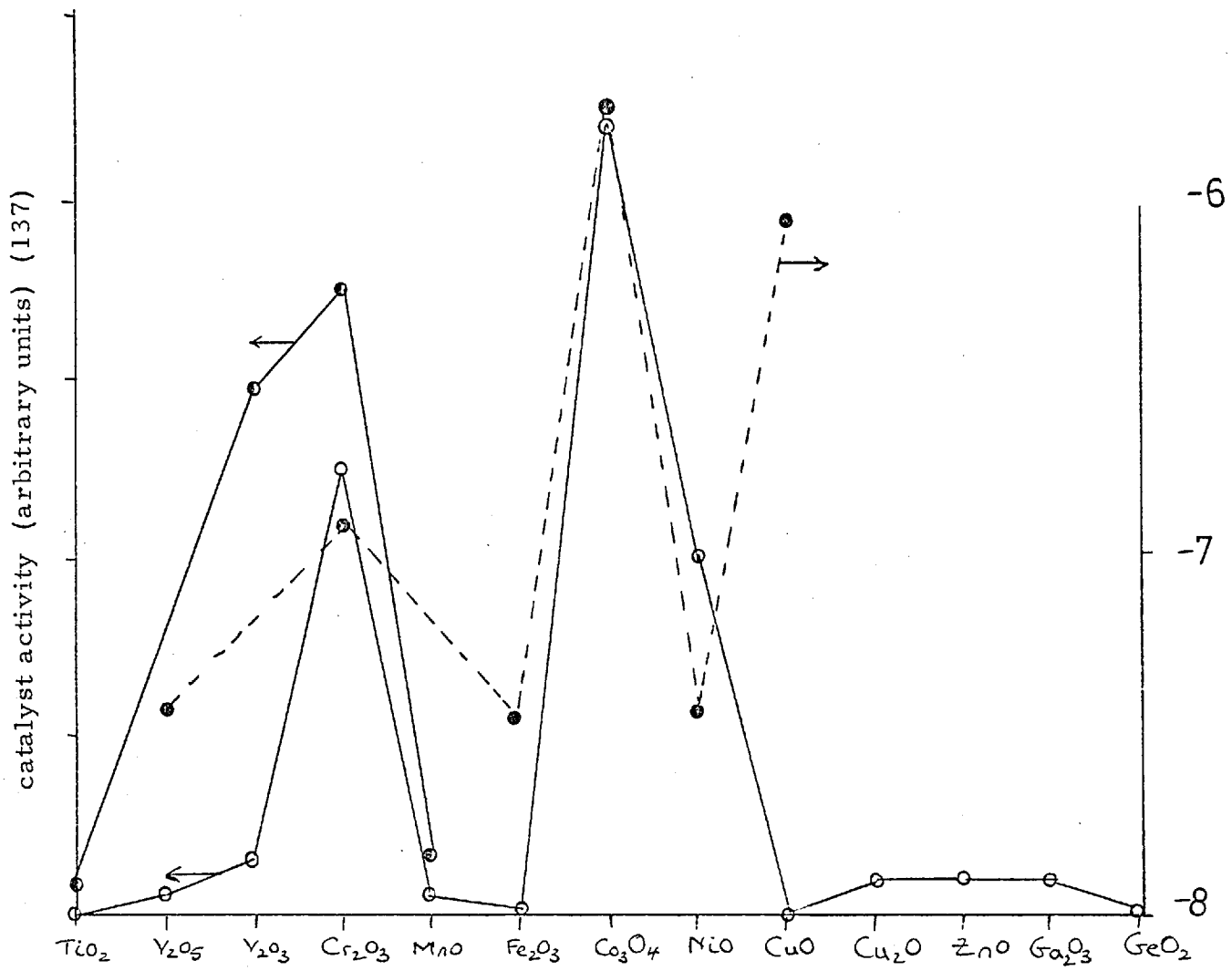
One such postulate rests on the temperature of light-off. Since the dopants are oxides, it could be suggested that they liberate heat by reacting with ammonia, this heat being given to the gauze and hence decreasing the heat needed to be supplied to the gauze, thus lowering the light-off temperature. As predicted from this, figure 5.2.3 shows that the greater the metal-oxygen bond strength the lower the light-off temperature.

This does assume that a chemical reaction is occurring on the dopant which may not give light-off. This in fact has been observed, the most notable example being V_2O_5 (Table 3.5.2).

It has been shown previously (Table 3.5.2) that some dopants give low running temperatures and low activity. This may be due to alloy formation during reaction. It can be assumed that alloy formation does not occur prior to catalyst light-off, but it is possible that, after light-off, the catalyst running temperatures ($800 - 1,000^\circ\text{C}$) will be sufficient for alloy formation to take place. Hence dopant species with d^5 or d^{10} electrons e.g. Mn and Zn oxides will not give linkage with platinum in alloy formation, and will not effect the activity of the platinum/rhodium catalyst. Alloy formation is possible with Zirconia and the mechanism of alloy formation is discussed later (Section 5.2.3).

Finally, reference must be made to the possibility of the influence of semiconductors on the reaction.

Fig 5.2.4.



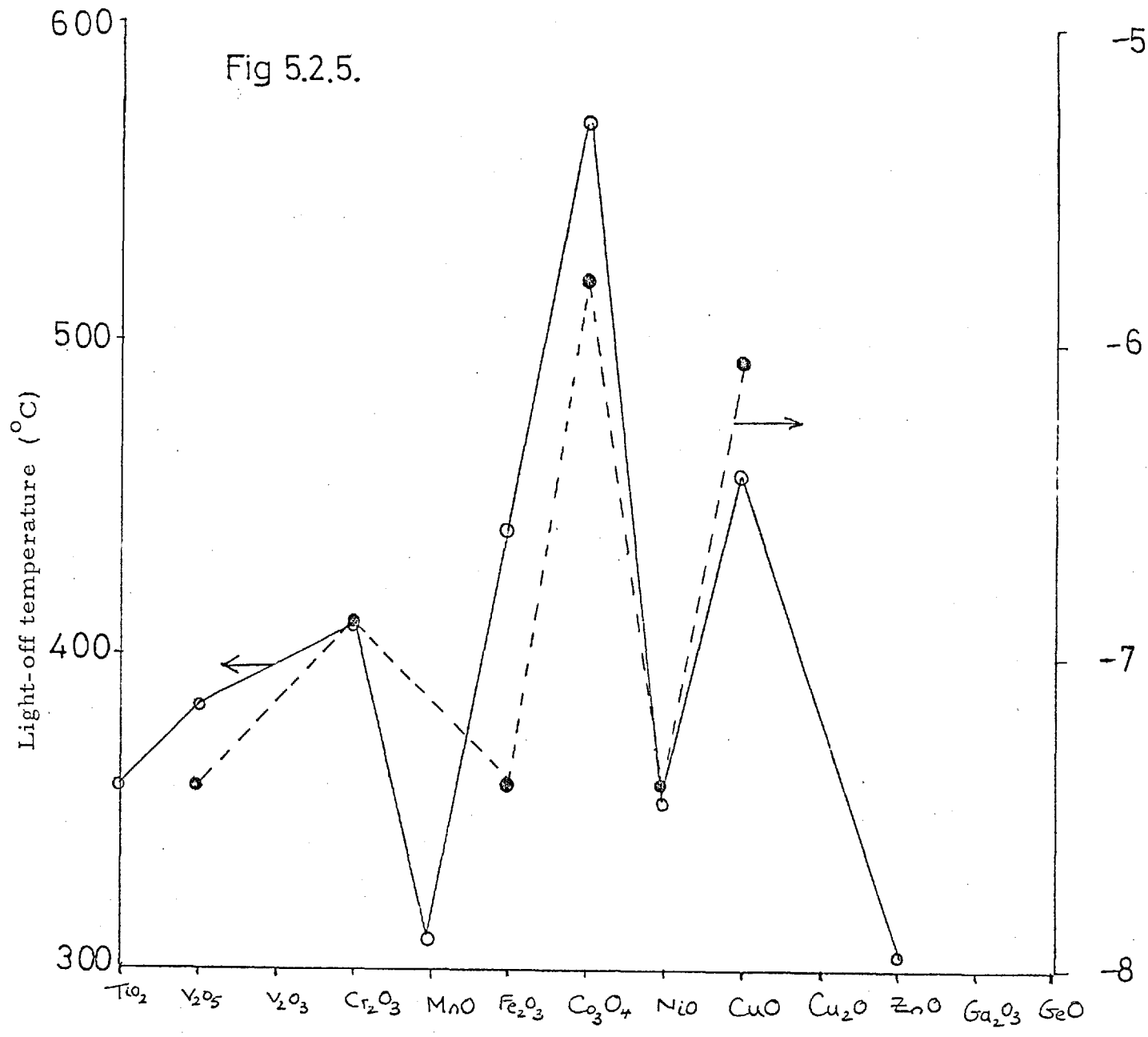
- H₂/D₂ Exchange
- Propylene oxidation
- Propane dehydrogenation

log V 300 (198)

-6

-7

-8



log V 300 (198)

Dixon and Longfield (110) have reviewed ammonia oxidation over metallic oxide catalysts and conclude that p-type oxides, which contain an excess of oxygen can act as initiators for the ammonia oxidation reaction, possibly via an oxygen atom. Giordano (199) has studied the catalytic behaviour of doped nickel oxides and concluded that increased lattice oxygen content favours the catalytic formation of nitrous oxide.

Krylov (200) has also studied the activity of metal oxides for ammonia oxidation to nitric oxide. He states that generally, high catalytic activity is obtained with p-type oxides, though this is with a proviso that the differences between p- and n-type conductivity is small. Experimentally it has been found that metal oxides which give high light-off temperatures (CuO , Co_3O_4 , Cr_2O_3) can be n-type or p-type. Metal oxides which give rise to low light-off temperatures are MnO (p-type) and ZnO which can be n - or p-type. Thus no clear correlation can be obtained for n - or p-type conductivity with light-off temperature. Whilst it has been shown that p-type oxides have the greatest activity (200), the exact nature of the conductivity of dopants used in these studies has not been determined. Heating the dopants in oxygen may result in changes in conductivity, and hence semiconductivity does not provide an exact explanation as to the effect of metal oxide dopants on light-off temperatures.

5.2.3 Dopant loss during reaction

Work undertaken in section 3.5.d has shown that, under industrial ammonia oxidation conditions all dopants shown in table 3.5.3 lower the activity of the catalyst. Both cobalt and chromium oxides substantially lower the activity and increase the light-off temperature. Vanadium pentoxide completely deactivates the gauze, giving no light-off at temperatures up to 500°C . Zirconium dioxide lowers the light-off temperature by 60°C and does not produce a catalyst of significantly lower activity than an undoped gauze.

However, a study of the gauze weight during reaction shows that a weight loss of 0.42 mg has occurred despite the fact that only 0.28 mg of dopant was deposited. Optical microscopy showed zirconia remaining on the gauze. This particular experiment was duplicated, giving a similar result.

It therefore must be concluded that the addition of zirconia causes increased weight loss, perhaps due to a chemical reaction between the platinum/rhodium catalyst and the zirconia dopant.

It has been noticed previously by Darling, Selman and Rushforth (201) that reactions can occur between platinum and refractory materials resulting in thermocouple failure. Further work by Darling, Selman and Rushforth (202) (203)(204) has shown that platinum has a very high affinity for zirconia. Whilst their work was carried out in argon arc furnaces and in vacuo, they have shown that when platinum thermocouples were heated in contact with zirconia powder, severe reactions occurred at temperatures as low as $1,100^{\circ}\text{C}$. The reaction occurred away from the wire surface and could be ascribed to platinum vapour moving away from the thermocouple to react with zirconia particles. Thick layers of Pt_3Zr have been identified on the surface of the zirconia particles and, where zirconia was in direct contact with the thermocouple, severe local reactions occurred with an intensity similar to that of the Thermit reaction. The reaction appears to have occurred by solid state diffusion processes. However these processes have been studied in the absence of oxygen in the surrounding atmosphere.

Darling, Selman and Rushforth further suggest (203) that geometry can influence the reaction system. They conclude that the reactions are controlled not only by the affinity of platinum for the metal evolved, (in this case zirconium) but also by the surface area of the reacting substances, and the rate at which oxygen can be removed from the reaction zone. Because the reactions proceed most rapidly in fine beds of powders with high surface areas, they conclude that vapour phase transfer accounts for most of the metal transfer observed.

Thus we can now draw parallels between this work and the effects observed when a Pt/10% Rh gauze doped with zirconia is used to oxidise ammonia.

Two effects may have led to the high weight loss with zirconia. Using zirconia in the ultra-fine powder form, only a small amount of the zirconia would have been in direct contact with the gauze. Thus it is possible that the PtO_2 formed in the reaction was condensing on the zirconia particles instead of being carried away in the gas stream or recondensing on the gauze. This would result in a reduced yield of nitric oxide which in fact is observed (graph 3.5.6) and give rise to a lower gauze running temperature (table 3.5.2). Finally, removal of the surface dopant by the flowing gas will also remove the platinum, giving a high weight loss. However this mechanism should theoretically apply to any dopant, because no chemical reaction is involved, and the platinum is being removed by physical transport of dopant particles away from the gauze.

Thus, the second process is more probable. In this process a chemical reaction is postulated to occur between the platinum and the zirconia, possibly similar to that outlined earlier (202). After chemical reaction, the dopant particles are removed by the gas stream, giving a high weight loss.

This second process relies on chemical reaction between the dopant and the gauze. However, according to work carried out earlier (202) these reactions can only occur in the absence of oxygen.

Earlier work with V_2O_5 in a 14% NH_3 / air stream has shown that there may be an oxygen deficiency at the surface. In a 10% NH_3 / air stream, this will not be the case unless mass transfer limitations are occurring to prevent oxygen reaching the catalyst surface. With a surface layer of dopant, it is possible that the reaction is mass transfer limited and a deficiency of oxygen is occurring. Under these circumstances a similar reaction between zirconia and platinum proposed earlier (202) is possible. Whilst oxygen must be evolved from the zirconia during the chemical reaction the rapid removal of this is essential (203). Hence either there is no excess oxygen at the

gauze surface and platinum dioxide is not the catalyst, which contradicts earlier work, or reaction can occur between zirconia and platinum under ammonia oxidation conditions, possibly leading to alloy formation (Pt_3Zr). This is then lost by physical transport of dopant particles away from the gauze. The high temperatures resulting from chemical reaction would not be observed because the majority of the zirconia would not be in contact with the Pt/10% Rh gauze.

Thus, to summarise, the doping studies have shown that oxygen must be adsorbed on the catalyst surface before reaction can occur. Also, all dopants lower the activity of the Pt/10% Rh catalyst, whilst zirconia may undergo a chemical reaction with the platinum/rhodium giving an increased weight loss.

It can be proposed that generally metal oxides with configurations d^0 , d^5 and d^{10} give rise to the lowest light-off temperatures. Light-off temperature is dependent on the dopant and not apparently on surface coverage.

Alloy formation and mass transfer limitations have combined to lower the catalyst efficiency.

5.3. The heterogeneous - homogeneous mechanism

It has been noted previously (section 1.2. a) that mass transfer processes may effect the mechanism of a catalytic reaction. Besides this, the volatilization of platinum as platinum dioxide into the vapour phase may in fact be the catalyst. It was to study this latter effect that work described in section 3.6 was undertaken.

Oxygen was passed through a conventional Pt/10% Rh catalyst which had previously been activated by solvent cleaning and heating in oxygen. The temperatures used varied from 950°C to $1,050^\circ\text{C}$. In an oxygen atmosphere, these temperatures should be sufficient to cause volatilization of platinum from the catalyst surface as platinum dioxide. This platinum dioxide enriched oxygen gas stream should then have reacted with ammonia which was added to the gas stream after the

catalyst gauze. Reference to graph 3.6.1 shows that no reaction occurred between oxygen and ammonia, which would have resulted in an exothermic reaction giving a rise in the temperature of the gas stream.

It therefore appears that the heterogeneous - homogeneous mechanism is not due to vapour phase platinum dioxide, and neither is platinum dioxide a catalyst in the vapour phase. Whilst this does not entirely rule out a heterogeneous - homogeneous reaction, it does show that any such reaction must involve species other than those formed from platinum and oxygen.

CONCLUSIONS

- (1) Solvent treatment lowers catalyst light-off temperature, due to the removal of specks of dirt which contain calcium compounds.
- (2) The activity of a solvent washed gauze is higher than an unwashed catalyst.
- (3) Boiling concentrated hydrochloric acid gives a clean gauze with a low carbon content due to the removal of oil deposits from the catalyst surface.
- (4) Activation in flowing oxygen at $1,000^{\circ}\text{C}$ produces a gauze with an activity comparable to that obtained from the hydrogen flame activation. Oxygen activation proved to be reproducible, unlike the hydrogen flame treatment.
- (5) Exposing the catalyst to air results in deposition of carbon on the surface. Moisture present in air causes an increase in light-off temperature.
- (6) The carbon content of the catalyst is reduced during activation and reaction, by movement to the surface where oxidising and reducing gases remove it. Carbon is also removed during the reaction.
- (7) Carbon does not penetrate the bulk platinum/rhodium alloy, and neither does oxygen. The oxide species present are only a few atomic layers thick.
- (8) Immersion in water removes surface platinum, possibly as the oxide, by dissolution.
- (9) During activation, rhodium moves to the surface, and moves back into the metal matrix during the reaction. Rhodium enrichment arises below 800°C due to the volatilization rate of Pt O_2 exceeding that of rhodium oxides. Above $1,000^{\circ}\text{C}$ no rhodium oxide is formed, and no rhodium enrichment occurs.

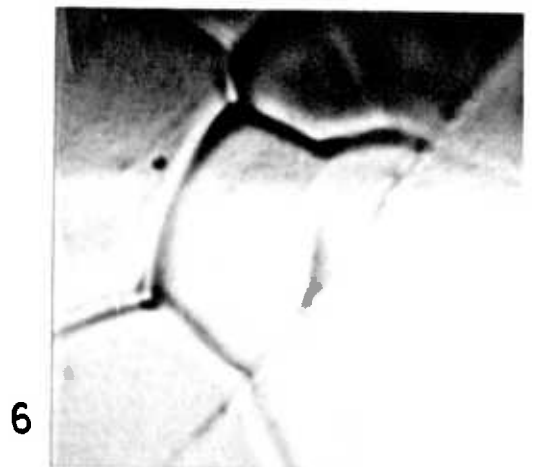
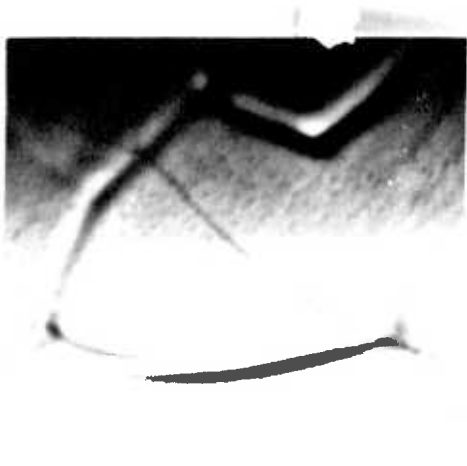
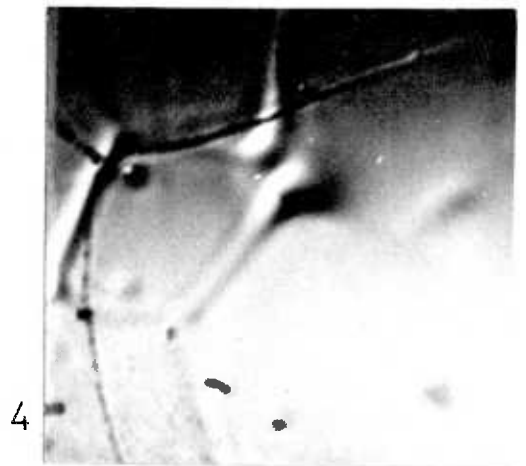
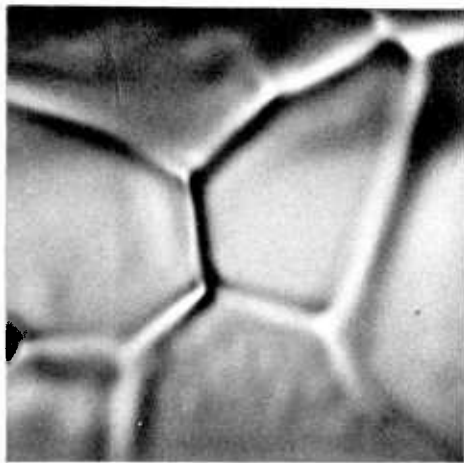
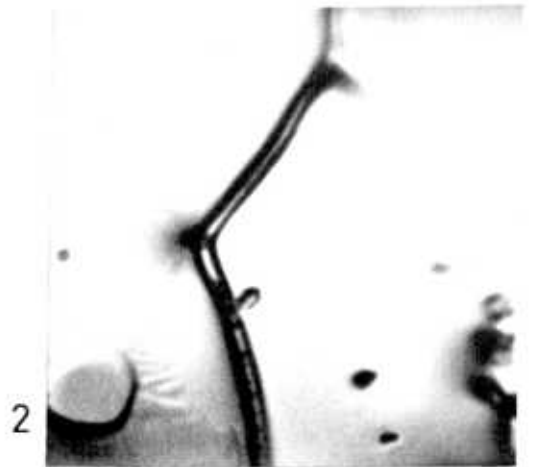
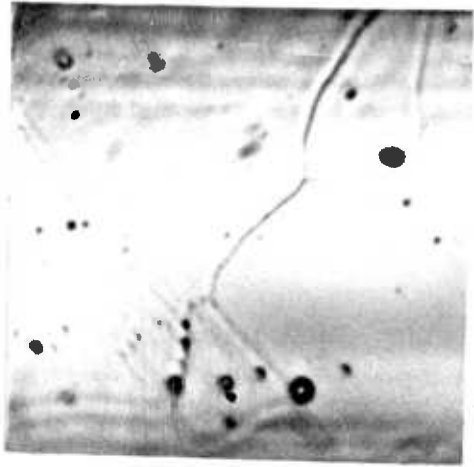
- (10) Increased rhodium enrichment occurs in the oxygen treatment compared with the hydrogen flame treatment, in which oxide formation and enrichment occur during cooling in air from the white heat temperatures of the hydrogen flame.
- (11) Activation produces a change in the oxidation state of the rhodium, but this oxide is not important in terms of the electronic state of the catalyst, and rhodium oxide does not take part in the reaction.
- (12) Hydrogen flame activation produces a molten metal surface, giving rise to extensive grain boundary grooving formation. Oxygen on the other hand produces extensive pitting. Reducing gases produce smoother metal surfaces and larger grain size.
- (13) The reorganisation is dependent on particular grains in the wire, on which rearrangement begins immediately the reaction commences.
- (14) Surface pitting definitely lowers light-off temperature and produces greater activity. Activation is not primarily connected with macro-geometric rearrangements on the surface, though for activation to occur, some surface rearrangement is necessary; this need not be as extensive as that associated with the hydrogen flame and oxygen treatments.
- (15) The pits induced by activation can be blocked with iron oxide which results in a lowering of the activity of the catalyst. The pits present on inactive gauzes have been shown not to contain any contaminant elements (e. g. Ca).
- (16) Grain boundary groove formation occurs by an evaporation - condensation process, and no preferential rhodium concentration arises at the grain boundaries.
- (17) Adsorption of oxygen is a precondition for ammonia oxidation and oxygen is the only gas adsorbed on the surface of the platinum/rhodium catalyst.

- (18) The activity of the catalyst is reduced by the presence of metal oxides on the surface. Minimum activity is obtained with Cr_2O_3 , Co_3O_4 and CuO dopants. Vanadium oxides poison the catalyst towards ammonia oxidation.
- (19) Metal oxides with configurations d^0 , d^5 , d^{10} give rise to the lowest light-off temperatures, and the greater the dopant metal-oxygen bond strength, the lower the light-off temperature.
- (20) No clear correlation has been established between semi-conductivity and dopant activity.
- (21) Light-off temperature is dependent on the dopant and not on the surface coverage.
- (22) The addition of zirconia causes an increased weight loss rate, which may be due to alloy formation.
- (23) Alloy formation and mass transfer limitations can combine to lower catalyst efficiency.
- (24) The heterogeneous - homogeneous mechanism is not due to vapour-phase platinum dioxide and neither is platinum dioxide a catalyst in the gas phase. Any heterogeneous - homogeneous mechanism must involve species other than those formed from platinum and oxygen.
- (25) Numerical calculations indicate that catalyst weight loss arises from the loss of platinum as platinum dioxide in the vapour phase in low and high pressure oxidation plants.

APPENDIX 1.

PHOTOGRAPHS

- (1) Activation for 20 seconds in a hydrogen flame. (held horizontal) (X 2,000)
 - (2) Activation for 1 second in a hydrogen flame. (held vertical) (X 2,000)
 - (3) Activation for 10 seconds in a hydrogen flame. No heating in oxygen. (X 2,000)
 - (4) As (3) + heating in oxygen.
Temperature 800^oC. Time 10 minutes.
Flow rate 900 cm³ min⁻¹ (X 2,000)
 - (5) As (3) + heating in oxygen.
Temperature 800^oC. Time 20 minutes
Flow rate 900 cm³ min⁻¹ (X 2,000)
 - (6) As (3) + heating in oxygen.
Temperature 800^oC. Time 30 minutes
Flow rate 900 cm³ min⁻¹ (X 2,000)
-



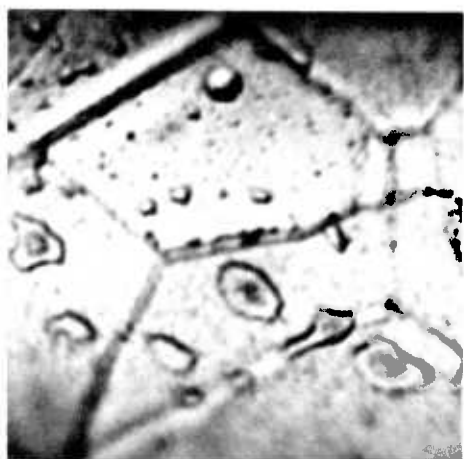
- (7) As (3) + heating in oxygen
Temperature 800°C. Time 45 minutes
Flow rate 900 cm³ min⁻¹ (X 2,000)
- (8) As (3) + heating in oxygen.
Temperature 800°C. Time 60 minutes
Flow rate 900 cm³ min⁻¹ (X 2,000)
- (9) As (3) + heating in oxygen
Temperature 800°C. Time 100 minutes
Flow rate 900 cm³ min⁻¹ (X 2,000)
- (10) As (3) + heating in oxygen
Temperature 800°C. Time 120 minutes
Flow rate 900 cm³ min⁻¹ (X 2,000)
- (11) Pt/10% Rh gauze wire before heating.
(X 2,000)
- (12) Activation Static H₂, 1000°C,
2 hours (X 2,000)



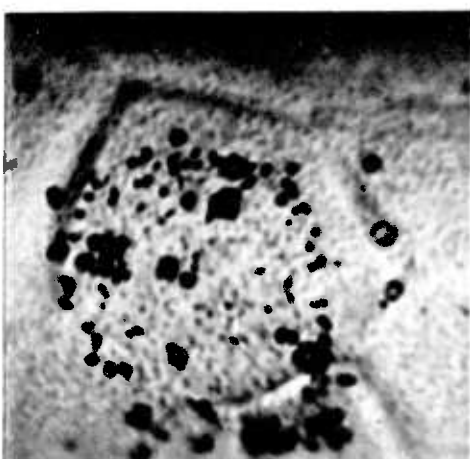
7



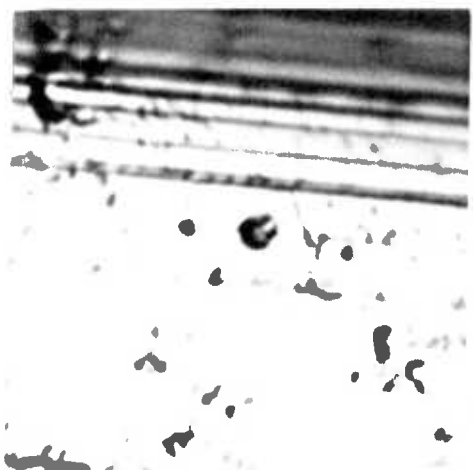
8



9



10



11



12

(13) Activation Static O₂, 1,000°C,
2 hours (X 2,000)

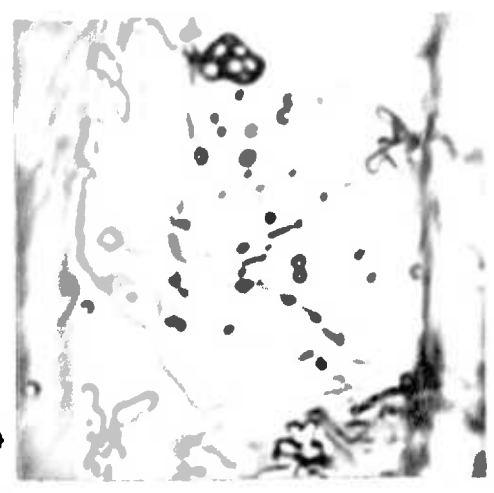
(14) Activation Static N₂, 1,000°C,
2 hours (X 2,000)

(15) Activation Static He, 1,000°C,
2 hours (X 2,000)

(16) Activation Static NH₃, 1,000°C,
2 hours (X 2,000)



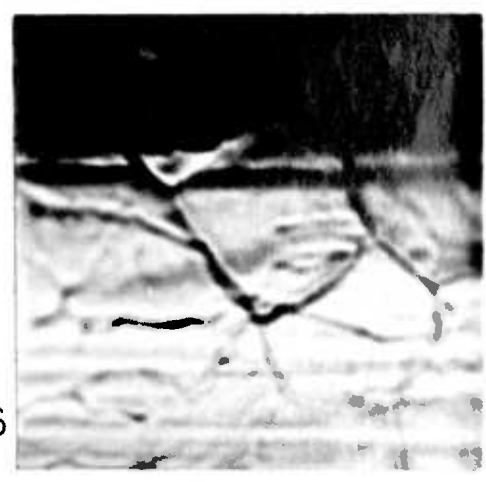
13



14



15



16

- (17) Activation O₂, 350°C, 2 hours
BEFORE REACTION
- (18) Activation as (17). After reaction in
10% NH₃ / air, 1,000 cm³ min⁻¹
TOP SURFACE
- (19) Activation as (17). After reaction in
10% NH₃ / air, 1,000 cm³ min⁻¹
BOTTOM SURFACE
- (20) Activation N₂, 800°C, 2 hours
BEFORE REACTION
- (21) Activation as (20). After reaction in
10% NH₃ / air, 1,000 cm³ min⁻¹.
TOP SURFACE
- (22) Activation as (20). After reaction in
10% NH₃ / air, 1,000 cm³ min⁻¹
BOTTOM SURFACE



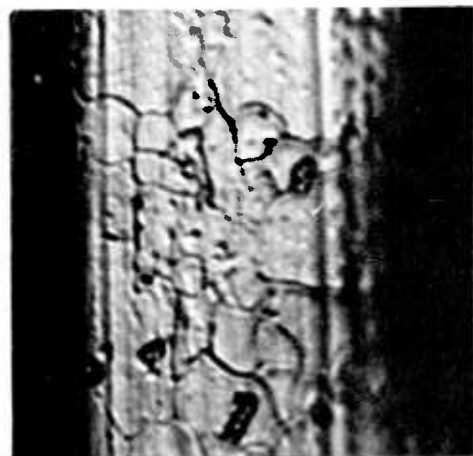
17



20



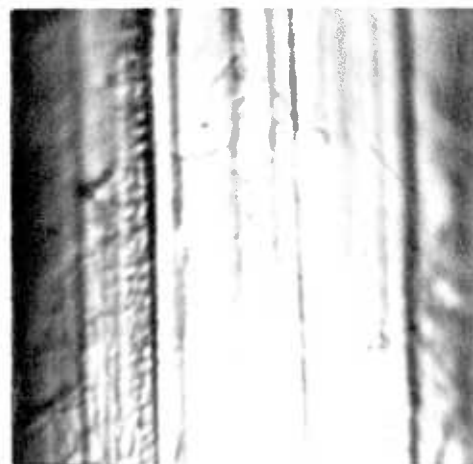
18



21



19

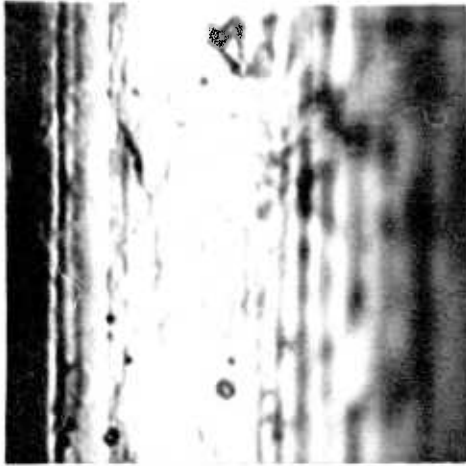


22

(23) Activation N_2 , 800°C , 2 hours
+
 O_2 , 350°C , 2 hours
BEFORE REACTION

(24) Activation as (23) After reaction in
 $10\% \text{NH}_3 / \text{air}$, $1,000 \text{ cm}^3 \text{ min}^{-1}$.
TOP SURFACE

(25) Activation as (23) After reaction in
 $10\% \text{NH}_3 / \text{air}$, $1,000 \text{ cm}^3 \text{ min}^{-1}$.
BOTTOM SURFACE



23



24

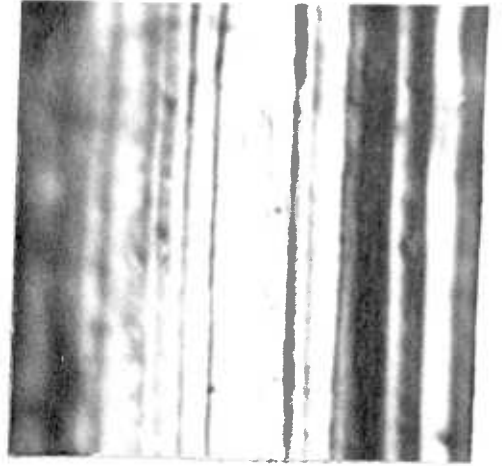


25

- (26) Activation Static O₂, 100°C, 2 hours
- (27) Activation Static O₂, 350°C, 2 hours
- (28) Activation Static O₂, 500°C, 2 hours
- (29) Activation Static O₂, 650°C, 2 hours
- (30) Activation Static O₂, 800°C, 2 hours
- (31) Activation Static O₂, 1,000°C, 2 hours



26



27



28



29



30



31

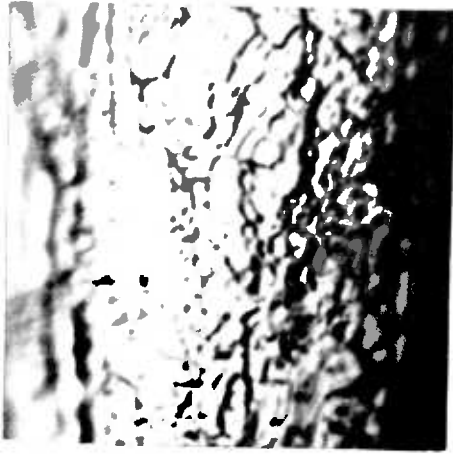
(32) Activation O₂, 1,000°C, 2 hours, 200 cm³ min⁻¹

(33) Activation N₂, 1,000°C, 2 hours, 200 cm³ min⁻¹

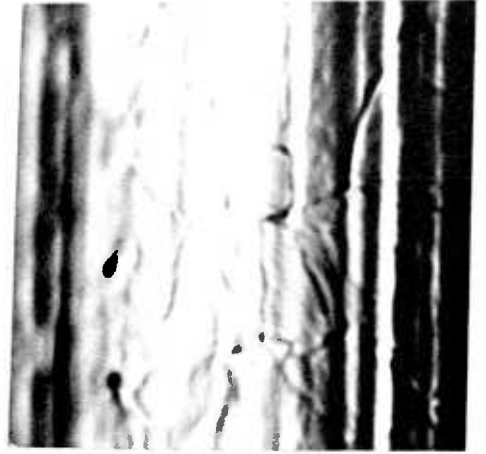
(34) Activation He, 1,000°C, 2 hours, 200 cm³ min⁻¹

(35) Activation H₂, 1,000°C, 2 hours, 200 cm³ min⁻¹

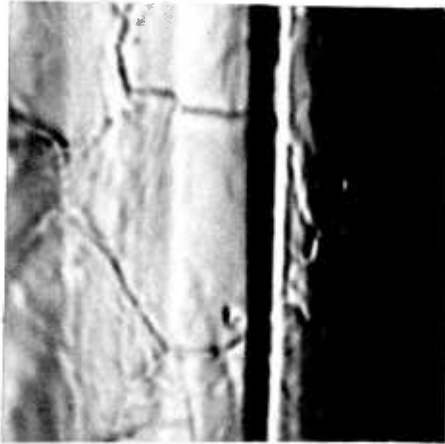
(36) Activation NH₃, 1,000°C, 2 hours, 200 cm³ min⁻¹



32



33



34



35



36

(37) Activation as (32). Reaction time 23 seconds
6 tons NH_3 m^{-2} catalyst day $^{-1}$

(38) Activation as (32). Reaction time 50 seconds
6 tons NH_3 m^{-2} catalyst day $^{-1}$

(39) Activation as (32). Reaction time 2 minutes
54 seconds
6 tons NH_3 m^{-2} catalyst day $^{-1}$

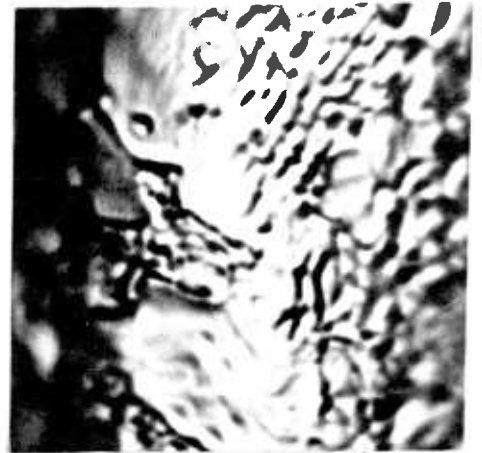
(40) Activation as (32). Reaction time 9 minutes
6 tons NH_3 m^{-2} catalyst day $^{-1}$

(41) Activation as (32). Reaction time 22 minutes
6 tons NH_3 m^{-2} catalyst day $^{-1}$

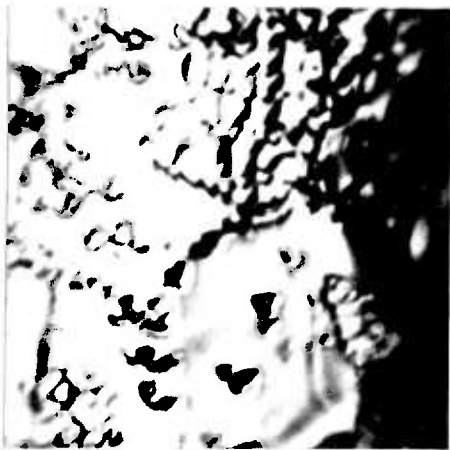
(42) Activation as (32). Reaction time 41 minutes
6 tons NH_3 m^{-2} catalyst day $^{-1}$



37



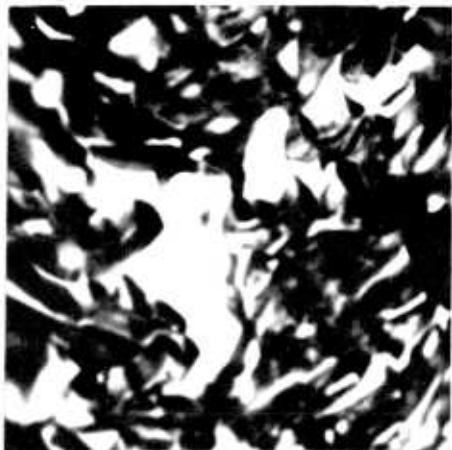
38



39



40

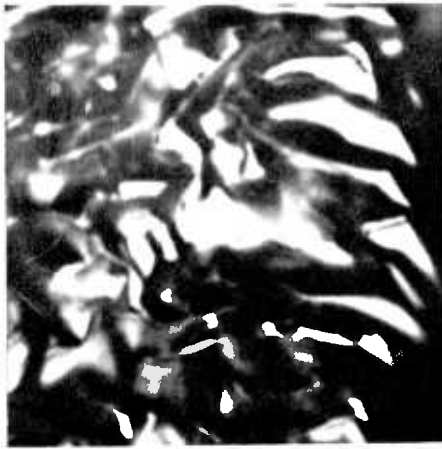


41



42

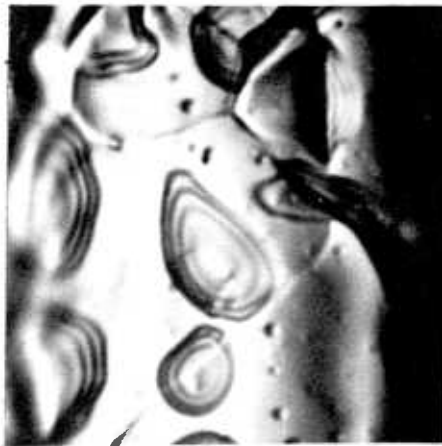
- (43) Activation as (32). Reaction time 60 minutes
6 tons NH_3 m^{-2} catalyst day⁻¹
- (44) Activation as (32). Reaction time 120 minutes
6 tons NH_3 m^{-2} catalyst day⁻¹
- (45) No Activation. Reaction time 120 minutes
6 tons NH_3 m^{-2} catalyst day⁻¹
- (46) Activation as (32). Reaction time 120 minutes
6 tons NH_3 m^{-2} catalyst day⁻¹
- (47) Untreated gauze.



43



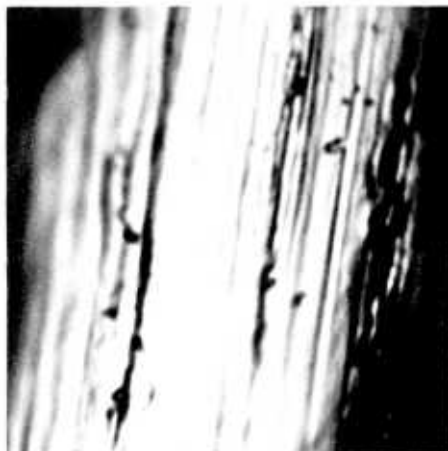
44



45



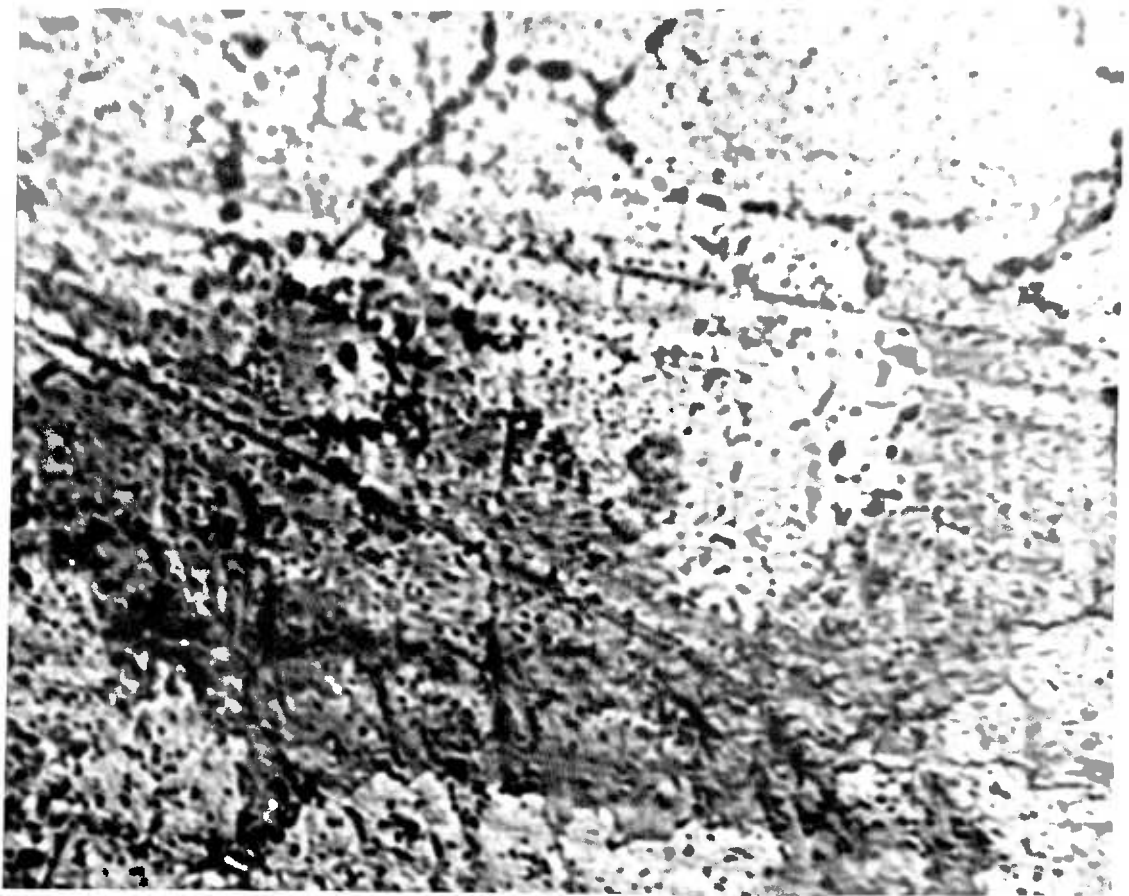
46



47

(48) Pt/10% Rh foil Activation Air, 72 hours,
800°C. (X2,000)

(49) Activation as (48) + reaction 2 hours in
10% NH₃ / air, 1,000 cm³ min⁻¹
(X 2,000)



48

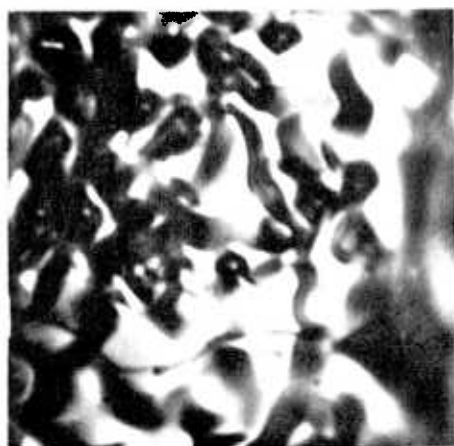


49

(50) Activation Air, 800°C, 2 hours.
Reaction time 2 hours in 10% NH₃ / air,
1,000 cm³ min⁻¹
TOP SURFACE (X 2,000)

(51) As (50)
BOTTOM SURFACE (X 2,000)

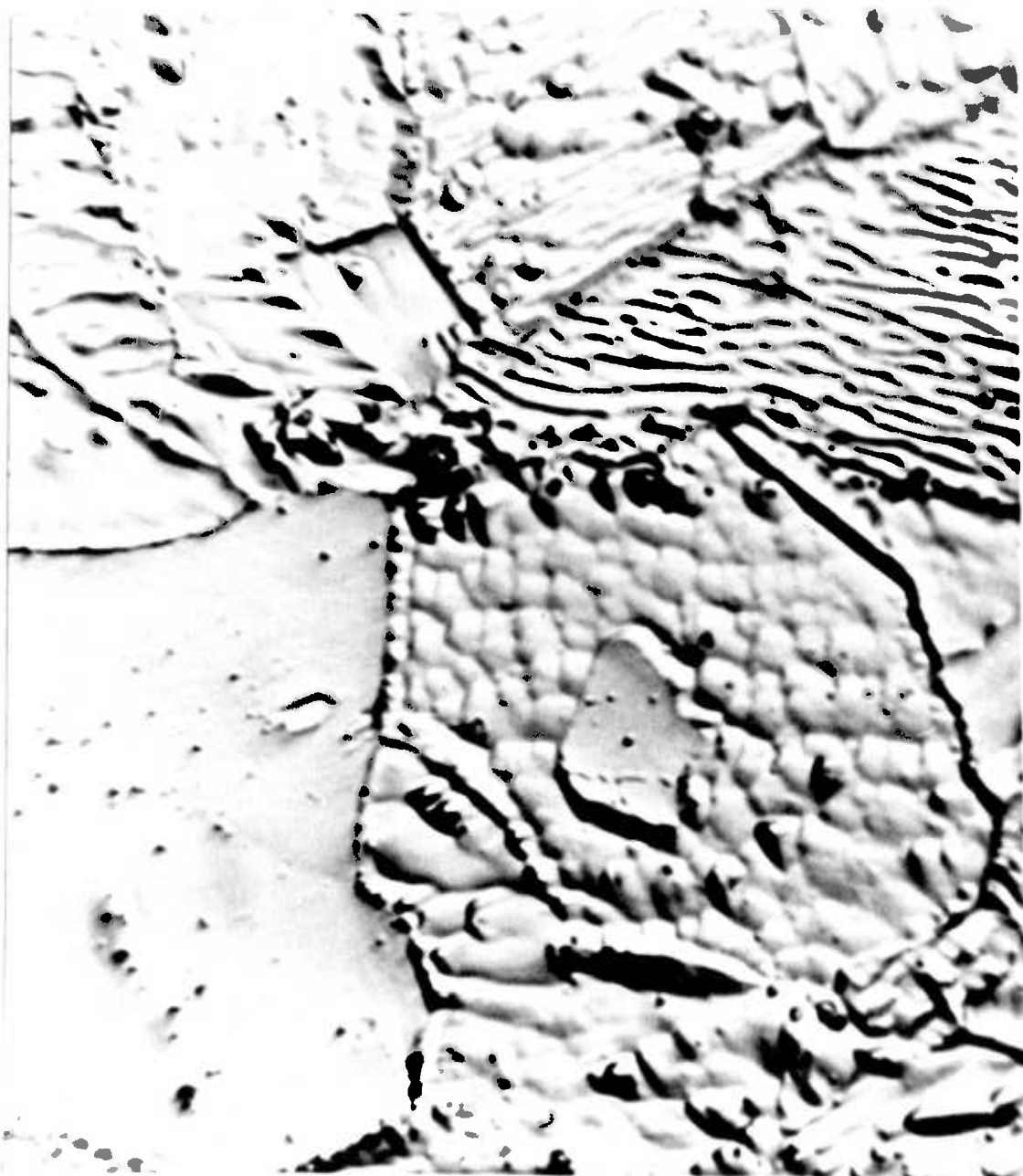
(52) Activation Hydrogen flame
Reaction time 2 hours in 10% NH₃ air,
1,000 cm³ min⁻¹ (X 2,000)



50



51



52

(53) Activation O_2 , $1,000^\circ C$, 2 hours
Dopant $Fe_2 O_3$
Reaction time 60 minutes
14% NH_3 / air, $4,300\text{ cm}^3\text{ min}^{-1}$ (X 2,000)
TOP SURFACE, TOP GAUZE

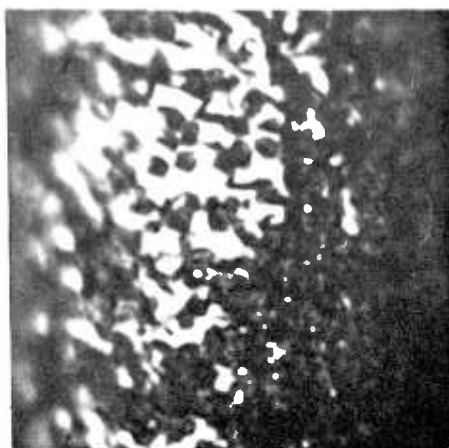
(54) As (53)
BOTTOM SURFACE, BOTTOM GAUZE

(55) Activation Solvent wash only
Dopant $Fe_2 O_3$
Reaction time 60 minutes
14% NH_3 / air, $4,300\text{ cm}^3\text{ min}^{-1}$ (X 2,000)

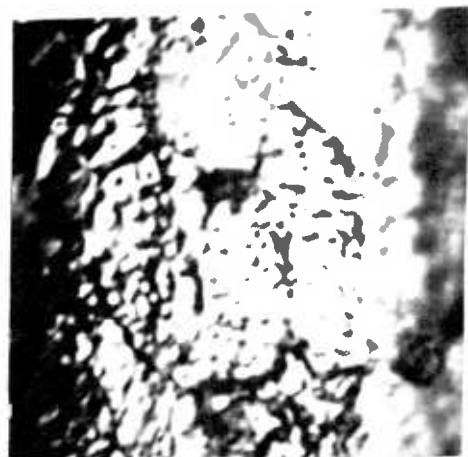
(56) As (55)
BOTTOM SURFACE, BOTTOM GAUZE

(57) Activation Solvent wash only
Dopant Au
Reaction time 60 minutes
14% NH_3 / air, $4,300\text{ cm}^3\text{ min}^{-1}$ (X2,000)
TOP SURFACE, TOP GAUZE

(58) As (57)
BOTTOM SURFACE, BOTTOM GAUZE



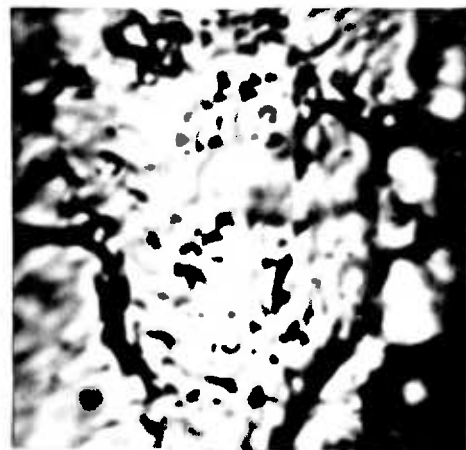
53



54



55



56

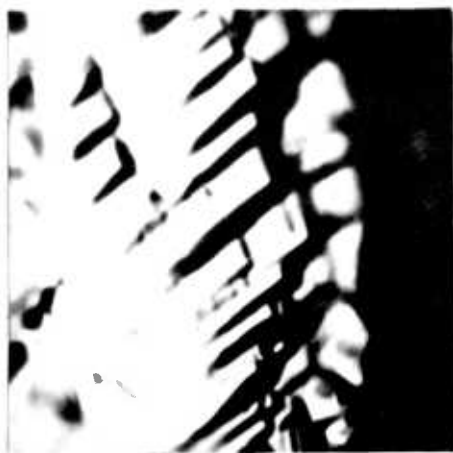


57



58

- (59) Activation Solvent wash only
Dopant Fe
Reaction time 60 minutes (X 2,000)
TOP SURFACE, TOP GAUZE
- (60) As (59)
BOTTOM SURFACE, TOP GAUZE
- (61) As (59)
BOTTOM SURFACE, BOTTOM GAUZE
- (62) Activation O₂, 1,000°C, 2 hours, 200 cm² min⁻¹
Dopant MgO
Reaction time 10 minutes (X 2,000)
- (63) Activation as (62)
Dopant CaO
Reaction time 10 minutes (X 2,000)



59



60



61



62



63

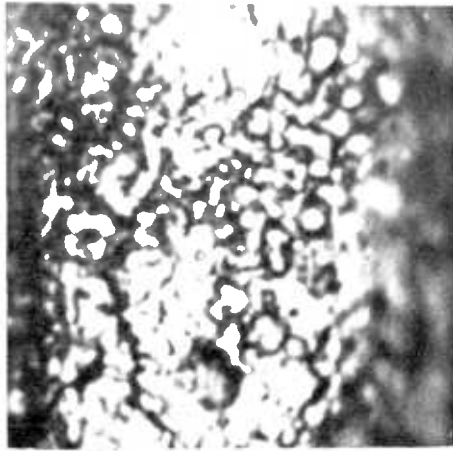
(64) Activation as (62)
Dopant BaO
Reaction time 10 minutes (X 2,000)

(65) Activation as (62)
Dopant TiO₂
Reaction time 10 minutes (X 2,000)

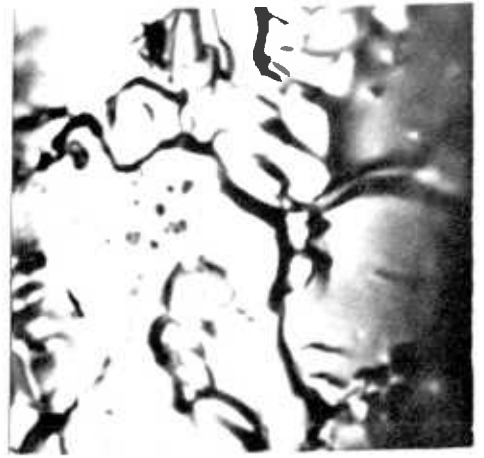
(66) Activation as (62)
Dopant ZrO₂
Reaction time 10 minutes (X 2,000)

(67) Activation as (62)
Dopant V₂O₅
Reaction time 10 minutes (X 2,000)

(68) As (67)



64



65



66



67



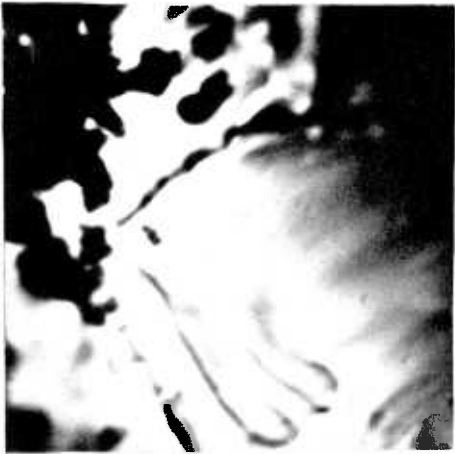
68

(69) Activation as (62)
Dopant Cr_2O_3
Reaction time 10 minutes (X 2,000)

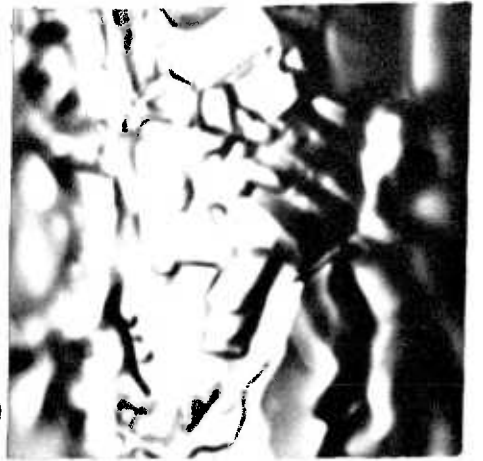
(70) Activation as (62)
Dopant MnO_2
Reaction time 10 minutes (X 2,000)

(71) Activation as (62)
Dopant Co_3O_4
Reaction time 10 minutes (X 2,000)

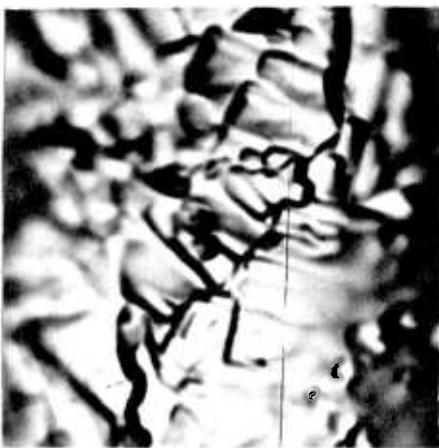
(72) Activation as (62)
Dopant NiO
Reaction time 10 minutes (X 2,000)



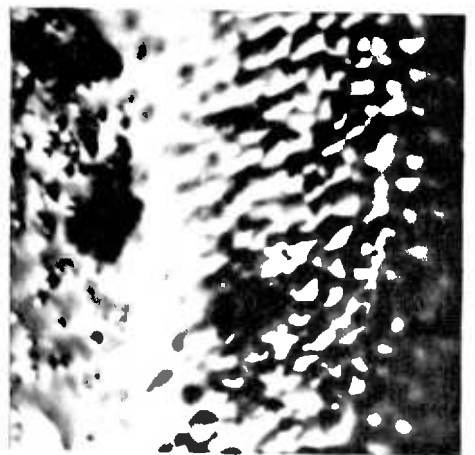
69



70



71



72

- (73) Activation as (62)
Dopant Ce O₂
Reaction time 10 minutes (X 2,000)
- (74) Activation as (62)
Dopant Th O₂
Reaction time 10 minutes (X 2,000)
- (75) Activation as (62)
Dopant La (NO₃)₃
Reaction time 10 minutes (X 2,000)
- (76) Activation As (62)
Dopant Si O₂
Reaction time 10 minutes (X 2,000)
- (77) Activation as (62)
Dopant Al₂ O₃
Reaction time 10 minutes (X 2,000)
- (78) Activation as (62)
Dopant K OH
Reaction time 10 minutes (X 2,000)



73



74



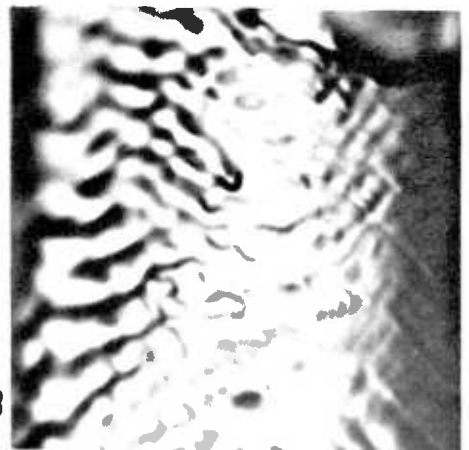
75



76



77



78

(79) Activation Hydrogen flame

No reaction

(X 500)

(80) As (79)

Reaction time 1 minute

(X 500)

(81) As (79)

Reaction time 10 minutes

(X 500)

(82) As (79)

Reaction time 30 minutes

(X 500)



79



80



81



82

(83) Activation Hydrogen flame

Reaction time 1 minute

(X 300)

(84) As (83)

Reaction time 11 minutes

(85) As (83)

Reaction time 31 minutes

(86) As (83)

Reaction time 91 minutes



85



83



86



84

REFERENCES

- (1) Parsons, C.L., Ind. Eng. Chem. II 541 (1919).
- (2) Hunt, L.B., Platinum Metals. Rev. 2, 129 (1958).
- (3) Handforth, S.L. and Tilley, J.N. Ind. Eng. Chem. 26, 1288 (1934).
- (4) Sikora, H., C.A. 73: 39016s.
- (5) Dobrovol'skaya, N.V., Miniovich, M.A., Epstein, D.A., Ovcharenko, B.G., Sverdlova, K.I., Yastrebov, Y.V., Molchanov, V.A., Botsman, G.A. and Avilova, M.K. C.A. 79: 68277g.
- (6) Epshtein, D.A., Tkachenko N.M., Miniovich, M.A., and Dobrovol'skaya, N.V., C.A. 54: 25617a.
- (7) Alkhozov, T.G., Adzhamov, K.Y., Lisovskii, A.E., Belen'kii, M.S., and Portyanskii, A.E., C.A. 72: 125424j.
- (8) Holbrook, L.L. and Wise, H. J. Catal. 27 (2). 322 (1972).
- (9) Delaney, J.E. and Manogue, W.H. Catal. Proc. Int. Congr. 5th 267, (1972).
- (10) Gillespie, G.R., and Kenson, R.E., Chemtech. 627, (1971).
- (11) Holzmann, H., Platinum Metals. Rev. 13, 2 (1969).
- (12) Holzmann, H., Chem. Ing. Tech. 40, (24), 1229 (1968).
- (13) Sorgenti, H.A., and Sachsel, G.F., Ind. Eng. Chem. 52 (2), 101, (1960).
- (14) Taylor, G.B., Ind. Eng. Chem. II, 1121 (1919).
- (15) Taylor, G.B., Chilton, T.H., and Handorth, S.L., Ind. Eng. Chem. 23, 860 (1931).
- (16) Kirk Othmer 9, 332.
- (17) Chilton, T.H., Chem. Eng. Prog. Monograph Series 3.
- (18) Miles, F.D., Nitric Acid - Manufacture and Uses O. U. P. (1961).
- (19) Bell, B.H.J., Platinum Metals Rev. 4 (4), 122 (1960).
- (20) Sloan, J.G., and Staats, H.C., Platinum Metals Rev. 5, 54, (1961).
- (21) Holmes, A.W., Platinum Metals Rev. 3 (1), 2, (1959).
- (22) Roudier, H., C.A. 74: 89168j.

- (23) Inskep, G. C., and Henry, T.H., Modern Chemical Processes. Vol. III. Reinhold (1954).
- (24) Bahari, E., Chem. + Proc. Eng. January, 16, (1965).
- (25) Platinum Metals Rev. 14 (2), 61 (1970).
- (26) Uronen, P., and Kiukanniemi, E., Brit. Chem. Eng. + Proc. Tech. 17, 323 (1972).
- (27) Oele, A.P., Chem. Reaction Eng., Meeting Europ. Federation Chem. Eng. 12th. Amsterdam 146 - 57, (1957).
- (28) Ervin., M.A., and Luss, D., Chem. Eng. Sci. 27 (2), 339 (1972).
- (29) Edwards, W.M., Worley, F.L., and Luss, D., Chem. Eng. Sci. 28, 1479 (1973).
- (30) Connor, H., Platinum Metals Rev. II (2), 60 (1967).
- (31) Connor, H., Platinum Metals Rev. II (1), 2 (1967).
- (32) Eyraud, C., Domanski, B., and Berger, C., C.A. 51: 6301d.
- (33) Nutt, C.W., and Kapur, S., Nature 220 (5168) 697 (1968).
- (34) Pignet, T.P., Schmidt, D.L., and Jarvis, N.L., J. Catal, 31, 145 (1973).
- (35) Harbord, N.N., Platinum Metals Rev. 18 (3) 97 (1974).
- (36) Arutyunyan, V.A., and Rozhkova, O.M., C.A. 81: 51710m.
- (37) Alcock, C.B., and Hooper, G.W., Proc. Roy. Soc. A. 254, 551 (1960).
- (38) Philpott, J.E., Platinum Metals Rev., 15 (2), 52 (1971).
- (39) Blair, J., and Gibb, J.G., Platinum Metals Rev., 11 (3) 100, (1967).
- (40) Sikora, H., and Kubicki, J., C.A. 67: 45638p.
- (41) Sedasheva, E.G., Atroschenko, V.I., and Zasorin, A.P., C.A. 74: 5095x.
- (42) Brack, G., and Guenzel, P., C.A. 123805w.
- (43) Nowak, E.J., Chem. Eng. Sci. 21, 19 (1966).
- (44) Nowak, E.J., Chem. Eng. Sci. 24, 421, (1969).
- (45) Bartlett, R.W., J. Electrochem. Soc. 114 (6), 547 (1967).

- (46) Raub, E., *J. Less Common Metals* 1, 3 (1959).
- (47) Lacroix, R., *Rev. Mét* 53, 809 (1956).
- (48) Krier, C.A., and Jaffe, R.I., *J. Less Common Metals* 5, 411 (1963).
- (49) Betteridge, W., and Rhys, D.W., 1st. Int. Cong. on Metallic Corrosion. London. April (1961).
- (50) Fryburg, G.C., *J. Phys. Chem.* 69 (10), 3660 (1965).
- (51) Fryburg, G.C., *J. Chem. Phys.* 42 (11), 4051 (1965).
- (52) Alcock, C.B., *Platinum Metals Rev.* 5, 134 (1961).
- (53) Schafer, H., and Tebben, A., *Z. Anorg. Alemg. Chem.* 304 (5/6), 317 (1960).
- (54) Norman, J.H., Staley, H.G., and Bell, W.E., *C.A.* 67 : 113259t.
- (55) Phillips, W.L., *C.A.* 60 : 129796b.
- (56) Chaston, J.C., *Platinum Metals Rev.* 8, 50 (1964).
- (57) Chaston, J.C., *Platinum Metals Rev.* 9, 51 (1965).
- (58) Chaston, J.C., *Platinum Metals Rev.* 9, 126 (1965).
- (59) Chaston, J.C., *Platinum Metals Rev.* 10, 91 (1966).
- (60) Chaston, J.C., *Platinum Metals Rev.* 13 (1), 28 (1969).
- (61) Fryburg, G.C., and Petrus, H.M., *J. Electrochem. Soc.* 108, 496 (1961).
- (62) Fryburg, G.C., *Trans. A.I.M.E.* 233 (11), 1986 (1973).
- (63) Heywood, A.E., *Platinum Metals Rev.* 17 (4), 118 (1973).
- (64) Akerman, K., Przemyslaw, M., Hoffmann, W.Z., Bialas, T., and Spiewak, Z., *C.A.* 61 : 10342h.
- (65) Akerman, K., *C.A.* 65 : 20609w.
- (66) Acres, G.J.K., Darling, A.S., and Selman, G.L., *Patent. Brit. Appl.* 37, 304/71 09 Aug. 1971.
- (67) Holzmann, H., *Patent. C.A.* 79 : 7509n.
- (68) Sikora, H., and Blasiak, E., *C.A.* 66 : 77796h.
- (69) Zasorin, A.P., Atroschenko, V.I., and Sedasheva, E.G., *C.A.* 74 : 14633y.
- (70) Atroschenko, V.I., Zasorin, A.P., Savenkov, A.S., Sedasheva, K.G., Kleschev, M.F., and Laboika, O.Y., *C.A.* 73 : 68087w.

- (71) Sikora, H., and Blasiak, E., C.A. 67 : 45629m.
- (72) Sikora, H., and Blasiak, E., C.A. 66 : 67389q.
- (73) Zasorin, A.P., Atroschenko, V.I., Sedasheva, E.G., and Laboiko, A.Y., C.A. 75 : 112150r.
- (74) Blasiak, E., Lugowska, M., and Swierczak, R., C.A. 75 : 131183h.
- (75) Janiczek, W., C.A. 70 : 109471a.
- (76) Janiczek, W., Krawiec, Z., Gajewski, A., and Karolewicz, S., C.A. 68 : 23198p.
- (77) Nishiyama, Y., and Wise, H., J. Catal. 32 (1), 50 (1974).
- (78) Ostermaier, J.J., Katzer, J.R., and Manogue, W.H., J. Catal. 33 (3), 457 (1974).
- (79) Darling, A.S., International Metallurgical Reviews 175 (1973).
- (80) Rand, D.A.J., and Woods, R., Proc. Symp. Electrocatal 140 (1974).
- (81) Damjanovic, A., Dey, A., and Bockric, J. O'M., J. Catal. 4 (6), 721 (1965).
- (82) Wilson, G.R., and Hall, W.K., J. Catal. 17, 190 (1970).
- (83) Somorjai, G.A., Catal. Rev. 7, 87 (1972).
- (84) Weinberg, W.H., Lambert, R.M., Comrie, C.M., and Linnett, J.W., Catal. Proc. Int. Congr. 5th 1, 513, (1972).
- (85) Baker, R.T.K., Thomas, R.B., and Notton, J.H.F., Platinum Metals Rev. 18 (4), 130 (1974).
- (86) Norris, L.F., and Parravano, G., Reactive Solids Proc. Int. Symp. 6th 149 (1968).
- (87) Blakely, J.M., Progress in Materials Science 10, 395 (1963).
- (88) Moore, A.J.W., Metal Surfaces. Am. Soc. for Metals. 155 (1963).
- (89) Mullins, W.W., J. Appl. Physics. 28 (3), 333 (1957).
- (90) Mullins, W.W., Trans. A.I.M.E. 218, 354 (1960).

- (91) Mullins, W.W., and Shewmon, P.G., *Acta. Met.* 7, 163 (1959).
- (92) Blakely, J.M., and Mykura, H., *Acta. Met.* 10, 565 (1962).
- (93) Fusy, J., Weber, B., and Cassuto, A., *C.A.* 71 : 53906x.
- (94) Andeeva, V.V., and Shishakov, N.A., *J. Appl. Chem.* 11, (10) 388, (1961).
- (95) Asanov, U.A., and Sakavov, I.E., *C.A.* 75 : 113489h.
- (96) Vaneslow, R., and Schmidt, W.A., *C.A.* 66 : 60008f.
- (97) Sandler, Y.L., and Durigan, D.D., *J. Phys. Chem.* 72 (3), 1051 (1968).
- (98) Dickens, P.G., Heckingbottom, R., Linnett, J.W., *Trans. Faraday Soc.* 65 (8), 2235, (1969).
- (99) Asanov, U.A., and Shishakov, N.A., *C.A.* 58 : 1118f.
- (100) Norton, F.J., *J. Appl. Phys.* 29, 1122 (1958).
- (101) Nutt, C.W., and Kapur, S., *Nature* 224 (5215), 169 (1969).
- (102) Fogel, Y.M., Nadykto, B.T., Rybalko, V.F., Svachko, V.I., Korobchanskaya, I.E., *Kinetics and Catalysis* 5, 431 (1964).
- (103) Fogel, Y.M., Nadykto, B.T., Rybalko, V.F., Shvachko, V.I., and Korobchaskaya, I.E., *C.A.* 61 : 7749e.
- (104) Molinari, E., *J. Catal.* 4, 341 (1965).
- (105) Norton, P.R., *Surf. Sci.* 47 (1), 98 (1975).
- (106) Gaillard, D.P., *Ind. Eng. Chem.* 11, 745 (1919).
- (107) Thomas, J.M., and Thomas, W.J., *Introduction to the Principles of Heterogeneous Catalysis*. A.P. (1967).
- (108) Bond, G.C., *Catalysis by Metals* A.P. (1962).
- (109) Bond, G.C., *Heterogeneous Catalysis - Principles and Applications*. Oxford Chemistry Series (1974).
- (110) Dixon, J.K., and Longfield, J.E., *Catalysis Vol VII* 281. Reinhold (1960).

- (111) Shah, M.A., and Roberts, D., Chemical Reaction Engineering 11. 422 (1974).
- (112) Satterfield, C.N., and Cortez, D.H., Ind. Eng. Chem. Fundam. 9, 613, (1970).
- (113) Gay, B., and Maughan, R., Int. J. Heat and Mass Transfer 6, 277 (1963).
- (114) Roberts, D., Gillespie, G.R., Advances in Chemistry Series 133, 600, (1974).
- (115) Ede, A.J., An Introduction to Heat Transfer Principles and Calculation. Pergamon Press (1967).
- (116) McAdams, W.H., Heat Transmission McGraw - Hill 3rd Edition.
- (117) London, A.L., Mitchell, J.W., and Sutherland, W.A., Journal of heat transfer 82, 199, (1960).
- (118) Somorjai, G.A., Principles of Surface Chemistry. Prentice Hall (1972).
- (119) Somorjai, G.A., and Szalkowski, F.J., J. Chem. Phys. 54, 389 (1971).
- (120) Morgan, A., and Somorjai, G.A., Surf. Sci. 12 (3), 405 (1968).
- (121) Morgan, A., and Somorjai, G.A., C.A. 70: 109392a.
- (122) Lewis, R., and Gomer, R., Surf. Sci. 12 (2), 157 (1968).
- (123) Mclean, M., and Mykura, H., Surf. Sci. 5 (4), 466 (1966).
- (124) Tucker, C.W., J. Appl. Phys. 35 (6), 1897 (1964).
- (125) Lyon, H.B., and Somorjai, G.A., J. Chem. Phys. 46 (7), 2539 (1967).
- (126) Clarke, T.A., Mason, R., and Tescar, M., Surf. Sci. 40 (1), 1 (1973).
- (127) Weber, B., and Fusy, J., C.A. 71: 42633e.
- (128) Voelter, J., Procop, M., and Berndt, H., Surf. Sci. 39 (2), 453 (1973).
- (129) Gwathmey, A.T., and Cunningham, R.E., Advances in Catalysis X, 57 (1958).

- (130) Farnsworth, H.E., and Woodcock, R.F. *Advances in Catalysis* IX, 123 (1957).
- (131) Alfons, K., and Anastazja, H., *C.A.* 53: 19543i.
- (132) Domanski, B., Lenoir, J., Eyraud, C., and Prettre, M., *Bull - Soc. Chim France* 688, (1960).
- (133) Schmidt, L.D., and Luss, D., *J. Catal.* 22 (2), 269 (1971).
- (134) Pan, B.Y.K., *J. Catal.* 21, 27 (1971).
- (135) McCabe, R.W., Pignet, T., and Schmidt, L.D., *J. Catal.* 32 (1), 114 (1974).
- (136) Sachtler, W.M.H., and Vander Plank, P., *Surf. Sci.* 18, 62 (1969).
- (137) Dowden, D.A., *Catal. Rev.* 5, 1 (1972).
- (138) Bond, G.C., *Disc. Faraday. Soc.* 41, 200 (1966).
- (139) Bond, G.C., *Platinum Metals Rev.* 10 (3), 87 (1966).
- (140) Siegbahn, K., *Third Int. Conf. Atomic Phys.* (1972).
- (141) Hercules, D.M., *Analytical Chemistry* 42 (1), 20 (1970).
- (142) Riviere, J.C., *Contemp. Phys.* 14(6), 513 (1973).
- (143) Brundle, C.R., *J. Vac Sci Technol* 11 (1), 212 (1974).
- (144) Riggs, W.M., *Electron Spectroscopy, Proc. Int. Conf.* 713, (1971).
- (145) Kim, K.S., Winograd, N. Davis, R.E., *J. Amer. Chem. Soc.* 93 (23), 6296 (1971).
- (146) Bahr, J.L., *Contemp. Phys.* 14 (4), 329 (1973).
- (147) McCall, J.L., and Strabel, G.R., *Amer. Soc. for Metals Tech. Rep.* W6 - 4.2.
- (148) Wittry, D.B., *Advances in X-ray Analysis* 3, 185 (1959).
- (149) Birks, L.V.S., *Electronprobe Microanalysis* N. York Interscience (1963).
- (150) Long, J.V.P., *Advances in X-ray Analysis* 6, 276 (1962).
- (151) McKinley, T.D., Heinrich, K.F.J., and Wittry, D.B., 'The Electron Microprobe'. *The Electrochemical Society* (1964).
- (152) Heinrich, K.F.J., *Advances in X-ray Analysis* 11, 40. (1967).

- (153) Russ, J.C., A.S.T.M. Special Technical Publications 485, 154 (1971).
- (154) Yakowitz, H., Proc. of 7th annual scanning electron microscopy symposium 1029 (1974).
- (155) Zawadzki, J., Disc. Faraday Soc. 8, 140 (1950).
- (156) Falk, F., and Pease, R.N., J. Amer. Chem. Soc. 76, 4746, (1954).
- (157) Ashmore, P.G., Catalysis and Inhibition of Chemical Reaction. Butterworths (1963).
- (158) Fogel, Y.M., Nadykto, B.T., Rybalko, V.F., Shvachko, V.I., Slabospitskii, R.P., and Korobchanskaya, I.E., C.A. 70: 31929j.
- (159) Fogel, Y.M., Nadykto, B.T., Ribalko, V.F., Slabospitskii, R.P., Korobchanskaja, I.E., and Shvachko, V.I., J. Catal. 4(2), 153 (1965).
- (160) Fogel, Y.M., Nadykto, B.T., Shvachko, V.I., Rybalko, V.F., and Korobchanskaya, I.E., C.A. 60: 12699b.
- (161) Fogel, Y.M., Nadykto, B.T., Shvachko, V.I., Rybalko, V.F., and Dorobchanskaya, I.E., Kinetics and Catalysis 5, 830 (1964).
- (162) Fogel, Y.M., Nadykto, B.T., Rybalko, V.F., Slabospitskii, R.P., Korobchanskaya, I.E., and Shvachko, V.I., Kinetics and Catalysis 5, 127 (1964).
- (163) Pignet, T., and Schmidt, L.D., Chem. Eng. Sci. 29(5), 1123 (1974).
- (164) Molinari, E., Cramarossa, F., Capitelli, M., and Pullo, A., C.A. 63: 14105h.
- (165) Wong, E.L., and Potter, A.E., J. Chem. Phys. 43(9), 3371 (1965).
- (166) Branch, M.C., and Sawyer, R.F., Proc. Int. Symp. Combust. 14, 967 (1972).
- (167) Bretsznajder, S., C.A. 53: 957i.
- (168) Bretsznajder, S., C.A. 53: 958a.
- (169) Vladov, D., C.A. 51: 9274g.

- (170) Vainshtein, F.M., and Polyakov, M.V., J. Phys. Chem. U.S.S.R. 15, 164 (1941).
- (171) Vladov, D., C.A. 53: 5844c.
- (172) Vladov, D., C.A. 54: 19130a.
- (173) Vladov, D., C.A. 56: 8061e.
- (174) Vladov, D., and Dyakovich, K., C.A. 59: 3348g.
- (175) Vladov, D., C.A. 55: 78f.
- (176) Atroschenko, V.I., Savenkov, A.S., Zasorin, A.P., C.A. 74: 130859a.
- (177) Atroschenko, V.I., Savenkov, A.S., and Zasorin, A.P., C.A. 75: 122692w.
- (178) Zasorin, A.P., and Atroschenko, V.I., C.A. 72: 6554s.
- (179) Zasorin, A.P., Atroschenko, V.I., and Kleshev, N.F., C.A. 77: 156854g.
- (180) Zasorin, A.P., Cherkashin, V.N., and Atroschenko, V.I., C.A. 74: 130860u.
- (181) Zasorin, A.P., Cherkashin, V.N., and Atroschenko, V.I., C.A. 71: 33804j.
- (182) Williamson, W.B., Flentge, D.R., and Lunsford, J.H., J. Catal 37, 258 (1975).
- (183) Bradley, J.N. Trans. Faraday Soc. 63 (12), 2945 (1967).
- (184) Atroschenko, V.I., C.A. 55: 21948c.
- (185) Bird, R.B., Stewart, W.E., and Lightfoot, E.N., 'Transport Phenomena' J. Wiley (1960).
- (186) Scott, W.W., Ind. Eng. Chem. 16, 74 (1924).
- (187) Simecek, A., and Vosolbe, J., C.A. 81: 30073r.
- (188) Dobrovol'skaya, N.V., C.A. 79: 68276f.
- (189) Ivanov, D.G., and Petrova, O., C.A. 55: 15777g.
- (190) Mazgaj, W., Gajewski, A., Jaromin, M., Bialas, T., Osiejko, J., C.A. 60: 9962d.
- (191) Miniovich, M.A., Shneerson, A.L., Arutyunyan, V.A., Ivakhenko, M.T., Oleinik, I.M., Molchanov, V.A., Prisyazhnyuk, V.I., Kovalenko, E.F., Rozhkova, O.M., C.A. 82: 48049t.

- (192) Zasorin, A.P., Cherkashin, V.N., Atroschenko, V.I.,
CA. 71: 51700b.
- (193) Kubik, O., Czech. Patent. 152,780 C.A. 81: 127350s.
- (194) Hunter, J.B., U.S. Appl. 186,630, 05 Oct. 1971.
- (195) Kurin, N.P., and Zakharov, M.S., C.A. 58: 5080g.
- (196) Kenson, R.E., Albert, H.J., and Accino, D.J.,
U.S. Appl. 239,652, 30 Mar. 1972.
- (197) Dowden, D.A., Mackenzie, N., and Trapnell, B.M.W.,
Proc. Roy Soc. A. 237, 245 (1956).
- (198) Morooka, Y., and Ozaki, A., J. Catal. 5, 116 (1966).
- (199) Giordano, N., Cavaterra, E., and Zema, D.,
J. Catal 5 (2), 325 (1966).
- (200) Krylov, O.V., Catalysis by Nonmetals. A.P. 1970.
- (201) Darling, A.S., Selman, G.L., and Rushforth, R.,
Platinum Metals Rev. 15 (1), 13 (1971).
- (202) Darling, A.S., Selman, G.L., and Rushforth, R.,
Platinum Metals Rev. 14 (2), 54 (1970).
- (203) Darling, A.S., Selman, G.L., and Rushforth, R.,
Platinum Metals Rev. 14 (3), 95 (1970).
- (204) Darling, A.S., Selman, G.L., and Rushforth, R.,
Platinum Metals Rev. 14 (4), 124 (1970).